Correlation between Unsteady Loading and Tip Gap Flow Occurring in a Linear Cascade with Simulated Stator-Rotor Interaction

by

Joshua K. Staubs

Thesis submitted to the Faculty of the Virginia Polytechnic Institute and State University in partial fulfillment of the requirements for the degree of

Master of Science

in

Aerospace Engineering

William J. Devenport, Chair

Ricardo A. Burdisso

Roger L. Simpson

May 2005
Blacksburg, Virginia

Keywords: compressor, cascade, unsteady pressure, unsteady velocity, blade tip loading, tip gap flow

Correlation between Unsteady Loading and Tip Gap Flow Occurring in a Linear Cascade with Simulated Stator-Rotor Interaction

Joshua K. Staubs

(ABSTRACT)

This thesis presents the results of a study performed in the Virginia Tech low speed linear cascade wind tunnel operating at a Reynolds number of 382,000 designed to model an axial compressor rotor. To simulate the flow created by the junction of a set of inlet guide vanes and the compressor casing, vortex generators were glued to a moving end wall. In this investigation, the tip clearance was varied from 0.83% to 12.9% chord. Measurements of the midspan and the tip blade loading were made using static pressure taps. The tip loading shows that the minimum suction surface pressure coefficient increases in magnitude linearly up to a tip clearance of 7.9% chord. Unsteady pressure was measured on the pressure and suction surfaces at the tip of two cascade blades using an array of 23 microphones mounted subsurface. These measurements reveal that the unsteady pressure at the blade tip is a linear function of tip clearance height. The instantaneous pressure shows that the surface pressure at the blade tip has the same character regardless of whether or not the blade is disturbed by the inflow vortices. This suggests that the vortex generators simply stimulate and organize the existing response of the blade. Single sensor hot-wire measurements were made within the tip clearance on the suction side of the blade 1mm from the tip gap exit. These measurements show that the mass flux through the tip clearance is closely related to the pressure difference across the tip gap.

Acknowledgements

I would like to begin by thanking my parents, Michael and Elizabeth Staubs, for all of your support and encouragement throughout my life. You have always stressed the importance of finding a subject that I would enjoy and applying my best effort to excel in that area. You have pushed me throughout my life to strive for only the best and to never settle for anything less. I am deeply indebted to both of you for all of the lessons you have taught me over the years.

I would like to thank my advisor, Dr. William Devenport, for all of your help and guidance throughout my undergraduate research work and continuing on into my graduate career. You have a gift of being able to talk anyone into staying in your research group as long as possible and I think no one knows this better than I do. I appreciate all of your insights and ideas into the experimental research that I have been involved in and for all of your help in completing this work.

I would also like to thank my committee members: Dr. Roger Simpson and Dr. Ricardo Burdisso for your insight and suggestions for improving this work.

The AOE shop people, Mr. Bruce Stanger and Mr. James Lambert, are appreciated for all of your help in getting this project underway and helping to make things go smoothly. I would also like to thank Mr. Steve Edwards for all of your help in instrumenting the cascade blades.

I would like to thank Dr. Patrick Mish for all of your guidance and help in my undergraduate research and for teaching me the methods of experimental research. I also appreciate all of the help given by Dr. Nanyaporn Intaratep in helping me take my data. I know many of the nights in the tunnel were not the greatest but we managed to get through it all. I also appreciate all of my colleagues: Dr. Ruolong Ma, Dr. J.V. Larssen, Mr. Aurelien Borgoltz, Mr. Nicolas Spitz, Mr. Dustin Grissom, Mr. Ben Smith, Ms. Liz Craig, Mr. Derek Geiger. We have had many fun times over the years.

The Office of Naval Research, in particular, Dr. Ki-Han Kim is thanked for his support of this work under grant N00014-99-1-0294.

Joshua Staubs

June 2005
Blacksburg, Virginia

Table of Contents

Nomenclature

$\langle C_p \rangle\|_{pressure}$	$\langle C_p \rangle$ on the pressure side of the blade
$\langle C_p \rangle\|_{suction}$	$\langle C_p \rangle$ on the suction side of the blade
$\langle C_p \rangle$	Phase averaged fluctuating pressure coefficient
$\overline{\langle C_p \rangle}$	Mean phase averaged $\langle C_p \rangle$
$\langle \Delta C_p \rangle_{norm}$	Normalized $\langle C_p \rangle$ difference across the blade tip
$\langle C_p \rangle_{rms}$	Root mean square of $\langle C_p \rangle$
$\langle \Delta C_p \rangle_{rms}$	Root mean square of $\langle C_p \rangle$ difference
c	Blade chord length (254mm), A/D converter offset
C_p	Mean pressure coefficient defined as $C_p = \frac{P - P_\infty}{P_{0\infty} - P_\infty}$
C_x	Force coefficient in the chordwise direction
C_y	Force coefficient in the normal to chord direction
$E[\ ]$	Expected value
e_0	Output from the A/D converter
e_0	Recorded raw microphone voltage signal
f	Frequency (Hz)
G_{pp}	Surface pressure auto-spectrum
i	Input to A/D converter
$\dot{m}$	Mass flow
$\langle \dot{m} \rangle$	Phase averaged fluctuating mass flow
$\langle \overline{m} \rangle$	Phase averaged mean mass flow
M	A/D converter slope

P	Mean static pressure
p	Unsteady pressure
p'^2	Mean square pressure given by $p'^2(x,y) = \int_{f_{\min}}^{f_{\max}} G_{pp}(f,x,y)df$
$P_{0\infty}$	Mean upstream total pressure
P_∞	Mean upstream static pressure
p_{ref}	Reference free stream pressure given by $p_{ref} = \frac{1}{2}\rho_\infty U_\infty^2$
p_{rms}	Root mean square pressure given by $p_{rms} = \sqrt{p'^2}$
q	Dynamic pressure
R	Gas constant given by $R = 287\frac{J}{kgK}$
Re	Reynolds number based on the blade chord
s	Blade spacing (236mm), Blade span (254mm)
S	Microphone sensitivity
T	Period given by $T = \frac{2\pi}{f}$, Temperature
t	Tip clearance
t	Time (sec)
$\langle u \rangle$	Phase averaged mean velocity
$\langle u'^2 \rangle$	Phase averaged fluctuating velocity
U_∞	Free stream velocity
U_c	Convection velocity
X, y, Z	Cascade coordinates
x, y, z	Downstream blade chord-aligned coordinates
δ	Uncertainty
ρ	Density
ρ_∞	Free stream density
τ	Time step
ω	Frequency (rad/sec)

List of Tables

List of Figures

1. Introduction

1.1 Tip clearance flow and its effect on the performance of turbomachinery

In the study of turbomachinery such as compressors, turbines, and propulsion pumps, there are many factors that affect the design of these machines. One main concern is that there must be a tip clearance between the rotor and the surrounding casing to prevent physical contact between these two surfaces. The clearance is usually small, about one percent of the blade span for compressors and less than one percent for turbines. The tip clearance for a propulsion pump is usually about three percent of the blade span. However, because this tip clearance exists, there is a flow under the tip of the blade that originates from the pressure difference across the blade tip section and the relative motion between the blade end and the end-wall.

The difference in pressure between the pressure and suction surfaces of the blades drives the flow through the tip gap region of a turbomachine. Upon exit from the tip clearance, the flow meets the flow from the blade passage and rolls up to form the tip leakage vortex. The tip clearance flow is extremely complex because it forms in the presence of a potential core, secondary flow, the endwall boundary layer, and the blade boundary layer. The relative motion between the rotor and the casing also creates both viscous and inviscid interactions that occur near the blade tip.

There have been many studies in the past that have investigated the flow through the tip clearance region of many types of turbomachinery. These studies have involved using combinations of velocity, pressure, and flow visualization to determine the

characteristics of the flow both within the tip clearance and within the blade passage. These studies have been made for different tip clearances to investigate the effects of tip clearance on overall efficiency and performance of turbomachinery.

For compressors, it is known that engine performance is strongly dependent upon the pressure ratio as well as the efficiency. It has been experimentally determined that the efficiency loss through a compressor is increased by increasing the tip clearance between the compressor rotor and the casing. At the back end of the compressor, where the pressure and density are the highest, the blade height is the smallest to ensure that the axial component of the average velocity is approximately the same for all stages. This means that the tip clearance normalized on the blade span is largest in the high pressure stages. The efficiency of these later stages is decreased drastically due to the increase in the ratio of the tip clearance to the blade height. It is also known that the high pressure differences across the tip clearance region in a compressor cause unsteady loading on the blade tips and thus the generation of noise. Because of increasing concerns with aircraft engine noise, this can become a significant problem. Therefore to decrease the noise created by this unsteady loading, we must have a better understanding of the tip clearance flow.

Turbines are generally more efficient than compressors because the fluid undergoes a pressure drop in a turbine whereas it undergoes a pressure rise in the compressor. However, the efficiency of turbines is also affected by the tip clearance height and is seen to decrease as the tip clearance is increased. Therefore, investigators are constantly trying to decrease the tip clearance height to improve the overall performance of the turbine. Because of the falling pressure in turbine flow passages, more turning in a turbine blade row is possible without causing flow separation than in an axial compressor blade row. This means that there is a higher pressure ratio per stage in the turbine. Again, this higher pressure ratio can lead to increased pressure differences across the tip gap region of the turbine blades. This pressure difference causes unsteady loading of the blades and thus a generation of unwanted noise within the turbine.

Propulsors have many of the same flow considerations as those seen in turbines and compressors, however, the problems seen in propulsors are primarily due to cavitation. Cavitation is caused by the rapid collapse of tiny low pressure bubbles in a

liquid. A primary source of cavitation has been determined to be in the tip clearance region. The pressure difference across the tip clearance causes the formation of cavitation near the suction surface of the propulsor blades. The cavitation has many detrimental affects on the blades within the propulsor as well as creating unwanted noise. Because of the rapid collapse of the low pressure bubbles, cavitation causes erosion of the propulsor blades and thus decreases the life of a propulsor. The collapsing bubbles hitting the blade surfaces also causes tiny pinging noises that can be heard from large distances underwater. Therefore it is beneficial to eliminate the source of the cavitation in order to extend the life of the propulsor blades as well as to prevent detection of submarines and other watercraft by sonar.

A better understanding of the tip clearance flow through turbomachinery such as compressors, turbines, and propulsors will provide a better means for designing and operating turbomachinery. Because this tip clearance flow has an extremely important effect on the performance and efficiency of turbomachinery, it is advantageous to understand the flow phenomena that occur because of the presence of this tip clearance.

1.2 Research motivation and focus

The specific application of the present work is to investigate the unsteady tip clearance flow in an axial propulsion pump. The flow under the rotor blade tip caused by the interaction of the upstream stator row and the rotor blades is very complex. There have been many studies on the flow through the tip clearance region of turbomachinery; however, there have been very few studies of the unsteady interaction between the stator and the rotor. In vehicles traveling in water (surface ships as well as underwater vehicles), the phenomenon of cavitation plays an important role in the design and operation of turbomachinery such as turbines, pumps, and shrouded propulsors. One of the areas that cavitation often occurs is within the tip clearance and thus it is important to understand the flow structure within the tip clearance. A better understanding of the tip clearance flow will lead to improved design and operation of turbomachinery of all types.

Consider the rotor of an axial propulsion pump operating downstream of a set of fixed stators or inlet guide vanes. As the flow enters the pump and encounters the inlet guide vanes, these vanes shed both vortical and non-vortical wakes. These wakes are then convected downstream to the rotor blades creating an unsteady inflow to the rotor. This unsteady inflow may be the primary cause of noise and vibration in aircraft engines. In shrouded marine propulsors, the unsteady inflow may be the source of intermittent cavitatation.

One area of primary focus in the study of the unsteady inflow created by the inlet guide vanes is near the casing junction where the casing wall and the inlet guide vanes are joined. In this area, there is a shedding of a vortical wake that is convected downstream and is the cause of a rotor blade tip response. The unsteady fluctuations seen by the blade tip may be a cause of the noise and vibration seen in aircraft engines. Studies have also found that this is a primary area of cavitation seen in axial propulsion pumps. Therefore a study of this interaction between the unsteady wake created by the stator vanes and the rotor blades downstream could lead to better design and operation of aircraft as well as marine engines.

1.3 Background on tip clearance flow

Following is a discussion of some of the studies that have been conducted to examine the flow through the tip clearance region of compressor cascades, axial compressor rotors, propulsion pumps, and turbines.

1.3.1 Measurements on compressor cascades

Measurements made in compressor cascades can be applied to specific applications of turbomachinery such as propulsors. Compressor cascades are generally composed of a linear set of blades designed to simulate a turbomachine with only a single stage. These types of investigations can then be used to understand the flow seen in a broad range of turbomachinery which makes these studies important for aerodynamicists

as well as hydrodynamicists. The following investigations have all been conducted in some form of a compressor cascade.

Kang and Hirsch (1993, 1994) investigated the tip leakage flow in a linear compressor cascade of seven NACA 65-1810 blades for tip clearance levels of 1, 2, and 3.3% chord with stationary wall. The test Reynolds number, based on blade chord, was approximately $2.9x10^5$, with a free-stream turbulence intensity of 3.4%. The blade aspect ratio was 1.0 with a blade chord of 200 mm. They explored the leakage flow using wall static pressure tappings and a Pitot tube to measure the gap velocity profiles. Also, detailed five-hole probe measurements were made as well as extensive surface flow visualizations. The static pressures on the blade surface were measured using tappings placed at 1.5, 15, and 50% span from the tip for tip clearance of 0, 1, 2, and 3.3% chord. Without any tip clearance, the pressure distribution was found to be the same at all spanwise locations. However, with increasing tip clearance, unloading (a significant drop in pressure and thus a blade force defect) was found to increase near the leading edge and the minimum pressure on the suction surface decreased. They also found that a strong reloading (increase in pressure) occurs from 15% chord downstream of the leading edge resulting from the low pressure core of the tip leakage vortex. These measurements show that the pressure difference near the blade tip increases with tip clearance indicating that the reloading at the blade tip is stronger at higher tip clearances. Using the measurements made in the tip clearance with the Pitot probe, they discovered that the tip leakage flow shows different behavior upstream and downstream of the minimum suction surface pressure at the blade tip. Downstream of this minimum pressure point, the profiles show a distinct wake, which becomes more apparent with distance. From their surface flow visualizations, Kang and Hirsch determined that there exists a weak horseshoe vortex formed from the blade leading edge at small tip clearances. In addition to this, they determined that there is a multiple tip vortex structure consisting of the tip leakage vortex, a tip separation vortex, and a secondary vortex. They determined that the flow inside the tip gap is fully three dimensional over the entire chord which is in contrast to the observations made by Rains (1954) who assumed that the tip leakage flow was two dimensional and normal to the camber line of the blade.

Storer (1989), Storer and Barton (1991), and Storer and Cumpsty (1991) examined the tip leakage and tip clearance flow in a linear compressor cascade composed of five blades for tip clearances from 0 to 4% with a stationary wall. The inlet Mach number was 0.03 leading to a test Reynolds number, based on the blade chord, of $5.0x10^5$. The blade chord was 300 mm with a span of 435 mm. They explored the tip leakage flow using a three-hole probe to determine the total pressure, flow speed, and direction of the flow leaving the tip gap on the suction side of the blade. They also used static pressure tappings on the blade surface and on the endwall to measure the blade loading and tip clearance flow. Using the static pressure tappings on the blades, they determined that the loading near the blade tip with zero clearance was less than that at midspan. There was a spanwise pressure gradient with higher pressure toward the blade tip, especially near the leading edge. However, the blade loading remained relatively high near the leading edge and was similar to that of the midspan. Upon testing the configuration with tip clearance, they determined that tip clearance causes the pressure on the pressure side to be lower near the tip, especially near the leading edge. On the suction side, the pressure near the tip was higher near the leading edge. The measurements made within the clearance gap were made at 10 chordwise locations for 25 points across the gap for tip clearances of 2 and 4% chord. The pattern of the leakage flow was found to be very similar for both tip clearances. The nature of the leakage flow was found to be different on either side of the position of minimum pressure measured on the endwall. This difference is marked by the appearance of a distinct fluid jet, which is apparent at all downstream measurement locations from this position of minimum pressure, first seen at 49% chord. From five-hole probe measurements made downstream of the blade trailing edges, they conclude that the rate of increase of total pressure loss with tip clearance was non-linear despite a linear relationship of tip leakage flow to tip clearance. This implies that the total pressure loss due to tip leakage must be attributed to other mechanisms besides the loss of kinetic energy of the tip leakage flow.

Kang and Hirsch (1993, 1994), Storer (1989), Storer and Barton (1991), and Storer and Cumpsty (1991) all used blade surface pressure taps and pressure probe measurements to study the flow through a linear compressor cascade as a function of the tip clearance. All of these studies found that the pressure was higher near the leading

edge on the suction side of the blade as the tip clearance was increased. They also all found that the behavior of the leakage flow was different upstream and downstream of the minimum suction surface pressure point with the downstream leakage flow showing a distinct wake.

1.3.2 Measurements on axial compressor rotors

Unlike the studies made in compressor cascades, the studies on axial compressor rotors are usually made in a compressor with multiple stages and thus these studies represent the actual turbomachinery that is encountered in industry. The discoveries made in this area can be used in the design and elimination of noise in many types of turbomachinery and are thus useful for general flow related problems such as efficiency and noise.

Foley and Ivey (1996) investigated the effect of tip leakage flow on the chordwise distribution of static pressure in a large-scale, low-speed, axial flow, compressor composed of 72 inlet guide vanes, followed by 4 identical stages each having 79 rotors and 72 cantilevered stators, and an exit row of 72 outlet guide vanes. The test Reynolds number of the rotors, based on the rotor blade chord of 59.2 mm, was 2.0×10^5. The rotor blade aspect ratio was 1.54. They studied the blade pressure distribution using static pressure tappings on the rotors and stators. These tappings were located at “root”, “mid”, and “tip” locations along the blade span with 14 taps on the pressure surface and 12 taps on the suction surface equally spaced along the blade chord from leading to trailing edge. In addition to the blade surface pressure, they also used three-hole pneumatic probes to obtain inlet and exit for both the stator and rotor. Measurements were made for tip clearances of 1.2 and 3% chord. The overall efficiency of the compressor was found to diminish as the rotor casing clearance was increased from 1.2 to 3% by approximately 0.6%. They found that there is a lower total pressure at the rotor hub than at the midspan resulting in the peak pressure difference moving forward from 30% chord at the midspan to about 20% chord at the hub. At the rotor tip, the suction peak pressure moves forward of the midspan, however, the pressure then remains nearly constant for the first 30% of the chord. The region of constant suction surface static pressure increases by

approximately 10% chord with an increase in tip clearance. They believe that the constant pressure region is caused by fluid traveling radially up the suction surface as it is entrained into the leakage jet.

Goto (1992) examined the effect of difference in rotor tip clearance on the mean flow fields and unsteadiness and mixing across a stator blade row in a low-speed, single-stage axial compressor consisting of 51 rotor blades and 36 stator blades operating at a Reynolds number, based on the rotor blade chord of 111 mm, of approximately 3.1×10^5. He made flow field measurements at rotor tip clearances of 0.7, 2, and 3% chord using hot-wire anemometry, pressure probes, flow visualization, and an ethylene tracer-gas technique. Goto measured the mean velocity vector and the turbulent stress 31 mm downstream of the rotor blades and 68 mm downstream of the stator blade trailing edges using hot-wire anemometry. He also used the ethylene tracer-gas method by injecting the gas at a constant rate upstream of the stator leading edge and sampling using a Kiel probe 20 mm downstream of the stator trailing edge. Based on his measurements, Goto determined that the overall compressor performance is largely independent of rotor tip clearance, however the total-to-static pressure rise coefficients decrease throughout the machine operating range when the rotor tip clearance is large. Using the hot-wire measurements, he determined that a strong unsteadiness is observed in the casing region for large rotor tip clearance and in the hub region for small clearance, which are both related with the blockage effect of the casing viscous region. He also found that the difference in rotor tip clearance had a minor effect on the mean flow field within the stator. The maximum value of the mixing coefficient in the casing region was found to increase linearly with the rotor tip clearance.

The investigations of Inoue and Kuroumaru (1988) involved determining the structure of the tip clearance flow by making hot-wire measurements in the clearance to examine the variation of a phase-locked flow pattern with the tip clearance. Their experiment was performed in a low-speed rotating cascade facility with two rotors operating at tip clearances of 0.5mm to 5mm. In their investigations, Inoue and Kuroumaru showed that at the small tip clearance, the flow field can be divided into two regions: a leakage flow region on the suction side and an incoming through flow region on the pressure side. The leakage flow was found to grow rapidly near the blade leading

edge and increased gradually downstream due to the large pressure difference between the pressure and suction side near the leading edge. The jet flow meets the incoming flow and causes violent interactions resulting in high turbulence intensity near the leading edge. They also found that the point of minimum wall pressure is located near the suction surface at the leading edge suggesting an onset of rolling-up of the leakage vortex. As the tip clearance increases, the position of maximum pressure difference between pressure and suction surfaces moves downstream so the leakage jet flow becomes stronger at the downstream locations.

Pandya and Lakshminarayana (1983a, 1983b) investigated the flow in the tip clearance region of a compressor rotor using a two-sensor hot-wire in combination with an ensemble averaging technique. The measurements were made in a compressor rotor consisting of a 45 blade inlet guide vane row followed by a 21 bladed rotor and then a stator vane row of 25 blades. They operated at an inlet velocity of 28.37 m/s. In this work, they measured two components of velocity within the tip clearance of the rotor as well as flow field measurements. The flow field was surveyed at various radial locations and at ten axial locations, four of which were in the blade passage in the clearance region and six of which were outside the passage. They determined that the flow-field at about mid-chord is very complex resulting from the interaction of the leakage flow, annulus-wall boundary layer, and the scraping vortex. Low velocities on either side of the blade near the annulus wall were accompanied by high velocities in the clearance region. The tangential velocities near the suction side of the blade near the wall were found to be very large. Near the blade trailing edge, they conclude that a small blade pressure difference and/or the fact that the blade thickness is small here lead to the less pronounced features of the trailing edge stations. Very low axial and tangential velocities here show the presence of a leakage vortex near the suction surface. The relative velocity vector plots show that near the blade leading edge, the velocity is nearly parallel to the blade, while at mid-chord and the trailing edge, the velocity is nearly perpendicular to the blade. Their measurements also involved the turbulence intensity profiles at the same measurement locations as described above. Near mid-chord, the turbulence intensity is found to be complicated with a high pressure difference across the blade tip leading to the expectation that the leakage flow velocity should be high. At approximately the three-

quarter chord location, there is a sudden decrease in both the tangential and the axial velocities inside the tip clearance because of a channelization of the leakage flow resulting in reduced turbulence intensities.

Lakshminarayana *et al*. (1987) and Murthy and Lakshminarayana (1986) both investigated the flow field in the tip clearance region of a compressor rotor using a Laser Doppler Velocimeter (LDV). The studies were performed in a single-stage axial flow compressor facility with an inlet guide vane row of 43 blades followed by a 21-bladed rotor and a 25-bladed stator. They operated at an inlet velocity of 29.5 m/s and tip clearances of 1.78 to 3% chord. The LDV measurements were made at ten axial locations and about 25 radial locations in order to map the velocity distribution within the blade passage. They found the axial velocity near the leading edge region of the suction surface to decrease substantially due to large flow turning. This results in a defect in the axial velocity near the blade surfaces at the leading edge. They also determined that the flow field past the three-quarter chord location is dominated by a mixing of the leakage jet with the main flow. Their data shows that the leakage flow and the tip clearance height have considerable influence on axial and tangential velocity profiles, momentum thickness, displacement thickness, outlet angles, losses, efficiency, pressure rise and annulus-wall boundary layer growth.

The investigators described above have used an axial compressor rotor as the basis for their measurements. Many of the investigators used either blade pressure measurements or some form of velocity measurements such as hot-wire, pitot probe, or LDV to determine the primary characteristics of the flow through the tip clearance of an axial compressor rotor. Foley and Ivey (1996) used blade surface pressure measurements at varying tip clearances to determine that the overall efficiency of a compressor decreases as the rotor tip clearance is increased. Goto (1992), Inoue and Kuroumaru (1988), and Pandya and Lakshminarayana (1983a, 1983b) used hot-wire anemometry to study the tip clearance and tip leakage vortex flows in an axial compressor. Lakshminarayana *et al*. (1987) and Murthy and Lakshminarayana (1986) both used LDV measurements within the blade passage and in the tip clearance to show that the leakage flow and tip clearance height have considerable effects on the complex flow within a compressor rotor. These studies demonstrate the importance of tip clearance on the

efficiency and other characteristics of the flow within an axial compressor rotor and can be used to better design a compressor to account for these phenomena.

1.3.3 Measurements on propulsion pumps

The flow within a propulsion pump has been studied by several investigators. These studies provide, amongst other things, a means of understanding the cause of cavitation within the pump. Cavitation is defined as the sudden formation and collapse of low-pressure bubbles in liquids as a result of mechanical forces. This collapse of bubbles leads to pitting and destruction to the surfaces at which the cavitation occurs, losses in machine efficiency, as well as noise and vibration. All of these effects are detrimental to the life of the turbomachine in which the cavitation is occurring and could potentially lead to the loss of human life in wartime situations where noise and vibration may lead to discovery of the ocean-going vessel. Therefore, it is beneficial to understand the phenomena within a propulsion pump that leads to the formation of cavitation. The studies described below attempt to understand this phenomenon.

Zierke *et al.* (1994) investigated the tip leakage vortices and the flow field of the entire pump resulting from varying the tip clearance from 1.07 to 5.89% chord for a high-Reynolds-number pump (HIREP) facility using surface flow visualization, a two-component laser-Doppler velocimeter, and static pressure taps embedded with the blade surfaces. The HIREP facility was operated at blade-chord Reynolds numbers of 3.9×10^6 and 5.5×10^6 with a free-stream turbulence intensity of approximately 0.107%. The pump includes a row of 13 inlet guide vanes followed by a row of 7 rotating blades. Their surface flow visualization shows that there is a line of separation at approximately 96% chord near the blade tip. Photographs also showed some cavitation bubbles originating in the tip clearance near the rotor blade leading edge with most of the cavitation beginning near the suction surface at 15% chord. This location is very close to the measured minimum pressure point on the suction surface. They conclude that the periodic interaction of the rotor blades with wakes from the upstream inlet guide vanes will affect the unsteadiness of the tip leakage vortex leading to averaging errors of time-averaged flow measurements. As the tip clearance decreases, the character of the velocity profile

along the vortex core changes from a jetlike profile to a wakelike profile related to the adverse pressure gradient in the region of the tip leakage vortex and the angle at which the vortex lines are wound into the vortex core. For small clearances, the presence and proximity of the casing endwall affects the roll-up, shape, dissipation, and unsteadiness of the tip leakage vortex.

Gearhart (1966) studied the mechanics of the tip clearance flow and was primarily concerned with the cavitation that occurs in the tip clearance region. The measurements were made in a wooden duct wind tunnel with wall motion to simulate the relative motion between the rotor and casing wall. The model was developed to create a scaled-up version of the tip clearance flow through a pump or compressor. In this study, Gearhart used four gap configurations consisting of uniform, uniform with rounded corner, divergent, and convergent shapes. Tip clearances were adjusted to vary the ratios within the range commonly found in turbomachines. He used static pressure taps across the channel surface adjacent to the belt and on the upstream and downstream faces of the test specimen to obtain the static pressure distribution across the blade end. The mass flow through the tip clearance was measured using a total pressure probe traversed through the exit plane of the tip clearance. He also used smoke flow to obtain the flow pattern into the tip clearance. From these studies, Gearhart determined that it is more effective to decrease the tip clearance than it is to increase the blade thickness since an increase in the normalized momentum thickness produces approximately twice as much change in the pressure coefficient as an increase in the normalized blade thickness by the same magnitude. The effect of endwall motion was determined to increase the occurrence of cavitation in all gap configurations tested, except for the convergent gap.

In these studies, Zierke *et al.* (1994) and Gearhart (1966) studied the flow through an axial propulsion pump in order to understand the aspects of the flow that cause the inception of cavitation. Zierke *et al*. (1994) primarily investigated the tip leakage vortices with varying tip clearance and found that most cavitation in the tip clearance occurred at about 15% chord on the suction surface. Gearhart (1966) primarily investigated the tip clearance flow. He found that it is more effective to decrease the tip clearance in order to eliminate cavitation than it is to increase the blade thickness. These

studies demonstrate that the cavitation forming within the tip clearance is an important consideration in the design and operation of propulsion pumps.

1.3.4 Measurements on turbines

The tip leakage flow can have an important impact on aerodynamic and thermodynamic losses and thus the performance of a system. This leakage flow is induced by the difference in pressure between the pressure and suction surfaces of a turbine blade and causes inefficiency in the machine. These losses are seen to increase with an increase in the tip clearance of the blades. The following studies present some of the advancements that have been made in the study of the tip clearance flow in turbines.

Bindon (1989) measured the detailed development of tip clearance loss from the leading edge to the trailing edge of a linear turbine cascade using pressure probes to measure the total pressure on the endwall, at the tip clearance exit, and inside the tip clearance. His measurement were made in a seven blade linear cascade with a 152 mm chord operating at a Reynolds number, based on this chord, of 2.0×10^5 to 3.0×10^5. The tip clearances studied by Bindon were 0, 1, 1.5, and 2.5% chord. Between the minimum and maximum clearances, the total loss was found to be linearly proportional to tip clearance. However, between 0 and 1%, the curve is not linear, showing that there are different loss mechanisms present. He determined that there are three components of total tip clearance loss on the endwall: internal gap loss making up 39% of the total, suction corner mixing loss contributing to 48%, and endwall/secondary loss forming the remaining 13%. Mixing loss was found to emerge only over the last 20% of the axial chord meaning that the leakage over the forward part of the blade contributes very little. Bindon also saw a rapid rise in total loss from 40 to 70% chord and contributes this to the growth of the boundary layer filling the clearance gap.

Dean (1954) experimentally investigated the phenomena arising from the presence of tip clearance and relative wall motion in a rectilinear cascade with a blade chord of 2.8 in and an inlet velocity of 119 ft/sec leading to a blade-chord Reynolds number of 1.75×10^5. He used a moving wall made of a smooth, gritless sanding belt at speeds between 0 and 213 ft/sec. The tip clearances used in this study were 0, 3.4, 5.2,

and 10% chord. The pressure distributions were measured by embedding static pressure taps at nine spanwise stations with 19 taps in each row on the suction surface and 17 taps in each row on the pressure surface. Based on these pressure measurements, Dean observed that significant pressure variations with changing tip clearance or wall speed are observed only close to the blade tip. Also he determined that the point of minimum pressure moves rearward on the suction surface with increasing tip clearance. This result was observed independently of wall speed.

Jin and Goldstein (2003) used a naphthalene sublimation technique to measure the mass transfer coefficients from a high pressure turbine blade near the tip surfaces in a linear cascade with tip clearance. The effects of tip clearance from 0.86 to 6.90% chord were investigated for a Reynolds number of 5.8×10^5 with a free-stream turbulence intensity of 0.2%. They determined that the high mass transfer near the blade tip is caused by the leakage flow being sucked into the tip clearance. At larger tip clearances, they saw much larger mass transfer rates, which was contrary to what they expected since they thought that the acceleration of the leakage flow into the tip clearance would be weaker for larger tip clearances. Near the leading edge of the blade, they observed that the effect of tip clearance on the mass transfer is not very evident on the suction surface. However, much higher mass transfer rates are caused further downstream by the tip leakage vortex at the smallest tip clearance, while at the largest tip clearance, the average mass transfer is lower that that at zero clearance.

Moore and Tilton (1988) made measurements of the velocity profiles of the endwall boundary layer using a pitot probe. They also made blade loading measurements at 45% span with static pressure taps and the pressure distribution through the tip clearance was measured using wall static pressure tappings on the bottom of one blade and on the endwall beneath the blade. This study was performed in a turbine cascade of five blades with an axial chord of 235.2 mm. They operated at a Reynolds number of 4.5×10^5 with a tip clearance of 2.1% of the span. The blade unloading was measured on the pressure surface with static pressure tappings at several different tip gap heights from the bottom of the blade. The tip gap exit velocity profile was measured at one location using a pitot probe 6 mm upstream of the tip gap exit. The static pressure on the endwall shows that the flow accelerates rapidly as the tip clearance is approached and it

accelerates until about 18% of the way through the gap. At this point, both the static pressure on the endwall and the blade bottom rise rapidly reaching the same pressure at the gap exit.

Sjolander and Amrud (1987) investigated the structure of the tip leakage flow and its effect on the blade loading in a large-scale planar cascade of turbine blades. They made pressure measurements and surface oil flow visualization at a Reynolds number of $4.3x10^5$ with a tip clearance that was varied from 0 to 2.86% of the blade chord. The loading near the blade tip was investigated using static pressure taps embedded within the blade surface with 14 rows of 73 static taps. They also used smoke flow visualization at a Reynolds number of $1.27x10^5$ since the smoke could not be seen at the higher Reynolds number. It may be noted that they determined that the change in Reynolds number did not result in any significant changes in the flow field. From the oil flow visualization, they determined that from about 10 to 50% of the chord length, the flow close to the tip wall is strongly turned and passes over the blade tip at nearly right angles to the camber line. On the suction side, the first 5% of the chord length has little leakage flow emerging from the tip gap. The blade loading measurements showed that the pressure varies slowly on the pressure surface. On the pressure side, the effect of the leakage flow is minor until very close to the tip where some unloading occurs. However, on the suction surface, the magnitude and locations of the suction peaks are very substantially altered. Closest to the tip, two suction peaks are evident at 20% and 60% of the chord and a third begins to appear at 75%. They attribute these peaks to the multiple tip leakage vortices observed in the flow visualization. With a variation in tip gap, they notice that the start of the first tip leakage vortex moves rearward with increasing gap.

Srinivasan and Goldstein (2003) measured the local mass transfer on the tip of a turbine blade. The measurements were made using a naphthalene sublimation technique in a five-blade linear cascade at varying tip clearances from 0.6 to 6.9% chord. They simulated relative motion between the turbine blades and the casing by using a moving wall apparatus made of a synthetic rubber belt moving from the suction side of the blades to the pressure side operating at a speed of 25 m/s. The wind tunnel was operated at a speed equal to half the belt speed, 12.5 m/s, to attain an engine-representative Reynolds number (about $2.72x10^5$). Detailed pressure measurements were also made on the blade

tip using a row of holes on a hollow blade located 12% chord from the blade tip together with a water manometer. From the pressure measurements, they noticed that at z/C=0.12, there is very little difference between the cases with and without endwall motion, indicating a highly localized effect. Using pressure taps on the tip surface itself, they noticed that the low pressure observed on the pressure side of the blade indicates that the largest leakage flow occurs at a location corresponding to the region of highest turning of the blade profile. With the introduction of the endwall, the overall pressure rises. At a tip clearance of 0.6% chord, the effect of endwall motion was to reduce the pressure gradients driving the tip leakage flow. The relative motion also causes a reduction of about 9% in the mass transfer levels at this same tip clearance, which is assumed to be due to the tip leakage vortex coming closer to the suction side of the blade and "blocking of the flow" leading to reduced tip gap velocities and therefore lower mass transfer.

Yaras *et al.* (1989) made measurements in the tip gap of a planar cascade of turbine blades for tip clearances from 2.0 to 3.2% of the blade chord by making detailed surveys of velocity magnitude, flow direction, and total pressure. These measurements were supplemented with blade surface and endwall static pressure measurements. The test section consists of a five-bladed cascade with each blade having a chord of 250 mm, an aspect ratio of 0.8, and a solidity of 1.667. The measurements were made at a free-stream velocity of 30 m/s corresponding to a blade-chord Reynolds number of 4.3×10^5. Measurements were made within the tip gap using a three-hole pressure probe and the blade surface pressure was measured using 14 rows of static taps from the blade tip to the midspan, with 37 taps on the pressure surface and 36 taps on the suction surface. The row closest to the blade tip is at 2% of the blade span. Detailed traverses were made along the blade mean line with the pressure probe, the flow development across the tip gap was examined at five chordwise stations, and static pressure measurements were made on the blade surface to clarify the pressure differences driving the flow into the gap. The measurements on the mean line were made at 10 to 14 points across the tip gap at 37 stations from leading edge to trailing edge. From this measurement, they found that close to the tip, the velocity vector varies rapidly in both magnitude and direction, particularly on the rearward portion of the blade, which they attribute to the separation bubbles that form on the blade tip at the pressure surface edge. On the rearward half of the blade and

close to the tip, they observed that the velocity vector is directed from the suction side to the pressure side, which is unexpected but is consistent with the bubble taking the form of a small vortex whose axis lies along the mean line. The centerline of the vortex is at about 20% of the gap for the tip clearance of 2.8%, which is evident from the reversal in the direction of the velocity vector at this height. Towards the endwall, the velocity was found to vary far more slowly in the chordwise direction and is nearly constant in the spanwise direction. They also found that there is no evidence of the endwall boundary layer even at the outermost plane, which is about 2 mm from the wall. From the total pressure distribution in the tip gap, it is seen that away from the separation vortices, the total pressure is essentially equal to the inlet free-stream value with the exception being in the upstream 10% of the gap where some loss is evident. From about 20% chord, regions of high total pressure loss are apparent near the blade tip. From the blade surface pressure, they noticed that the stronger suction peak near the blade tip is caused by the tip leakage vortex that begins to form in the blade passage at about 20% chord. Sjolander and Amrud (1987) believed that the distortion of the blade loading near the tip would complicate the prediction of the gap mass flow, since this flow is generally assumed to be driven by the blade pressure difference. However, Yaras *et al.* believe this concern was not justified because their data indicates that the fluid closest to the blade tip does not contribute greatly to the leakage mass flow. In this study they also observed that the flow experiences its accelerating pressure difference before it enters the gap, which decouples the acceleration process from the pressure distortion that occurs locally near the blade tip on the pressure and suction surfaces.

The investigations presented above have made important studies on the flow through the tip clearance region of turbines using pressure, velocity, and flow visualization measurements. Jin and Goldstein (2003) and Srinivasan and Goldstein (2003) also used naphthalene sublimation techniques to investigate the mass flow rates at the blade tips. These studies have revealed the importance of the tip clearance height on the flow through the tip clearance region.

1.3.5 Measurements on unsteady stator/rotor interaction

An important investigation in the study of the flow through any type of turbomachinery is the study of the unsteady interaction that occurs between the stator and the rotor. This unsteady interaction results from the inlet flow passing over the stator vanes, causing turbulent wakes which then impinge upon the rotor blades. Since this is the actual problem encountered in turbomachines and is not an idealized model, many investigators have chosen to study this particular problem to determine the characteristics of the flow that result from this unsteady interaction.

Gallus *et al.* (1994) studied the static pressure distribution on the rotor blade surface and the rotor exit flow field using three-dimensional hot-wire and pneumatic probes. Their primary goal was to determine how well a simple, steady multiple-blade-row calculation predicted the time-averaged flow distributions at the exit of each blade row. The experiment was performed in a single stage axial turbine at a Reynolds number, based on the rotor blade chord, of 4.9×10^5. The flow was surveyed with a pneumatic five hole probe, three-wire hot-wire probes, and a laser velocimeter. A pneumatic boundary layer probe and a two-wire hot-wire probe were used near the endwall, while a rotating scanivalve was used to measure the static pressure distribution on the rotor blade. From their experimentation, they found that the time-averaged blade loadings are adequately calculated using a steady stage calculation. The unsteady effects on the time-averaged loading are relatively small even in transonic turbine stages and therefore this result is not surprising. They also found that the passage vortex near the hub of the rotor is transported toward the mid-span due to the unsteady interaction between the stator exit secondary flow and the rotor flow field. The steady stage calculation was not able to model this phenomenon. Overall, the steady state calculation was able to calculate most of the time-averaged flow field accurately enough for design applications. However, the radial distribution of the flow angle at the exit of the stage was not properly calculated using the steady approach. Based on these measurements they determined that further research is necessary to improve the steady multiple-blade-row calculation method.

Moyle *et al.* (1996) measured high-response pressure data in the tip gap, relative to the upstream stator, over a range of flow and tip gap conditions in a compressor test section with three stages with inlet and exit vanes. The Reynolds number for their experiment was $4.2x10^5$. From this experiment, they determined that the pressure magnitude was typically uniform from leading to trailing edge on the pressure side of the stator blade. They also found that the pressure distribution and levels varied substantially in the region near the suction side of the rotor, with this variation dependent on the stator relative position of the pressure sensor. The pressure trace and level on the pressure side of the rotor blade, however, was found to be roughly constant regardless of sensor position. The pressure difference across the tip of the rotor blade was determined to fluctuate by as much as 30% of the average along the rotor chord. When they correlated the position of the rotor and stator, Moyle *et al*. found that the pressure across the tip region undergoes a rapid change from the minimum differential to the maximum differential as the rotor passed out of the stator shadow. However, they found that the pressure levels at the inlet and outlet of the tip gap were only slightly affected by the stator relative position of the rotor.

Yamamoto *et al.* (1993) made detailed unsteady flow measurements before, within, and after the second stage stator passage of a 1.5-stage axial flow turbine using single slanted hot-wire anemometry. Their test section consisted of 16 stator blades and 20 rotor blades with the test Reynolds number for the rotor approximately $0.9x10^5$ and about $1.5x10^5$ for the stator. From their experimentation, they determined that the rotor wake is cut by the downstream cascade leading edges and then is separated into two parts within the cascade passage. The tip leakage vortex generated in the downstream cascade passage was determined to be influenced by the rotor-stator interaction and over time both the strength and size changes. The differences between the relative locations of the rotor and stator were found to effect the performance of the cascade.

Zechsky and Gallus (1993) made measurements in a subsonic, axial-flow turbine stage using static pressure tappings on the rotor blade surface accompanied by measurements of the rotor exit flow field using three-dimensional hot-wire and pneumatic probes. The test Reynolds number for their experiment was $6.8x10^5$ for the stator and $4.9x^5$ for the rotor. They determined that the pressures on the suction side of

the rotor blades increase considerably starting at about 25%*c*. The pressure decrease on the pressure side starts at about 50%*c* leading to reduced blade forces in the tip region. They also found that the highest fluctuations of the velocity, flow angle, and the turbulence intensity occur in the hub and tip region since the stator wakes and the cutting of stator secondary vortices leads to periodically high turbulence levels and intensified crossflow components toward the suction side.

These studies have experimentally examined the effects of unsteady stator/rotor interaction in order to provide more accurate quantification of the flow through a "real-world" turbomachine. Because the wake generated by the stator is unsteady, this has a very important effect on the performance of the rotor and must be examined to better understand the physics that occurs within a turbine.

1.4 Prior studies on the present configuration

The linear cascade used in this research has been previously studied by several researchers. The details of both prior and simultaneous research will be discussed.

The first of these studies made by Muthanna (1998, 2004) measured the flow field downstream of the cascade with stationary endwall using four-sensor hot-wire anemometry combined with oil flow visualizations made on the endwall underneath the blade row. The hot-wire measurements were made at 5 axial locations from 1.366 to 4.64 axial chords downstream of the blade trailing edge. He also studied the effects of tip gap on the tip leakage vortex for tip gaps of 0.83%*c*, 1.65%*c*, and 3.3%*c*. From these studies, he determined that the pressure difference across the blade tip induces flow through the tip gap which is almost perpendicular to the blade chord line. The tip gap flow then rolls up to form the tip leakage vortex which dominates the lower endwall flow region. This tip leakage vortex was found to be a source of high turbulence in the flow field. He also found that there is a secondary vortical structure that has the opposite vorticity and is much weaker than the tip leakage vortex. Muthanna also found that increasing the tip gap increases the strength of the tip leakage vortex, which then influences a larger region near the endwall. This study revealed the complex nature of the downstream flow field

of a compressor cascade. A simultaneous study made by Wenger (1999, 2004) used two point measurements at a tip gap of 1.65%c to further understand the flow downstream of the linear cascade. Analysis of these profiles showed that the tip leakage vortices are not subject to low frequency wandering motions. He also determined that the turbulence structure in the tip leakage vortices is highly anisotropic. The turbulent eddies in the vortex were found to be aligned along an axis that lies at an angle of 20° with the axis of the vortex.

Wang (2000, 2004) modified the linear cascade so that this configuration could be tested with a moving endwall to simulate the effects of relative motion between the blades and the casing. He made four-sensor hot-wire measurements downstream of the linear cascade. These measurements were made at three locations of 1.51, 2.74, and 3.75 axial chords downstream of the central passage. Measurements were made at one location, namely x/c_a=2.74, for tip gaps of 0.83%c, 1.65%c, and 3.33%c. He determined that both with and without the moving wall, the tip leakage vortex dominates the downstream flow field near the endwall. He also found that the difference between a stationary endwall and a moving endwall are substantial. The moving endwall reduces that strength of the tip leakage vortex and causes the vortex region to be swept further in the direction of wall motion. The wall motion also stretches the shape of the vortex region and disturbs the flow structure in the tip leakage flow. These results verify the importance of simulating relative motion between rotor blade and casing for the measurements in this cascade configuration.

de la Riva (2001, 2004) made detailed hot-wire anemometry measurements of a turbulent flow field past the linear cascade and compared these measurements to those predicted using Rapid Distortion Theory (RDT). The measurements were made with the stationary endwall for a tip gap of 1.65%c. He used a turbulence grid made of 10 vertical and 4 horizontal steel rods welded together to generate isotropic and homogeneous turbulence that was fully developed by the time it reached the blade row. He determined that the RDT calculations plus the viscous considerations were able to provide the general trend of the evolution of the turbulent fluctuations through the cascade within 10% of the measured values. The most important difference that he noted was in the integral length scales. He concluded that a proper RDT model could predict the

characteristics of a turbulent flow quite well with a good level of accuracy if viscous and blade blocking effects were included in the model.

Muthanna (2002) made further investigations to reveal the structure of the flow through the same linear cascade as it evolved through the cascade at a tip gap of 1.65%*c*. He also made measurements to reveal the effects of grid generated turbulence on the flow field for the same grid used by de la Riva (2001). Measurements were made at 8 axial locations, 0.8 and 0.23 axial chords upstream and 0 to 1.6 axial chords downstream of the leading edge of the blade row for the cascade without the grid generated turbulence and with the turbulence. In this study he determined that the tip leakage vortex becomes apparent at X/c_a=0.27 then grows to dominate the endwall flow region by the time it approaches X/c_a=0.77. This tip leakage vortex produces regions of positive vorticity near the vortex center and regions of negative vorticity underneath the tip leakage vortex due to the crossflow from the tip gap. The tip leakage vortex was also found the produce high levels of turbulence kinetic energy primarily due to gradients in the streamwise velocity direction. From his studies of the grid generated turbulence, Muthanna determined that the grid turbulence is suppressed near the endwall as it approaches the cascade. The blade loading showed a 4% reduction as a result of the free stream turbulence levels, the mean streamwise vorticity levels were reduced by about 20%, the size of the vortex core was increased by 30%, and the circulation was decreased by 2.5%. The path of the vortex center was shifted closer to the suction side of the blade passage at the trailing edge due to the higher turbulence levels.

Ma (2003) made measurements of the vortical inflow to the cascade produced by vortex generators attached to the moving endwall. The generators were designed to model the periodic unsteady vortical inflow similar to that shed by the junction of the casing wall and a row of inlet guide vanes. He also made measurements of the mean blade loading at mid-span as well as the downstream tip leakage flow. Ma measured both phase and time averaged three-component turbulence and pressure fluctuation measurements. The measurements were made for tip gaps from 0.83%*c* to 3.3%*c* at streamwise locations from 0.772% to 1.117% blade spacing axially downstream of the cascade. The vortex generators were found to have a symmetric pattern of two counter rotating vortices with the total circulation of these vortices about two orders of magnitude

smaller than the circulation in the cascade tunnel. The time averaged measurements show that the height, circulation, and maximum turbulence kinetic energy of the tip leakage vortex increases with increasing tip gap for the case with no generators. The vortical inflow produced by the generators was capable of producing significant fluctuations in the size, strength, structure, and position of the tip leakage vortex. These effects were seen to increase in magnitude with increase in tip gap. The phase averaged data also reveals that the tip leakage vortex center zigzags as it passes downstream of the rotor blade trailing edge for large tip gaps. The variation of the location of the center reduces as the tip gap is reduced, however, at very small tip gaps the variation in the location of the center increases again. This suggests that the shedding of vorticity from the blade tip is periodically influenced by the vortical inflow, however when the tip gap is decreased this influence is weakened. At small tip gaps the shedding of the tip leakage vortex as well as the tip leakage vortex itself is influenced by the vortical inflow. The microphone measurements made downstream of the cascade show that periodic fluctuating pressure waves move across the measurement section at a speed that is lower than the generator passing speed. These measurements show the importance of the counter-rotating vortices created by the inlet guide vanes on the flow within the tip leakage vortex.

Tang (2004) made measurements of the tip gap turbulent flow structure in the linear cascade using endwall pressure measurements, oil flow visualizations, and three-component laser-Doppler velocimetry. The measurements were made for a stationary wall at tip gaps of 1.65%c and 3.3%c. He also performed some initial experiments with the moving wall. The endwall static pressure distributions show that there is a strong cross-flow that is driven by lateral pressure gradients below the blade tip. This cross-flow relies on the local tip pressure loading. In the LDV measurements, four profiles inside the tip gap were made at each of nine chordwise locations. The cross-flow velocity was found to be nearly uniform in the middle of the tip gap but was found to increase from the pressure to the suction side. The turbulence kinetic energy did not vary much within the tip gap except near the endwall and the blade tip. The tip clearance was determined to affect the starting point of the tip leakage vortex with a shift from 16%c to 36%c as the tip clearance was increased from 1.65%c to 3.3%c. With endwall motion, he

found the near wall flow was skewed and the corresponding flow angles changed substantially. Further investigations are currently being made to better examine the effects of the moving endwall on the tip gap flow structure.

Mish (2003) made unsteady pressure measurements on both the suction and pressure sides of the cascade blades with an array of 24 microphones mounted subsurface. His measurements were made at tip gaps from 0.83%*c* to 12.9%*c* and were phase averaged with the passage of the vortex generators. He also made measurements without the periodic disturbance created by the generators. These measurements reveal that the blade response is a complex interaction of both the inviscid response and viscous phenomena. A close relationship between unsteady tip loading and the tip leakage vortex circulation was found to exist. Predictions made using inviscid theory agreed well with the measured levels of unsteady tip loading but were not able to capture the details of this loading. The measurements made by Mish were the primary motivation for the study presented in this thesis.

Intaratep *et al*. (2004) measured streamwise mean velocity and turbulence quantities as well as three-component mean velocity and turbulence distributions in the center of the blade passage for the linear cascade. Measurements were made at three axial locations downstream of the blade leading edge: 55.5%, 75.5%, and 98% of the axial chord length. These measurements were phase averaged with the passing of the vortex generators. Single component hot-wire measurements were made at all three axial locations while three-component hot-wire measurements were made at x/c_a=0.755 and 0.98. In this study she found that the flow structure inside the blade passage is composed primarily of shear layers which are shed by the tip leakage jet exiting from the tip gap on the suction side. The initial jet thickness was found to be the same as the tip gap height but expands as the jet encounters the tip leakage vortex in the middle of the blade passage. The phase averaged measurements show that a direct influence of the inflow vortices is only evident at x/c_a=0.555. Downstream of this location, the size and shape of the mean velocity structure are only slightly changed. Intaratep (2005) made similar measurements using three-component hot-wire at tip gaps of 1.65%*c*, 3.3%*c*, and 5.7%*c*. These measurements were made in planes horizontal to the endwall to document the movement of the inflow vortices through the blade passage. The purpose of this research

is to determine how the unsteadiness was affecting the tip leakage vortex and the blade tip loading.

The studies made in previous years on this linear cascade configuration have revealed many important aspects of the flow through a compressor cascade such as the effects of tip clearance height on the tip leakage vortices as well as the effects of relative motion between rotor and endwall. These studies are important in understanding the basic fundamentals of the flow through a single stage turbomachine and will help in further design and operation of turbines, compressors, and propulsors.

1.5 Research objectives and approach

The goal of this research is to better understand the flow through the tip clearance region of a linear cascade. The flow will be studied for disturbances like those caused by the inlet guide vanes in front of a rotor. Measurements were phase-locked to determine the correlation between the relative position between the rotor blade and the stator. The approach is to model this phenomenon in a laboratory environment in order to make accurate measurements.

To achieve these objectives, a linear cascade model was used. The model consists of a stationary blade row with a moving endwall to simulate relative motion between the rotor and casing. To simulate the affects of the inlet guide vanes, we have attached small vortex generator pairs to the moving endwall. These generator pairs are designed to simulate the flow created at the junction of the inlet guide vanes and the compressor casing. This is obviously a highly idealized model; however, we found it impossible to attach large devices to a moving belt to correctly simulate the flow over the entire span of the inlet guide vanes. Therefore we have chosen to ignore the effects of the spanwise turbulence created by the inlet guide vanes.

In order to study the flow through the tip gap, several different measurements have been made. These include:

1. A 23 microphone array embedded beneath the blade surface was used to measure the unsteady pressure fluctuations on the pressure and suction side of the two central blades in the linear cascade.
2. These measurements were made at tip clearances from 0.83%*c* to 12.9%*c* for several different generator configurations to determine the effect of generator spacing and size on the unsteady loading at the blade tip.
3. Single-wire hot-wire anemometry was used to measure the unsteady velocity perpendicular to the blade camber line at the exit of the tip clearance at 9 locations (6 corresponding to the microphone locations) along the blade chord. The unsteady velocity was made at a tip clearance of 3.3%*c*.
4. Mean surface pressure measurements were made using pressure taps at the blade tips to investigate the blade loading at the tip for tip clearances from 0.83%*c* to 12.9%*c*.
5. Mean surface pressure measurements were also made at the mid-span for the stationary wall case at tip clearances of 1.65%, 3.3%, and 5.7%*c*.
6. The combination of these measurements were then used to determine how the pressure difference across the blade tip clearance was driving the flow through the tip gap and how this pressure difference affected the mass flow rate through the tip gap.

1.6 Outline of thesis

This thesis documents the experimental study used to investigate the flow through the tip clearance of a linear compressor cascade. Hopefully these results will lead to a better understanding of the fundamentals of the flow through the tip clearance region of turbomachinery.

Chapter 2 describes the apparatus and instrumentation used to perform this study. The Virginia Tech linear cascade wind tunnel is described along with the moving wall system used to simulate relative motion. The microphone system used to measure the unsteady pressure, the pressure tap system used to measure the mean pressure, and the

hot-wire system used to measure the velocity through the tip gap is discussed. The data acquisition and reduction is also presented in this chapter.

Chapter 3 provides the results of the measurements of the blade tip loading made using the pressure tappings on both the pressure and suction side of the cascade blades. These results are presented at tip clearances ranging from 0.83%*c* to 12.9%*c*. The results with no wall motion and wall motion with no vortex generators are presented for all of the tip clearances. However, measurements made with the generators present are presented for only tip clearances from 0.83%*c* through 3.3%*c*. This is because of the similarity of the mean pressure with no generator effects and that with the generator effects.

Chapter 4 presents the measurements of the unsteady pressure near the tip of the cascade blades using the microphone system. Results are presented for the stationary wall case as well as the moving wall case with no vortex generators at a tip clearance of t/c=3.3% to provide a baseline for further discussions. Results are then presented for three cases: the cascade in periodic disturbance of the "baseline" case, the effect of the vortex generator spacing on the unsteady pressure, and the effect of the generator size on the unsteady pressure. These results are presented for tip clearances ranging from 0.83%*c* to 12.9%*c*.

Chapter 5 describes the measurements made using a single sensor hot-wire placed perpendicular to the camber line of the cascade blades. These measurements only provide one component of the velocity at the exit of the tip gap. Also presented is the mass flow calculations that were determined based on these single component velocity measurements.

Chapter 6 summarizes the results presented in this thesis and provides some conclusions that can be found from the measurements made in this investigation.

2. Apparatus and Instrumentation

2.1 Test facilities and configuration

2.1.1 Linear cascade wind tunnel

The measurements detailed in this study were performed in the Virginia Tech low speed linear cascade wind tunnel shown in Figure 2.1. This tunnel was built to simulate the flow through an aircraft engine fan rotor by Muthanna (1998) and was modified by Wang (2000) who added a moving wall system to study the effects of relative motion between the blade tips and the endwall. Ma (2003) also modified the tunnel to adapt it for the attachment of vortex generators to the moving wall. In this configuration the facility models a blade row, such as a propulsion pump rotor, operating downstream of a set of inlet guide vanes.

The cascade wind tunnel has a centrifugal fan powered by a 15hp AC motor. Air passes through a diffuser and a settling chamber and undergoes a contraction of 6.43:1. The air then enters a rectangular duct of 762mm x 304.8mm located upstream of the test section. This rectangular duct directs the flow onto the blade row, which consists of 8 aluminum GE Rotor B blades mounted at an angle of 24.9° to the axis of the upstream inlet section (inlet angle of 65.1°). The blade coordinates are detailed in Muthanna (2002). Ma (2003) modified the location of the blade row in order to attach vortex generators to the moving wall upstream of the blade row. He moved the blade row about 170mm downstream, along the upstream flow direction. The blades are mounted on a

superstructure that allows adjustments to be made to each blade in order to adjust the tip gap to the correct value. This superstructure also allows for the tip clearance of the entire blade row to be adjusted by placing shims under the superstructure. The blades are mounted with a stagger angle of 56.9° and have a chord length of 254mm and a span of approximately the same depending on the tip clearance. The spacing between successive blades is 236mm. Tip clearances used for this investigation are 2.1, 4.2, 5.6, 8.4, 11.4, 14.5, 20.1, and 32.8mm corresponding to 0.83%, 1.65%, 2.2%, 3.3%, 4.5%, 5.7%, 7.9%, and 12.9% of the blade chord, *c*. Boundary layer trips 6.4mm wide were attached to both sides of the blades at 25.4mm downstream of the blade leading edge. These trips were made of 0.51mm diameter glass sanding beads spread over a single layer on double sided tape and held in place using a coating of clear lacquer. The trips serve the purpose of eliminating the undesirable effects associated with natural boundary layer transition.

Located on the upper and lower endwall of the cascade are 19.1mm high boundary layer scoops that remove the upstream boundary layers. The scoops are 187.6mm axially upstream of the blade leading edge plane as shown in Figure 2.1. Attached to the lower scoop was a 2.4mm square boundary layer trip located 7mm downstream of the leading edge of the scoop to obtain the desired momentum thickness at the location of the vortex generators. On the floor of the upstream section of the tunnel is a 762mm x 63.5mm rectangular bleeding area that was added because the boundary layer thickness was not uniform at the leading edge of the boundary layer scoops. The bleeding area reduces the size of the boundary layer on the floor of the upstream section of the tunnel since the boundary layer thickness was found to be larger than the height of the scoops near the long upstream sidewall and would spill over the scoops without the bleeding area resulting in uneven endwall flow entering the blades (See Muthanna, 2002 for details).

To guide the flow through the tunnel, adjustable angle tailboards were hinged to blades 1 and 8 downstream of the cascade. The tailboards were made so that there was a small gap between the lower endwall and the bottom of the tailboard so that the moving wall could pass under the tailboards without rubbing against them. The tailboards were placed at an angle of 11.8°, the turning angle of the flow, so that the downstream flow was periodic in the pitchwise direction.

At the exit of the tunnel, two screens were clamped in order to raise the pressure inside the test section for the proper operation of the boundary layer scoops.

2.1.2 Moving wall system

To simulate the relative motion between the blades and the casing of a real turbomachine, a moving end wall was installed under the blade row by Wang (2000) and modified by Ma (2003). The moving wall is made of a 0.254-mm thick Mylar belt moving over a lower end wall. The lower end wall is made of a 3200mm x 80mm rectangular plywood bed. The windward side of the lower end wall is connected to the lower boundary layer scoop. The plywood bed is covered by a 1.6-mm Teflon sheet which helps reduce friction between the end wall and the moving Mylar belt. The moving belt is 686-mm wide and extends approximately 124-mm axially upstream and 423-mm downstream of the blade row.

The Mylar belt is made by overlapping the two ends of the Mylar sheet and creating a belt joint approximately 80-mm wide by welding the Mylar using a soldering iron at several hundred points across the width of the belt. Heavy duty clear tape was placed on the bottom and the top of the belt joint to keep the joint from wearing down and breaking during normal operation of the moving wall system. The belt joint was created at an angle of approximately 45° to improve the alignment and stability of the belt position. Since the belt joint is more than twice as thick as the rest of the Mylar sheet, this provides a large stimulation at the blade tips as the belt joint passes under the blade row. This problem was solved by eliminating any measurement points that were taken while the belt joint was near the passage between blades 4 and 5 (see Figure 2.1 for the blade numbering scheme).

Since the leading edge of the belt is exposed to the free-stream, a leading edge cover was made of a 25.4-mm wide x 0.254-mm thick Mylar strip. This strip was taped to the lower boundary layer scoop and overlapped the leading edge of the belt in order to prevent lifting of the belt inside of the test section.

The Mylar belt is driven using a 15hp AC synchronous motor. The belt speed can be adjusted using a TOSHIBA Tosvert-130G2+ digital variable-frequency controller

which is connected to the motor and allows the speed of the belt to be kept within 1% of the correct speed. The correct belt speed is given by $U_\infty \cos(24.9°)$ where U_∞ is the free-stream velocity. Therefore, at the typical free-stream velocity of 24.8 m/s, the correct belt speed is 22.5 m/s. This speed corresponds to the pitchwise component of the free stream so that an object moving with the belt would only see the axial component of the inflow. The belt is propelled and controlled using two 203-mm diameter, 762-mm wide rollers located outside of the tunnel on either side. The rollers are installed 3760-mm apart. The location of the belt was controlled using the driven roller on the upstream side of the tunnel. This roller was mounted on take-up bearings whose position in the pitchwise direction can be manually adjusted using two large screws connected to the roller. These screws allow both the tension on the belt and the angle of the driven roller to be adjusted. This allows for proper control of the belt so there was minimal drift from the mean location. The drift of the belt from its mean position is approximately ±4.2mm. The amplitude of the vibration of the belt was measured by Ma (2003) by imaging the tip gap of one of the center blades in the method described by Wang (2000). Ma averaged the tip gap measurements from a set of 20 photographs and determined that the r.m.s vibration was lower than 0.05mm (2.4% of the 0.825%*c* tip gap and 0.6% of the 3.3%*c* tip gap). This was the smallest vibration measurable using this method. Belt heating measured by Wang (2000) was found to be negligible.

2.1.3 Vortex generators

2.1.3.1 Vortex generators

To simulate the wake created by the junction of the casing and an upstream stator blade (or inlet guide vanes) half delta wing vortex generator pairs were glued to the belt. These generator pairs produce a highly idealized inlet guide vane flow but the design is necessary due to constraints with attaching the generators to the moving wall. The vortex generators shown in Figure 2.3 were based on the design of Pauley and Eaton (1989). They are made of 0.5-mm thick sheet metal, have an axial chord length of 24-mm, a height of 10-mm, and an angle of attack of ±18°. The generators were placed 12.7-mm

apart at mid-chord in pairs to produce a 'common-flow down' counter-rotating vortex pair. This vortex pair is an idealization of a necklace vortex wake. The generators were glued to the belt with their trailing edges 68.6±4.2mm axially upstream of the blade row to generate an unsteady, periodic vortical inflow representing an array of stator necklace vortices. The axes of the generator pairs were aligned perpendicular to the blade row, since in the frame of reference moving with the belt, this is the free-stream direction. Therefore, the counter-rotating vortices shed by the generator pairs grow in the axial direction as they are translated tangentially with the belt. The inflow disturbance caused by the vortex generators was thoroughly studied by Ma (2003) using a single sensor hot-wire rotation technique. The inflow disturbances were found to be roughly twice the height of the 3.3%*c* tip clearance and the leading vortex was found to be stronger and larger than the trailing one due to the relative motion between the stationary lower scoop and the moving belt. A picture of the inflow vortices is shown in Figure 2.4.

2.1.3.2 Baseline generator configuration

The vortex generator pair configuration used for the unsteady pressure and velocity measurements is shown in Figure 2.5. The vortex generators are the same as the generators used to make the unsteady measurements presented by Ma (2003), Mish (2003), and Intaratep (2005). Except at the belt joint, these generators are separated by a distance equal to the spacing of the cascade blades which is approximately 9.29" or 236 mm. The distance between generator pairs was chosen so that the unsteady boundary conditions of the flow would be periodic, which is an important consideration for computational modeling. Since the length of the belt was not an integer multiple of the blade spacing, there had to be one uneven spacing between generator pairs. This uneven spacing coincided with the location of the belt joint so that the location of the belt joint could be determined by measuring the passage of the generator pairs. Measurements taken during the passing of the belt joint under the blade row could then be eliminated in the data processing.

2.1.3.3 Widely spaced generator configuration

In order to investigate the effect of generator spacing on the unsteady pressure at the blade tip, a second generator configuration was studied and is shown in Figure 2.6. The only change was the spacing between the vortex generator pairs. The new configuration places the generator pairs at a distance of approximately 641 mm apart or 2.72 times the blade spacing. A distance of 641 mm was chosen because it was thought to be large enough that the effects of only one vortex generator pair should be seen in the blade surface pressure distribution at any given moment of time, and also because it is not an integer multiple of the blade spacing. This essentially eliminates any effects caused by the interactions between the inflow vortices from any two pair of generators or from simultaneous multiple blade interactions. The hypothesis is that possibly some of the effects that are seen in the fluctuating surface pressure distribution on the blade tip could be caused by the simultaneous interactions of separate inflow vortex pairs with adjacent blades. This new generator spacing was designed to eliminate this possibility.

2.1.3.4 Half-height generator configuration

To investigate the variation in the unsteady pressure on the blade tip as a function of disturbance size, a half-size set of vortex generators was used and is shown in Figure 2.7. The half-height generators are 5mm in height and were mounted at intervals equal to the blade spacing.

It is assumed that decreasing the height of the vortex generators will also decrease the size of the inflow vortices created by the generator pairs. Ma (2003) measured the height of the inflow vortices using hot-wire anemometry and determined that the inflow vortices were approximately twice the height of the 3.3%*c* tip clearance. For this investigation, time was a limiting factor and therefore the height of the inflow vortices created by the half-height generators was not measured. The assumption here is that decreasing the height of the generators by a factor of 2 will decrease the height of the inflow vortices by roughly the same factor.

2.1.4 Coordinate systems

Two coordinate systems are used for the discussion of the measurements made in this study. These coordinate systems are shown in Figure 2.1. The cascade coordinates (X,y,Z) places the X-axis in the axial direction of the cascade and the Z-axis parallel to the blade leading edge line. The origin of the cascade coordinate system is on the lower endwall at the center of the leading edge plane of the cascade. The blade chord-aligned coordinates (x,y,z) places the x-axis in the downstream flow aligned direction. The origin of the blade chord-aligned coordinates is at the intersection of the blade tip and the blade leading edge. The y-axis is the same for both systems and is normal to the endwall. The coordinate systems used are right-handed coordinate systems.

2.1.5 Tunnel calibration

The cascade tunnel was calibrated before testing to correctly model the flow conditions that exist in a turbomachine. This requires that:

1. There is no acceleration or deceleration when the upstream flow passes the boundary layer scoops.
2. There is no pitchwise velocity gradient in the potential core upstream of the blade row.
3. There is no pitchwise pressure gradient across the test section downstream of the blade row.
4. The back pressure is correct.

In order to remove the downstream pitchwise pressure gradient, the downstream tailboard angles were adjusted to obtain a uniform downstream pitchwise pressure distribution. Figure 2.8 shows the upstream pressure and velocity distribution for X/s=-0.54. Figure 2.9 shows the downstream pressure and velocity distribution for X/s=1.533. The pressure coefficients, C_p and C_{p0} are defined as

$$C_p = \frac{P - P_\infty}{P_{0\infty} - P_\infty}$$

$$C_{p0} = \frac{P_0 - P_\infty}{P_{0\infty} - P_\infty}$$

where P is the static pressure, P_0 is the total pressure, P_∞ is the reference static pressure and $P_{0\infty}$ is the reference total pressure. From these figures it can be seen that the pressure at both the upstream and downstream locations is uniform and there is no pressure gradient across the tunnel test section. The velocity gradient across the tunnel at the upstream location and the downstream location is minimal. The measurements were made at the blade mid-span (y/s=0.54) using a Dwyer Instruments Standard Model 160 Pitot probe. The pressure signals were obtained using 3 Setra model 239 electronic pressure transducers with ranges of 0-5 in. of water, 0-15 in. of water, and -2.5-2.5 in. of water.

2.2 Static pressure, microphone and hot-wire anemometry system

2.2.1 Static pressure system

2.2.1.1 Blade mid-span static pressure system

The blade loading at the mid-span was measured for tip clearances of 1.65%, 3.3%, and 5.7%c for the case of the stationary wall. The measurements were made with pressure ports located on the pressure side of blade 5 and the suction side of blade 4. There are 46 ports on the pressure side and 46 ports on the suction side. However, some of the ports were determined to be damaged and therefore the data from the damaged pressure ports is not presented. The locations of the mid-span pressure ports are given in Table 2.1 for the pressure side of blade 5 and in Table 2.2 for the suction side of blade 4 at a 123mm from the blade tip corresponding to a spanwise location of y/s=0.50.

Table 2.1 Mid-span pressure port locations for blade 5 (pressure side).

Port No.	*x/c*	*z/c*	X/c_a	Z/c_a
1	0.9867	0.0031	0.9909	-2.3621
2	0.9706	-0.0002	0.9697	-2.3407
3	0.9546	-0.0033	0.9489	-2.3192
4	0.9374	-0.0065	0.9268	-2.2960
5	0.9211	-0.0092	0.9064	-2.2737
6	0.9046	-0.0120	0.8857	-2.2511
7	0.8888	-0.0144	0.8663	-2.2293
8	0.8731	-0.0166	0.8470	-2.2073
9	0.8569	-0.0190	0.8272	-2.1848
10	0.8412	-0.0210	0.8085	-2.1627
11	0.8259	-0.0227	0.7905	-2.1410
12	0.8100	-0.0246	0.7718	-2.1185
13	0.7940	-0.0262	0.7532	-2.0955
14	0.7778	-0.0277	0.7348	-2.0723
15	0.7618	-0.0292	0.7165	-2.0492
16	0.7466	-0.0304	0.6995	-2.0270
17	0.7291	-0.0317	0.6801	-2.0014
18	0.7004	-0.0335	0.6486	-1.9593
19	0.6683	-0.0352	0.6138	-1.9116
20	0.6363	-0.0366	0.5797	-1.8640
21	0.6060	-0.0378	0.5476	-1.8186
22	0.5740	-0.0388	0.5142	-1.7704
23	0.5429	-0.0394	0.4821	-1.7234
24	0.5075	-0.0398	0.4462	-1.6694
25	0.4749	-0.0396	0.4138	-1.6192
26	0.4412	-0.0392	0.3807	-1.5671
27	0.4091	-0.0386	0.3496	-1.5172
28	0.3769	-0.0377	0.3187	-1.4669
29	0.3456	-0.0363	0.2897	-1.4175
30	0.3137	-0.0346	0.2604	-1.3669
31	0.2836	-0.0329	0.2330	-1.3189
32	0.2654	-0.0315	0.2169	-1.2895
33	0.2487	-0.0302	0.2021	-1.2626
34	0.2331	-0.0290	0.1885	-1.2375
35	0.2174	-0.0275	0.1751	-1.2119
36	0.2010	-0.0260	0.1610	-1.1852
37	0.1844	-0.0243	0.1470	-1.1580
38	0.1708	-0.0228	0.1358	-1.1356
39	0.1544	-0.0209	0.1222	-1.1086
40	0.1370	-0.0188	0.1081	-1.0798
41	0.0909	-0.0126	0.0716	-1.0028
42	0.0766	-0.0103	0.0607	-0.9785

43	0.0604	-0.0077	0.0484	-0.9511
44	0.0430	-0.0050	0.0354	-0.9217
45	0.0285	-0.0024	0.0247	-0.8969
46	0.0142	0.0001	0.0144	-0.8724

Table 2.2 Mid-span pressure port locations for blade 4 (suction side).

Port No.	*x/c*	*z/c*	X/c_a	Z/c_a
1	0.9927	-0.0079	0.9800	-2.3822
2	0.9777	-0.0136	0.9563	-2.3650
3	0.9622	-0.0189	0.9326	-2.3464
4	0.9467	-0.0239	0.9094	-2.3276
5	0.9313	-0.0286	0.8868	-2.3087
6	0.9162	-0.0332	0.8647	-2.2902
7	0.9003	-0.0379	0.8416	-2.2704
8	0.8848	-0.0420	0.8197	-2.2507
9	0.8692	-0.0461	0.7979	-2.2309
10	0.8520	-0.0503	0.7743	-2.2087
11	0.8374	-0.0533	0.7551	-2.1892
12	0.8219	-0.0564	0.7348	-2.1686
13	0.8059	-0.0595	0.7140	-2.1472
14	0.7907	-0.0621	0.6949	-2.1264
15	0.7746	-0.0649	0.6745	-2.1044
16	0.7589	-0.0674	0.6549	-2.0829
17	0.7431	-0.0694	0.6362	-2.0606
18	0.7098	-0.0734	0.5968	-2.0135
19	0.6783	-0.0763	0.5607	-1.9680
20	0.6476	-0.0785	0.5267	-1.9232
21	0.6168	-0.0803	0.4933	-1.8777
22	0.5846	-0.0813	0.4595	-1.8292
23	0.5534	-0.0818	0.4275	-1.7819
24	0.5221	-0.0821	0.3958	-1.7342
25	0.4907	-0.0816	0.3651	-1.6855
26	0.4592	-0.0807	0.3350	-1.6362
27	0.4273	-0.0794	0.3052	-1.5858
28	0.3948	-0.0774	0.2757	-1.5340
29	0.3638	-0.0752	0.2481	-1.4843
30	0.3322	-0.0726	0.2205	-1.4331
31	0.2997	-0.0690	0.1936	-1.3796
32	0.2698	-0.0653	0.1694	-1.3302
33	0.2385	-0.0612	0.1445	-1.2780
34	0.2228	-0.0587	0.1325	-1.2513
35	0.2067	-0.0560	0.1206	-1.2240
36	0.1922	-0.0537	0.1097	-1.1993

37	0.1777	-0.0510	0.0993	-1.1744
38	0.1630	-0.0482	0.0890	-1.1491
39	0.1471	-0.0452	0.0777	-1.1216
40	0.1319	-0.0420	0.0673	-1.0951
41	0.1155	-0.0384	0.0565	-1.0663
42	0.0810	-0.0304	0.0343	-1.0055
43	0.0644	-0.0263	0.0241	-0.9759
44	0.0471	-0.0219	0.0135	-0.9448
45	0.0327	-0.0180	0.0051	-0.9189
46	0.0113	-0.0090	-0.0025	-0.8770

2.2.1.2 Blade tip static pressure system

The static pressure at the blade tip was measured using pressure taps located on the pressure and suction surface of the blade. 25 pressure taps were located on the suction surface of blade 4 and 25 taps were on the pressure surface of blade 5, 6.4mm above the blade tip corresponding to a spanwise location of y/s=0.025. The location of the pressure taps on the pressure side of the blade is shown in Table 2.3. The location of the pressure taps on the suction side of the blade is shown in Table 2.4.

Table 2.3 Blade tip pressure port locations on the pressure side of the blade

Port No.	*x/c*	*z/c*
1	0.0126	0.0057
2	0.0322	0.0022
3	0.0521	-0.0012
4	0.0721	-0.0044
5	0.0921	-0.0074
6	0.1422	-0.0142
7	0.1924	-0.0199
8	0.2426	-0.0245
9	0.2929	-0.0283
10	0.3433	-0.0311
11	0.3936	-0.0331
12	0.4441	-0.0343
13	0.4945	-0.0347
14	0.5449	-0.0343
15	0.5953	-0.0332
16	0.6456	-0.0314
17	0.6958	-0.0289
18	0.7460	-0.0256

19	0.7960	-0.0212
20	0.8460	-0.0157
21	0.8958	-0.0087
22	0.9157	-0.0056
23	0.9356	-0.0021
24	0.9554	0.0016
25	0.9752	0.0055

Table 2.4 Blade tip pressure port locations on the suction side of the blade.

Port No.	*x/c*	*z/c*
1	0.0091	-0.0059
2	0.0289	-0.0123
3	0.0486	-0.0177
4	0.0684	-0.0228
5	0.0882	-0.0276
6	0.1381	-0.0387
7	0.1884	-0.0482
8	0.2389	-0.0564
9	0.2897	-0.0631
10	0.3406	-0.0684
11	0.3917	-0.0725
12	0.4429	-0.0753
13	0.4941	-0.0769
14	0.5453	-0.0772
15	0.5966	-0.0762
16	0.6478	-0.0738
17	0.6990	-0.0696
18	0.7500	-0.0636
19	0.8008	-0.0555
20	0.8512	-0.0452
21	0.9009	-0.0326
22	0.9206	-0.0269
23	0.9402	-0.0208
24	0.9597	-0.0143
25	0.9789	-0.0075

2.2.2 Microphone system

Unsteady pressure measurements on the blade surface were performed using Sennheiser microphones embedded within the tip of two cascade blades (pressure side of blade 5 and suction side of blade 4)-the same system used by Mish (2003). Two blades

were used for the unsteady pressure measurements due to constraints on the size of the blades. Namely, one blade was too small to embed all 23 microphones within its surface. Blade 4 (suction side) was equipped with 12 microphones and blade 5 (pressure side) was equipped with 11 microphones. On blade 4, 7 microphones were placed along the blade chord and 5 microphones were placed along the blade span. Blade 5 was equipped with 6 microphones along the blade chord and 5 microphones along the blade span. The microphone numbers and location are given in Table 2.5. The location of the microphones was given so that the pressure difference is computed in the direction of the lift vector. The coordinate system that corresponds with the microphone locations in Table 2.5 is given in Figure 2.10. The coordinate system is defined with the origin at the

Table 2.5 Microphone locations on blades 4 and 5

Microphone No.	***x/c***	***y/c***
Blade 5-pressure side		
1	0.7625	0.025
2	0.55	0.025
3	0.39375	0.025
4	0.29375	0.025
5	0.23125	0.01875
6	0.175	0.025
7	0.23125	0.05
8	0.23125	0.075
9	0.23125	0.15
10	0.23125	0.25
11	0.23125	0.45
Blade 4-suction side		
12	0.75625	0.025
13	0.55625	0.025
14	0.40625	0.025
15	0.30625	0.025
16	0.24375	0.01875
17	0.1875	0.025
18	0.1375	0.025
19	0.24375	0.05
20	0.24375	0.075
21	0.24375	0.15
22	0.24375	0.25
23	0.24375	0.45

leading edge corner of the blade tip with *x* pointing downstream along the blade chord, *y* pointing up along the blade span, and *z* pointing away from the blade completing the right hand rule. The microphone system was powered using 2 custom built quiet power supplies detailed in Mish (2003). The system was operated using an Agilent VXI system described in detail in below.

To ensure that the data from this system was accurate, all 23 microphones were calibrated individually while they were embedded within the blade surface. For accurate measurements, full amplitude and phase versus frequency calibrations are required for each individual microphone. This was done using a calibrator adapted from a NASA design and built by Mish (2003). The calibrator is shown in Figure 2.11. The calibrator is made of a small wide-range loudspeaker. The speaker is driven from an audio amplifier using a white noise signal, compensated for the response of the speaker/amplifier system. The white noise was generated by the HPE1432A described in detail below. The cross spectrum between the input signal and the microphone signal is then compared with a similar measurement made using a B&K reference microphone with a know calibration. The calibrator was held over the pinhole for the microphones and data was taken with a sampling rate of 25.6kHz using a 2048 point record length of 200 averages. This sampling scheme provided accurate frequency resolution between 100 and 5000Hz. The response of the microphones was found to be nearly flat over this range. A typical amplitude and phase calibration for the Sennheiser microphones is shown in Figure 2.12. The calibrations were applied over the full frequency range (0 Hz to 12800 Hz) in order to ensure accuracy.

2.2.3 Hot-wire anemometry system

Single component velocity and turbulence measurements were made using a single sensor model 1218 TSI standard boundary layer probe shown in Figure 2.13. This type of probe allows measurements to be made very close to an end wall and was thus determined to be the best available means of taking data very close to the moving end wall. The probe was mounted perpendicular to the mean blade camber line on the suction side of the blade approximately 1mm from the exit of the tip gap. Nine measurement

locations along the blade chord were used corresponding to a superset of the locations of the microphones used for the unsteady pressure measurements. The unsteady velocity was measured at x/c = 0.19, 0.24, 0.31, 0.36, 0.41, 0.48, 0.56, 0.67, 0.76. The hot-wire probe was mounted in a mounting device shown in Figure 2.14. The probe was traversed vertically within the tip clearance region at approximately 50 points between the blade tip and the moving endwall for each measurement location.

The hot-wire sensor was operated using a Dantec Type 55M01 bridge with a DISA Type 55M10 CTA standard constant-temperature anemometer unit. The anemometer bridge was optimized to give a frequency response greater than 25 kHz. The output voltage from the bridge was sampled by the Agilent data acquisition system (see below for details on this system). The hot-wire signal was buffered by a 10x buck-and-gain amplifiers containing calibrated RC-filters to limit their frequency response to 50 kHz.

2.2.4 Vortex generator detector system

For this experiment, it was vital to know the location of the vortex generator pairs at any instant of time. Therefore, a photodiode was mounted underneath the Teflon bed at a location 80.5-mm axially upstream of the center of the cascade leading edge line between blades 4 and 5. The detector was illuminated with a laser beam that was mounted on top of the tunnel and was shined vertically downward through a hole in the Plexiglas. The laser was positioned directly above a hole in the Teflon bed underneath which the photodiode was mounted. The beam of the laser was interrupted by the passing of the vortex generators. The signal from the photodiode was then amplified and was sampled simultaneously along with the hot-wire and microphone measurements. For further details on this system see Ma (2003).

2.2.5 Agilent data acquisition system

For data acquisition, an Agilent VXI system was used. The system is composed of an Agilent E1432A module, an Agilent E8491A interface and an Agilent E8408A VXI mainframe. The Agilent E1432A module is a 16-channel digitizer used for data acquisition. It is a C-size, one-slot, register-based VXI module that includes DSP, transducer signal conditioning, alias protection, digitization, and high-speed measurement computation. The module is installed in the Agilent E8408A VXI mainframe which consists of 4 C-size slots, in which the Agilent E1432A module and the Agilent E8491A interface are installed. The Agilent E8491A links the VXI mainframe backplane to the IEEE 1394 serial bus. The bus links the VXI mainframe to the PC. The system can deliver a maximum of 51,200 simultaneous samples per second per channel at 16-bit resolution. The input residual DC of the Agilent E1432A is ≤±1% of the range, ±10mV. The r.m.s noise for a 23 kHz span in dynamic range is less than 45μV r.m.s.

2.3 Data acquisition and reduction

2.3.1 Data acquisition

2.3.1.1 Static pressure acquisition

Static pressures at the blade mid-span and the blade tip pressure taps were measured using a scannivalve system consisting of a solenoid scanning system, 2 pressure transducers, and a data acquisition system. The scannivalve, model CTLR2P/S2-S6 Scannivalve Corp., can obtain data from a single pressure tap at a time and was operated using a Data Translation DT2801-A A/D converter installed in a PC. The system was set to collect 2 kilosamples at a frequency of 1000 Hz. Once a measurement was completed for one pressure tap, the system would switch to the next pressure tap motor. The pressure from each tap was read after 3 seconds of settling time until the data from all of the pressure taps was completed. One of the pressure transducers (a Setra model 239 electronic pressure transducer with a range of ±2.5 in. of

water) was used to measure the difference between the free-stream and the local static pressure. The other transducer (a Setra model 239 electronic pressure transducer with a range of ±5 in. of water) was used to measure the free-stream dynamic pressure.

2.3.1.2 Unsteady pressure acquisition

The data acquisition for the unsteady pressure measurements was controlled using a PC using programs encoded in Agilent VEE. The programs were used to sample the free-stream temperature using a thermocouple, the free-stream pressure using a pressure transducer, the voltage output from the vortex generator detector, as well as collecting data from 23 microphones simultaneously. All of the microphone measurements were performed using a sampling rate of 25.6 kHz with a record length of 16384. A total of 100 averages were taken for each tip clearance. This sampling scheme ensures that data was taken for at least one full revolution of the moving belt.

2.3.1.3 Hot-wire anemometry data acquisition

Data acquisition for the unsteady tip clearance velocity was also made using a laptop PC with programs encoded in Agilent VEE. The programs controlled the Agilent digitizer to sample the free-stream temperature and pressure using a thermocouple and a pressure transducer, respectively, the voltage output from the vortex generator detector, as well as collecting the voltage data from the hot-wire anemometry system. At each measurement point within the tip clearance, 100 records of 16384 samples of the hot-wire signal were recorded at a sampling frequency of 25.6 kHz.

2.3.1.4 Other instrumentation

The free-stream temperature for all measurements was measured using an Omega copper-constantan thermocouple connected to an Omega Model DP80 digital thermometer and the free-stream pressure was measured using a 3.1mm diameter Dwyer

Pitot-static probe connected to a Setra model 239 pressure transducer. The position of this reference Pitot-static probe is given in Figure 2.1.

2.3.2 Data reduction

2.3.2.1 Vortex generator signal reduction

The signal from the photodiode underneath the Teflon bed was sampled simultaneously with the hot-wire and microphone measurements in order to provide a phasing signal for averaging of the data. The vortex generator signal was processed using HPvee to construct a phasing signal by subdividing the time intervals between the passing of successive vortex generator pairs into 256 equal periods. These periods represent the instantaneous position of the vortex generator pair as shown in Figure 2.15. A phase number of 0 corresponds to the instant of time when the center of the vortex generator pair is axially upstream of the center of the passage between two successive blades, phase 128 indicates the instant of time when the center of the vortex generator pair is axially upstream of the blade leading edge, and phase 256 indicates the instant of time when the center of the generator pair is axially upstream of the center of the passage between the next two blades. One phase number corresponds to a movement of 236/256=0.92mm of the generator pair. The processing of the phasing signal allows any bad periods to be excluded from the measurement results by setting limits on belt speed as well as belt position. This allows the passing of the belt joint to be processed out of the measurement results since the period of time between successive generator pairs passing through the generator detector is much longer at the belt joint. It also allows any bad periods that may result from movement of the belt away from its mean position as well as increases/decreases in belt speed. It is beneficial to remove these bad periods in order to ensure the accuracy of the collected data. This method of processing the phasing signal was used for both the hot-wire measurements and the microphone measurements.

2.3.2.2 Phase averaged data reduction

The processed phasing signal was used for the reprocessing of the microphone and hot-wire voltage signals. The phase averaged mean value at each phase time, *i*, can be calculated using Equation 2.1.

$$\langle a \rangle_p = \frac{1}{N} \sum_{n=0}^{N-1} a(i + nT) \tag{2.1}$$

Here $\langle\ \rangle$ represents the phase averaged value, N is the number of samples at phase time i, and T represents the period time for the vortex generator pair passing through one blade passage.

2.4 Summary

The Virginia Tech low speed linear cascade tunnel was used to simulate the flow through an axial propulsion pump rotor operating in the wakes of a set of inlet guide vanes. The inlet guide vane wakes were simulated by attaching vortex generator pairs to the moving end wall to generate the wake created at the junction of the inlet guide vane and the casing wall. The cascade tunnel, the moving wall system, and the vortex generator configurations used in this investigation were described in full detail. The static pressure system, the hot-wire anemometry system, and the microphone system were also described. The phase signal processing and hot-wire and microphone reprocessing were discussed.

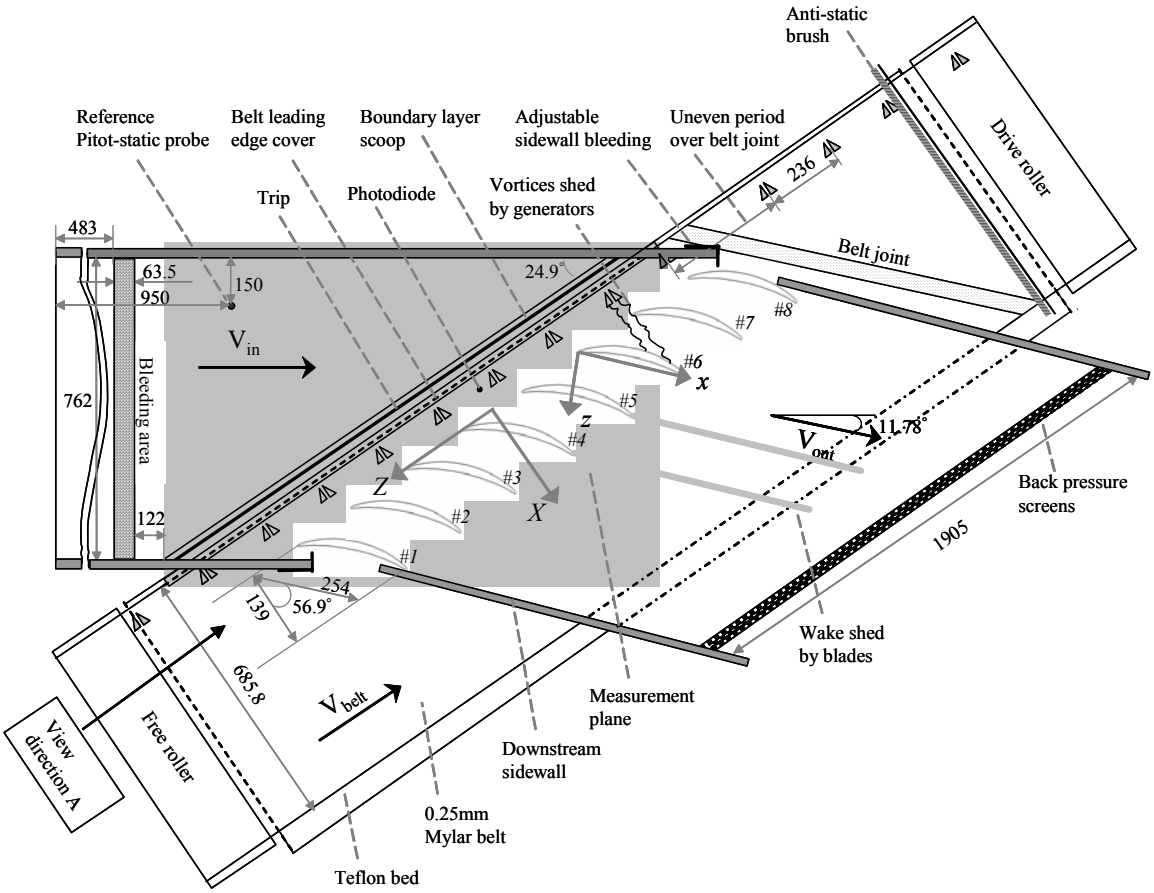

Figure 2.1 Plan-view of the Virginia Tech linear cascade wind tunnel (Adapted from Ma 2003).

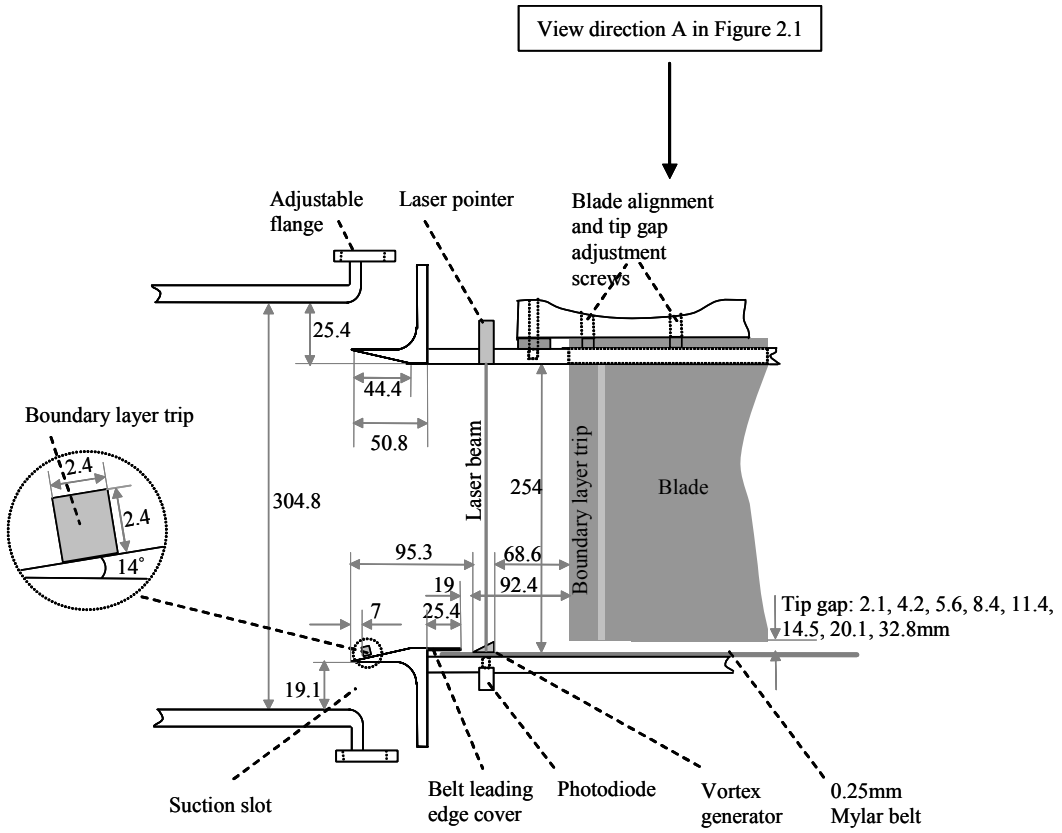

Figure 2.2 Cross section through the cascade along the axial direction (Adapted from Ma 2003).

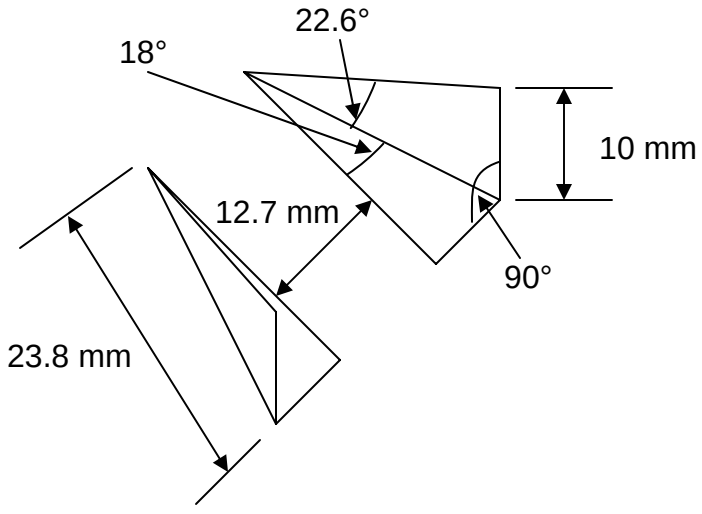

Figure 2.3 Delta wing vortex generator pair.

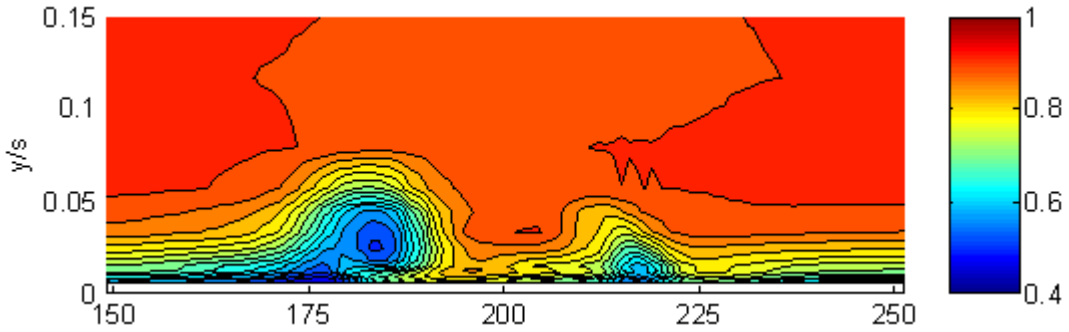

Figure 2.4 Streamwise velocity, $\langle u_s \rangle / U_{eX}$, the phase averaged velocity in the cascade coordinates on the stator frame normalized on the axial component of the velocity at the edge of the boundary layer.

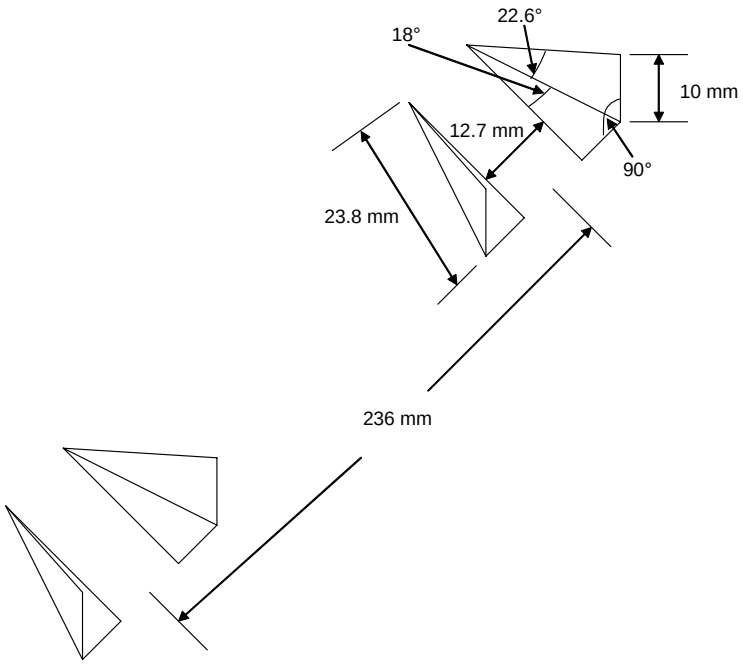

Figure 2.5 Baseline configuration of vortex generator pairs.

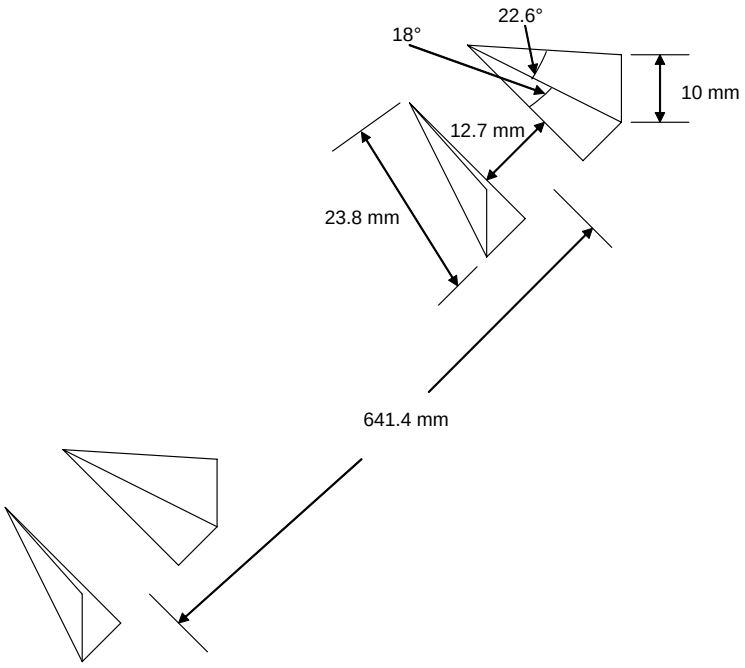

Figure 2.6 New configuration of vortex generator pairs to study the effects of generator spacing on the blade surface pressure distribution.

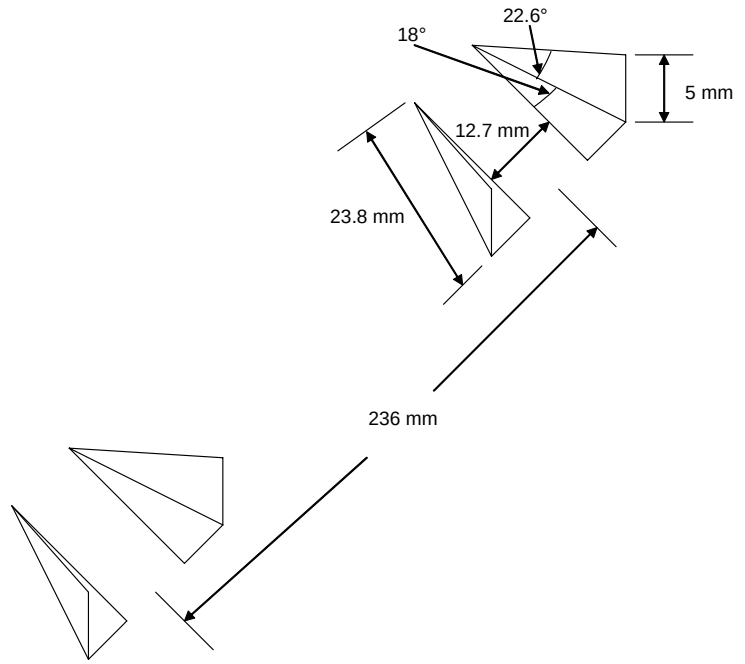

Figure 2.7 New size of vortex generator pairs to study the effects of generator size on the blade surface pressure distribution.

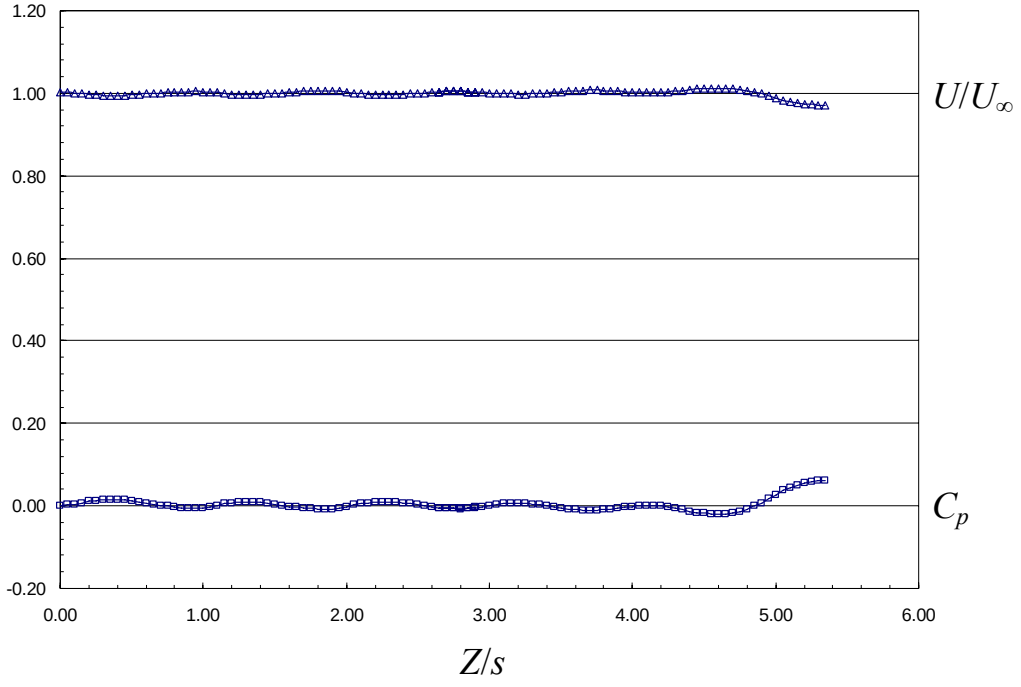

Figure 2.8 Cascade tunnel upstream pressure and velocity distribution at X/s=-0.54, y/s=0.54.

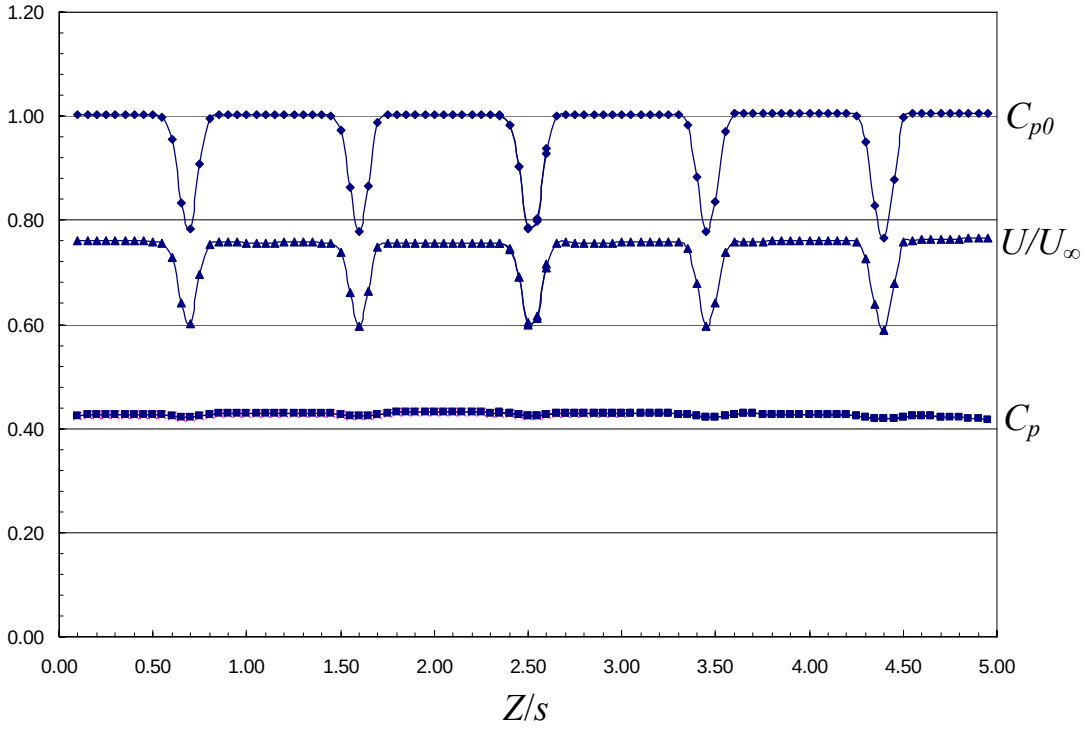

Figure 2.9 Cascade downstream pressure and velocity distribution at X/s=1.534, y/s=0.54.

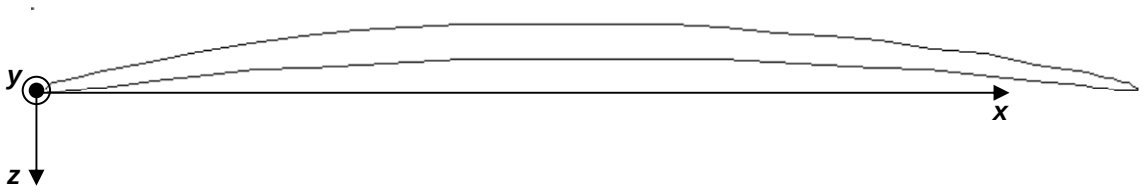

Figure 2.10 Coordinate system for microphone locations.

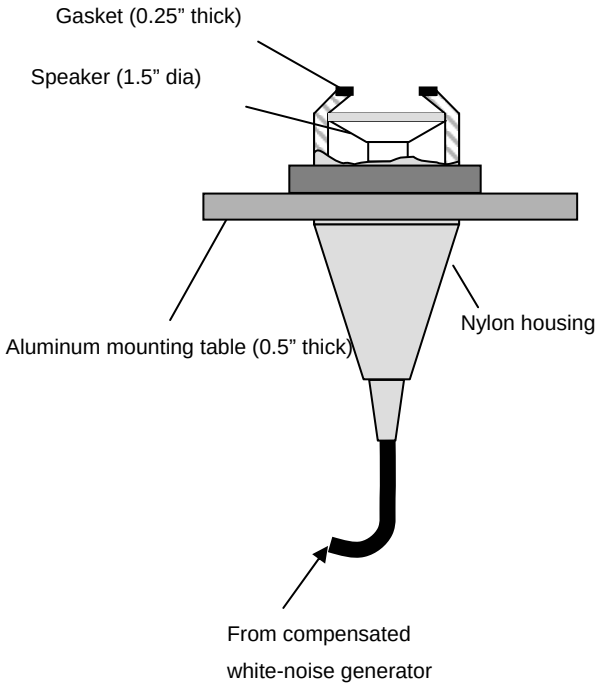

Figure 2.11 Handheld microphone calibrator (Adapted from Mish 2003).

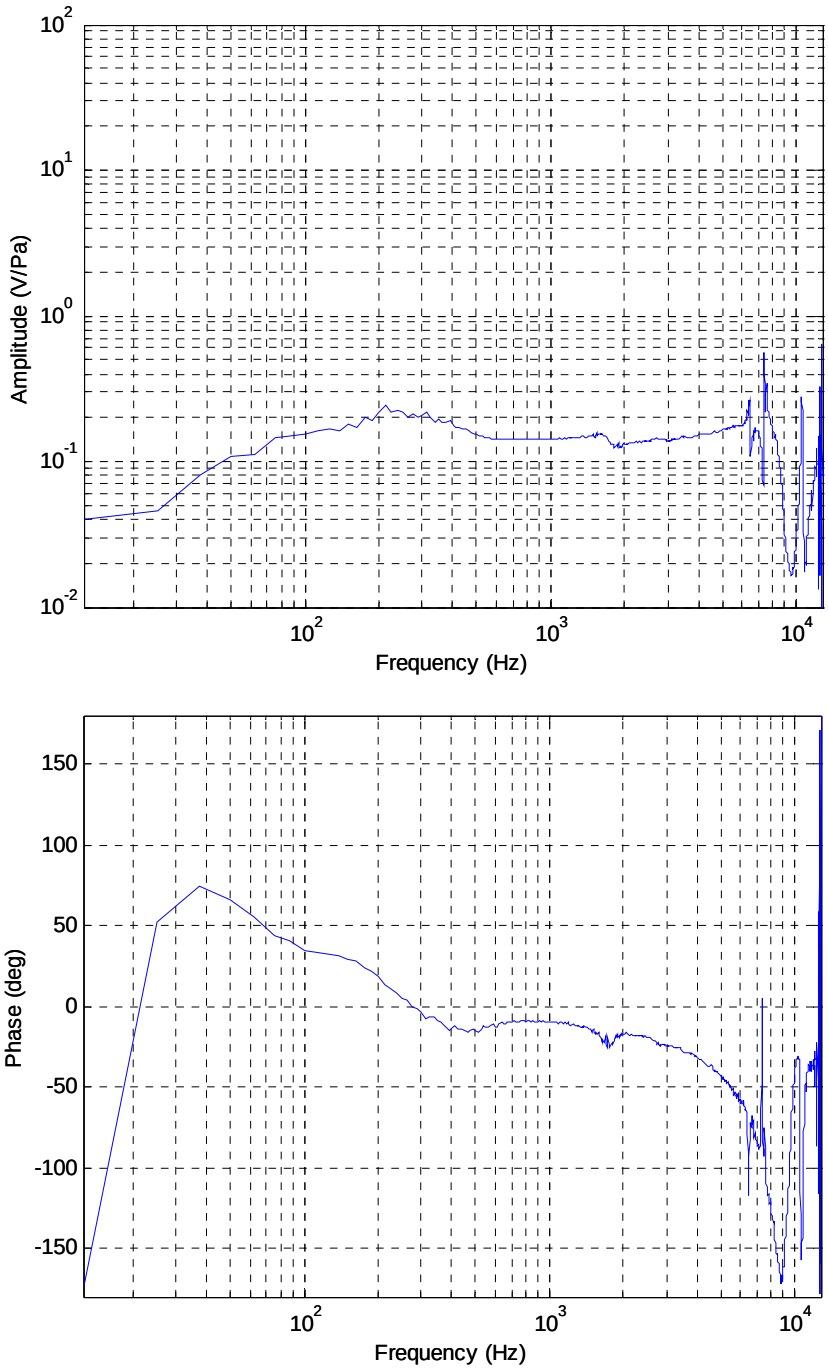

Figure 2.12 Typical amplitude and phase calibration for the Sennheiser microphones.

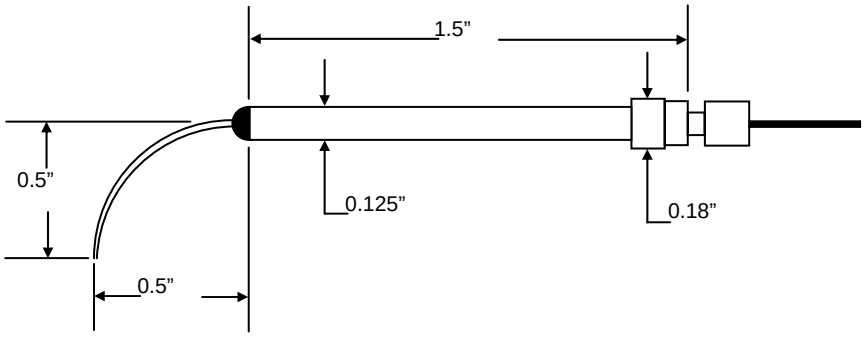

Figure 2.13 Boundary layer probe used for tip gap velocity measurements.

Figure 2.14 Boundary layer probe mounted in probe holder.

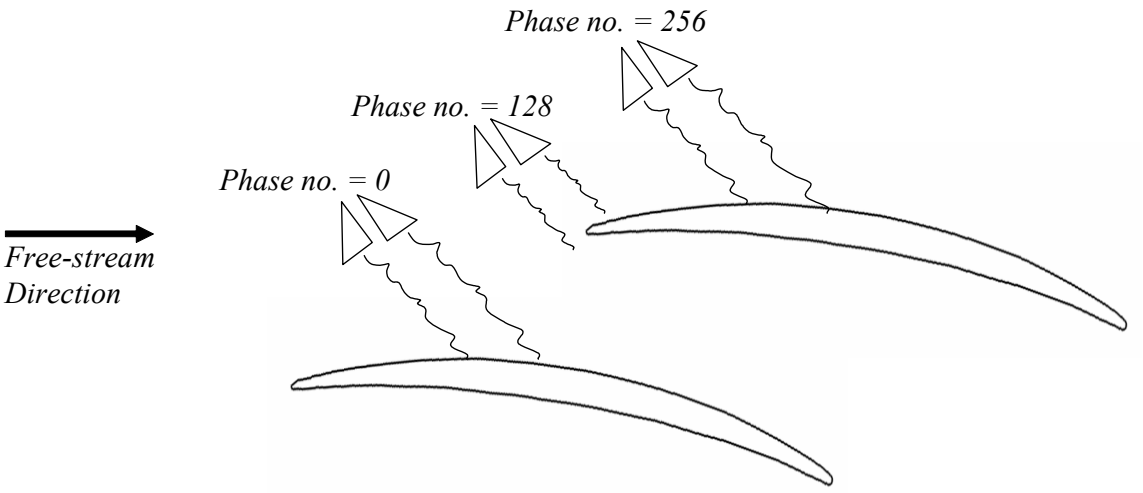

Figure 2.15 Definition of phase number.

3. Analysis of Blade Loading

3.1 Introduction

It is important to understand the loading that occurs near the blade tip in order to better understand the interactions between the blades and the tip clearance flow. In this section, mean blade pressure distributions measured at both the mid-span and the blade tip are presented for tip clearances from 0.83%*c* to 12.9%*c* for three cases: stationary wall, moving wall, and moving wall with unsteadiness from the vortex generator pairs.

3.2 Flow conditions

The cascade tunnel was operated at a Reynolds number based on the blade chord of 382,000. This corresponds to a tunnel free-stream velocity of 24.8 m/s. The free-stream velocity was measured using a 3.1mm diameter Dwyer Pitot-static probe connected to a Setra model 239 pressure transducer. The free-stream conditions were measured at a location 950 mm downstream of the entrance of the upstream section and 150 mm from the wall of the upstream section, which is approximately 1 m upstream of the center of the blade row.

3.3 Mean pressure uncertainty analysis

The mean pressure coefficient is defined as $C_p = \frac{P - P_\infty}{P_{0\infty} - P_\infty}$. For this study, the quantities in the numerator and the denominator were measured using very similar transducer systems so it can be assumed that $\delta(P - P_\infty) = \delta(P_{0\infty} - P_\infty)$ and therefore the uncertainty of C_p can be calculated using Equation 3.1

$$\frac{\delta C_p}{C_p} = \delta(P - P_\infty)\sqrt{\frac{1}{(P - P_\infty)^2} + \frac{1}{(P_{0\infty} - P_\infty)^2}} \tag{3.1}$$

where

$$\delta(P - P_\infty) = \sqrt{\delta^2(P - P_\infty)|_{Rand} + \delta^2(P - P_\infty)|_{Bias}} \tag{3.2}$$

The random uncertainty in the measured pressure was found to be 1.24 Pa (0.005 in of water) based on half of the digital resolution. The bias uncertainty in the measured pressure was checked to be negligible. Therefore, the uncertainty in the mean pressure measurement is 1% of C_p.

3.4 Mid-span blade loading

The blade loading at the mid-span was measured for tip clearances of 1.65%, 3.3%, and 5.7%*c* for the case of the stationary wall. The measurements were made with pressure ports located on the pressure side of blade 5 and the suction side of blade 4. There are 46 ports on the pressure side and 46 ports on the suction side. However, some of the ports were determined to be damaged and therefore the data from the damaged pressure ports is not presented. The locations of the mid-span pressure ports are detailed in Chapter 2 and are located at a 123mm from the blade tip corresponding to a spanwise location of y/s=0.50. Figure 3.1 presents the pressure coefficient, C_p, at the blade midspan (y/s = 0.54) where s is the blade span and C_p is defined by Equation 3.3.

$$C_p = \frac{P - P_\infty}{P_{0\infty} - P_\infty} \tag{3.3}$$

In this equation, P is the measured mean static pressure, $P_{0\infty}$ and P_{∞} are the mean reference total and static pressure, respectively. This figure shows that the mid-span pressure decreases on both the suction and pressure side of the blade as the tip clearance is increased. The small peak in the pressure near the leading edge on the pressure surface and the large peak on the suction surface can be attributed to the boundary layer trip strips on the blades.

Measurements presented by Ma (2003) were made for all three endwall cases: the stationary wall case, the moving wall case, and the moving wall with vortex generator case at a tip clearance of 3.3%*c*. These results show that there is only a slight difference in the mid-span pressure for the three different cases; however he states that the difference in the pressure may be due to the uncertainty of the measurements. Therefore, it was not deemed necessary for the current measurements to be made for the three cases since there is very little effect of the moving wall at the mid-span.

From the mid-span pressure data, it can be concluded that the pressure at the mid-span of the blade is affected by the height of the tip gap. However, the difference is small and could be due to the uncertainty of the measurements. This result is quantified by Figure 3.2 and Figure 3.3. Figure 3.2 presents the maximum C_p on the pressure side of the blade for tip clearances of 1.65, 3.3, and 5.7%*c*. From this figure it can be seen that the maximum C_p on the pressure side of the blade decreases linearly as the tip clearance is increased. Figure 3.3 presents the minimum C_p on the suction side of the blade for the same tip clearances. Note the minimum C_p values do not include the pressure measured by the very leading edge ports since the pressure values here are expected to be affected by the boundary layer trip strip located near these locations. From Figure 3.3 it can be seen that the minimum C_p on the suction decreases up to a tip clearance of 3.3%*c* and then increases at a tip clearance of 5.7%*c*. It is interesting that the linear effect is seen on the pressure side of the blade and not on the suction side. This suggests that the flow on the suction side of the blade is much more complex and may be a result of the tip leakage vortex rolling up on the suction side of the blade. The flow through the tip clearance region may also be contributing to this non-linear trend on the suction side. The mid-span pressure data at the tip gaps studied is useful for comparison with the loading at the blade tip to investigate the differences between the two measurement locations.

3.5 Mid-span loading versus tip loading

Figure 3.4-Figure 3.6 shows the variation in the mean pressure coefficient at the mid-span for the stationary wall case versus the mean pressure coefficient at the blade tip for the stationary wall case for tip clearances of 1.65%, 3.3%, and 5.7%*c*. From these figures, it can be seen that there is a significant variation between the pressure at the mid-span and the pressure at the blade tip, which is seen to increase as the tip clearance is increased. The tip pressure clearly shows the effects of the increasing tip clearance, while the mid-span pressure shows very little variation with tip clearance. This is an expected result since most of the interactions associated with the tip clearance flow are concentrated in the tip clearance region. Thus as we move farther away from the tip gap, we expect to see less and less of the effects from the tip clearance flow. Again, the abnormalities in the pressure near the leading edge are caused by the boundary layer trip strips attached to the surface of the blades. This allows us to concentrate our investigations in the vicinity of the tip clearance and not have to worry about making measurements at large distances up the blade span.

3.6 Tip loading versus tip gap

3.6.1 Tip loading with stationary wall

To provide a baseline for all of the mean tip pressure measurements made, the blade tip loading was measured for the case with no wall motion. Pressure taps located on the pressure and suction surface of the blade were used. 25 pressure taps were located on the suction surface of blade 4 and 25 taps were on the pressure surface of blade 5 6.4mm above the blade tip corresponding to a spanwise location of y/s=0.025. The location of the pressure taps at the blade tip is detailed in Chapter 2.

It can be expected that the case of the stationary wall will have different pressure distributions along the blade chord than the case with a moving wall and the case with the

unsteady effects of the vortex generators present. The C_p distribution along the blade chord for the stationary wall is presented in Figure 3.7 for all tip gaps from 0.83%*c* to 12.9%*c*. This figure clearly shows that the height of the tip clearance has a significant effect on the pressure distribution at the blade tip. Namely, the point of minimum pressure on the suction side of the blade moves closer to the blade trailing edge as the tip clearance is increased. This result is consistent with the measurements made by Dean (1954). Along with this effect, this figure shows that the minimum pressure on the blade suction side continues to decrease as the tip clearance is increased. This effect is evident up to a tip gap of 7.9%*c*. Along the pressure side of the blade, the pressure decreases with an increase in tip gap, however the pressure is nearly constant along the blade chord.

3.6.2 Tip loading with moving wall

The case for the moving wall with no vortex generators attached was also studied to provide a baseline for the unsteady measurements. Figure 3.8 presents the pressure coefficient distribution along the blade chord for all tip gaps from 0.83%*c* to 12.9%*c* for the moving wall with no unsteady effects from the vortex generators. The addition of wall motion seems to have only a small impact on the pressure variation along the blade chord on the suction side when compared with the case of the stationary wall, however the addition of wall motion has a larger impact on the pressure variations on the pressure side of the blade. This point is demonstrated by Figure 3.9 and Figure 3.10. Figure 3.9 presents the maximum C_p at the blade tip on the pressure side. From this figure it can be seen that the addition of wall motion causes the pressure coefficient to increase for tip clearances between 0.83 and 2.2%*c* and tip clearances between 5.7 and 12.9%*c* by as much as 0.03 at the smaller tip clearances. The trend shown in this figure is not a simple relationship, especially since the addition of wall motion causes C_p to decrease for tip clearances of 3.3 and 4.5%*c*. However, Figure 3.10, which presents the minimum C_p at the blade tip on the suction side, shows that the addition of wall motion causes a smaller change in the C_p (about 0.01) for smaller tip clearances between 0.83 and 4.5%*c*. Here the addition of wall motion causes the minimum C_p to decrease at tip clearances between 0.83 and 3.3%*c* and tip clearances between 7.9 and 12.9%*c*. The suction surface

minimum pressure follows a linear trend for tip clearances between 0.83 and 7.9%*c* while the pressure surface maximum pressure does not seem to follow any trend. The point of minimum pressure on the suction side of the blade, like the stationary wall case, also moves closer to the blade trailing edge as the tip clearance is increased. The minimum pressure on the suction side also continues to decrease as the tip clearance is increased. It can be expected that the fundamentals of the flow should be the same whether a moving wall or a stationary wall is implemented since the wall motion should only affect the magnitude of the pressure since it causes a skewed flow through the tip clearance.

3.6.3 Unsteady tip loading

One might expect the effects of the unsteady inflow created by the vortex generators attached to the moving endwall to be noticeable in the pressure distribution along the blade tip. The results of the measurements taken with the unsteadiness are presented in Figure 3.11-Figure 3.14. Each of these figures presents the pressure distribution along the blade chord for all three cases (stationary wall, moving wall with no unsteadiness, and moving wall with unsteadiness) at each tip gap measured. From these figures, it can be seen that there is a slight difference in the pressure between all three cases. However, the cases of moving wall with no generators and moving wall with generators are very similar and differ in magnitude only slightly. Therefore, only tip gaps from 0.83%*c* to 3.3%*c* were measured with the effects of the generators. Because of the similarity between the two cases for the four tip clearances measured, we can predict that the similarity will exist for all tip gaps and thus the measurements made with wall motion with no unsteadiness are valid for the higher tip gaps (4.5%*c* to 12.9%*c*).

Figure 3.11-Figure 3.14 clearly shows that the trends in the pressure along the blade chord as a function of tip clearance are dependent almost solely on the height of the tip clearance. This suggests that there must be a simple relationship between the pressure distribution at the blade tip and the tip clearance. This relationship can be explained by Figure 3.15-Figure 3.18. Figure 3.15 presents the maximum pressure coefficient on the blade pressure side as a function of tip clearance. Figure 3.16 presents the chordwise location of maximum C_p on the pressure side of the blade as a function of tip clearance.

The relationship between maximum C_p and tip clearance seems to be a parabolic relationship up to a tip clearance of 5.7%c. Above this tip clearance there does not seem to be any relationship between the maximum C_p and the tip clearance. There does not seem to be any simple relationship between the location of maximum C_p and the tip clearance. Since the pressure side of the blade is not subject to the rolling up of the tip leakage vortex, it is intuitive that the relationship between the maximum C_p and the tip clearance would be much simpler than a parabolic relationship. However, the pressure side of the blade may be affected by the tip leakage vortex and the tip clearance flow from the blade next to it and therefore the relationship seen on the pressure side of the blade is more complex that that seen on the suction side.

Figure 3.17 presents the minimum pressure coefficient on the blade suction side as a function of tip clearance. The straight line on the plot is a linear fit to the data. Figure 3.18 presents the chordwise location of minimum C_p as a function of tip clearance. It can be clearly seen that there is a linear relationship between the minimum suction surface pressure and the tip clearance up to a tip gap of 7.9%c. This linear trend is verified by the location of minimum C_p. The location of the minimum C_p on the suction side of the blade follows a nearly linear trend up to a tip clearance between 5.7 and 7.9%c. The location of the minimum C_p continues to move from leading edge to trailing edge as the tip clearance is increased. This is a startling result. Because of all of the interactions that occur within the blade tip clearance, we should expect that the pressure distribution along the blade chord would be a more complex phenomenon. The tip clearance flow forms in the presence of a potential core, secondary flow, an end wall turbulent boundary layer, and a blade boundary layer. Therefore we would expect to see very complex interactions at the blade tip at small tip clearances and much simpler interactions at higher tip clearances. The blade pressure distribution at these higher tip clearances obviously is not affected by the boundary layer formed by the endwall. This linear increase in the minimum suction surface C_p as the tip clearance is increased suggests that there must be a simpler model of a marine propulsor.

3.7 Blade Loading

To provide further insight into the forces on the blade at the tip, the pressure distributions presented above can be integrated to give the components of the force acting at the blade tip. In order to obtain the force coefficients acting on the blade, the detailed geometry of the blade given in Muthanna (2002) was interpolated using the tip pressure port locations detailed in Chapter 2 to get the corresponding axial, tangential, edgelength, and normal to chord locations of the pressure ports. The force coefficients, C_x and C_z, can then be determined in the chordwise (x) and normal to chord (z) directions by integrating the pressure distributions using the trapezoidal rule and are given by Equations 3.4 and 3.5.

$$C_x = \frac{1}{2}\sum_{i=1}^{n-1}(C_{p_{i+1}} + C_{p_i})(x_{i+1} - x_i) \tag{3.4}$$

$$C_z = \frac{1}{2}\sum_{i=1}^{n-1}(C_{p_{i+1}} + C_{p_i})(z_{i+1} - z_i) \tag{3.5}$$

In these equations, n is the number of pressure ports, C_p is the pressure difference across the blade tip measured using the pressure ports, x is the chordwise locations along the blade normalized on the blade chord, and z is the normal to chord location normalized on the blade chord. The results of this analysis are presented in Figure 3.19 and Figure 3.20. These figures present the force coefficients for the case of no moving wall, moving wall with no generators, and moving wall with generators for tip clearances from 0.825% to 12.9%c. From these figures it can be seen that the chordwise force coefficient varies nearly linearly up to a tip clearance of 7.9%c especially for the case of no moving wall. The cases of moving wall with no generators and moving wall with generators seem to follow this linear trend up to a tip clearance of 3.3%c at which point the chordwise force coefficient versus tip clearance relationship does not appear to remain linear. This is a strange relationship since this linear trend is the same that was seen in the chordwise pressure distribution as a function of tip clearance. Figure 3.20 presents the normal to chord force coefficient as a function of tip clearance for the three cases. From this figure, it can be seen that there is almost no change in the normal to chord force coefficient as the tip clearance is increased. This suggests that the force normal to the blade does not

depend upon the tip clearance which seems to be an interesting result since one would expect the force normal to the blade chord to vary as the tip clearance is increased. However, the pressure distributions suggest that C_z should remain constant as the tip clearance is increased while C_x should vary. This is because the pressure distribution for each tip clearance, although different in magnitudes and shapes, has approximately the same area. This result could be investigated further to better understand the blade tip loading and to confirm that this is indeed correct.

3.8 Summary

The mean blade loading at the blade mid-span and at the blade tip were investigated for tip clearances from 0.83%*c* to 12.9%*c* for three cases: a stationary wall case, a moving wall case, and a moving wall case with unsteady inflow created by vortex generator pairs. These measurements were made using pressure ports located on the suction and pressure surfaces of blades 4 and 5, respectively. From these measurements, we can make several conclusions:

1. From the mid-span pressure data, it can be concluded that the pressure at the mid-span of the blade is affected by the height of the tip gap. This is an unexpected result since the effects of the moving wall are not expected to travel up the blade span over a very large distance.
2. The maximum pressure side C_p at the midspan decreases linearly as the tip clearance is increased. There is not enough information to make a conclusion about the trend in the minimum suction side $C_{p.}$ This suggests that the flow on the suction side of the blade is much more complex and may be a result of the tip leakage vortex rolling up on the suction side of the blade. The flow through the tip clearance region may also be contributing to this non-linear trend on the suction side.
3. For the stationary wall case, the mid-span blade loading and the tip loading are significantly different, especially at higher tip gaps, showing that the

effects of the tip clearance primarily affects the region of the blade closest to the tip.

4. There is very little difference in the blade tip loading between the three cases studied showing that the effects of the moving wall and unsteadiness play a small role in the mean tip loading of the blade.
5. Consistent with the measurements made by Dean (1954), the point of minimum pressure on the suction side of the blade moves closer to the blade trailing edge as the tip clearance is increased.
6. The minimum pressure on the blade suction side continues to decrease as the tip clearance is increased. This effect is evident up to a tip gap of 7.9%c.
7. There exists a very simple relationship between the suction surface minimum pressure at the blade tip. The decrease in the suction side minimum pressure is found to be a linear function of the tip clearance for tip clearances up to 7.9%c.
8. The force coefficient along the blade chord varies linearly up to a tip clearance of 7.9%c while the force coefficient perpendicular to the blade chord remains nearly constant as the tip clearance is increased.

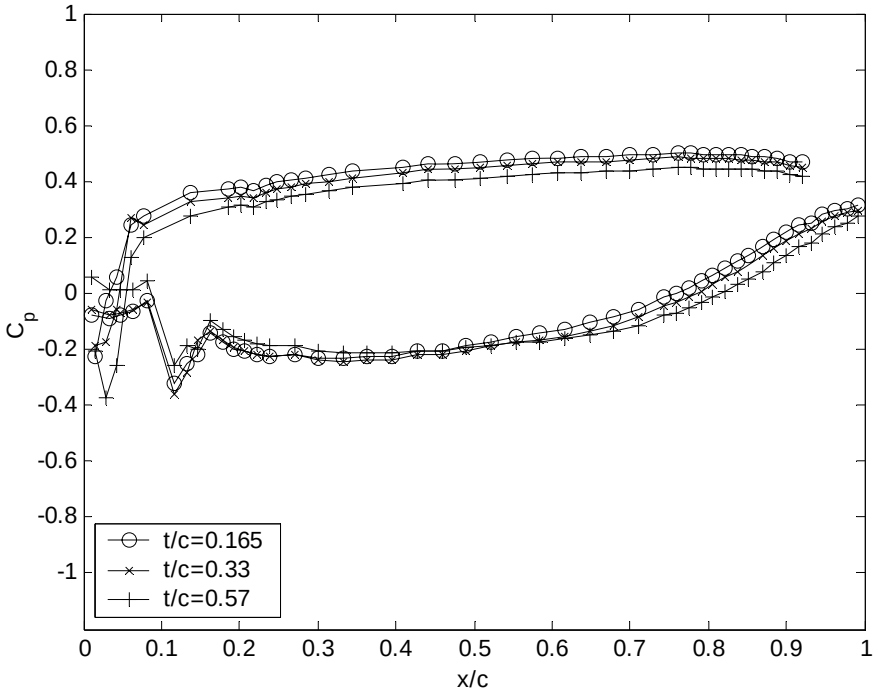

Figure 3.1 Chordwise mean pressure coefficient at the mid-span for the stationary wall case for tip gaps of 1.65%*c*, 3.3%*c*, and 5.7%*c*.

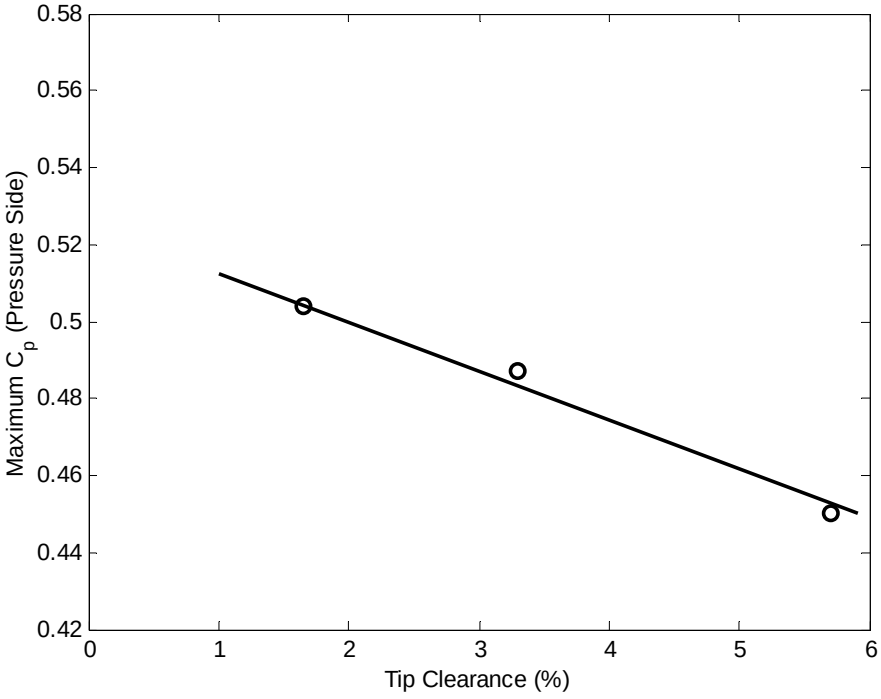

Figure 3.2 Maximum C_p on the pressure side for tip clearances of 1.65, 3.3, and 5.7%*c*.

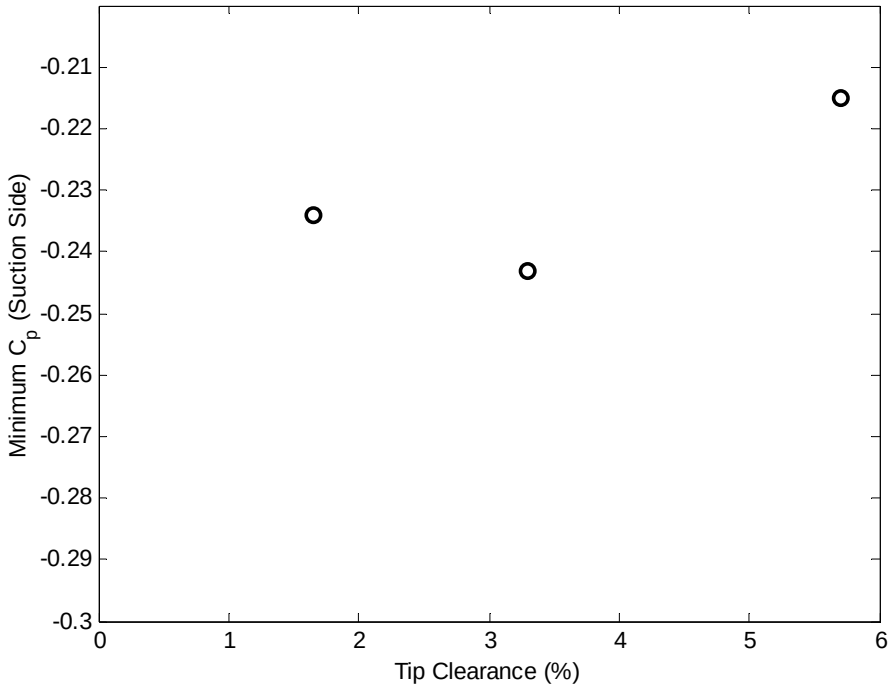

Figure 3.3 Minimum C_p on the suction side for tip clearances of 1.65, 3.3, and 5.7%*c*.

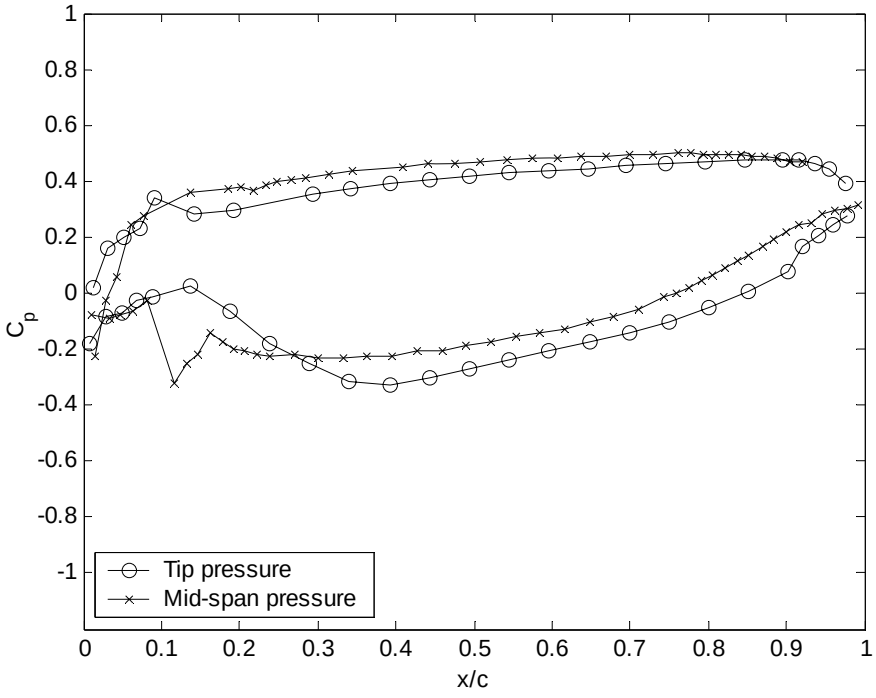

Figure 3.4 Chordwise mean pressure coefficient at the mid-span and the tip for the stationary wall case at a tip gap of 1.65%*c*.

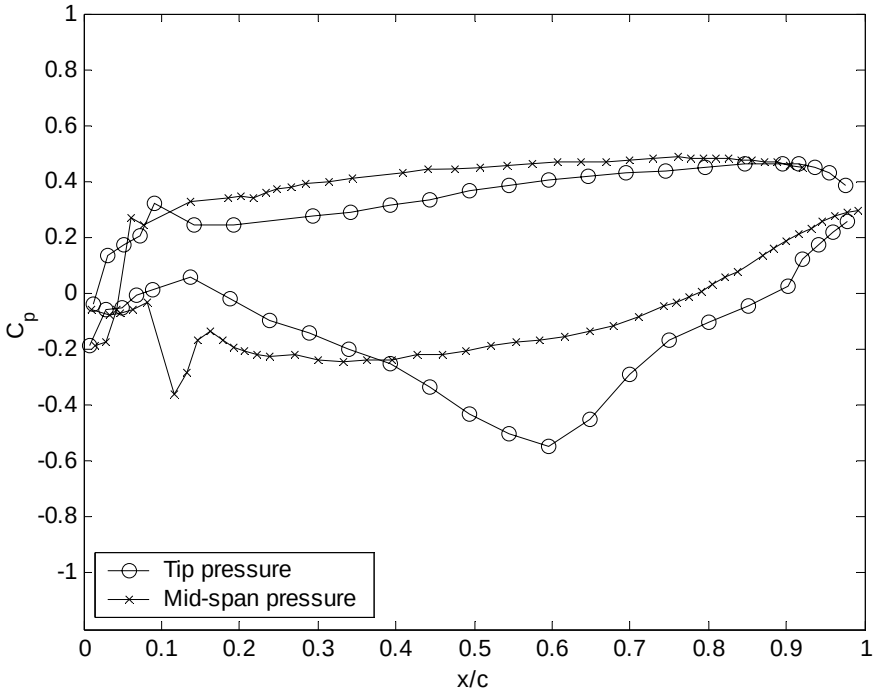

Figure 3.5 Chordwise mean pressure coefficient at the mid-span and the tip for the stationary wall case at a tip gap of 3.3%*c*.

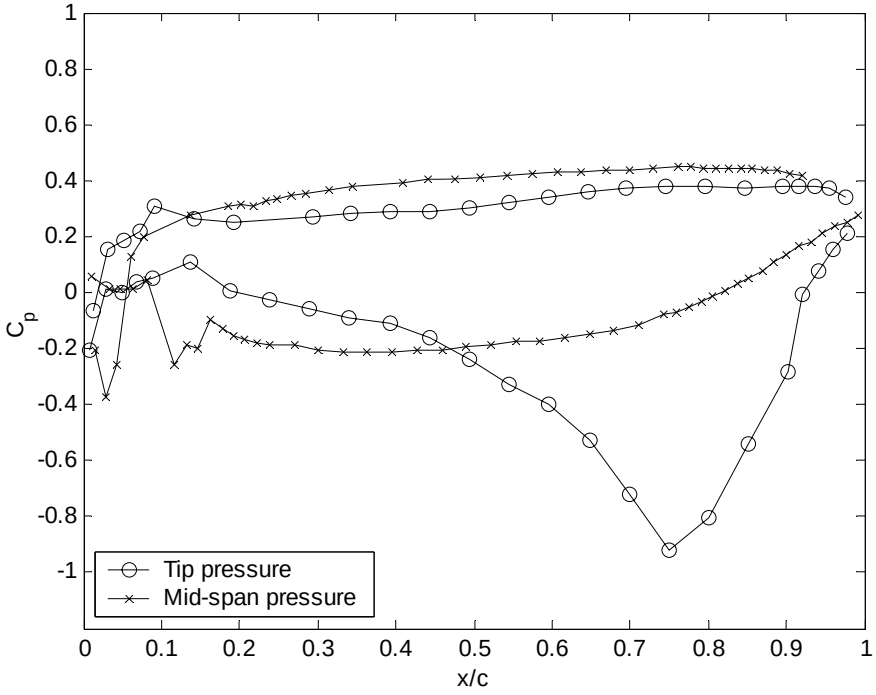

Figure 3.6 Chordwise mean pressure coefficient at the mid-span and the tip for the stationary wall case at a tip gap of 5.7%*c*.

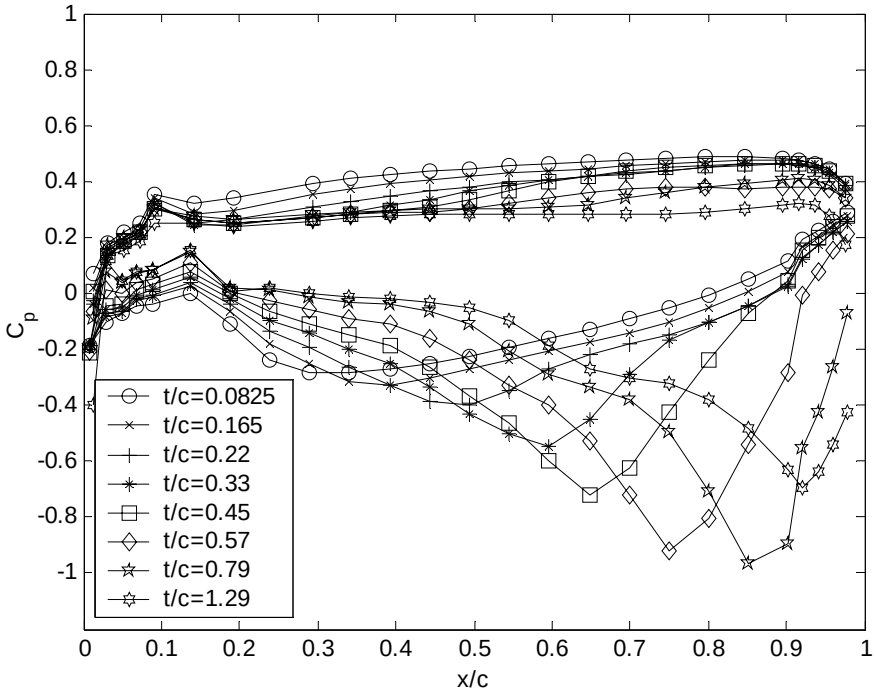

Figure 3.7 Chordwise mean pressure coefficient at the blade tip for the stationary wall case for tip gaps from 0.83%*c* to 12.9%*c*.

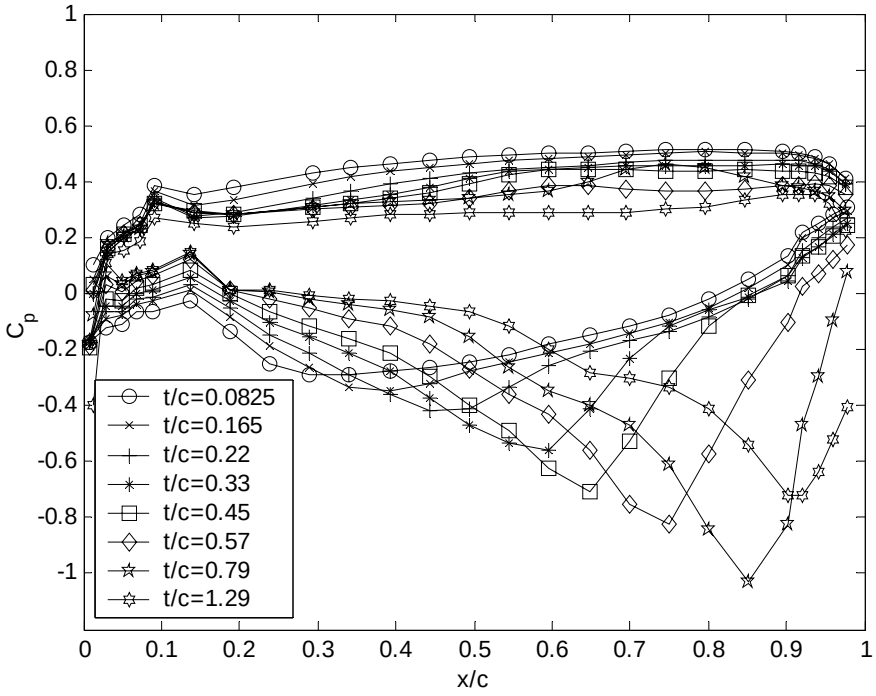

Figure 3.8 Chordwise mean pressure coefficient at the blade tip for the moving wall with no vortex generators for tip gaps from 0.83%*c* to 12.9%*c*.

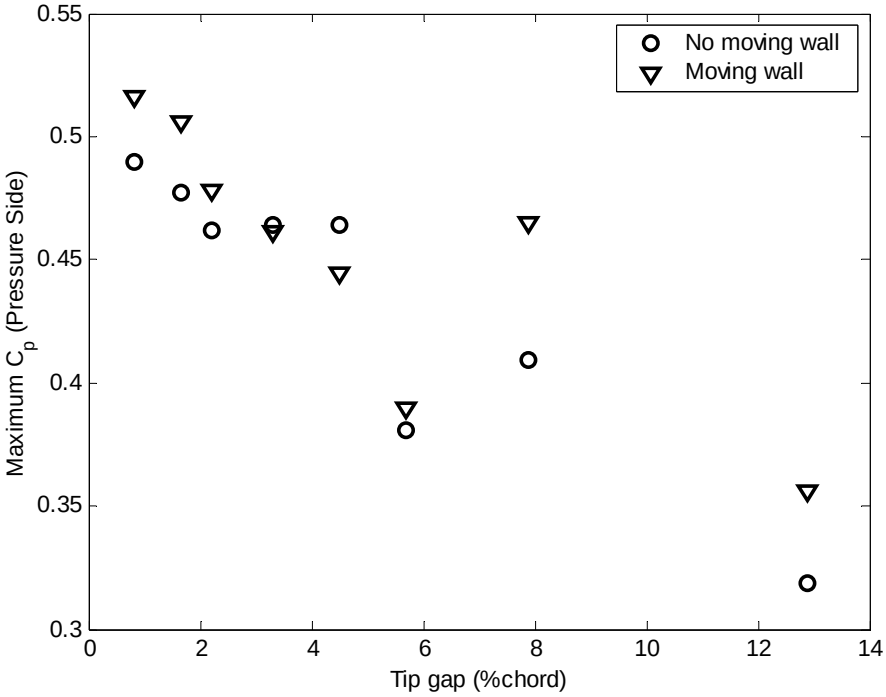

Figure 3.9 Maximum C_p at the blade tip on the pressure side for no moving wall and moving wall cases.

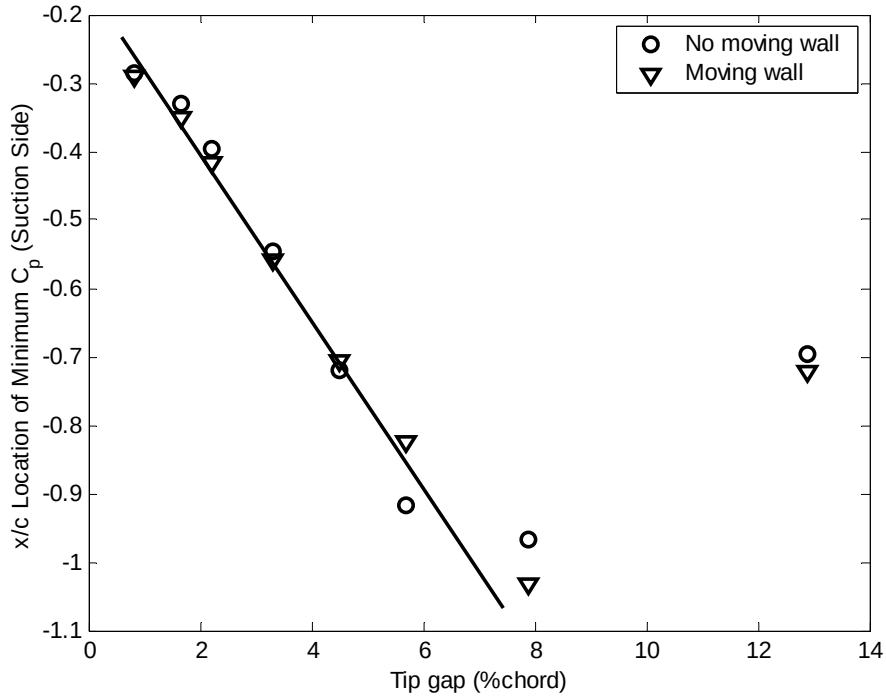

Figure 3.10 Minimum C_p at the blade tip on the suction side for no moving wall and moving wall cases.

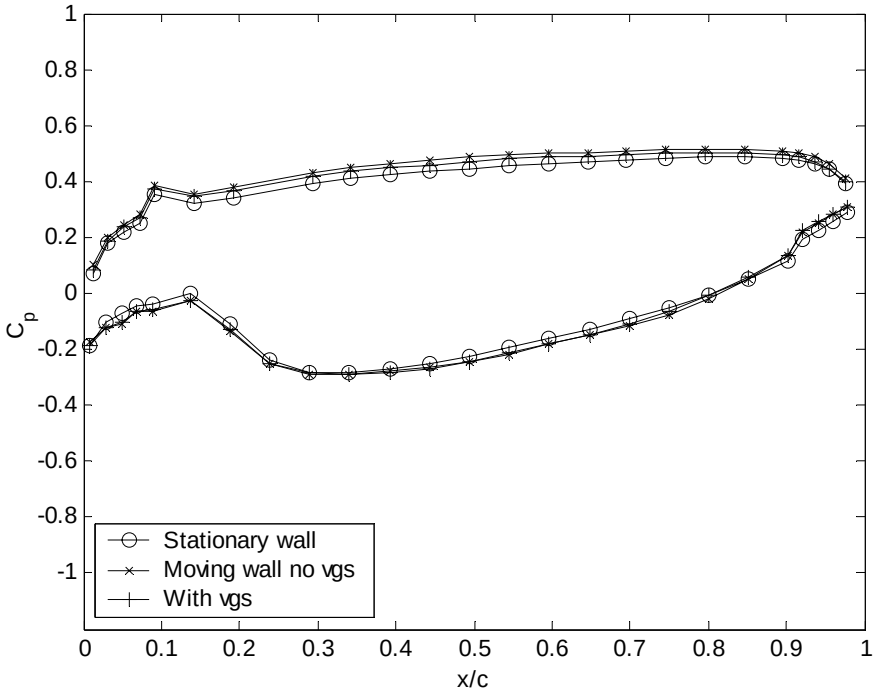

Figure 3.11 Chordwise mean pressure coefficient at the blade tip for all three cases for 0.83%*c* tip gap.

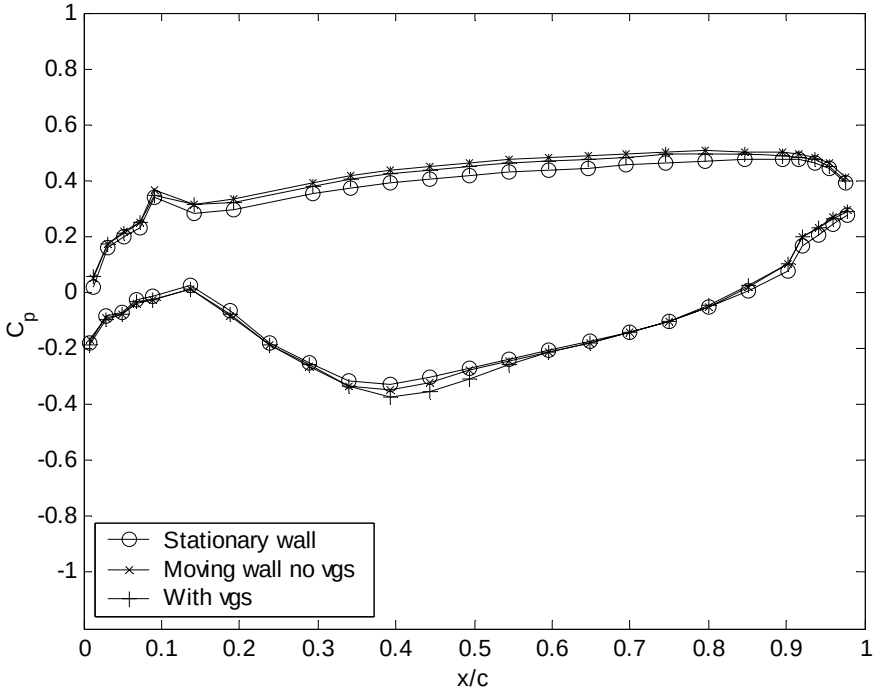

Figure 3.12 Chordwise mean pressure coefficient at the blade tip for all three cases for 1.65%*c* tip gap.

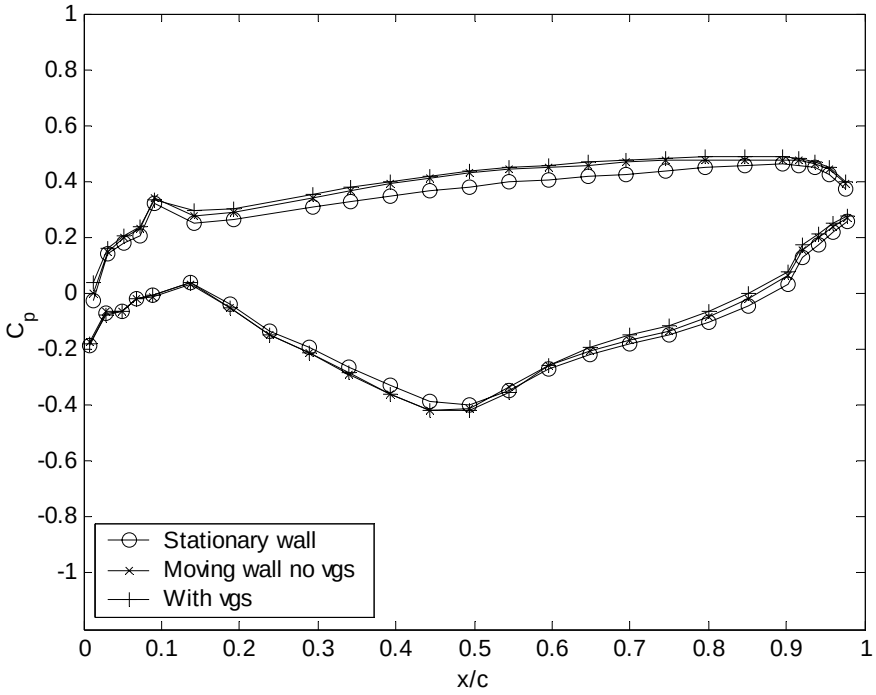

Figure 3.13 Chordwise mean pressure coefficient at the blade tip for all three cases for 2.2%*c* tip gap.

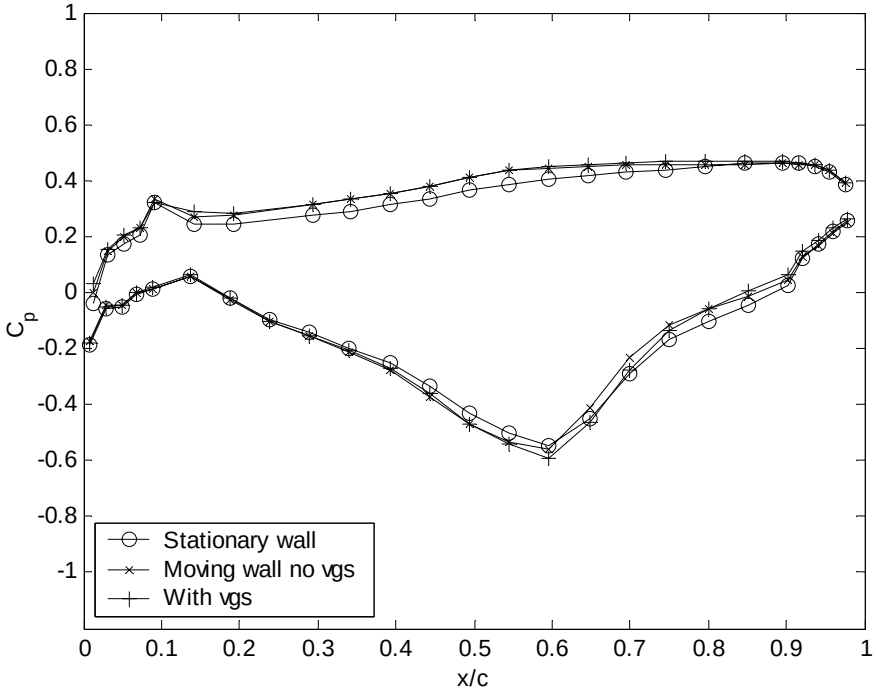

Figure 3.14 Chordwise mean pressure coefficient at the blade tip for all three cases for 3.3%*c* tip gap.

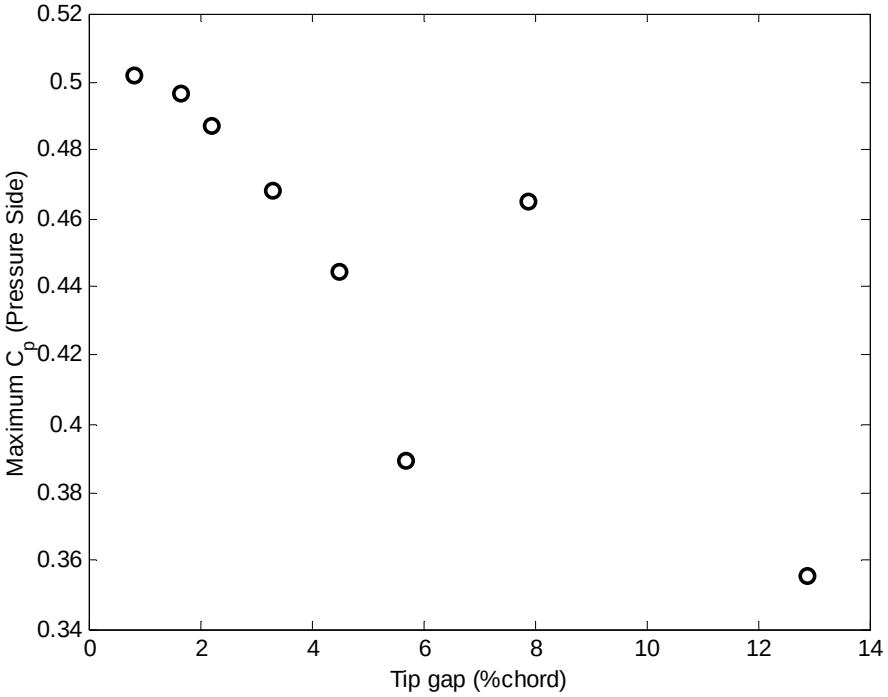

Figure 3.15 Maximum pressure surface C_p at all tip gaps.

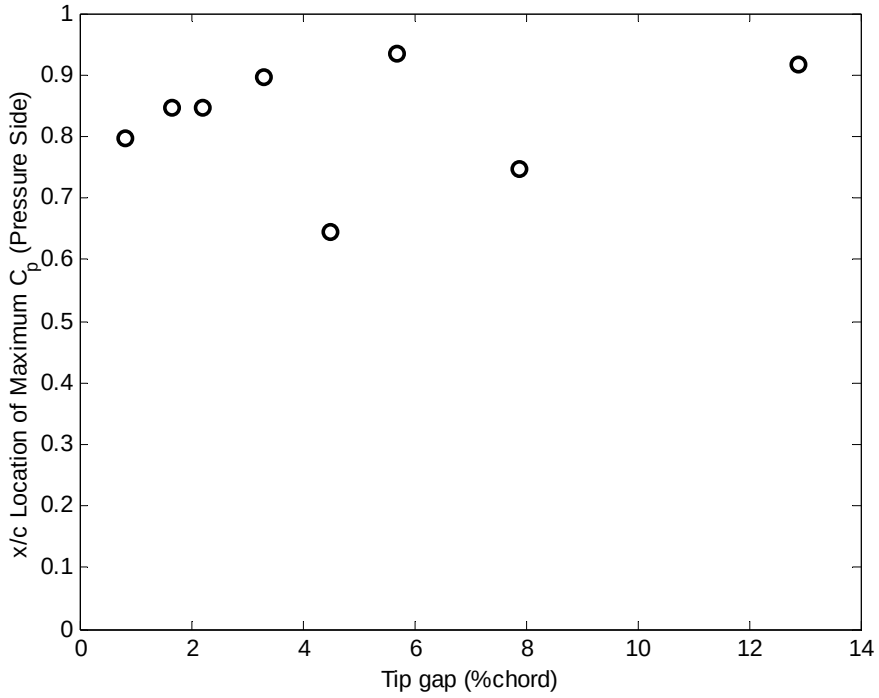

Figure 3.16 Chordwise location of maximum C_p on the pressure side of the blade for all tip clearances.

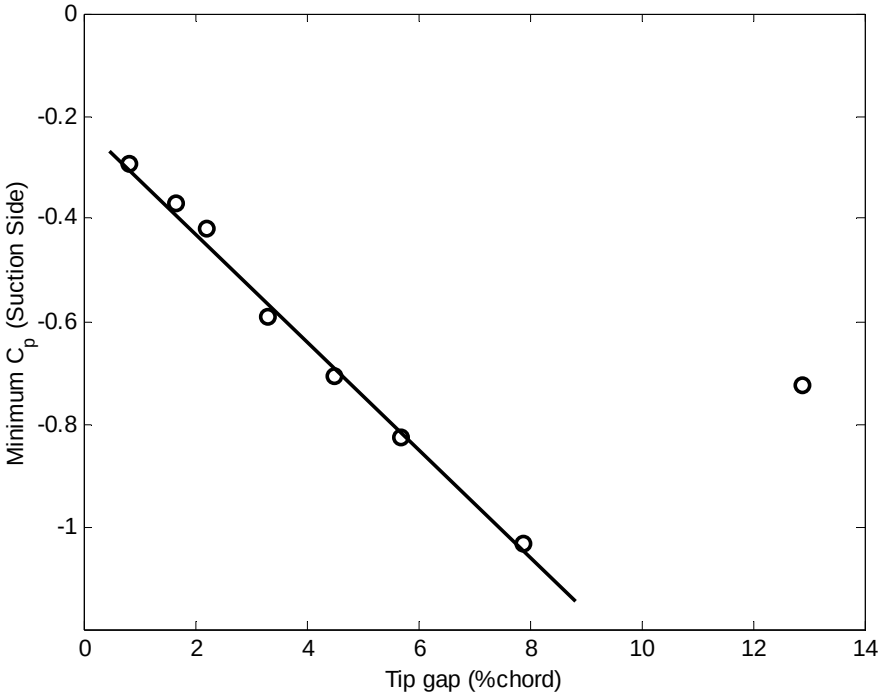

Figure 3.17 Minimum suction surface C_p at all tip gaps.

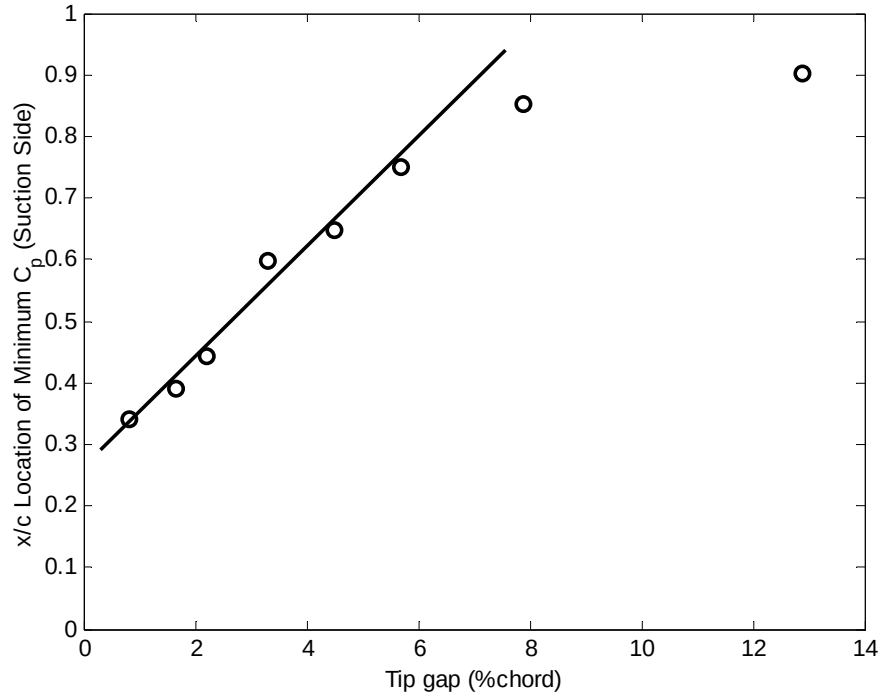

Figure 3.18 Chordwise location of minimum C_p on the suction side of the blade for all tip clearances.

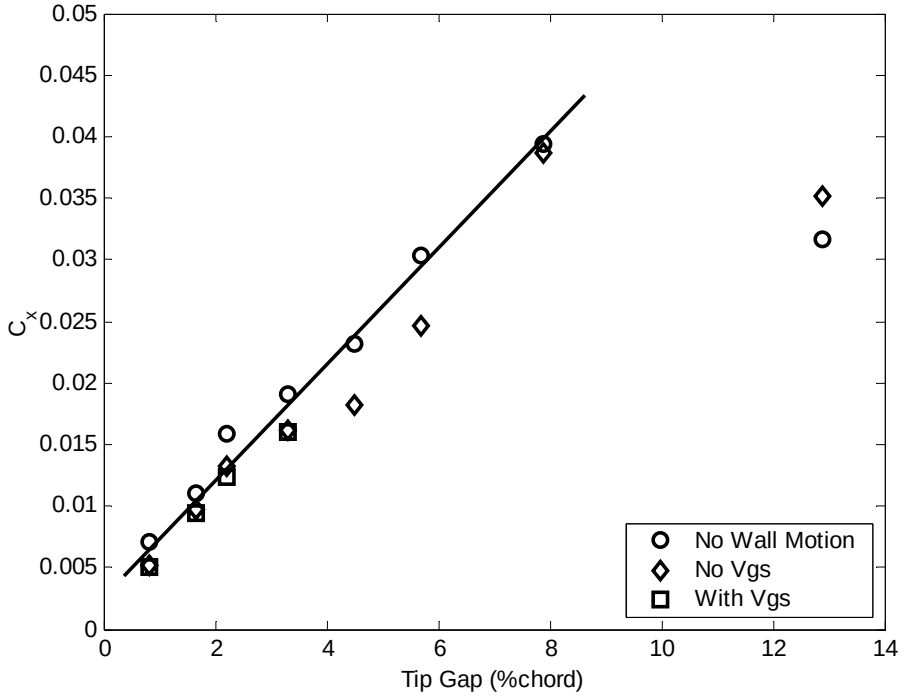

Figure 3.19 Chordwise force coefficient, C_x, versus tip clearance for three cases: no wall motion, wall motion with no generators, and wall motion with generators.

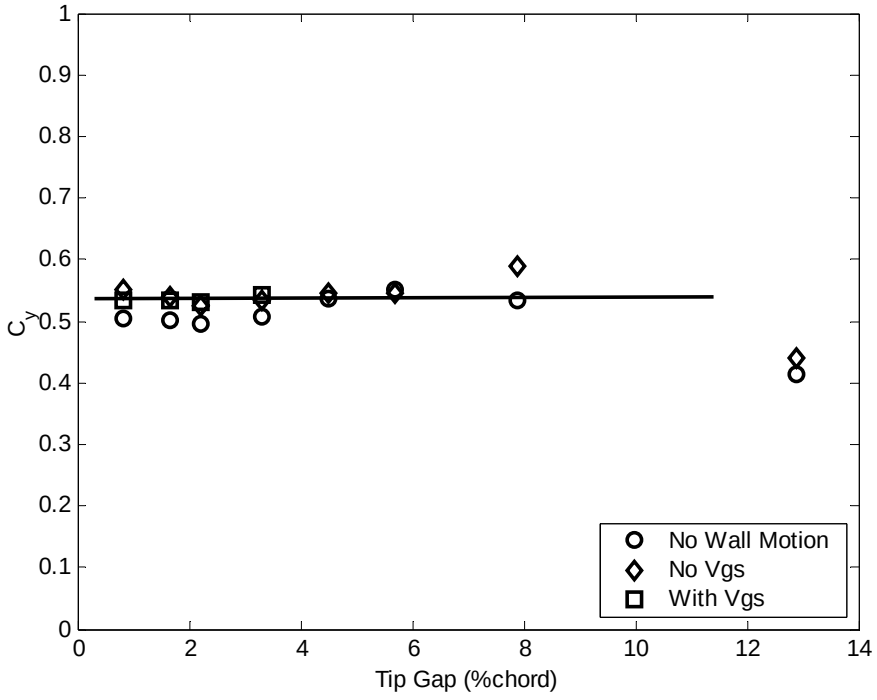

Figure 3.20 Normal to chord force coefficient, C_z, versus tip clearance for three cases: now wall motion, wall motion with no generators, and wall motion with generators.

4. Analysis of Unsteady Pressure

4.1 Introduction

The flow through the tip clearance of a compressor cascade is important for understanding some of the sources of noise in a turbomachine. The flow can also be applied to marine propulsors to understand how the flow through the tip clearance leads to cavitation. In the previous section, the mean pressure at the blade tip was investigated using pressure taps placed along the blade chord from leading edge to trailing edge. In addition to the mean pressure at the blade tip under the influence of an unsteady flow, it is important to understand how the pressure fluctuates as a function of time. A better understanding of the effects of the unsteady inflow on the blade surface pressure fluctuations across the tip gap can help to solve some of the problems associated with tip clearance flow such as the noise created by the pressure fluctuations as well as the noise and damage to the blades created by cavitation.

To study the unsteady pressure fluctuations across the blade tip, two cascade blades were instrumented with Sennheiser microphones. The pressure side of blade 5 and the suction side of blade 4 were instrumented with 23 of these microphones with 11 microphones on the pressure side of blade 5 and 12 microphones on the suction side of blade 4. The microphones were placed beneath the blade surface in rows along the blade

chord and the blade span. On the pressure side of blade 5, 6 microphones were placed along the blade chord, 0.25" from the blade tip, and 5 microphones were placed along the blade span, 2.3" from the blade leading edge, at the locations detailed in Chapter 2. On the suction side of blade 4, 7 microphones were placed along the blade chord and 5 microphones were placed along the blade span. These microphones allow instantaneous surface pressure measurements and these measurements were phase locked with the passing of the vortex generator pairs in order to study the effects of unsteady inflow on the blade tip pressure. The measurements were made for 3 cases: non-moving wall, moving wall with no vortex generators, and moving wall with vortex generators to compare the effects of relative motion between the casing and the blade tips and to compare the effects of the unsteady inflow created by stator vanes.

The unsteady pressure measurements presented in this chapter were made for tip clearances from 0.83 to 12.9%*c* in order to understand the effects of tip clearance on the unsteady blade surface pressure. The unsteady pressure measurements were also made for several different configurations of vortex generators. These configurations are detailed in Chapter 2. The three configurations include: the baseline generator configuration, the widely spaced vortex generators, and the half-height vortex generators. These three configurations were studied in order to understand how the surface pressure distribution varies as a function of the inflow disturbance to the cascade. The baseline generator configuration is the same measurement performed by Mish (2003). The measurements made by Mish (2003) showed inconsistencies in the spectral data between the case of moving wall with no vortex generators and moving wall with vortex generators. Namely, the similarity that is to be expected between these two cases was not found and since Mish (2003) was unable to determine the source of the inconsistency, it was decided that it would be worthwhile to retake the data for the baseline generator configuration. This chapter documents the results of these measurements.

4.2 Unsteady pressure uncertainty analysis

The equation $e = Mi + c$ is used to represent the A/D converter, where M is the slope, c is the offset, i is the input, and e is the output. There are three kinds of errors that may result from the Agilent 1432 A/D converter: A/D conversion random error $\delta_c(e)$, A/D offset error $\delta(c)$, and A/D slope error $\delta(M)$. Only $\delta_c(e)$ is random, the other two are bias. The two bias errors are given by

$$\delta(e)|_{rand} = \delta_c(e) \tag{4.1}$$

$$\delta(e)|_{Bias} = 0 \tag{4.2}$$

For the Agilent 1432, the rms random error $\delta_c(e)$ was taken to be 45μV according to its specifications.

The measured unsteady pressure p is determined from e_0 using the relationship $p = \frac{e_0}{S}$ where e_0 is the microphone voltage signal and S is the microphone sensitivity. The uncertainty in S is taken to be 2.5mV/Pa. The microphone sensitivity is taken to be 0.132 V/Pa when connected to the amplifier. The uncertainty in the measured unsteady pressure can be calculated using

$$\frac{\delta^2(p)}{p^2} = \frac{\delta^2(e_0)}{e_0^2} + \frac{\delta^2(S_0)}{S_0^2} \tag{4.3}$$

Since $C_p = \frac{p}{\frac{1}{2}\rho_\infty U_\infty^2} = \frac{p}{p_{ref}}$

So

$$\frac{\delta(C_p)^2}{C_p^2} = \left(\frac{\delta(p)}{p}\right)^2 + \left(\frac{\delta(p_{ref})}{p_{ref}}\right)^2 \tag{4.4}$$

where the uncertainty in the reference pressure, $\delta(p_{ref})$, is 0.0005 inches of water based on half of the digital resolution of the manometer. Therefore, the uncertainty in the unsteady pressure measurements is 1.9% of C_p calculated at 20:1 odds.

4.3 Basic flow definition

4.3.1 Contribution of noise sources

Unsteady pressure measurements were made with the 23 microphone array with no moving wall as well as for the moving wall without vortex generators attached to establish a baseline level for sources of tunnel contamination. With no vortex generators attached to the moving wall, the primary sources of pressure fluctuations are expected to be the ambient acoustic field and the aerodynamic pressure fluctuations seen in the turbulent boundary layer. With the effect of the vortex generators, the pressure fluctuations should include the ambient acoustic field and the aerodynamic pressure fluctuations as well as aerodynamic and acoustic pressure fluctuations created by the passing of the vortex generator pairs. The spectral data from the two cases is presented for a tip clearance of 3.3%*c* to examine the sources of tunnel contamination.

4.3.2 No generator and generator comparisons

Figure 4.1 presents the spectral data on the pressure side of blade 5 along the blade chord for the moving wall with no vortex generators and the moving wall with vortex generators. This figure presents the pressure auto-spectrum as a function of frequency normalized on the square of the dynamic pressure. G_{pp}, the pressure-pressure auto-spectrum can be calculated by taking the fast Fourier transform of the pressure time series using Equation 4.5.

$$G_{pp} = \lim_{\tau \to \infty} \left(\frac{\pi}{T} \right) E\left[p^*(\omega) p(\omega) \right] \tag{4.5}$$

In this equation, the τ is the time step between samples, p represents the pressure at a particular instant of time, and f is the frequency. The dynamic pressure, q can be calculated using Equation 4.6

$$q = \frac{1}{2} \rho U_{ref}^2 \tag{4.6}$$

where ρ is the density of air calculated from the ideal gas equation given by Equation 4.7

$$\rho = \frac{p}{RT_{ref}} \tag{4.7}$$

and U_{ref} is the inlet free-stream velocity. In Equation 4.7, p is the atmospheric pressure, R is the gas constant for air given by R = 287 J/kg/K and T_{ref} is the free-stream temperature. It can be expected that the spectral data for the case of the moving wall with vortex generators should be slightly different than the case of the moving wall with no vortex generators. This is because the generators should cause pressure fluctuations that would not be seen if the generators are not present. The difference between the two cases should be due to a combination of the acoustics of the tunnel coupled with fan tones from the blower, which would likely affect the broadband part of the spectrum, and the turbulent pressure fluctuations experienced by the microphones, which would certainly affect the broadband part of the spectrum. Looking at Figure 4.1, it appears that the turbulent pressure fluctuations may be dominant since the acoustic field should not vary much over a distance that is small compared with 1 wavelength. From this figure, significant chordwise variation in the pressure auto-spectrum can be seen which suggests that the turbulent pressure fluctuations are dominant. There are spikes in the pressure spectra for the case with the generators that cannot be seen in the case with no generators. These spikes occur because of the phase-locked response of the blade in the presence of the vortex generators. While all of these phase-locked pressure fluctuations will end up in these spikes, any non-phase locked effects such as greater generation of turbulent pressure fluctuations or change in average flow structure will not. These spikes occur at the vortex generator passing frequency of approximately 100 Hz or harmonics of this frequency. Figure 4.2 presents the spectral data on the pressure side of blade 5 along the blade span for the two different cases. Similarly, this spectral data should also only show slight differences in the pressure spectra for the two different cases. From Figure 4.2, it can be seen that the only differences occur at harmonics of the passing frequency of the vortex generators.

Figure 4.3 and Figure 4.4 present the spectral data on the suction side of blade 4 along the blade chord and span, respectively, for the moving wall with no vortex generators and the moving wall with vortex generators. The different cases for both the

chordwise measurements and the spanwise measurements show that the only difference occurs at the passing frequency of the vortex generators or harmonics of this frequency. This indicates that the unsteady blade tip response produced by the disturbance is effectively superimposed upon the existing turbulent flow around the blade tip. This can be better shown by examining Figure 4.5, which presents a comparison of the spectra for the case of moving wall with no generators and moving wall with generators for a tip clearance of 3.3%*c* for two chordwise microphone locations. This figure shows that there is no difference between the two cases except for the peaks in the spectra from the moving wall with generators. This minor difference will be discussed in more detail in subsequent sections by calculating the rms pressure from just the broadband part of the spectrum (*i.e.* with the peaks from at the generator passing frequency removed). The consistency found here clears up the discrepancy found by Mish (2003) who observed significant differences between the moving wall without vortex generators and the moving wall with vortex generator cases for the same configuration that could not be explained at that time.

4.4 Cascade in periodic disturbance of baseline case

4.4.1 Unsteady pressure versus tip gap

4.4.1.1 Chordwise surface pressure distribution

The phase-locked surface pressure distribution was investigated 0.25" from the blade tip in terms of the phase averaged mean pressure coefficient, $\langle C_p \rangle$ which is defined in Equation 4.8

$$\langle C_p(x,y,t) \rangle = \frac{\langle p'(x,y,t) \rangle}{\frac{1}{2}\rho U_\infty^2} \tag{4.8}$$

where p' is the unsteady pressure, ρ is the density, and U_∞ is the mean free-stream velocity. The phase-averaging of the data eliminates any contamination not keyed to the passage of the vortex generators, such as that due to fan noise. Figure 4.6-Figure 4.13

presents movies of $\langle C_p \rangle$ on the pressure and suction side of the blade as a function of chordwise location for all eight tip gaps measured. The movies are embedded in the plots and can be played by double clicking the plots. These movies provide a simple yet important means of viewing the surface pressure fluctuations as a function of phase number. There is a counter at the top of each plot that indicates the phase number.

For the tip clearance of 0.825%*c*, there is little fluctuation of $\langle C_p \rangle$ over all phase numbers. There is a slight fluctuation near the blade leading edge for phase numbers greater than 200, which is the period of time when the vortex generator pair has already moved past the leading edge of the blade. As the tip clearance is increased, the fluctuations in $\langle C_p \rangle$ become greater in magnitude up to a tip clearance of 7.9%*c*, at which point the $\langle C_p \rangle$ fluctuations begin to decrease in magnitude. As the tip clearance is increased from the smallest tip gap, the $\langle C_p \rangle$ fluctuations become more evident along the entire length of the blade chord. At tip clearances above 2.2%*c*, significant fluctuations can be seen over the length of the chord, while the fluctuations are primarily confined to the first 50% of the chord for the smaller tip clearances. This indicates that the tip clearance plays a important role in the interaction between the blade tip and the inflow vortices from the passing of the vortex generators. These results can be quantified by investigating the minimum suction side $\langle C_p \rangle$ as a function of tip gap as well as the root mean square $\langle C_p \rangle$ as a function of tip gap. The root mean square $\langle C_p \rangle$ is defined by Equation 4.9

$$\langle C_p \rangle_{rms} = \sqrt{\frac{1}{nm}\sum_{i=1}^{m}\sum_{j=1}^{n}\left[\langle C_p \rangle_{ij} - \overline{\langle C_p \rangle_{ij}}\right]^2} \tag{4.9}$$

where n is the number of phases in the measurement and m is the number of microphones. The mean pressure coefficient $\overline{\langle C_p \rangle}$ is zero for the microphones used in this study since the microphones can only measure fluctuations from the mean. The minimum suction side $\langle C_p \rangle$ and the r.m.s. $\langle C_p \rangle$ as a function of tip clearance are

presented in Table 4.1. The results from Table 4.1 are presented in Figure 4.14. From these results, it can be seen that the minimum pressure coefficient on the suction side

Table 4.1 Minimum $\langle C_p \rangle$ and r.m.s $\langle C_p \rangle$ averaged over all phases and all microphone locations on the suction side as a function of tip clearance.

Tip clearance	*Suction side minimum* $\langle C_p \rangle$	*Suction side r.m.s* $\langle C_p \rangle$
0.83%	0.00336	0.000544
1.65%	0.00569	0.001168
2.2%	0.00752	0.001528
3.3%	0.01262	0.002155
4.5%	0.01291	0.002371
5.7%	0.02023	0.003185
7.9%	0.01745	0.002294
12.9%	0.00263	0.000434

increases as the tip clearance increases, up to a tip gap of 5.7%*c*. The trend shown by this figure shows that the minimum pressure increases approximately linearly for tip clearances between 0.83 and 5.7%*c*. This supports the conclusions presented in Chapter 3 from the mean pressure measurements that the effects of tip clearance have a linear effect on the blade tip pressure. Figure 4.15 presents the r.m.s pressure coefficient averaged over all phases and all microphone locations on the suction side as a function of tip clearance. This figure shows the same trend as the minimum pressure coefficient up to a tip clearance of 5.7%*c*. To determine how large the pressure fluctuations are in relationship to the mean pressure across the tip clearance measured with the static pressure taps, it is useful to present the results of these two measurements simultaneously. The results are presented in Table 4.2. The suction side $\langle C_p \rangle$ ' is the fluctuation in the $\langle C_p \rangle$ as measured by the microphones and the suction side mean C_p is the mean pressure measured using the static pressure taps. From this table, it can be seen that the minimum C_p measured using the static pressure taps is approximately 2 orders of magnitude larger than the $\langle C_p \rangle$ fluctuations measured using the microphones. This says that there is a large pressure difference across the blade tip with slight fluctuations from the mean caused by the passing of the vortex generators. However, it is these slight

pressure fluctuations across the tip gap that contributes to the unwanted effects of the tip clearance flow such as cavitation and noise.

Table 4.2 Minimum suction side C_p fluctuation and mean as a function of tip clearance.

Tip clearance	*Suction side minimum* $\langle C_p \rangle$ *'*	*Suction side minimum* C_p
0.83%	0.00336	0.29288
1.65%	0.00569	0.37141
2.2%	0.00752	0.42000
3.3%	0.01262	0.59046
4.5%	0.01291	0.70637
5.7%	0.02023	0.82593
7.9%	0.01745	1.03240
12.9%	0.00263	0.72335

Contours of the phase averaged pressure coefficient for both the pressure and suction side of the blade are presented in Figure 4.16. In this figure, the phase number is presented as normalized time $\frac{tU_\infty}{c}$ where t is the time, U_∞ is the free-stream velocity, and c is the blade chord length is plotted on the abscissa versus the microphone locations $\frac{x}{c}$ plotted on the ordinate. Here the normalized time $\frac{tU_\infty}{c}$ can be related to the phase number by Equation 4.10

$$x = U_c t \Rightarrow t = \frac{x}{U_c} \tag{4.10}$$

and Equation 4.11.

$$\frac{i}{255} \times \frac{s}{c\cos(24.9°)} = \frac{x}{c}\frac{U_\infty}{U_c} \tag{4.11}$$

Equation 4.10 defines the location, x, of the inflow vortices at any instant of time, t, if the inflow vortices were convected at a velocity given by U_c. The phase number can then be related to the normalized time by Equation 4.11. In this equation, i is the phase number between 0 and 255, s is the blade spacing (9.29”), c is the length of the blade chord (10”), x is the location along the blade chord described above, U_∞ is the free-stream velocity,

and U_c is the convection speed of the inflow vortices. The microphone locations plotted on the top of each plot are for the microphones on the pressure side of the blade (i.e. the positive x/c), while the microphone locations on the bottom of each plot are for the microphones on the suction side of the blade (i.e. the negative x/c). The normalized time corresponds to the phase number and thus it is possible to view the pressure along the blade chord as the vortex generators travel past the blade. All eight tip gaps are plotted together on this figure in order to show the variation in the pressure with tip gap. Figure 4.16 provides an intuitive view into the variation of the pressure as a function of phase number. The dashed lines on the figures represent the approximate path that would be traced by across the blade surfaces assuming convection at the inlet velocity. This figure clearly shows the nature of the leading edge response. It can be seen that the inflow vortices produce a local disturbance to the blade tip loading that travels down the chord at almost the free stream velocity. This is strongest for the tip gap equal to approximately about 6-8% chord. Based on the conclusions of Ma (2003), the height of the inflow vortices is approximately twice the height of the 3.3%*c* tip clearance. Therefore, this gap is large enough for the inflow vortices to pass completely though it without the blade tip destroying the structure of the vortices. Interestingly, traces can be seen on the pressure as well as the suction side in antiphase. It seems more intuitive that the largest pressure fluctuations would be concentrated on the pressure side of the blade where the inflow vortices first impact the blade. However, larger pressure fluctuations are seen on the suction side of the blade at any instant of time. Since this is a startling result, it may be more revealing to look at the pressure difference across the blade to see how this varies as a function of tip gap.

Contours of the pressure difference across the blade tip as a function of tip gap are presented in Figure 4.17. The pressure difference was normalized according to Equation 4.12.

$$\left\langle \Delta C_p \right\rangle_{norm} = \frac{\left\langle C_p \right\rangle_{pressure} - \left\langle C_p \right\rangle_{suction}}{\left\langle \Delta C_p \right\rangle_{rms}} \tag{4.12}$$

In this equation, $\left\langle C_p \right\rangle_{pressure}$ is the phase averaged pressure coefficient on the pressure side of the blade, $\left\langle C_p \right\rangle_{suction}$ is the phase averaged pressure coefficient on the suction side

of the blade and $\left\langle \Delta C_p \right\rangle_{rms}$ is the root mean square of the pressure difference across the blade tip given by Equation 4.13.

$$\left\langle \Delta C_p \right\rangle_{rms} = \sqrt{\frac{1}{nm}\sum_{i=1}^{m}\sum_{j=1}^{n}\left[\left\langle C_p\,|_{pressure} - C_p\,|_{suction}\right\rangle_{ij} - \overline{\left\langle C_p\,|_{pressure} - C_p\,|_{suction}\right\rangle_{ij}}\right]^2} \qquad (4.13)$$

In this equation, n is the number of samples in the measurement, m is the number of microphones, $\left\langle C_p \right\rangle_{pressure}$ and $\left\langle C_p \right\rangle_{suction}$ are the same as defined above and $\overline{\left\langle C_p\,|_{pressure} - C_p\,|_{suction}\right\rangle}$ is defined by Equation 4.14.

$$\overline{\left\langle C_p\,|_{pressure} - C_p\,|_{suction}\right\rangle} = \frac{1}{n}\sum_{i=1}^{n}\left\langle C_p\,|_{pressure} - C_p\,|_{suction}\right\rangle_i \qquad (4.14)$$

For the microphones used here, the quantity given by Equation 4.14 is zero. The pressure difference across the blade was normalized in this manner to provide a method of comparing the pressure contours at different tip clearances. The normalized time is plotted versus the microphone locations for tip gaps from 0.825%c to 12.9%c. From these contours it appears that the normalized pressure difference is independent of tip clearance. This similarity between the different tip clearances measured in this study is startling. It almost seems as though the larger tip gap pressure fluctuations are scaled variations of the smaller tip gaps. This is unexpected since the flow through the tip clearance region is a highly complex flow and since there are many factors that contribute to the unsteady pressure fluctuations on the blade surface. As the tip clearance is increased, the blade is being withdrawn from the inflow vortices and therefore sees a different disturbance at each tip clearance. From Figure 4.17 it can be hypothesized that the flow through the blade passage is not nearly as complex as was originally believed. This can be clearly demonstrated by Figure 4.18.

Figure 4.18 presents the phase-averaged difference between suction and pressure side C_p, adjacent to the blade tip, root-mean-square averaged along the chord and over phase time versus tip gap. The root-mean-square $\left\langle C_p \right\rangle$ presented in this figure is the same quantity defined in Equation 4.13. From this figure, it can be seen that the amplitude in fluctuations of $\left\langle C_p \right\rangle$ across the blade tip appear to vary nearly linearly with tip gap up to a tip clearance of 5.7%c. This suggests that the flow through the blade row

may not be as complex as previously thought. Because of this, it seems as if there may be a simple model for describing the unsteady response of a propulsor or compressor tip gap.

The root mean square pressure can be calculated from the spectral data for the microphones along the chord as well as the microphones along the span for each tip clearance measured. The RMS pressure is calculated from the mean square pressure where the mean square pressure is given by Equation 4.15.

$$p'^2(x,y) = \int_{f_{\min}}^{f_{\max}} G_{pp}(f,x,y)df \tag{4.15}$$

In this equation, f_{min} = 0Hz and f_{max} = 10000Hz. The values of x and y are the locations of the microphones along the chord and the span, respectively. The RMS pressure is then calculated by Equation 4.16.

$$p_{rms} = \sqrt{p'^2} \tag{4.16}$$

The results from these calculations for the chordwise microphone locations are presented in Figure 4.19. This figure presents p_{rms} normalized on the dynamic pressure, q, for the chordwise microphones as a function of tip clearance for all three generator configurations: the baseline configuration, the widely spaced generators, and the half-height generators. From this figure it can be seen that p_{rms} increases as the tip clearance is increased from 0.83% to 5.7%c for the baseline configuration. At tip clearances above 5.7%c, the RMS pressure decreases rapidly as the tip clearance is increased. The changes in the RMS pressure as the tip clearance is increased are mainly noticeable at the trailing edge. Near the leading edge, there are slight variations in the RMS pressure; however the changes at the trailing edge are much larger. This supports the idea that most of the pressure fluctuations are concentrated near the trailing edge of the blade. It can also be seen that the RMS pressure is greater on the pressure side of the blade than on the suction side of the blade. This may be because of the interaction of the blade with the inlet flow or the interaction of the blade with the tip leakage vortex from the blade next to it. This is certainly an interesting result since the pressure contours suggested that the fluctuations in pressure were largest on the suction side of the blade. The effects of different generator configurations will be discussed in following sections.

To verify that the spectral data and the phase averaged data are consistent, it is beneficial to calculate the rms pressure from the spectral data and the rms pressure from the phase averaged data. These two quantities should be exactly the same since the spectral data is calculated from the Fourier transform of the pressure data. The rms pressure at a tip clearance of 3.3%*c* calculated in two different manners is presented in Figure 4.20 and Figure 4.21. Figure 4.20 presents the comparison of p_{rms} normalized on the dynamic pressure, q, on the pressure side of the blade calculated from the spectral data and the phase averaged data, while Figure 4.21 presents the comparison on the suction side of the blade. These figures present the normalized rms pressure versus the chordwise location along the blade. From these figures, it can be seen that the values of the rms pressure calculated in two different manners are nearly identical which verifies the consistency of the data.

Figure 4.22-Figure 4.25 presents the comparison of the rms pressure on the pressure and suction sides of the blade for the case of moving wall with no generators and the case of moving wall with generators for a tip clearance of 3.3%*c* for both the chordwise microphones and the spanwise microphones. The rms pressure presented in these figures is from just the broadband part of the spectrum. The spectral spikes at the generator passing frequency and multiples of this were removed from the case of moving wall with generators for comparison purposes. From these figures, it can be seen that there is only a slight difference between the two cases. These figures verify that there is little difference in the rms pressure on the blade surface regardless of the presence of the vortex generators, which suggest that the generators may not have a significant effect upon the blade surface pressure.

4.4.1.2 Spanwise surface pressure distribution

Since there were microphones embedded along the span of the blade at approximately 24%*c*, the pressure coefficient along the blade span can be investigated in a similar manner to that along the chord. Figure 4.26 presents the phase-averaged pressure coefficient along the blade span as a function of tip clearance. The normalized time corresponding to phase number is plotted on the abscissa and the normalized

microphone location $\frac{y}{c}$, where y is the microphone location in question, is plotted on the ordinate. From this figure, it can be seen that there is little variation in the pressure coefficient along the blade span as the tip gap is increased. There are slight variations, however, near the blade tip that continues to increase up to a tip clearance of 5.7%*c*. This simply verifies the conclusion that there is a simple relationship between the pressure distribution along the blade surface as a function of tip clearance that was hypothesized based on the variation in the pressure distribution along the chord.

The RMS pressure along the blade span for tip clearances from 0.83% to 12.9%*c* for the three generator configurations is presented in Figure 4.27. From this figure it can be seen that the RMS pressure on the pressure side of the blade increases as the tip clearance is increased from 0.83% to 12.9%*c* for the baseline case. The effects of increasing the tip clearance are mostly noticeable near the mid-span of the blade as opposed to the tip of the blade. This is an unusual result since the RMS pressure should vary the most near the tip of the blade as the blade is drawn up through the inflow vortices. On the suction side of the blade, the exact opposite phenomena can be seen. The largest variation in the RMS pressure can be seen at the tip of the blade as the tip clearance is increased. The maximum RMS pressure at the blade tip is seen at a tip clearance of 3.3%*c*. The RMS pressure continues to increase near the blade tip up to this tip clearance, but as the tip clearance is increased above 3.3%, the RMS pressure decreases. This is startling since all of the other information found in this study has led to the determination that the maximum pressure occurs near a tip clearance of 5.7% to 7.9%*c*. However a significant portion of the RMS pressure is contained in the spectral spikes from the passing of the vortex generators. And since the effects of the inflow vortices should decrease as the tip clearance is increased because the inflow vortices are only approximately twice the height of the 3.3%*c* tip clearance, it is possible that the RMS pressure would decrease above a tip clearance of 3.3%*c*.

4.5 Effect of generator spacing on unsteady pressure

4.5.1 Introduction

In the previous section, it was concluded that there is a linear variation in the r.m.s. pressure difference across the blade as a function of tip clearance. In order to investigate the effect of generator spacing on the unsteady pressure on the blade tip, a new generator configuration was studied. The only change is the spacing between the vortex generator pairs. This new generator spacing should essentially eliminate any effects caused by the interactions between the inflow vortices from any two pair of generators or from simultaneous multiple blade interactions. The hypothesis is that possibly some of the effects that are seen in surface pressure distribution are caused by the interactions of separate inflow vortex pairs. This new generator spacing should eliminate the possibility that this phenomenon is occurring.

4.5.2 Modification of phase averaging to account for new spacing

Because the spacing of the vortex generator pairs was changed to investigate the effects of generator spacing on the unsteady pressure at the blade tip, the definition of phase number had to also be modified to account for the generator spacing. The phase numbers from 0 to 256 are defined in the same manner as they were for the baseline generator configuration. A phase number of 0 corresponds to the instant of time when the center of the vortex generator pair is axially upstream of the center of the passage between two corresponding blades, phase 128 is the instant of time when the center of the vortex generator pair is axially upstream of a blade leading edge, and phase 256 is the instant of time when the center of the generator pair is axially upstream of the next blade passage. Phase numbers from 256 to 696 are defined as shown in Figure 4.28. Phase numbers greater than 256 are the times when the vortex generators are past the blade at the center of the passage and therefore at phase numbers greater than 256, the effects of the vortex generators should not be seen on either the pressure or suction surface of the blade at the center of the blade row.

4.5.3 Unsteady pressure versus tip gap

4.5.3.1 Chordwise surface pressure distribution

Figure 4.29-Figure 4.36 presents movies of $\langle C_p \rangle$ on the pressure and suction side of the blade as a function of chordwise location for all eight tip gaps measured. These movies show almost the same phenomena that the movies of $\langle C_p \rangle$ for the baseline generator spacing showed. Namely, they show that at the smaller tip clearances, the fluctuations along the blade chord seem to be confined to the leading edge and are contained in the phase numbers between 150 and 300, which is the period of time slightly after the generator pair has passed the leading edge of the blade. At a tip clearance of 0.825%*c*, there is almost no variation in the $\langle C_p \rangle$ over all phase numbers suggesting that the inflow vortices do not significantly contribute to the surface pressure distribution at small tip clearances. At phase numbers lower than 150 and greater than 300, there is little fluctuation in the $\langle C_p \rangle$ along the entire length of the blade since the generators are well past the blade leading edge at this period of time. As the tip clearance is increased, the effects of the generators can be seen along the entire length of the blade for phase numbers between 150 and 300. It is interesting to note, however, that at the larger tip clearances (4.5%*c* to 7.9%*c*), a large pressure difference can be seen at the trailing edge of the blade. This pressure difference is almost constant as a function of phase number which suggests that it is not caused by the passing of the vortex generators but is caused by the flow over the blade. As with the baseline spacing, the fluctuations in $\langle C_p \rangle$ continue to increase in magnitude up to a tip clearance of 7.9%*c*. These results demonstrate that the fluctuations in the pressure along the blade surface are independent of the generator spacing, which can be further explained by plotting the contours of $\langle C_p \rangle$ for the wide generator spacing and comparing these with the baseline spacing.

Contours of the phase averaged pressure coefficient for both the pressure and suction side of the blade for the widely spaced vortex generators are presented in Figure

4.37. As with the contour plots presented before, the normalized time $\frac{tU_\infty}{c}$ is plotted on the abscissa versus the microphone locations $\frac{x}{c}$ plotted on the ordinate. As with the contour plots for the baseline generator configuration, it can be seen that there is an increase in $\langle C_p \rangle$ for increasing tip clearance up to a tip clearance of 7.9%*c*. It also appears that there is a larger number of oscillations that occur near the blade trailing edge in the widely spaced generator case. These oscillations appear to occur at a different frequency than those seen in the baseline case and may be a result of the viscous response stimulating the inviscid response of the trailing edge. The pressure difference across the blade tip normalized on the root mean square pressure difference is plotted in Figure 4.38. Again, it appears that there is a self-similarity between the pressure difference and the tip clearance for tip clearances of 1.65%*c* and above. The measurements at a tip clearance of 0.83%*c* seem to deviate from this similarity. Figure 4.39 presents the phase-averaged difference between suction and pressure side C_p, adjacent to the blade tip, root-mean-square averaged along the chord and over phase time $\sqrt{\overline{\langle \Delta C_p \rangle^2}}$ versus tip gap. From this figure, it appears that there is not a simple relationship between the r.m.s pressure difference across the blade tip and the tip clearance. This is contrary to the results from the baseline generator configuration where the r.m.s. pressure difference across the blade tip varied linearly with tip clearance. It can also be noted that the r.m.s. pressure difference for the widely spaced generators is approximately one order of magnitude smaller than that for the baseline generator configuration. This may be due to the larger sampling time with the widely spaced generators (696 phases compared with 256 phases with the baseline configuration). Since a large part of the sampling time for the widely spaced generators consisted of a large time period when the generators were well past the blade leading edge and thus the blade tip was not seeing any significant pressure fluctuations from the passing of the generators.

Returning to Figure 4.19, it can be seen that the effects of the different generator spacing causes an insignificant variation in the RMS pressure when compared with the baseline generator configuration. The same conclusions that were presented for the

baseline case are also valid for the widely spaced generators. The RMS pressure increases as the tip clearance is increased from 0.83% to 5.7%*c*. At tip clearances above 5.7%*c*, the RMS pressure decreases rapidly.

This result implies that there is little effect on the blade surface pressure distribution as a function of generator spacing. Therefore, it seems that the hypothesis that there was a significant effect on the surface pressure distribution because of the vortices from multiple vortex generator pairs impacting the blade at the same time is incorrect. This hypothesis can be further examined by presenting a comparison for the new generator spacing and the baseline generator spacing at a tip clearance of 3.3%*c*.

4.5.3.2 Spanwise surface pressure distribution

Returning to Figure 4.27, it can be seen that there is a slight difference in the spanwise RMS pressure on the pressure side of the blade at a tip clearance of 12.9%*c*. This could be a result of the different generator spacing; however the difference in the RMS pressure is not large enough to come to this conclusion. On the suction side of the blade, the differences in the RMS pressures as the tip clearance is increased are much smaller than that seen for the baseline configuration, especially well above the blade tip.

4.5.3.3 3.3%c comparison with baseline generator spacing

Figure 4.40 presents a comparison of the pressure difference across the blade tip normalized on the root mean square pressure difference for the baseline generator configuration and the widely spaced generator configuration. It can be seen that there is little difference between the two cases for phase numbers between 0 and 256. Because the new generator configuration required a larger number of phases (namely 696 with the higher phase numbers corresponding to a period of time when the generator pairs are well past the blade leading edge), $\langle C_p \rangle$ at higher phase numbers varies insignificantly. However this is to be expected since outside of 256 phases, the generators should have almost no impact upon the blade surface pressure distribution. At phase numbers greater than 256, there should be almost no impact on the blade caused by the inflow vortices.

However, at phase numbers greater than 256, there is a significant variation of the pressure fluctuations only at the trailing edge of the blade. This suggests that the impact of the inflow vortices continues to play an important role in the blade surface pressure distribution near the trailing edge. This is verified by the $\langle C_p \rangle$ movies where large pressure differences can be seen at the trailing edge at higher phase number. However, the physical aspects of the blade surface pressure distribution between the two configurations are interesting. Since this invalidates the idea that the generator spacing is playing a key role in the linear variation of the pressure difference with the tip clearance, it would be useful to further examine the cause of this linear variation in $\langle C_p \rangle$.

Figure 4.41 and Figure 4.42 presents the chordwise movies of the fluctuating $\langle C_p \rangle$ with the movies for the widely spaced generator pairs and the baseline spacing presented together in one movie. Figure 4.41 presents the $\langle C_p \rangle$ movie for the pressure side of the blade while Figure 4.42 presents the $\langle C_p \rangle$ movie for the suction side of the blade. The movies are embedded in the plots and can be played by double clicking the plot. From these movies, it can be seen that there are some fluctuations in the $\langle C_p \rangle$ for the baseline configuration at lower phase numbers that cannot be seen in the surface pressure distribution for the widely spaced generator pairs. This can be contributed to the spacing of the generator pairs. When the generator pairs are spaced at the same distance apart as the blade spacing (the baseline configuration), the effects of multiple generator pairs can be seen as a 'thump' on the blade resulting in a reverberation effect on the $\langle C_p \rangle$ fluctuations. This effect cannot be seen when the generator pairs are spaced far enough apart to eliminate any of these kinds of effects. Since the pressure fluctuations between the baseline case and the widely spaced generators are almost exactly the same, it can be concluded that the spacing of the generators does not factor significantly into the surface pressure distribution. Therefore it is important to further investigate the cause of the linear variation in the root mean square of the pressure fluctuation by investigating the effects of generator size on the surface pressure distribution.

4.6 Effect of generator size on unsteady pressure

4.6.1 Introduction

In the previous section it was determined that the generator spacing plays only a small role in the variation of the pressure difference across the blade tip with tip clearance, it is useful to further examine the cause of such a relationship. Therefore, it was decided that the variation in the unsteady pressure as a function of tip clearance should be examined for a different size of vortex generators. The vortex generators used for this investigation are half the height of the vortex generators used in the baseline case. These half-height generators will demonstrate whether the blade surface pressure distribution is dependent upon the size of the vortex generators, which directly affects the size of the inflow vortices.

For this investigation, it is assumed that decreasing the height of the vortex generators will also decrease the size of the inflow vortices created by the generator pairs. Ma (2003) measured the height of the inflow vortices using hot-wire anemometry and determined that the inflow vortices were approximately twice the height of the 3.3%*c* tip clearance. For this investigation, time was a limiting factor and therefore the height of the inflow vortices created by the half-height generators was not measured. The assumption here is that decreasing the height of the generators by a factor of 2 will decrease the height of the inflow vortices by the same factor. To better quantify the results presented in this section, a further investigation would measure the height of the inflow vortices using the same techniques used by Ma (2003).

4.6.2 Unsteady pressure versus tip gap

4.6.2.1 Chordwise surface pressure distribution

Figure 4.43-Figure 4.50 presents the movies of fluctuating $\langle C_p \rangle$ versus phase number for tip clearances from 0.825%*c* to 12.9%*c* for the half-height generators. These movies also provide similar results to those presented for the full-size generators. The

pressure fluctuations are small for the lowest tip clearance of 0.825%*c* and are confined primarily to the first 50% of the chord for this tip clearance. As the tip clearance is increased, the fluctuations become larger in magnitude and can be seen over the entire length of the blade chord for tip clearances up through 5.7%*c*. This is different from the full size generators since the fluctuations were seen to increase up to a tip clearance of 7.9%*c*. At tip clearances of 7.9%*c* and 12.9%*c*, the pressure fluctuations begin to decrease in magnitude. At a tip clearance of 12.9%*c*, there is almost no variation in the pressure with the phase number suggesting that the inflow vortices are not large enough to impact the blade tip at this large tip clearance. The differences between the pressure fluctuations on the blade surface with the full-size generators and the half-height generators are almost negligible except at tip clearances of 5.7% and 7.9%*c*. The size of the vortex generators should affect the size of the inflow vortices, and since the half-height generators should be expected to create inflow vortices that are smaller in size than those created by the full size generator, this result is to be expected. This suggests that the size of the inflow vortices plays a minor role in the pressure fluctuations near the blade tip. This can be better examined by investigating the pressure contours.

Figure 4.51 presents the chordwise $\langle C_p \rangle$ contours for the pressure and suction side of the blade for tip clearances from 0.825%*c* to 12.9%*c*. These contours are similar to those presented for the full-size generators. At tip clearances up to 5.7%*c*, the plots are almost the same as those presented for the full-size generator case. However, for the full-size generators, the $\langle C_p \rangle$ fluctuations continue to increase up to a tip clearance of 7.9%*c*. For the half-height generators, the fluctuations increase up to a tip clearance of 5.7%*c*. This result is not surprising since the half-height generators are expected to create inflow vortices that are smaller in size than those created by the full-size generators. It is assumed that the half-height generators will create a pair of inflow vortices that is half the size of the inflow vortices created by the full-size generators. The investigation of Ma (2003) showed that the inflow vortices created by the full-size generators were twice the height of the 3.3%*c* tip clearance, which means the inflow vortices are approximately 6.6%*c* in height. Therefore, the half-height generators should create a pair of inflow vortices that are only 3.3%*c* in height. The contour plots show that this is not the case. If

this assumption that the half-height generators create inflow vortices that are only 3.3%*c* in height, the contours would show that the $\langle C_p \rangle$ fluctuations begin to decrease at a tip clearance of 3.3%*c*. However, the contours show that the $\langle C_p \rangle$ fluctuations continue to increase up to a tip clearance of 5.7%*c*. To verify the actual height of the inflow vortices created by the half-height generators, a further investigation similar to that made by Ma (2003) would have to be performed using hot-wire anemometry to measure the height of the inflow vortices.

Figure 4.52 presents a comparison of the pressure difference across the blade tip normalized on the root mean square pressure difference. Here the same self similarity shown by the full-size vortex generators can be seen between the different tip clearances studied. However, again the increasing effects on the $\langle C_p \rangle$ fluctuations can be seen only up to a tip clearance of 5.7%*c*. However because of the self similarity between tip clearances, it can be concluded that the size of the vortex generators does not play a significant role in the variation in $\langle C_p \rangle$. This verifies that the phenomenon that is displayed by the pressure distribution along the blade chord is real and is not affected by different vortex generator configurations.

From Figure 4.19, it can be seen that the effects of the half-height generators are negligible when compare with the baseline case and the widely spaced generators on both the pressure and suction sides of the blade. The RMS pressure on both sides of the blade continues to increase as the tip clearance is increased from 0.83% to 5.7%*c*. At tip clearances above 5.7%*c*, the RMS pressure then decreases rapidly. These are the same results seen in the baseline case and the widely spaced generator case.

4.6.2.2 Spanwise surface pressure distribution

The RMS pressure along the span of the blade for all three configurations is presented in Figure 4.27. It can be seen that there are differences between the half-height generator case and the other two cases. These differences are mainly noticeable at tip clearances of 3.3% and 7.9%c. This is an unusual result since the only noticeable

differences occur at two tip clearances. This result may need to be investigated further. However, since the only noticeable differences occur at these two tip clearances, there is no reason to believe that the half-height generators have a significant effect on the flow across the tip gap.

4.6.2.3 3.3%c comparison with baseline generator size

Figure 4.53 presents a comparison of the pressure difference across the blade tip normalized on the root mean square pressure difference for the baseline generator configuration and the widely spaced generator configuration. At this tip clearance, there is not a noticeable difference between the full-size generators and the half-height generators. This suggests that there is no effect on the $\langle C_p \rangle$ fluctuations as a result of the size of the inflow vortices. This is not an expected result since the fluctuations should be significantly greater for the full-size generators at this tip clearance. It is expected that the fluctuations should be approximately twice as large for the full-size generators. However, this simply verifies the results described above that the size of the generators does not affect the surface pressure distribution along the blade chord.

Figure 4.54 and Figure 4.55 presents the chordwise movies of the fluctuating $\langle C_p \rangle$ with the movies for the half-height generator pairs and the full-size generators presented together in one movie. Figure 4.54 presents the $\langle C_p \rangle$ movie for the pressure side of the blade while Figure 4.55 presents the $\langle C_p \rangle$ movie for the suction side of the blade. The movies are embedded in the plots and can be played by double clicking the plot. These movies show that the fluctuations for the full-size generators and the half-height generators are similar and verify that there is almost no difference in the $\langle C_p \rangle$ fluctuations as a function of the generator size.

Figure 4.56 presents the phase-averaged difference between suction and pressure side C_p, adjacent to the blade tip, root-mean-square averaged along the chord and over phase time $\sqrt{\overline{\langle \Delta C_p \rangle^2}}$ versus tip gap. This figure clearly shows a linear variation in the

scaled pressure difference as a function of tip gap up to a tip clearance of 4.5%*c*. At tip clearances higher than this, the linear trend no longer exists. This is a similar result to that shown by the scaled pressure for the full-size generators. This similarity is shown in Figure 4.57. This figure shows the scaled pressure difference across the tip for the full-size generators and the half-height generators. The linear trends exhibited by both cases are similar in slope suggesting that the vortex generator size does not play a major role in the scaled pressure across the blade tip. However, the half-height generators break the linear trend at a tip clearance of 4.5%*c* while the full-size generators break this linear trend at a tip clearance of 5.7%*c*.

4.7 Instantaneous pressure

4.7.1 Introduction

The instantaneous pressure is valuable because the phase-averaging of the data may cause the overall picture of what is occurring across the blade tip gap to be lost. The instantaneous pressure is not processed in the same manner as the phase-averaged pressure since the unsteady pressure needs to be known at any given instant of time and therefore it is not important to know the exact position of the generators in the blade passage. The instantaneous pressure allows the overall effects of the inflow and the inflow vortices to be seen on the blade surface pressure distribution. For the processing of the instantaneous pressure, disturbances associated with low frequencies (less than 100Hz) and high frequencies (greater than 5000Hz) are eliminated. This should help eliminate any effect of ambient acoustics such as the vibration of the tunnel, noise from the fan, etc. This section will present the results of the instantaneous pressure for the moving wall with no vortex generators and the moving wall with vortex generators at a tip clearance of 3.3%*c*. The results from the moving wall with vortex generators will also be presented for tip clearances of 1.65%, 3.3%, and 5.7%*c*.

4.7.2 Comparison between no generator and generator cases

Figure 4.58 presents the instantaneous pressure difference across the tip clearance for the case of moving wall with no generators and moving wall with generators for a tip clearance of 3.3%*c*. The normalized time is plotted on the abscissa and the microphone locations are plotted on the ordinate. For the instantaneous pressure, a normalized length of time equal to 256 phases (1.024) is presented for comparison with the phase averaged data. From this figure it can be seen that there is no noticeable difference between the case with no generators and the case with generators. This is a startling result since it seems intuitive that the effects of the generators would appear in the instantaneous pressure taken with the generators attached to the moving wall. Namely, there should be pressure fluctuations across the blade tip that should not be seen in the case with no generators. This suggests that the pressure fluctuations across the tip gap are the same whether or not the generators are present suggesting that the vortical wakes created by the passing of the vortex generators may not play a major role in the blade surface pressure distribution. The inflow vortices seem to organize the pressure distribution but may not be the primary source of the pressure fluctuations. This is something that has not been seen previously for this cascade configuration. To understand what is happening, it may be beneficial to investigate the effects of no generators for all tip clearances to see whether or not the effects shown here increase with increasing tip gap. This may be something that can be investigated in future studies.

4.7.3 Instantaneous pressure vs. tip gap

Figure 4.59 presents the time averaged instantaneous pressure difference across the tip clearance as a function of tip clearance. Here only three tip clearances are presented: 1.65%, 3.3%, and 5.7%. From this figure it can be seen that as the tip clearance is increased, the instantaneous pressure difference across the tip clearance also increases. This is expected since the phase averaged data led to this conclusion. However, this is an interesting result since it supports the hypothesis that this

phenomenon is present regardless of whether or not the data is phase averaged. It seems as if the inflow vortices simply stimulate this response of the blades.

4.8 Summary

In this investigation, the effect on the surface pressure distribution from several different vortex generator configurations was studied for tip clearances from 0.825%*c* to 12.9%*c*. To determine whether the surface pressure distribution is influenced by multiple inflow vortices impacting the blade at the same instant of time, the vortex generators were placed far enough apart to eliminate this effect. The size of the vortex generators and thus the size of the inflow vortices were also investigated by using half-height generator pairs. This allows an investigation of the surface pressure for inflow vortices that should be almost twice as small as those for the baseline vortex generator configuration. From this study, several conclusions can be made:

1. The baseline generator configuration shows a self-similarity in the $\langle C_p \rangle$ contours when the pressure difference across the blade tip is normalized on the root mean square pressure difference.
2. The baseline generator configuration shows that the phase-averaged difference between suction and pressure side C_p, adjacent to the blade tip, root-mean-square averaged along the chord and over phase time varies nearly linearly up to a tip clearance of 5.7%*c* with an increasing pressure difference up through this tip clearance.
3. At tip clearances between 0.825%*c* and 5.7%*c*, the pressure fluctuations along the blade chord increase in magnitude as the tip clearance is increased.
4. At small tip clearances (0.825% and 1.65%*c*) the pressure fluctuations are primarily confined to the first 50% of the blade chord while at higher tip clearances, the pressure fluctuations can be seen along the entire length of the blade chord.
5. At tip clearances greater than 5.7%*c*, the pressure fluctuations along the blade chord begin to decrease in magnitude for the baseline generator configuration.

6. The RMS pressure increases as the tip clearance is increased from 0.83% to 5.7%*c* for the baseline configuration. At tip clearances above 5.7%*c*, the RMS pressure decreases rapidly as the tip clearance is increased. The changes in the RMS pressure as the tip clearance is increased are mainly noticeable at the trailing edge. It can also be seen that the RMS pressure are greater on the pressure side of the blade than on the suction side of the blade. This may be because of the interaction of the blade with the inlet flow or the interaction of the blade with the tip leakage vortex from the blade next to it. This is certainly an interesting result since the pressure contours suggested that the fluctuations in pressure were largest on the suction side of the blade.
7. The spacing of the vortex generators shows that there is almost no effect on the blade surface pressure distribution resulting from multiple inflow vortices impacting the blade at the same instant of time.
8. The study of the vortex generator size shows that there is almost no effect on the blade surface unsteady pressure distribution at tip clearances smaller than 5.7%*c*.
9. The half-height generators show an increase in $\langle C_p \rangle$ up to a tip clearance of 4.5%*c* while the full-size generators show an increase in $\langle C_p \rangle$ up to a tip clearance of 5.7%*c*.
10. The half-height generators show that the phase-averaged difference between suction and pressure side C_p, adjacent to the blade tip, root-mean-square averaged along the chord and over phase time varies nearly linearly up to a tip clearance of 4.5%*c* with an increasing pressure difference up through this tip clearance.
11. There are only minor effects on the blade surface pressure distribution as a result of using widely spaced generator pairs and half-height generator pairs in place of the full-size generator pairs spaced 9.29" apart. Therefore, the pressure on the blade surface near the tip is affected primarily by one pair of inflow vortices and is not significantly affected by the size of these inflow vortices.

12. The instantaneous pressure results show that the response of the blade is independent of whether or not the vortex generators are present. It appears as though the inflow vortices stimulate the response of the blade. These results also show that the tip gap effect is real and is not simply a result of the phase averaging of the measurements.

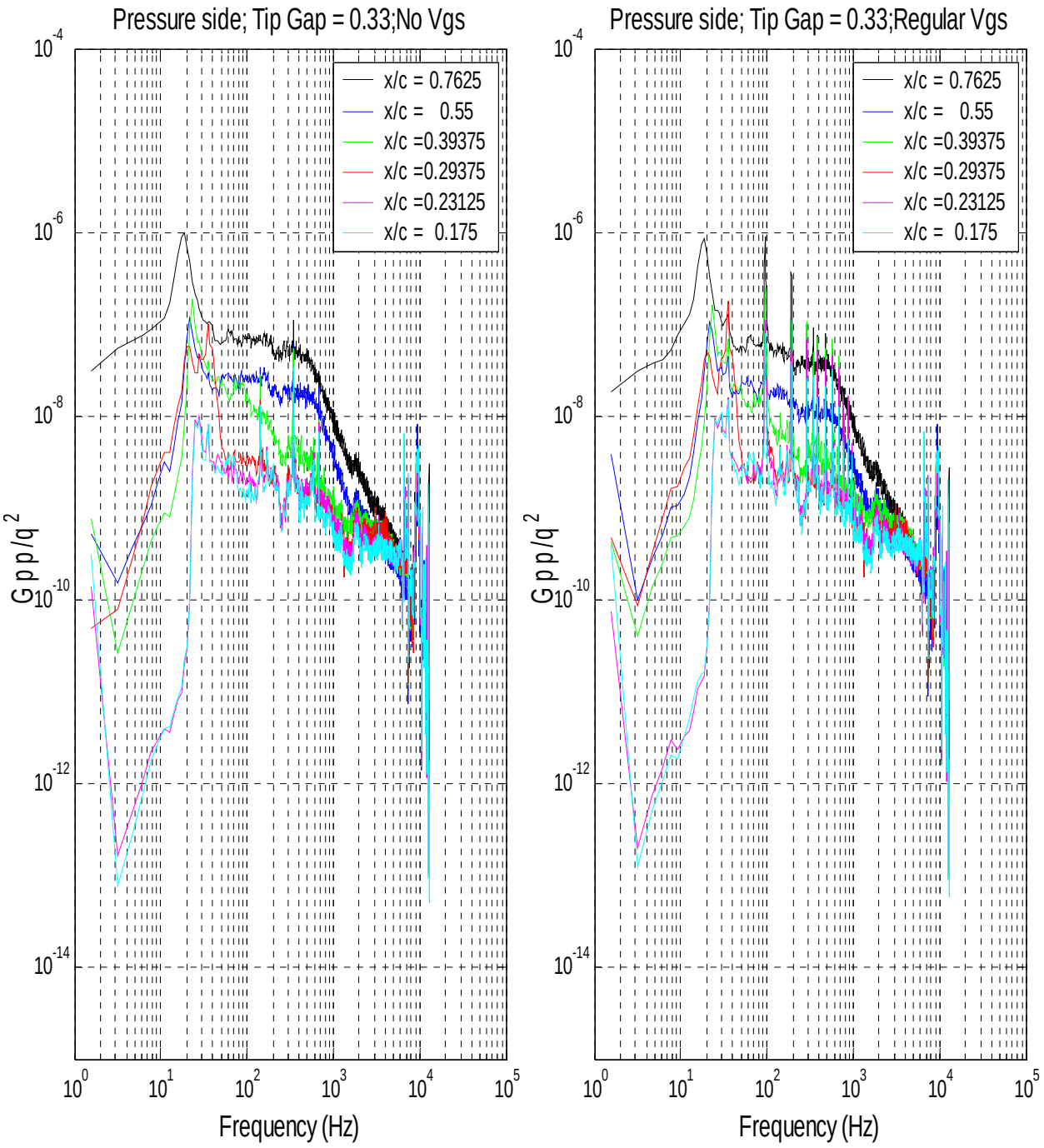

Figure 4.1 Comparison of time averaged pressure spectra on *pressure* side of the blade along the chord for a tip clearance of 3.3%*c* for wall motion with no vortex generators and wall motion with vortex generators.

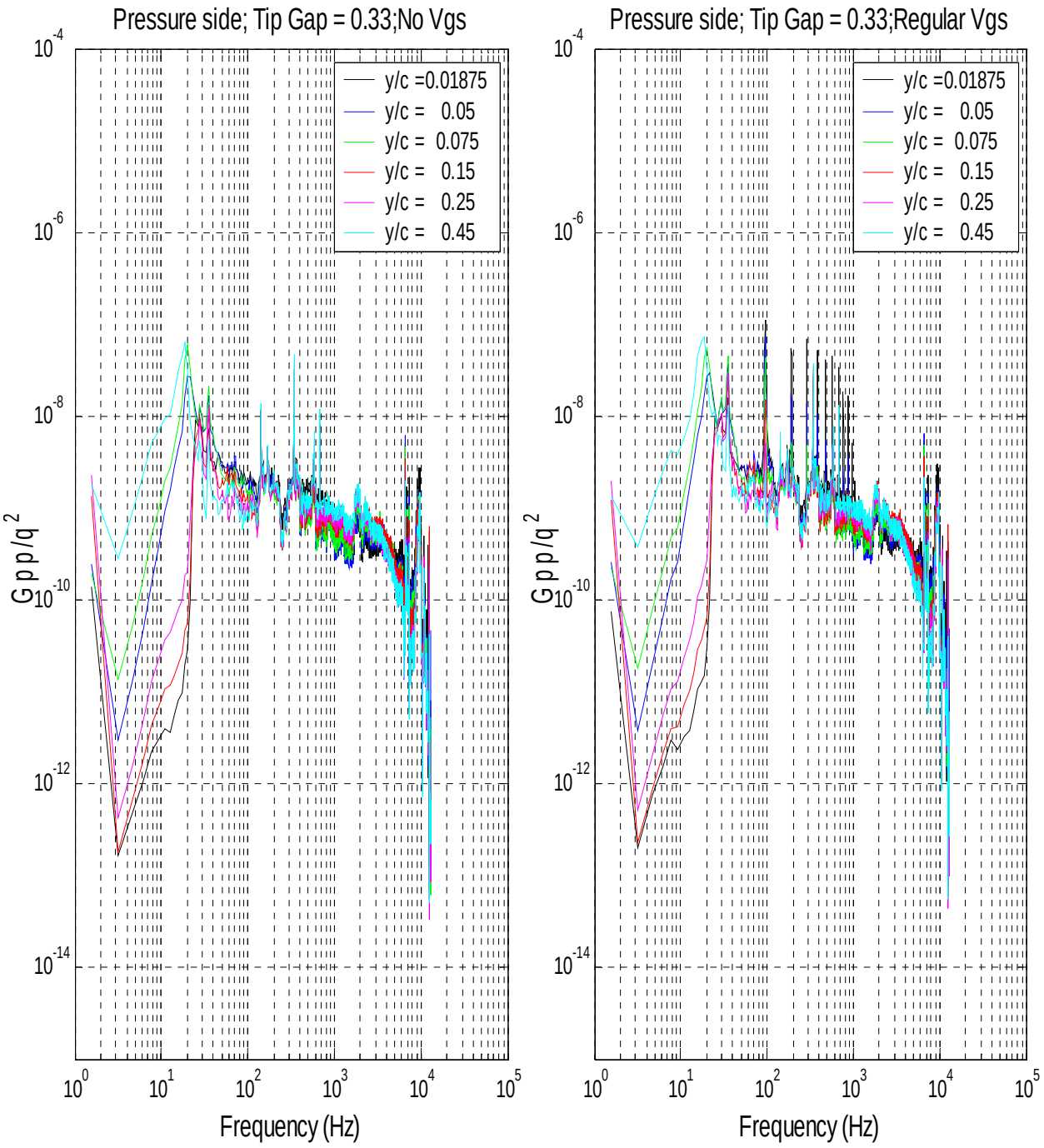

Figure 4.2 Comparison of time averaged pressure spectra on *pressure* side of the blade along the span for a tip clearance of 3.3%*c* for wall motion with no vortex generators and wall motion with vortex generators.

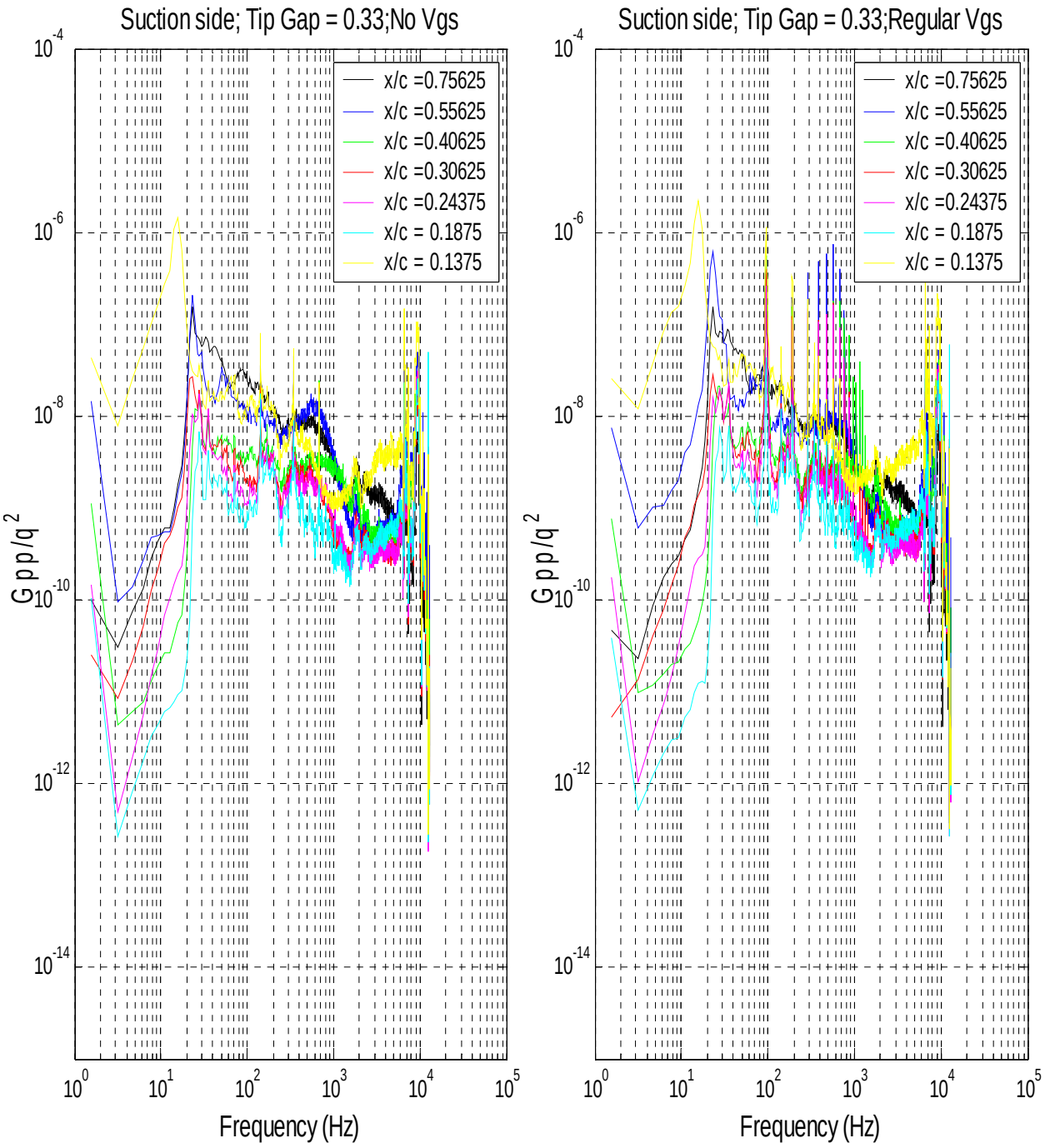

Figure 4.3 Comparison of time averaged pressure spectra on *suction* side of the blade along the chord for a tip clearance of 3.3%*c* for wall motion with no vortex generators and wall motion with vortex generators.

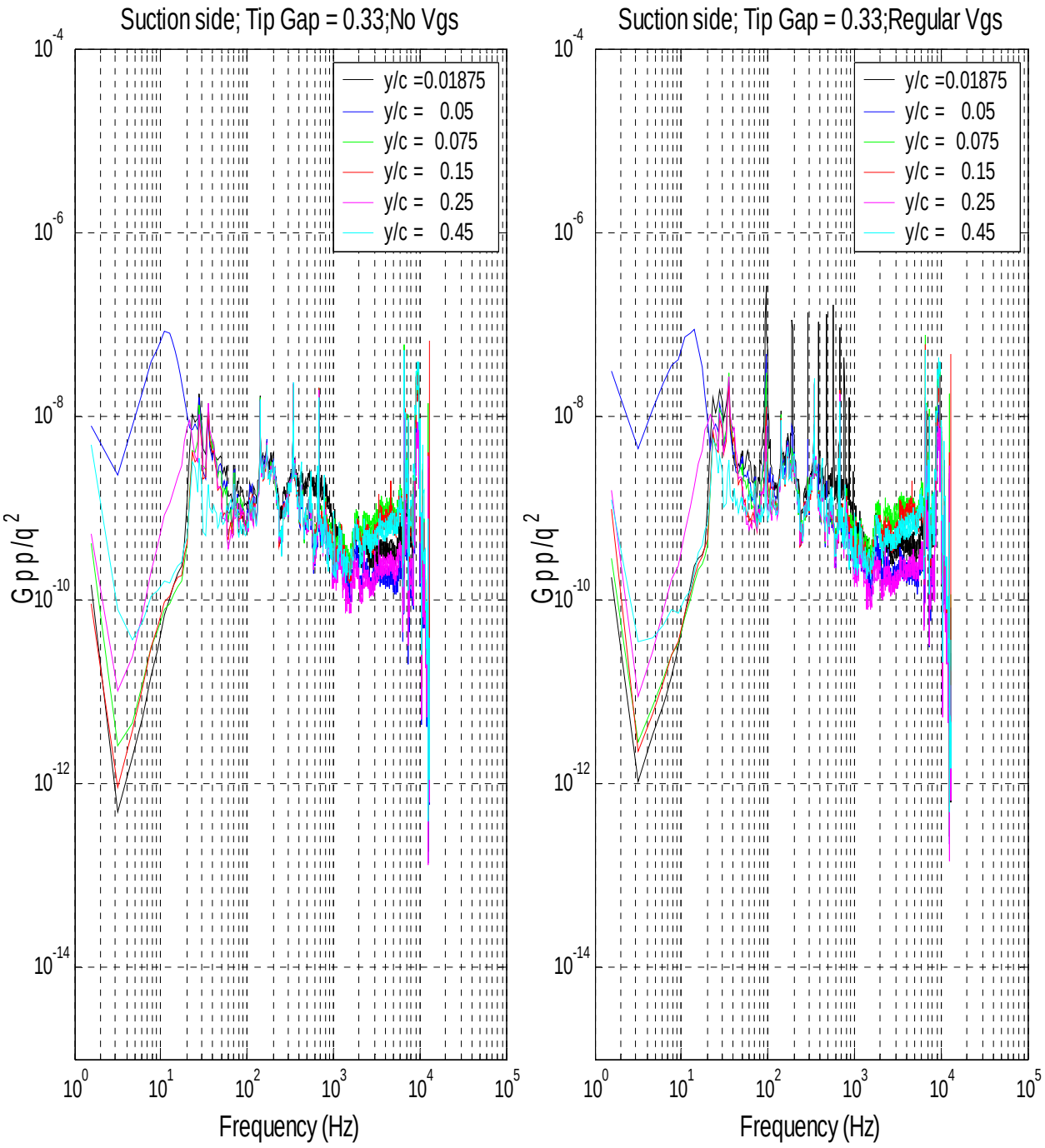

Figure 4.4 Comparison of time averaged pressure spectra on *suction* side of the blade along the span for a tip clearance of 3.3%*c* for wall motion with no vortex generators and wall motion with vortex generators.

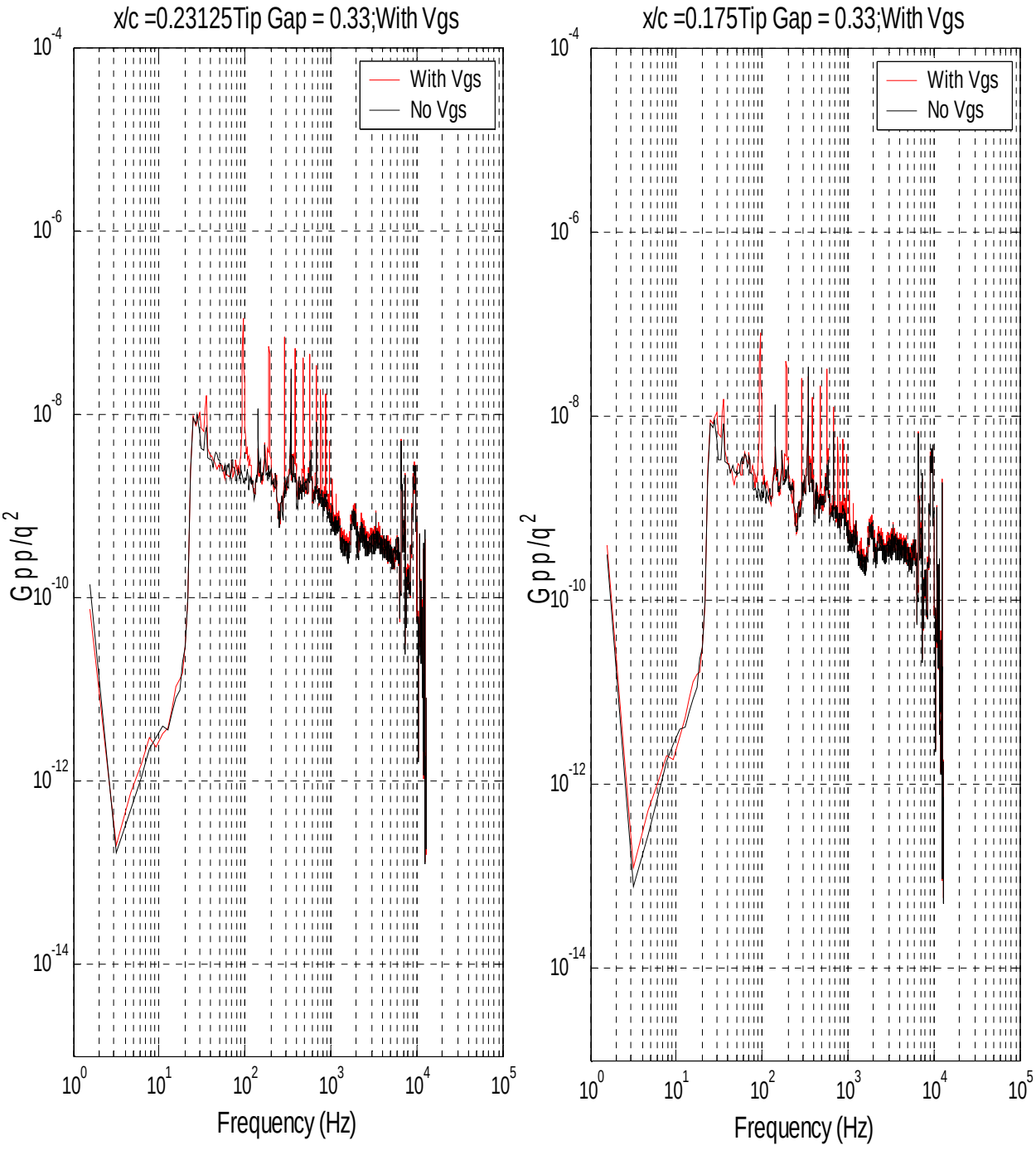

Figure 4.5 Comparison of time averaged pressure spectra for two separate microphones along the chord for a tip clearance of 3.3%*c* for wall motion with no vortex generators and wall motion with vortex generators.

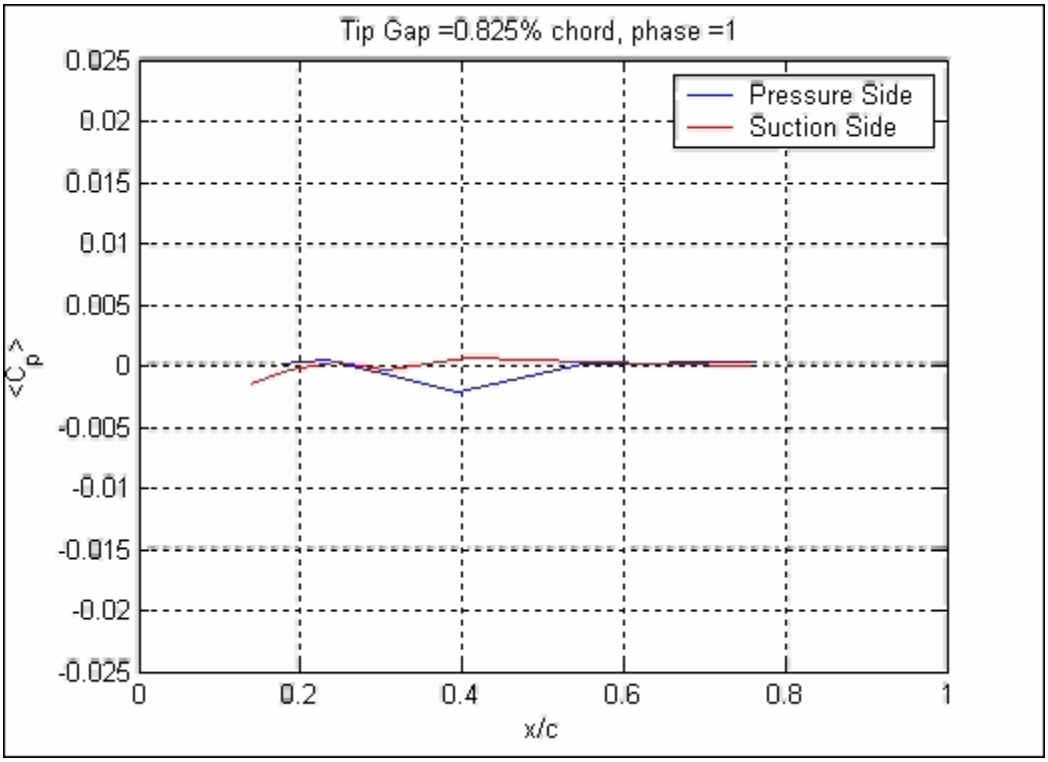

Figure 4.6 Movie of unsteady pressure fluctuation as a function of phase number along blade chord for baseline generator configuration for a tip clearance of 0.825%*c*.

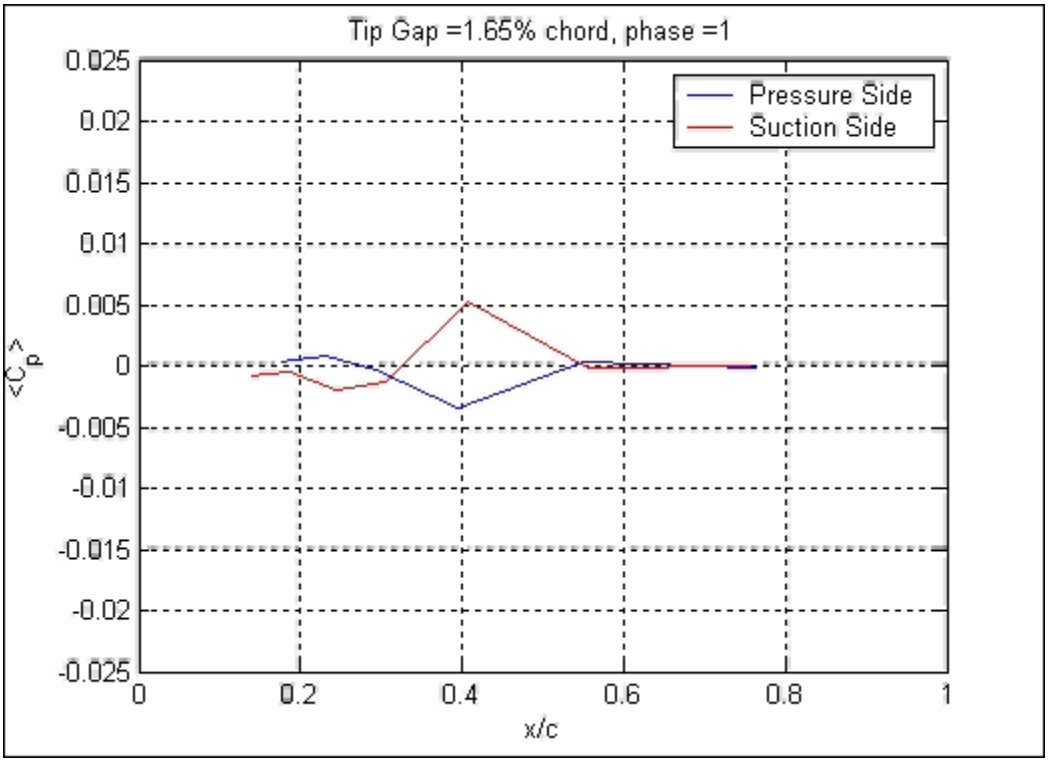

Figure 4.7 Movie of unsteady pressure fluctuation as a function of phase number along blade chord for baseline generator configuration for a tip clearance of 1.65%*c*.

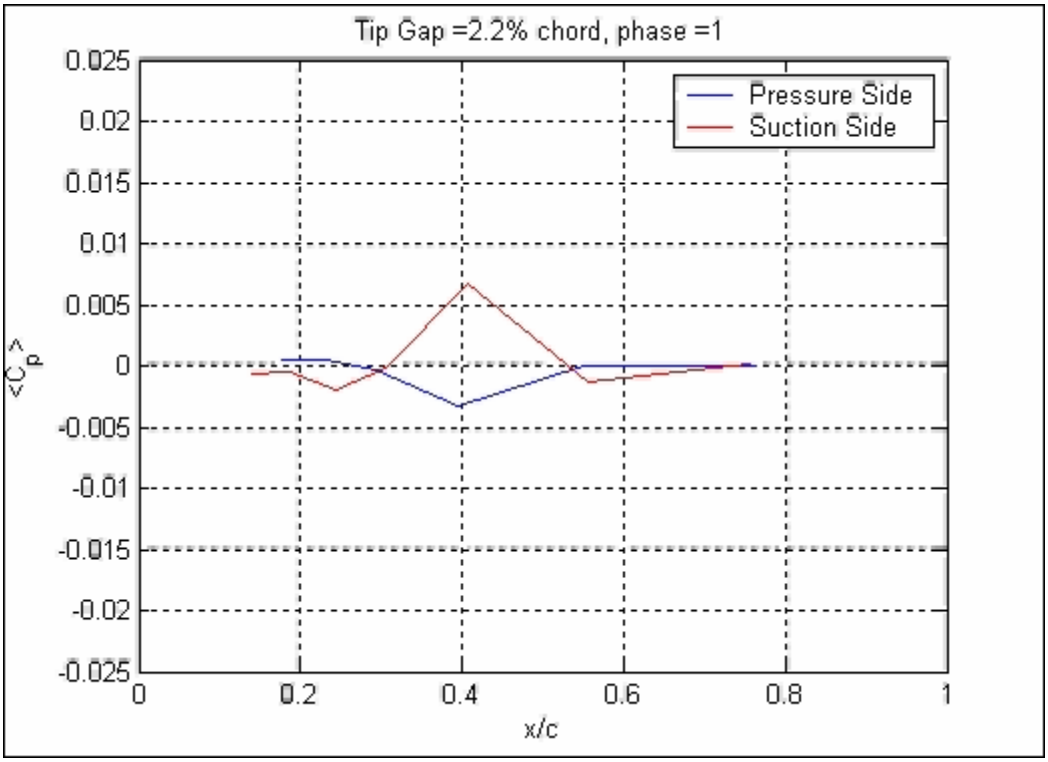

Figure 4.8 Movie of unsteady pressure fluctuation as a function of phase number along blade chord for baseline generator configuration for a tip clearance of 2.2%*c*.

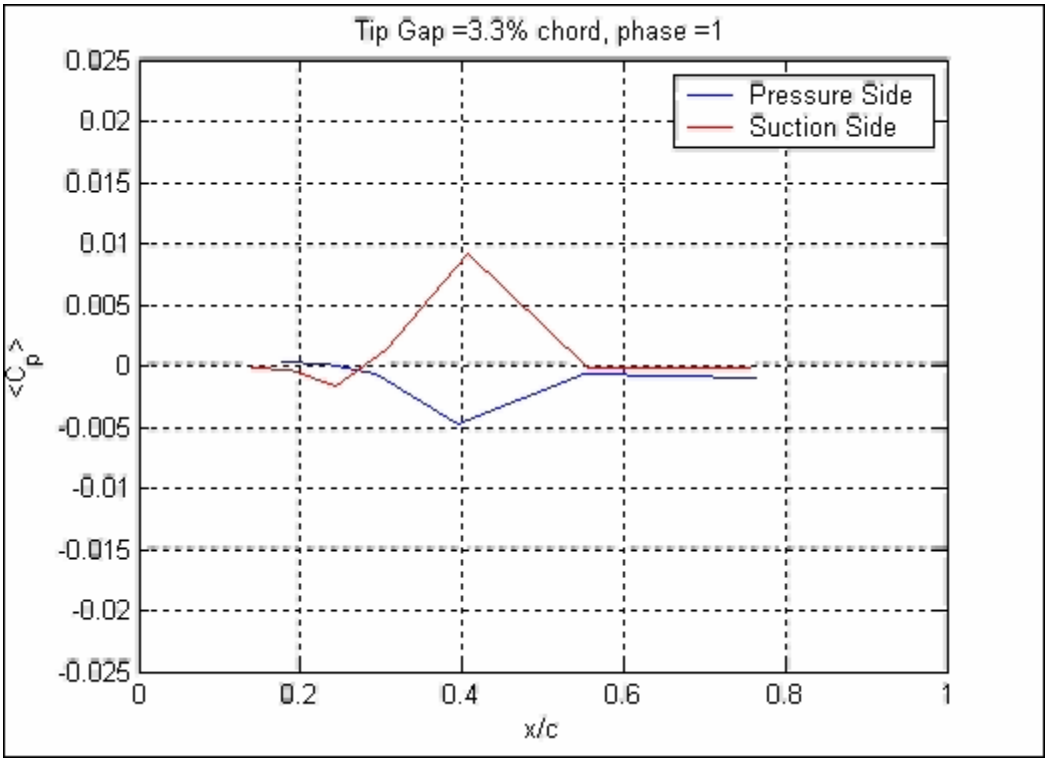

Figure 4.9 Movie of unsteady pressure fluctuation as a function of phase number along blade chord for baseline generator configuration for a tip clearance of 3.3%*c*.

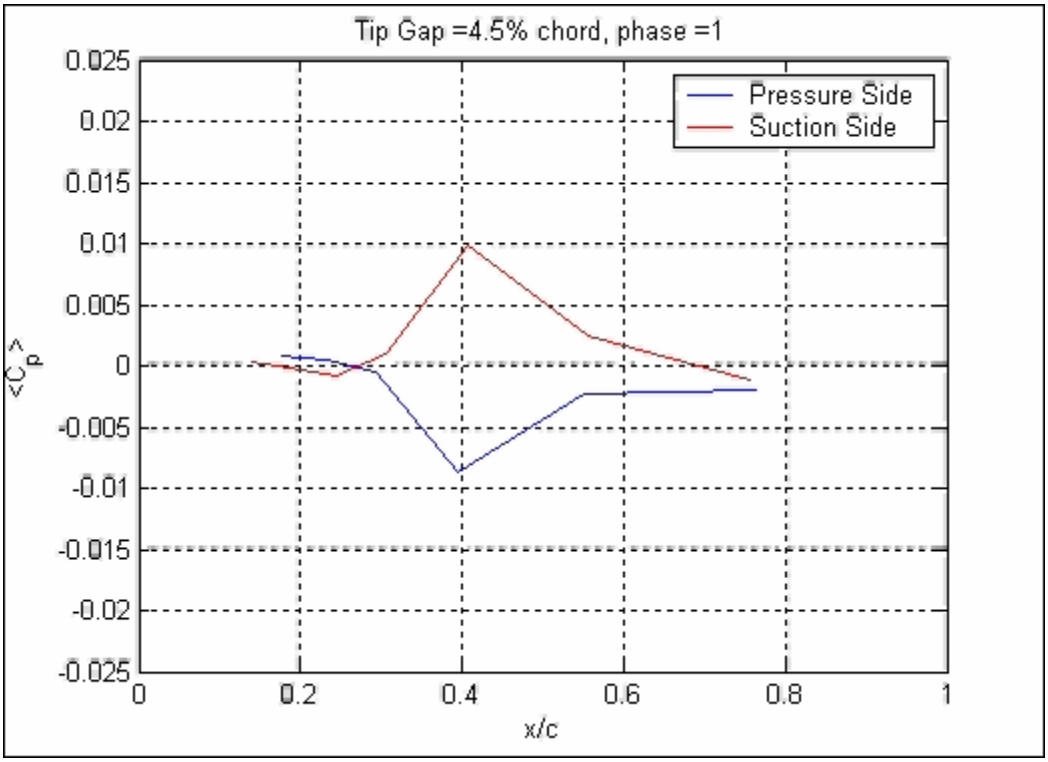

Figure 4.10 Movie of unsteady pressure fluctuation as a function of phase number along blade chord for baseline generator configuration for a tip clearance of 4.5%*c*.

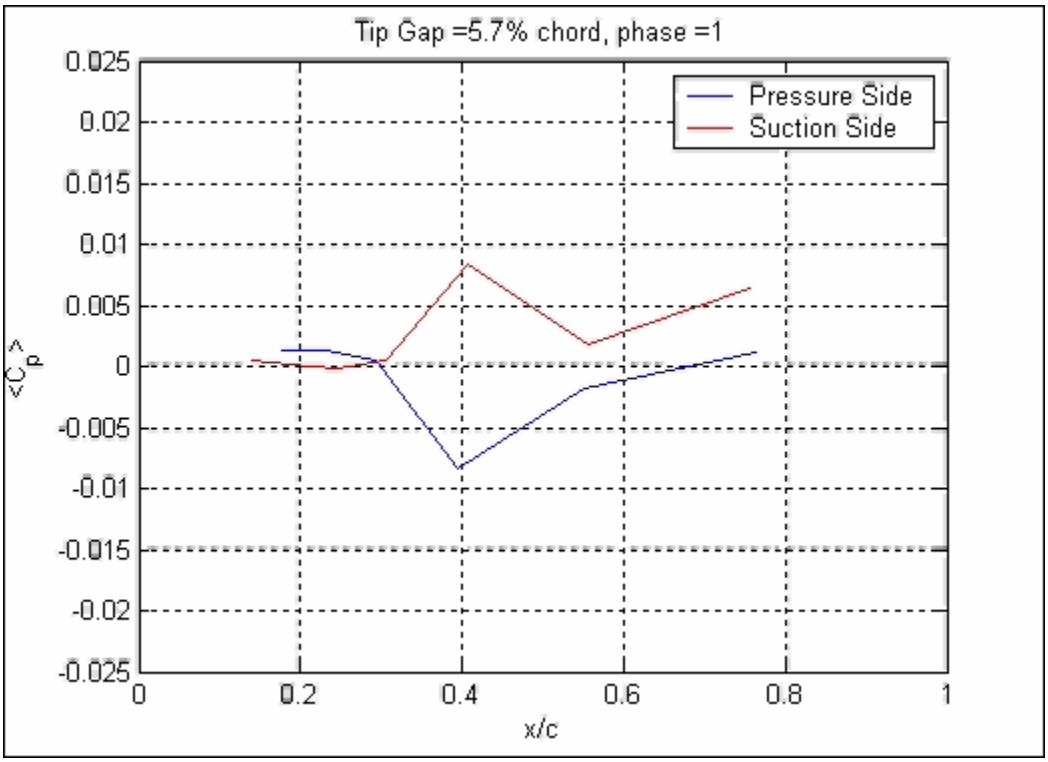

Figure 4.11 Movie of unsteady pressure fluctuation as a function of phase number along blade chord for baseline generator configuration for a tip clearance of 5.7%*c*.

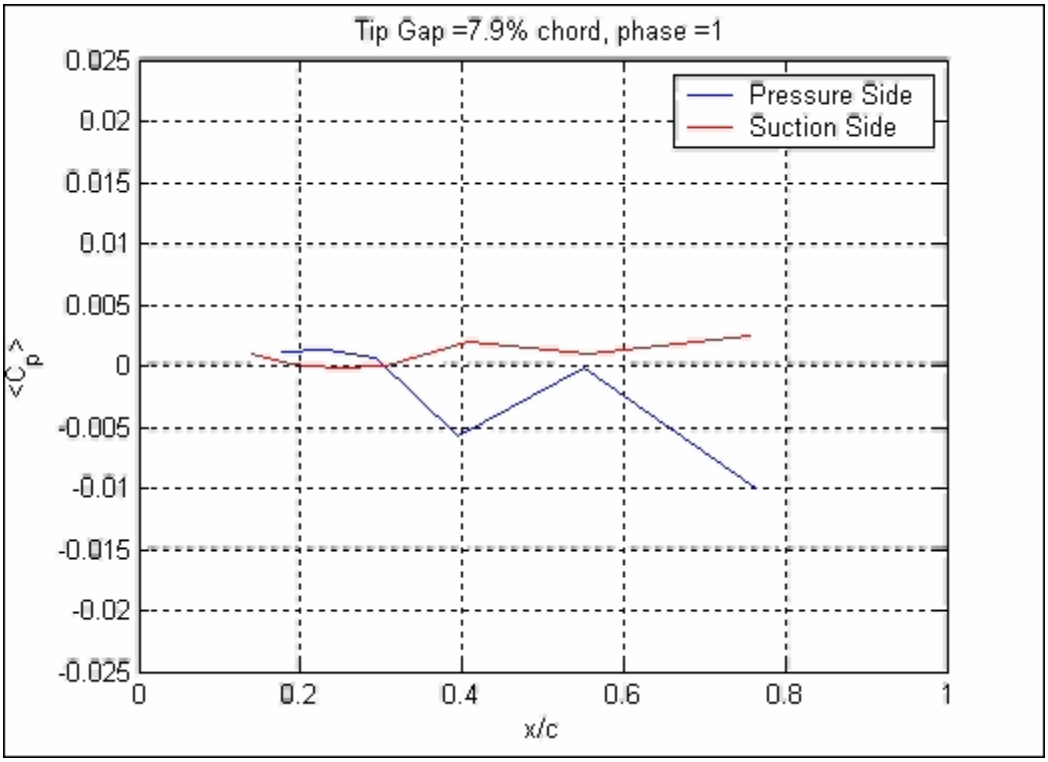

Figure 4.12 Movie of unsteady pressure fluctuation as a function of phase number along blade chord for baseline generator configuration for a tip clearance of 7.9%*c*.

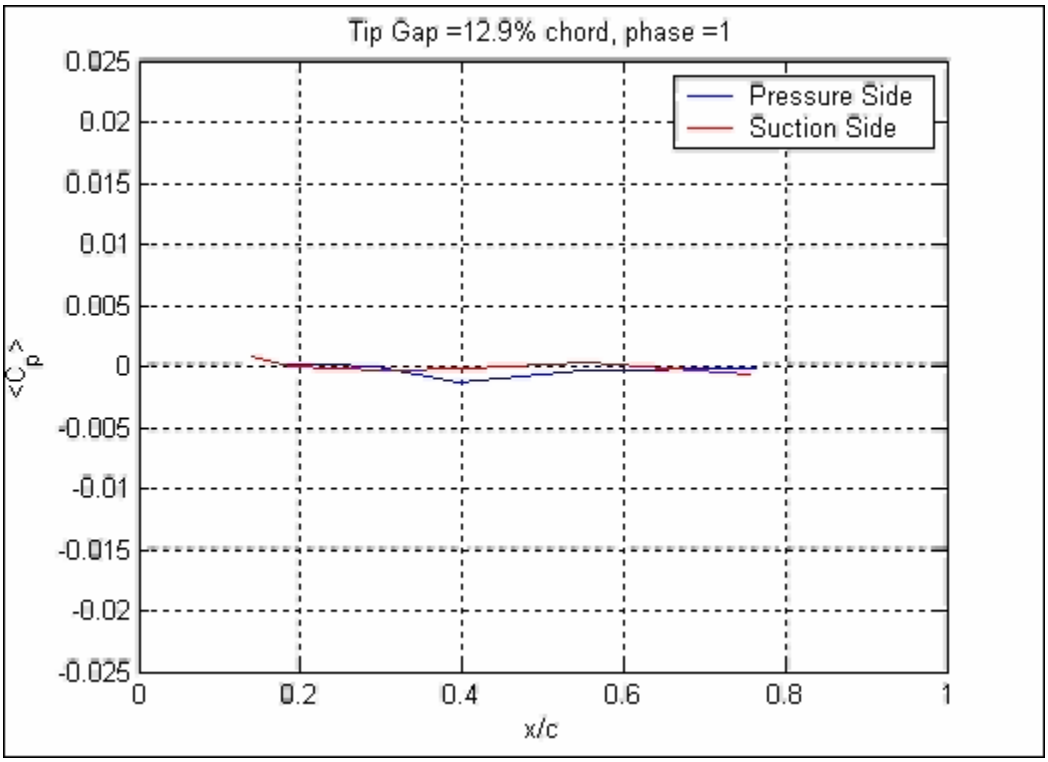

Figure 4.13 Movie of unsteady pressure fluctuation as a function of phase number along blade chord for baseline generator configuration for a tip clearance of 12.9%*c*.

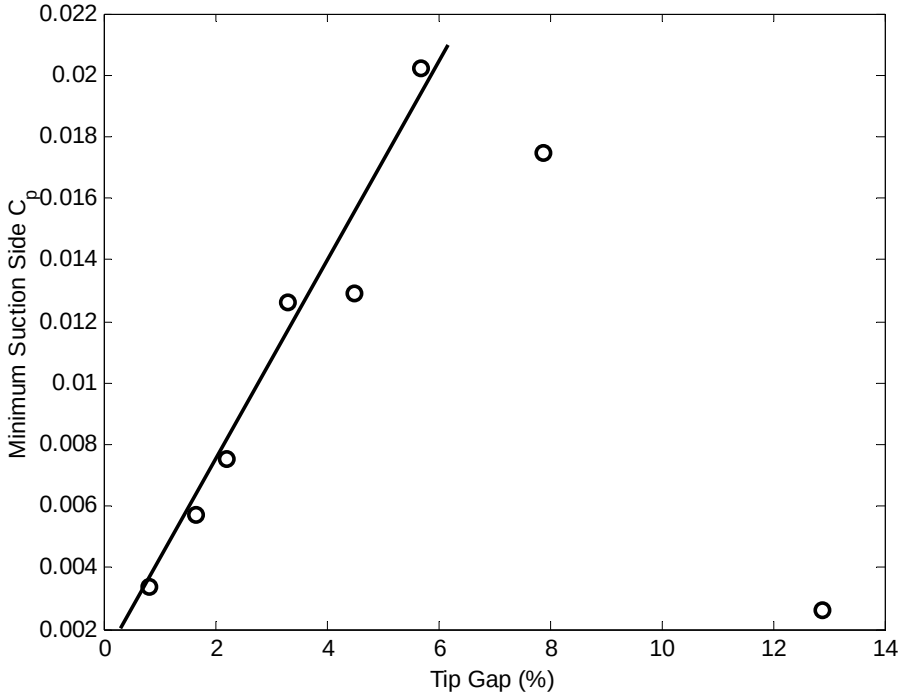

Figure 4.14 Minimum suction side C_p as a function of tip clearance.

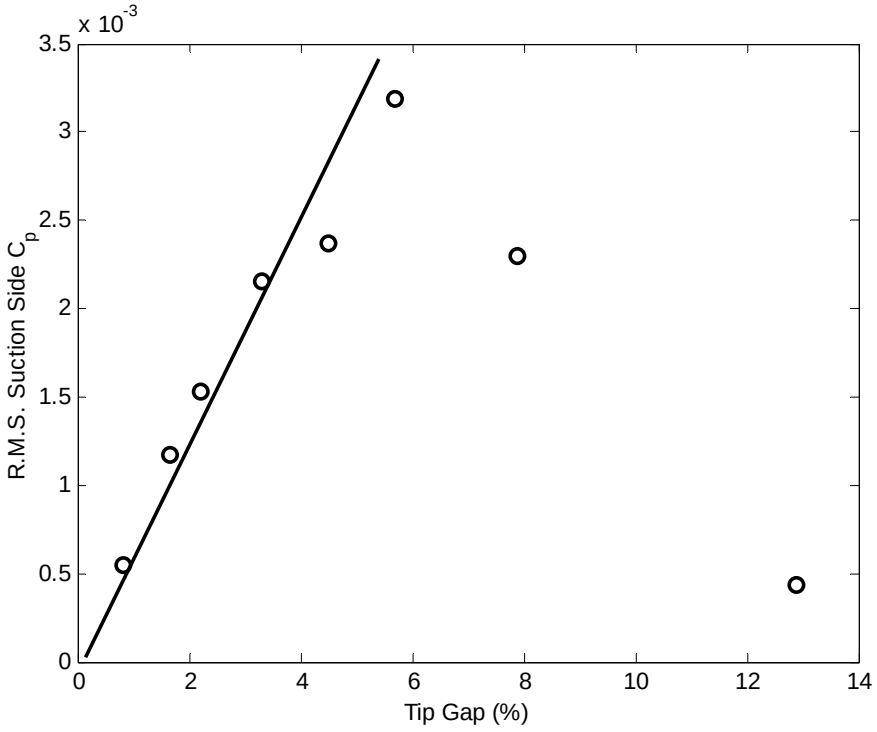

Figure 4.15 r.m.s suction side C_p as a function of tip clearance.

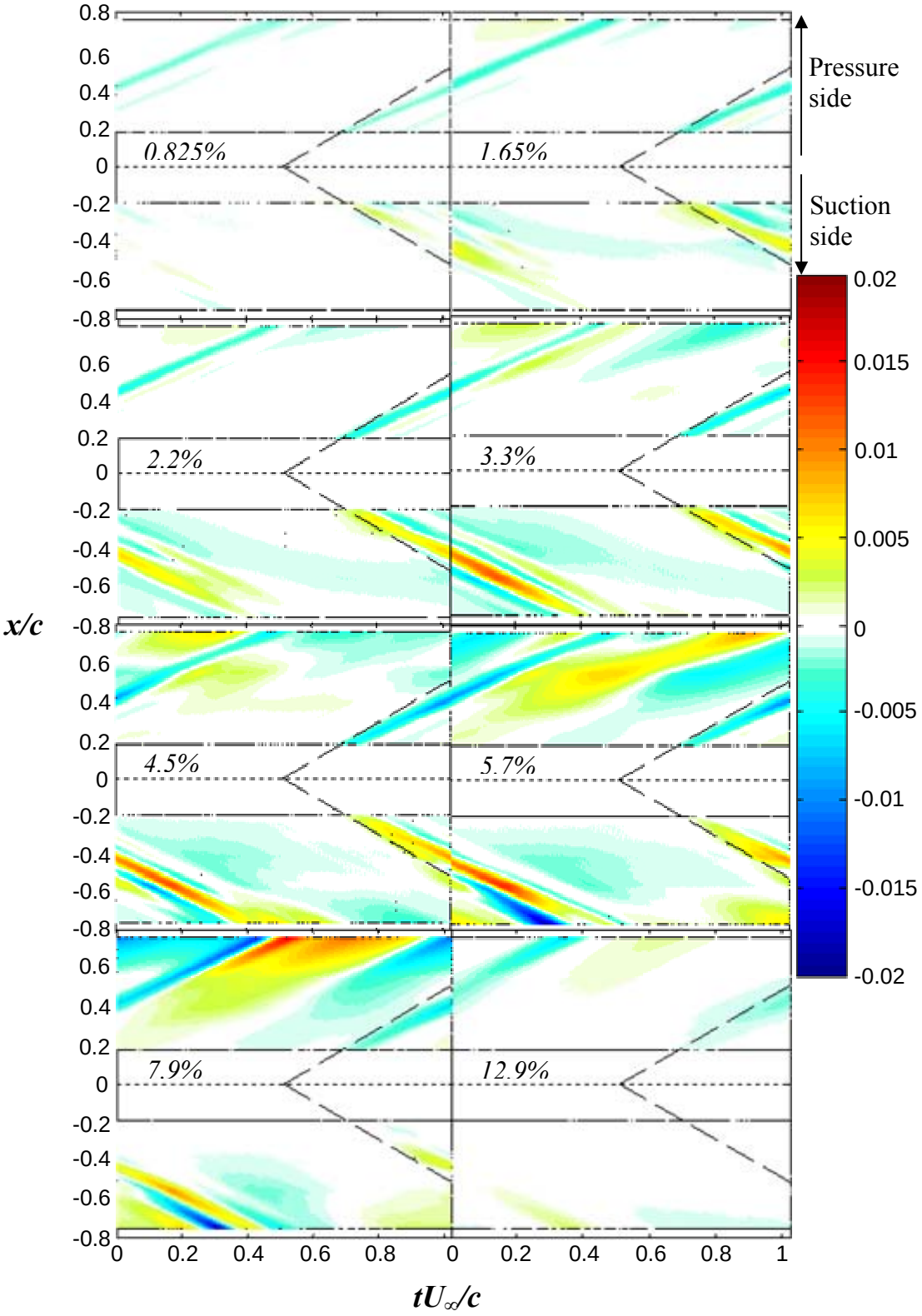

Figure 4.16 Chordwise pressure coefficient (C_p) contours for microphones on pressure and suction sides of blade for baseline configuration.

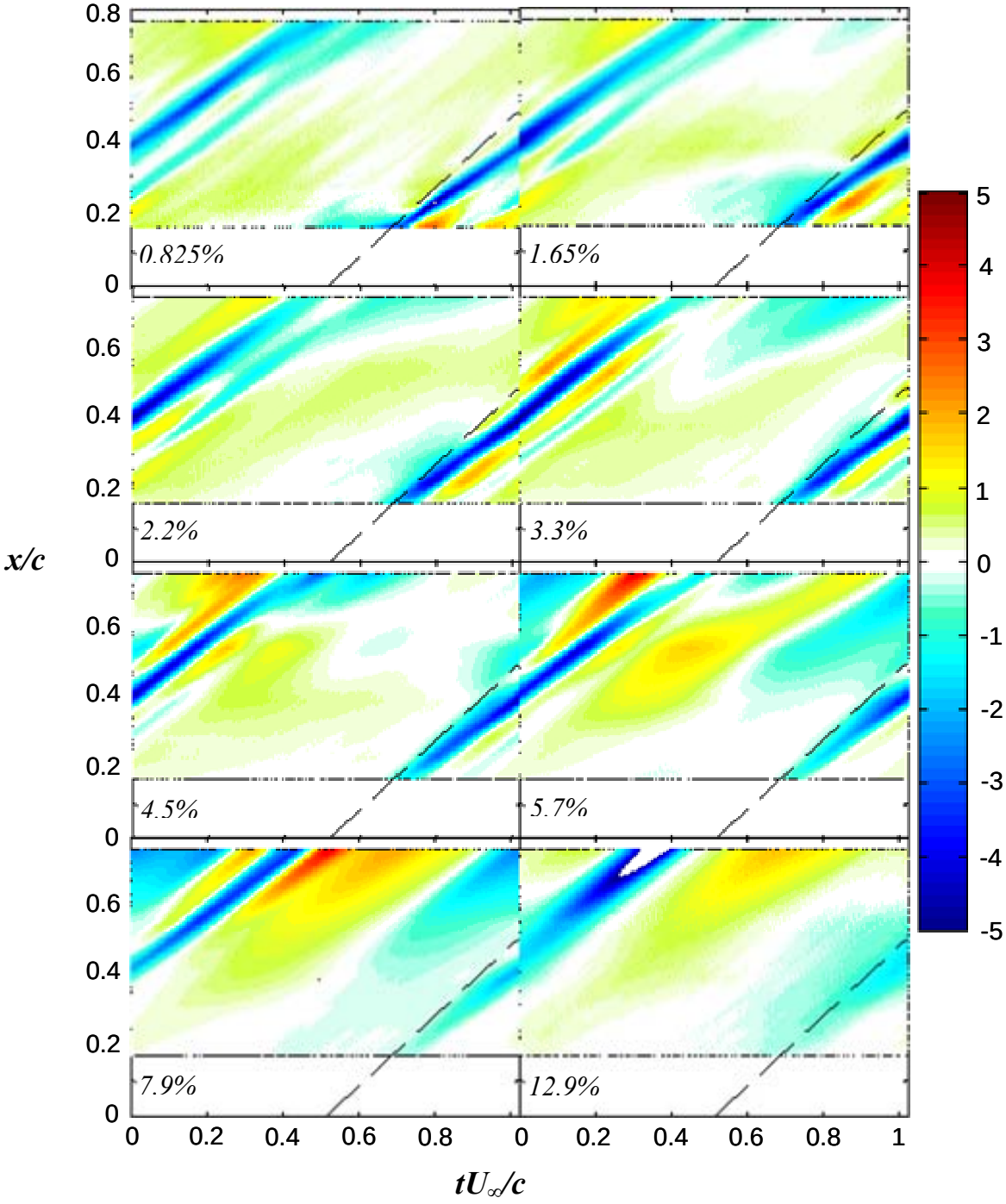

Figure 4.17 Pressure difference across blade tip normalized on the r.m.s. pressure difference across the blade tip for the baseline configuration.

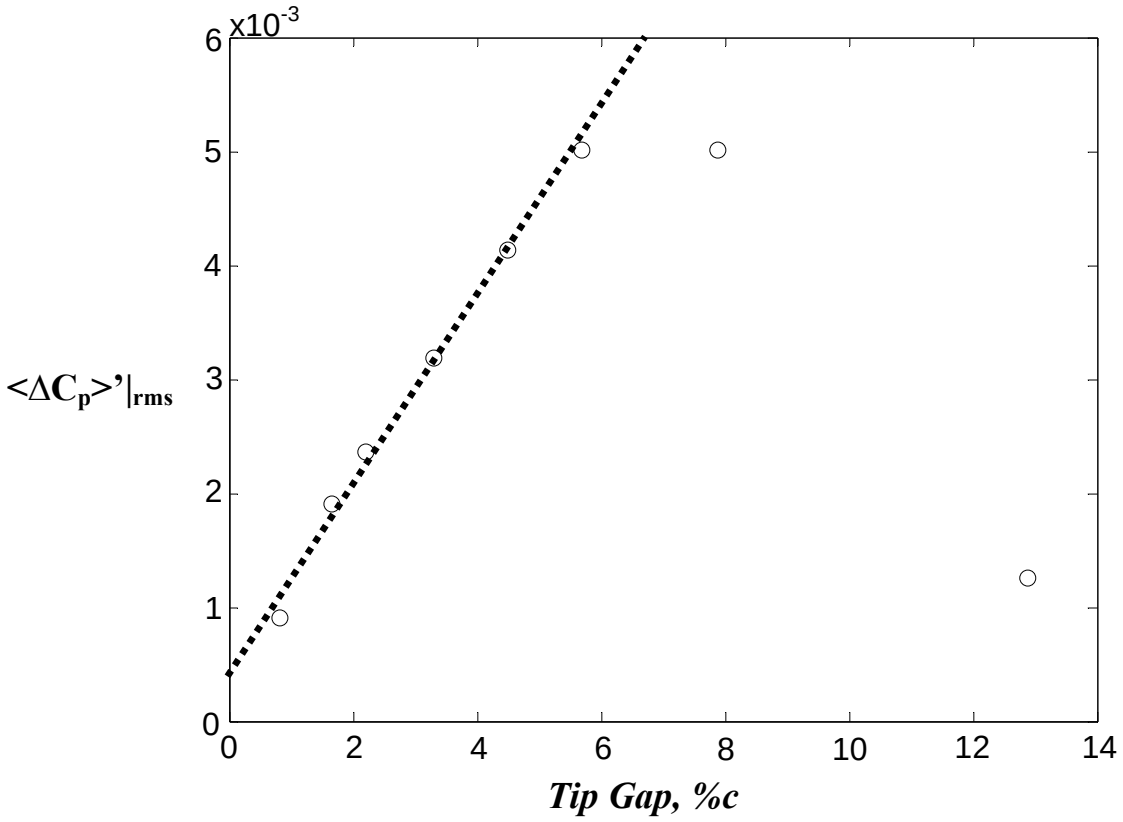

Figure 4.18 Scaled tip loading versus tip gap for baseline configuration.

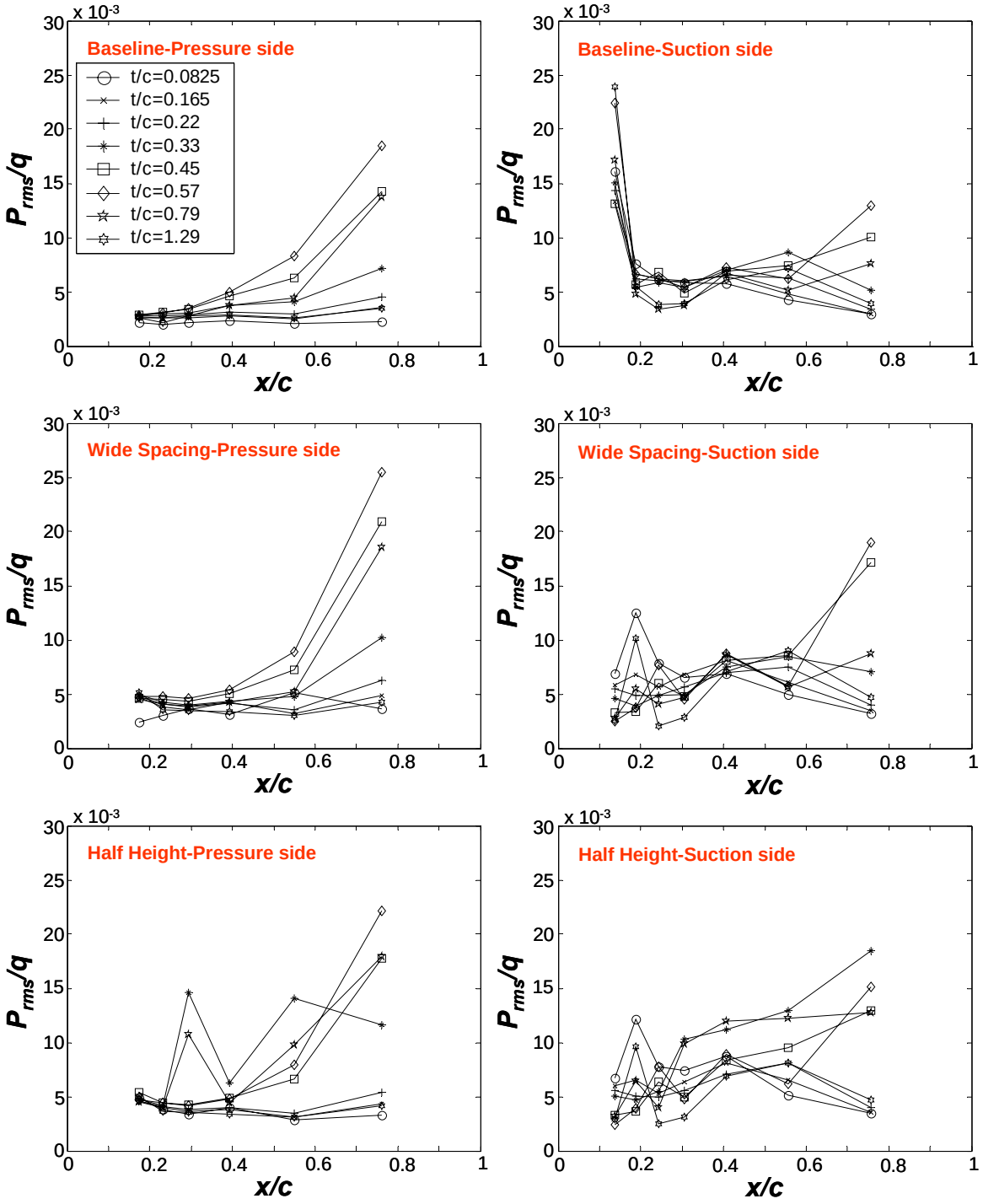

Figure 4.19 Normalized p_{rms} along the blade chord for the pressure and suction side of the blade as a function of tip clearance for baseline generator configuration, widely spaced generators, and half-height generators.

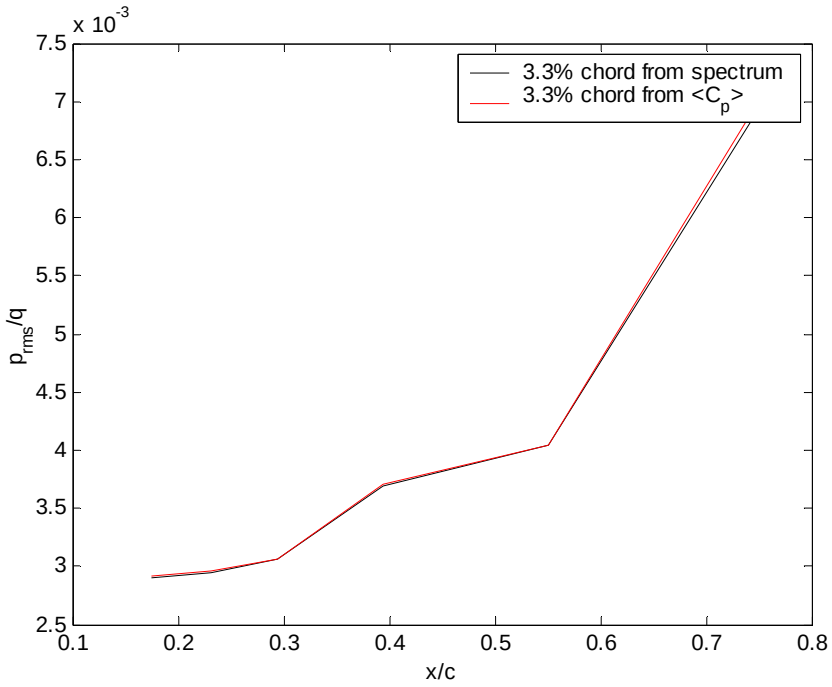

Figure 4.20 Comparison of chordwise p_{rms} on the pressure side of the blade calculated from spectra and from phase averaged $<C_p>$ at a tip clearance of 3.3%c.

Figure 4.21 Comparison of chordwise p_{rms} on the suction side of the blade calculated from spectra and from phase averaged $<C_p>$ at a tip clearance of 3.3%c.

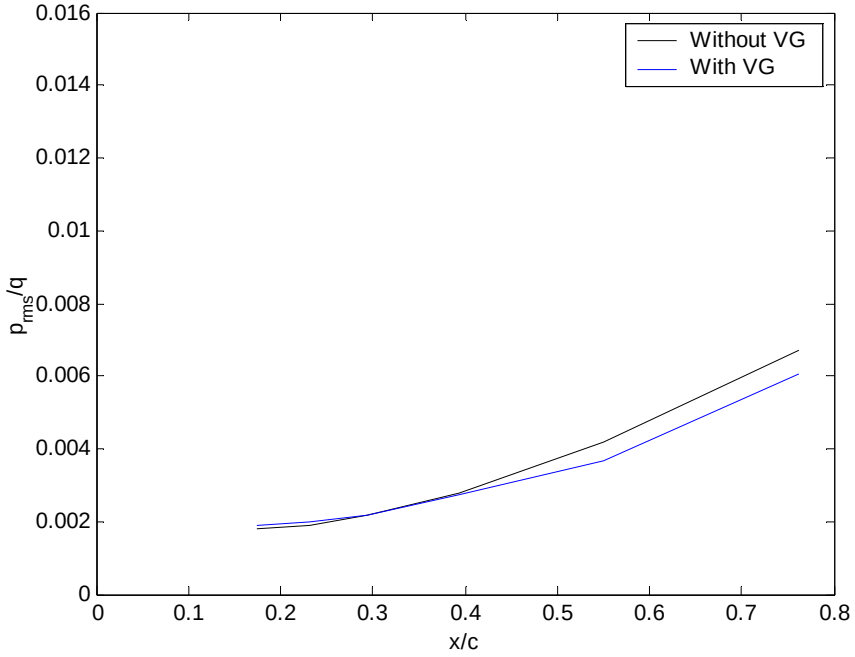

Figure 4.22 Comparison of chordwise p_{rms} on the pressure side of the blade calculated from the spectra for the moving wall with no generator case and the moving wall with generator case for a tip clearance of 3.3%*c*.

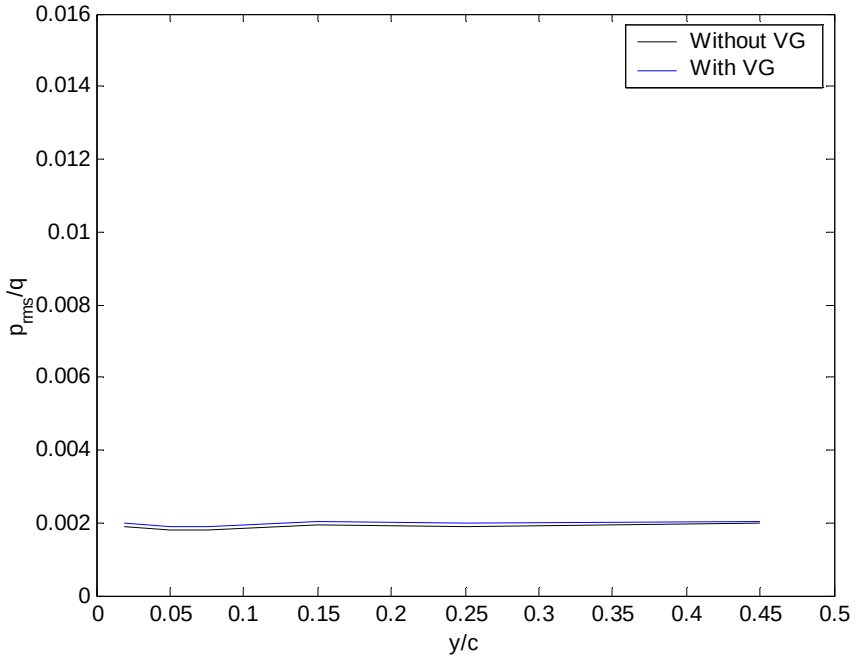

Figure 4.23 Comparison of spanwise p_{rms} on the pressure side of the blade calculated from the spectra for the moving wall with no generator case and the moving wall with generator case for a tip clearance of 3.3%*c*.

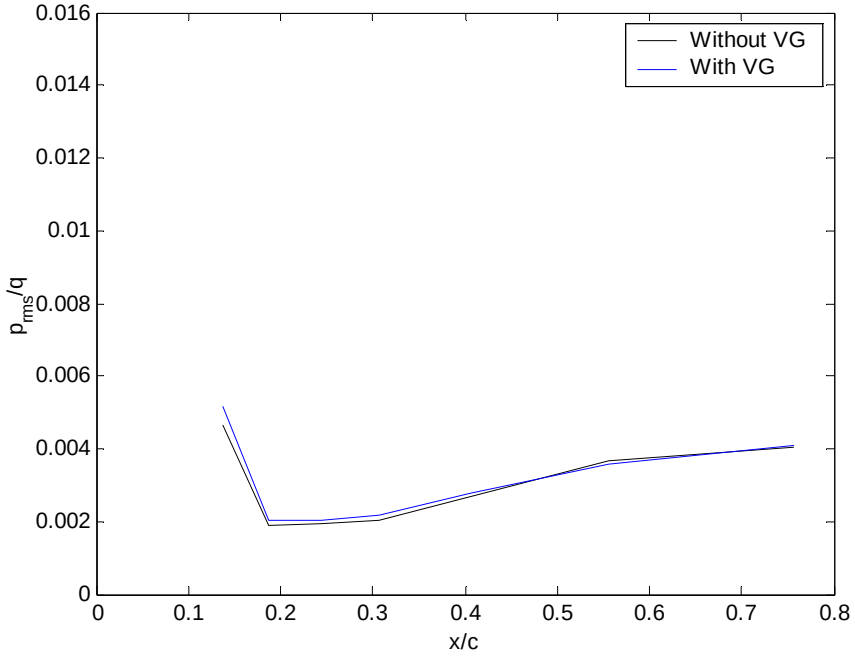

Figure 4.24 Comparison of chordwise p_{rms} on the suction side of the blade calculated from the spectra for the moving wall with no generator case and the moving wall with generator case for a tip clearance of 3.3%*c*.

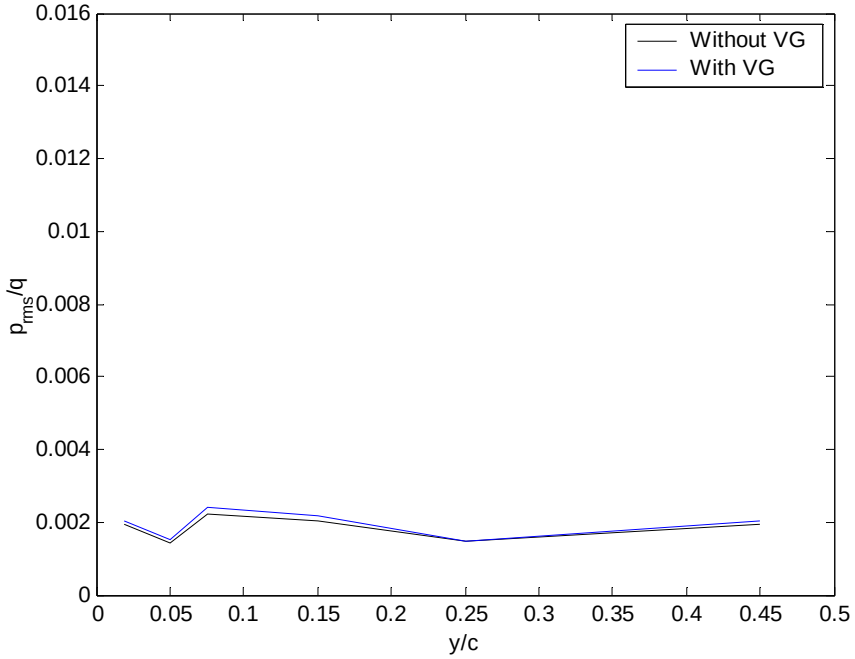

Figure 4.25 Comparison of spanwise p_{rms} on the suction side of the blade calculated from the spectra for the moving wall with no generator case and the moving wall with generator case for a tip clearance of 3.3%*c*.

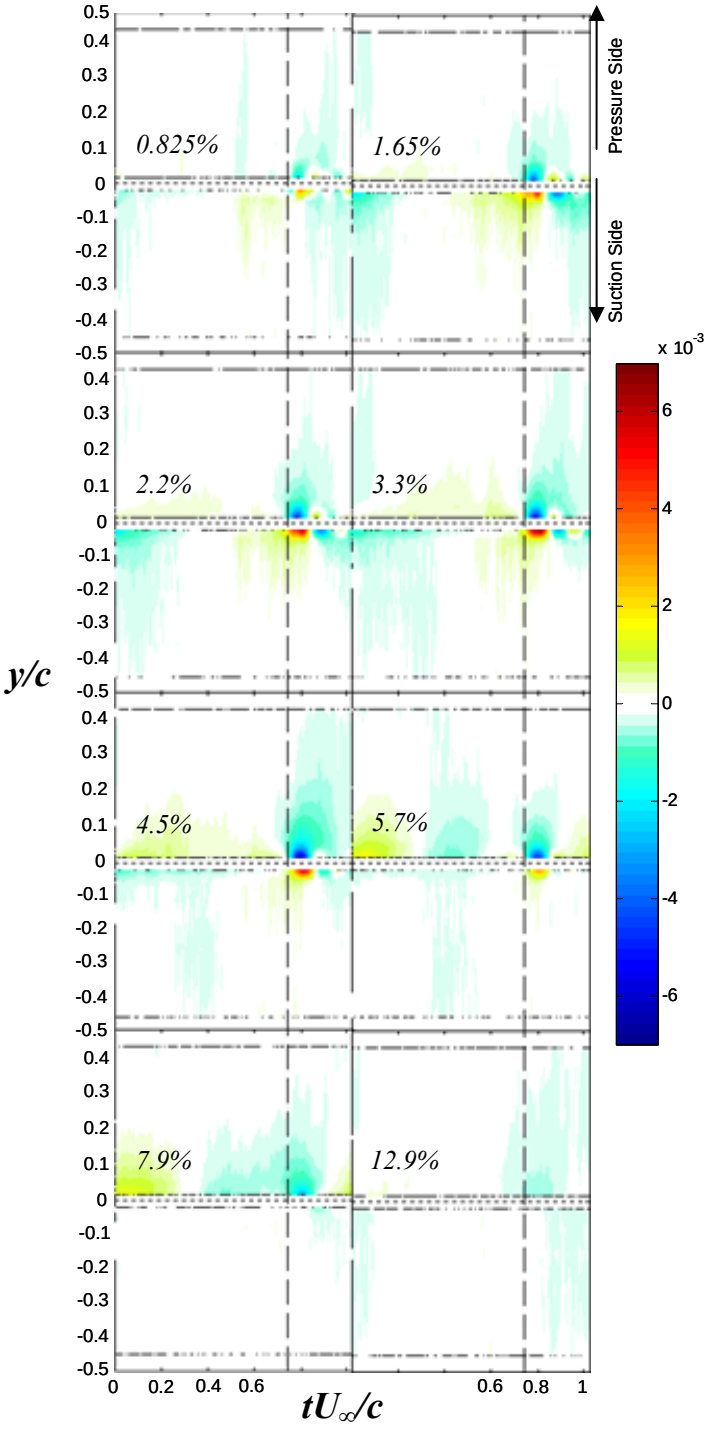

Figure 4.26 Spanwise pressure coefficient (C_p) contours for microphones on pressure and suction sides of blade for baseline configuration.

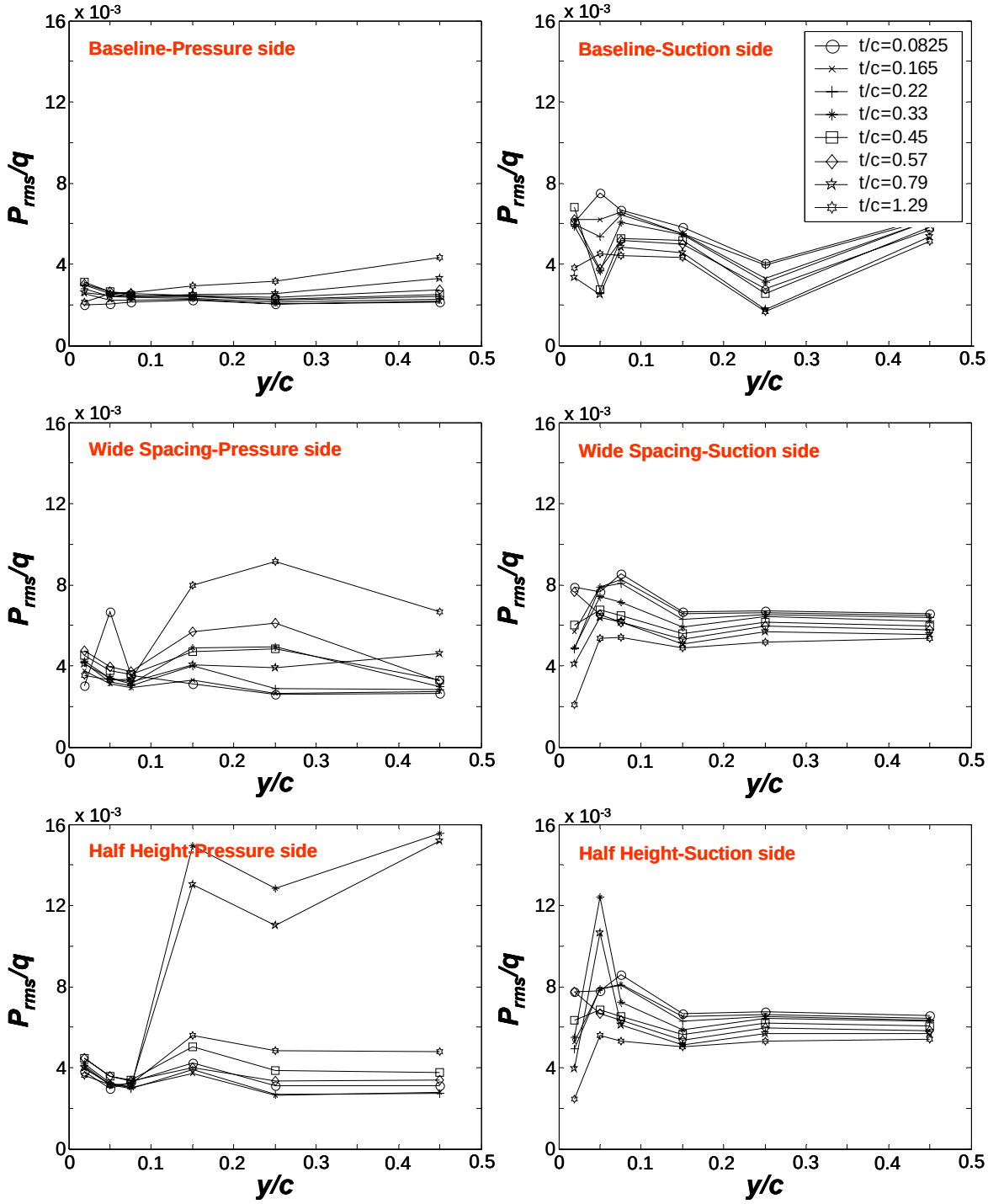

Figure 4.27 Normalized p_{rms} along the blade span for the pressure and suction side of the blade as a function of tip clearance for baseline generator configuration, widely spaced generators, and half-height generators.

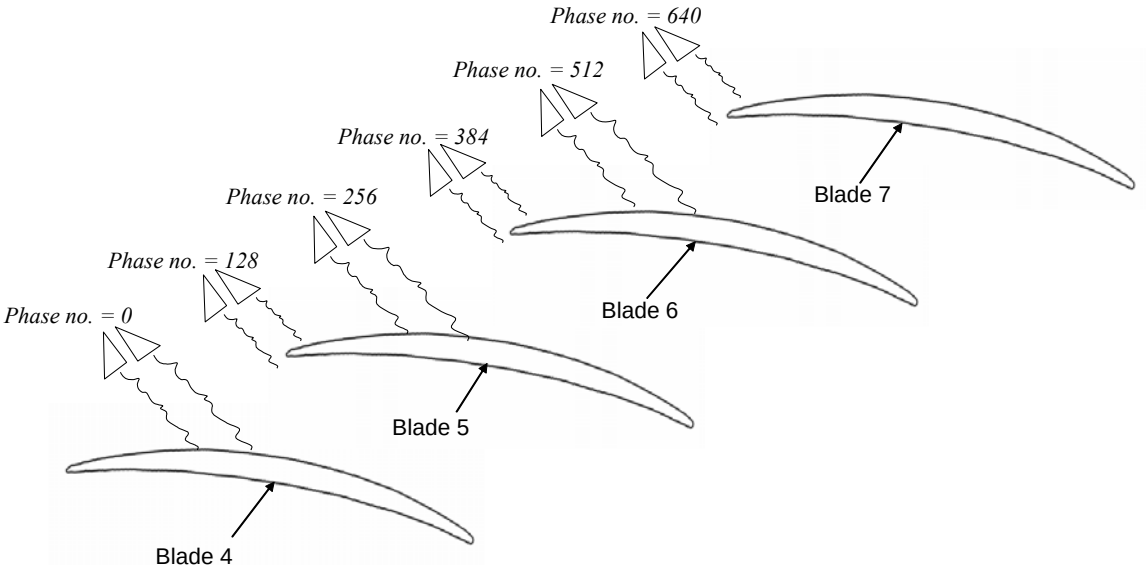

Figure 4.28 Phase numbers for widely spaced generators.

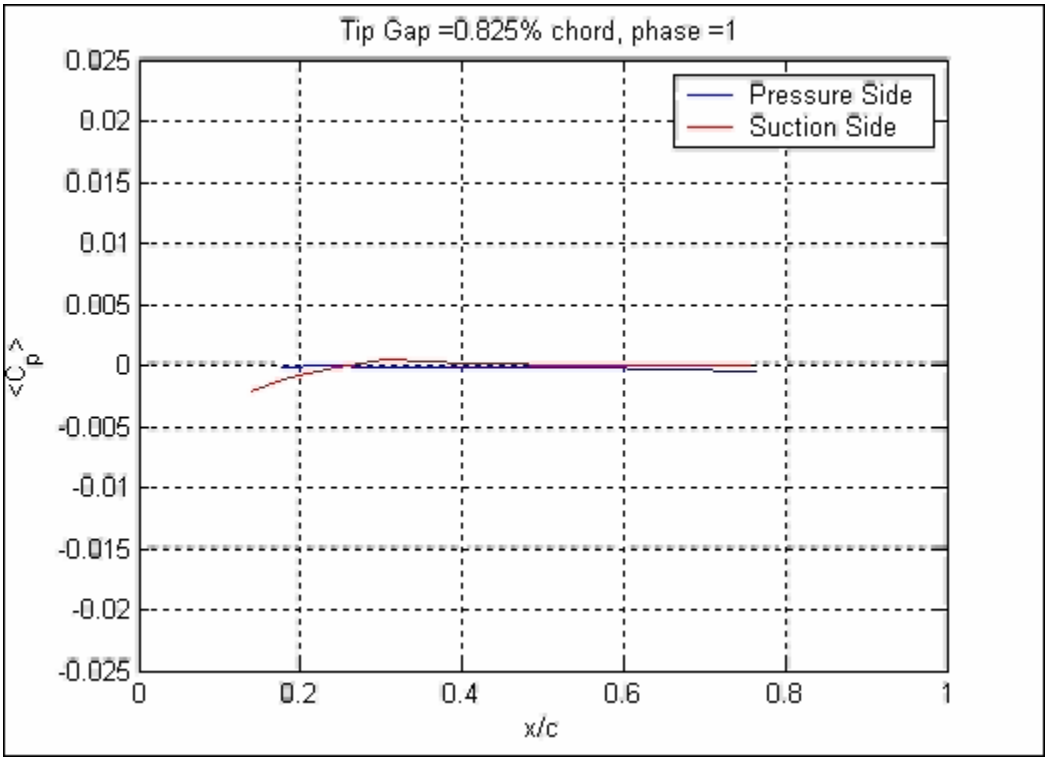

Figure 4.29 Movie of unsteady pressure fluctuation as a function of phase number along blade chord for widely spaced generators for a tip clearance of 0.825%*c*.

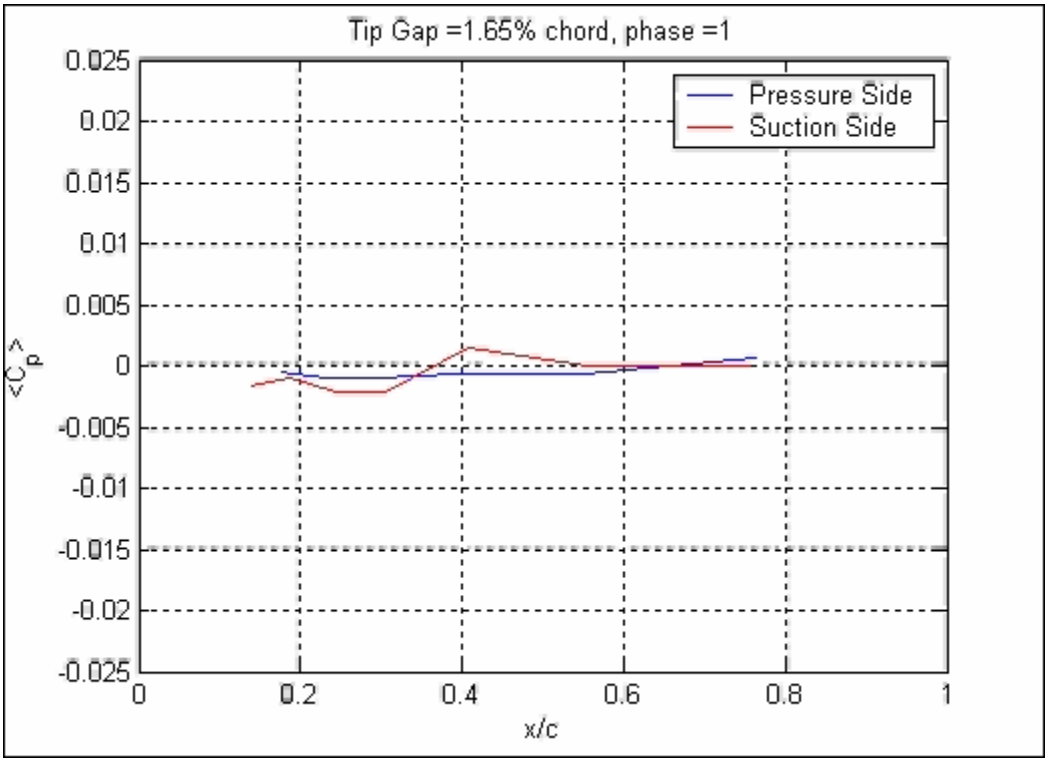

Figure 4.30 Movie of unsteady pressure fluctuation as a function of phase number along blade chord for widely spaced generators for a tip clearance of 1.65%*c*.

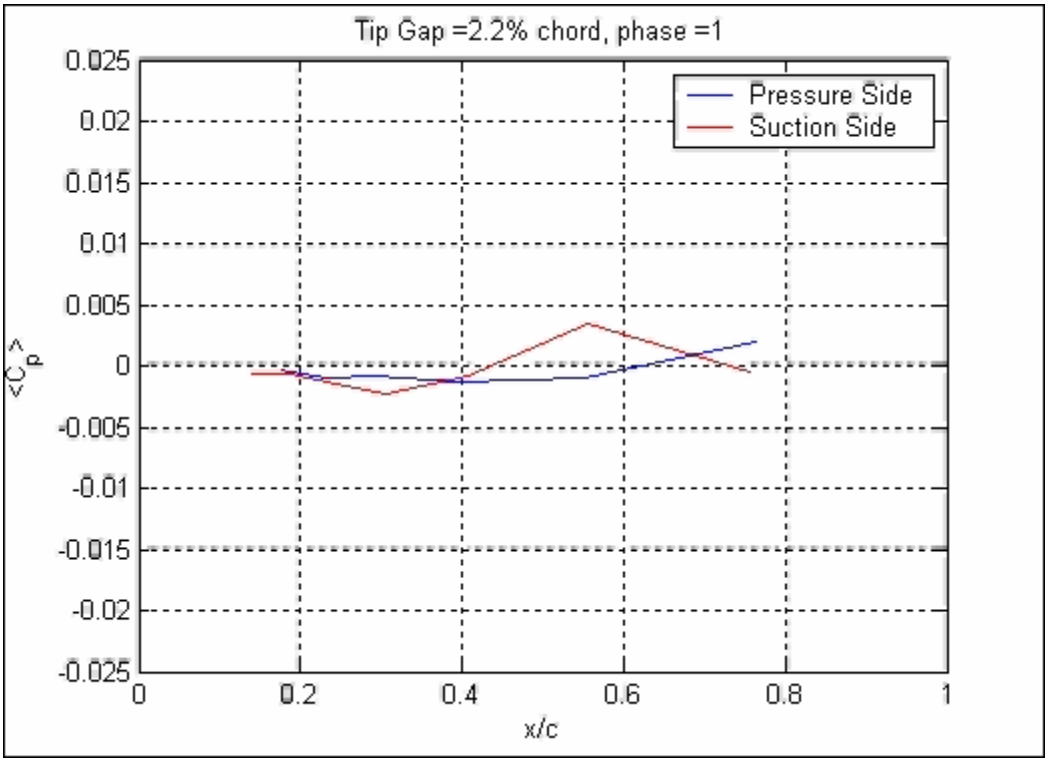

Figure 4.31 Movie of unsteady pressure fluctuation as a function of phase number along blade chord for widely spaced generators for a tip clearance of 2.2%*c*.

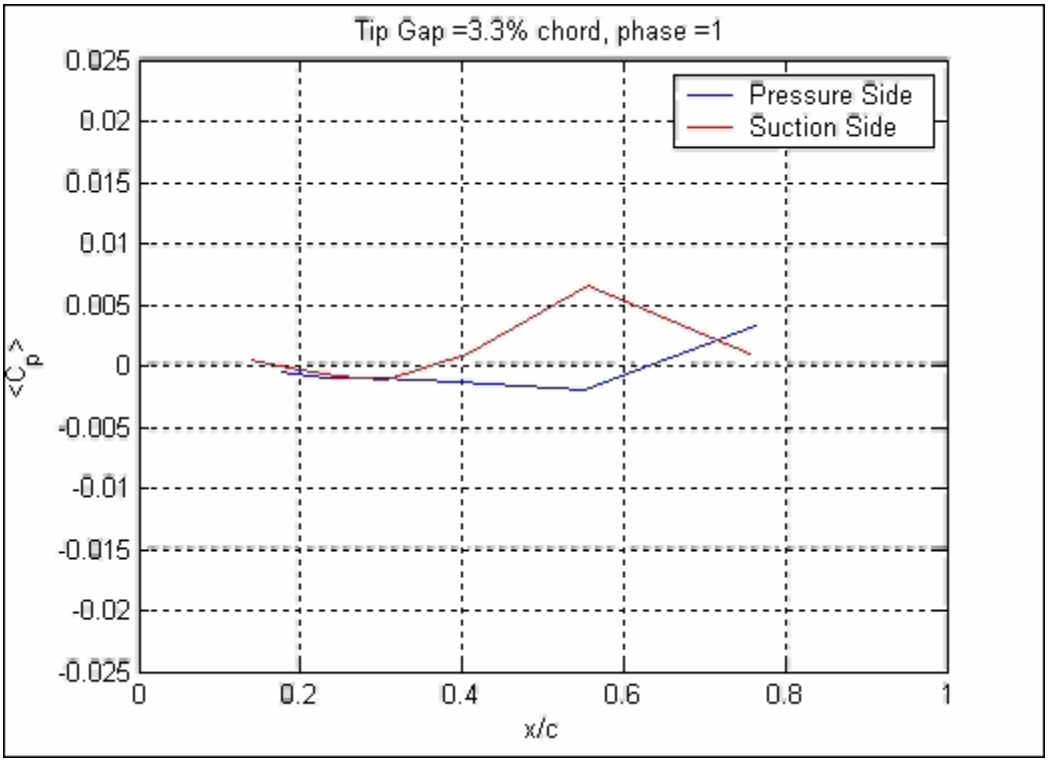

Figure 4.32 Movie of unsteady pressure fluctuation as a function of phase number along blade chord for widely spaced generators for a tip clearance of 3.3%*c*.

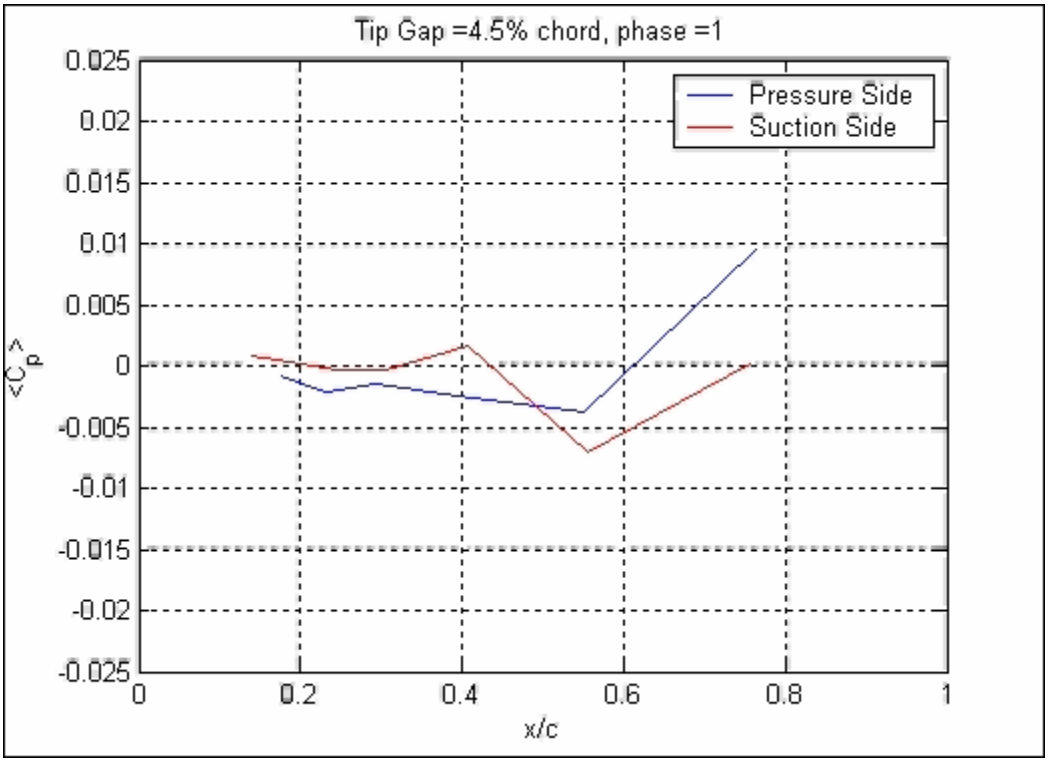

Figure 4.33 Movie of unsteady pressure fluctuation as a function of phase number along blade chord for widely spaced generators for a tip clearance of 4.5%*c*.

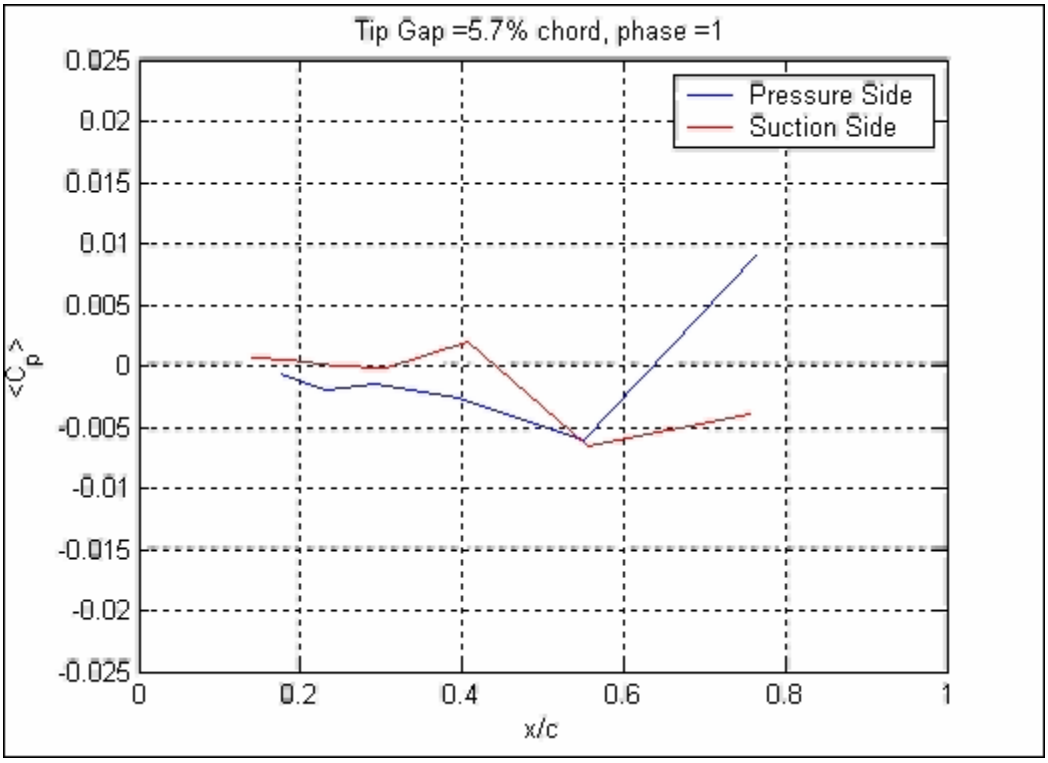

Figure 4.34 Movie of unsteady pressure fluctuation as a function of phase number along blade chord for widely spaced generators for a tip clearance of 5.7%*c*.

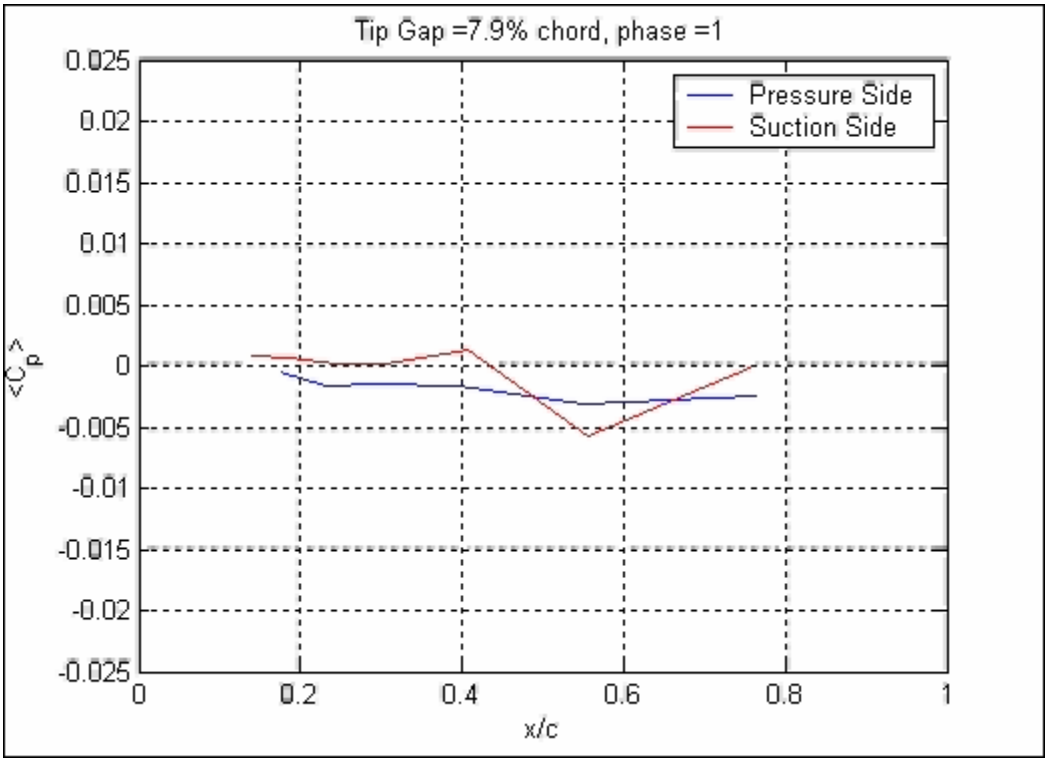

Figure 4.35 Movie of unsteady pressure fluctuation as a function of phase number along blade chord for widely spaced generators for a tip clearance of 7.9%*c*.

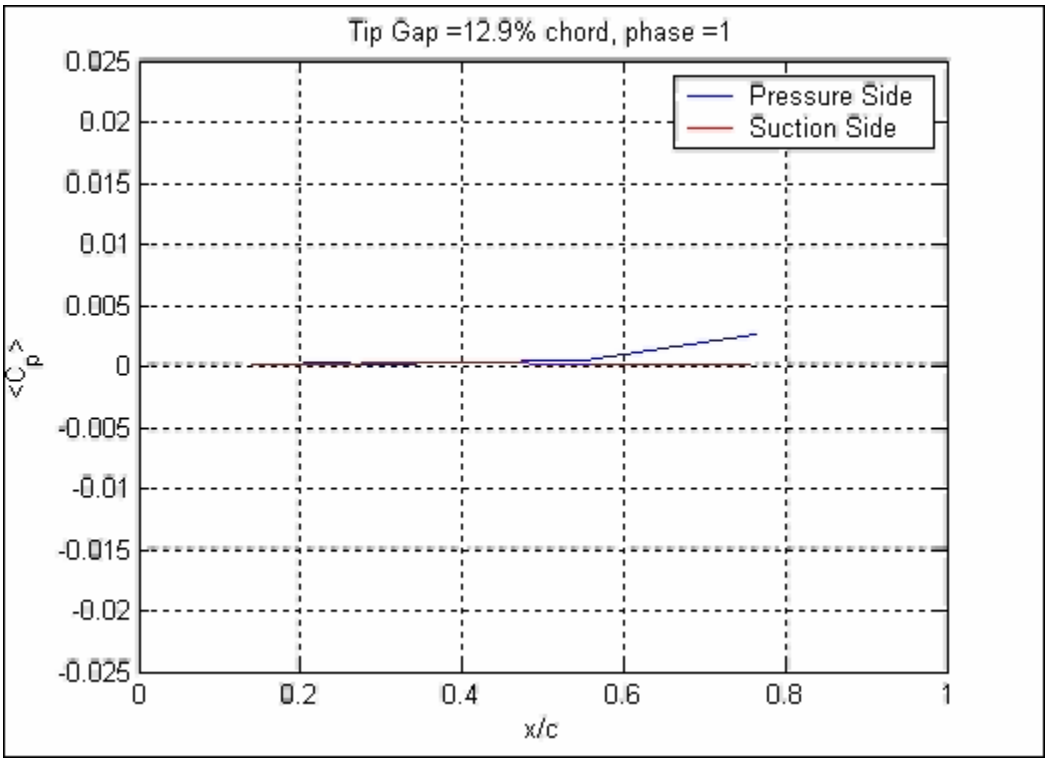

Figure 4.36 Movie of unsteady pressure fluctuation as a function of phase number along blade chord for widely spaced generators for a tip clearance of 12.9%*c*.

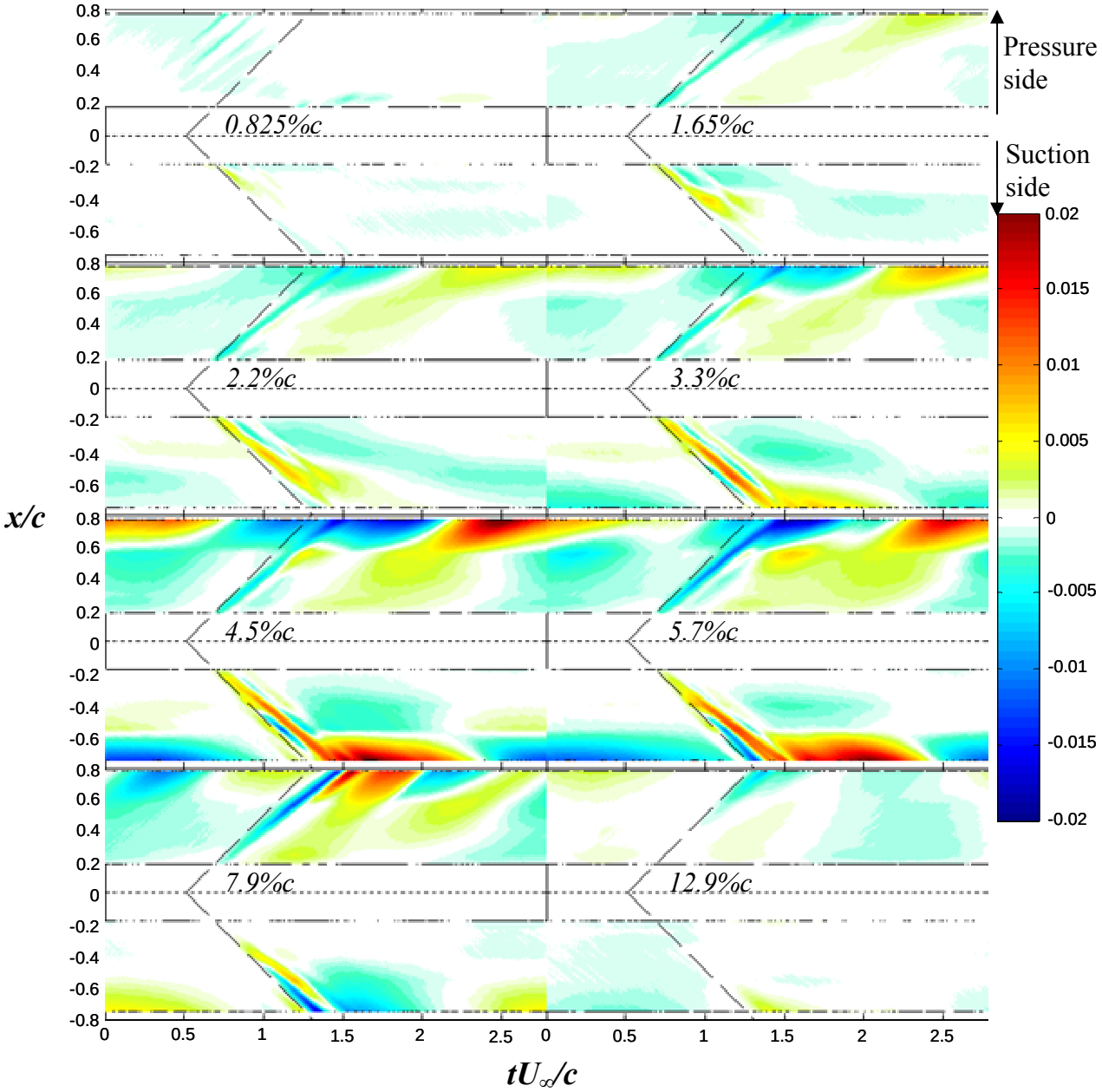

Figure 4.37 Chordwise pressure coefficient (C_p) contours for microphones on pressure and suction sides of blade for new generator spacing.

.

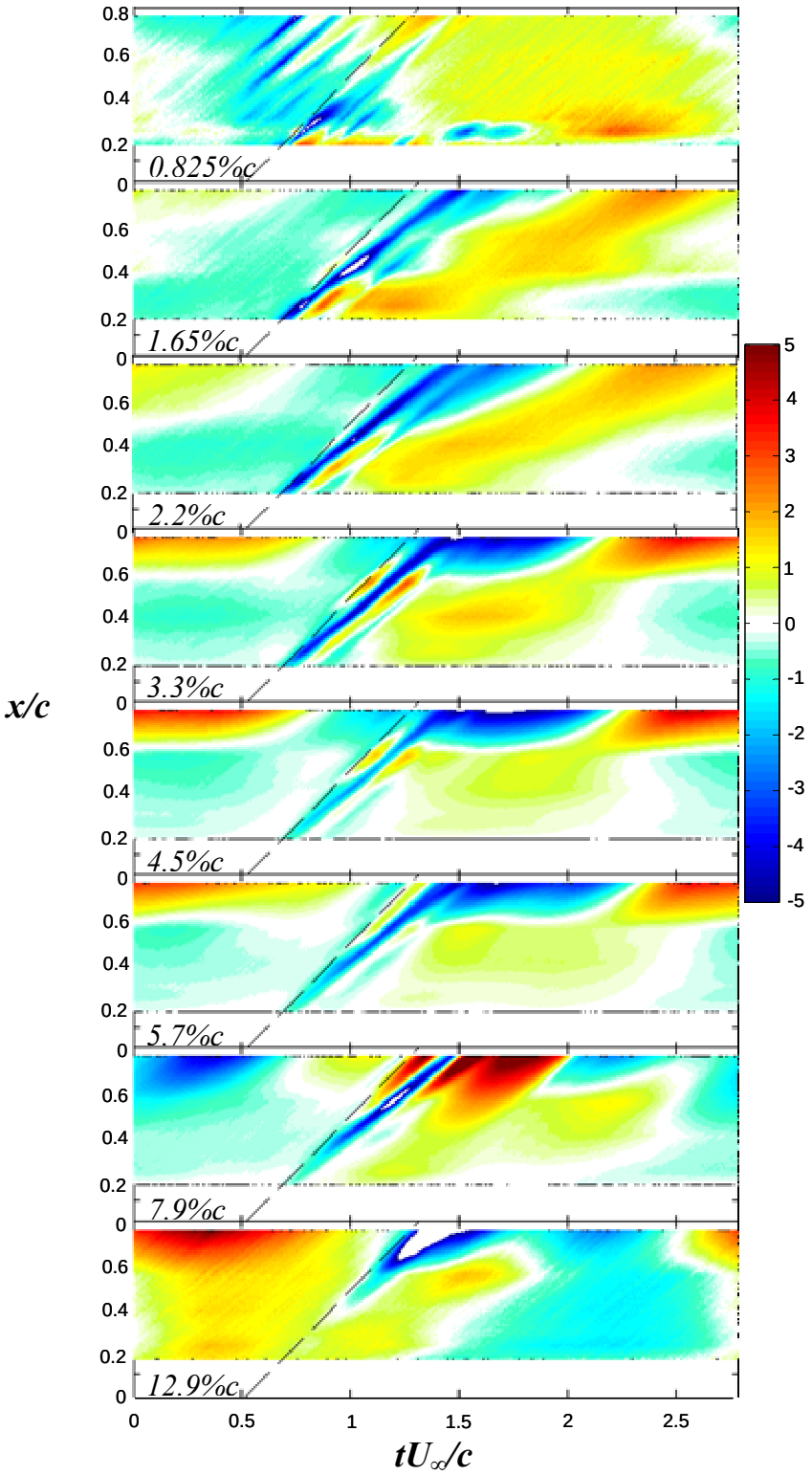

Figure 4.38 Pressure difference across blade tip normalized on the r.m.s. pressure difference across the blade tip for the new generator spacing.

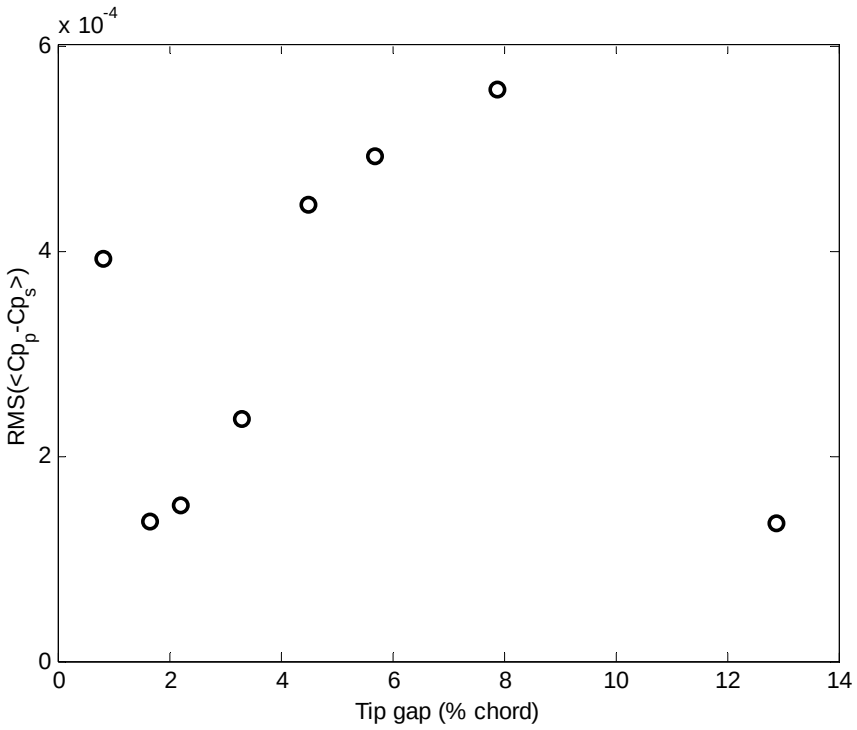

Figure 4.39 Scaled tip loading versus tip gap for widely spaced generators.

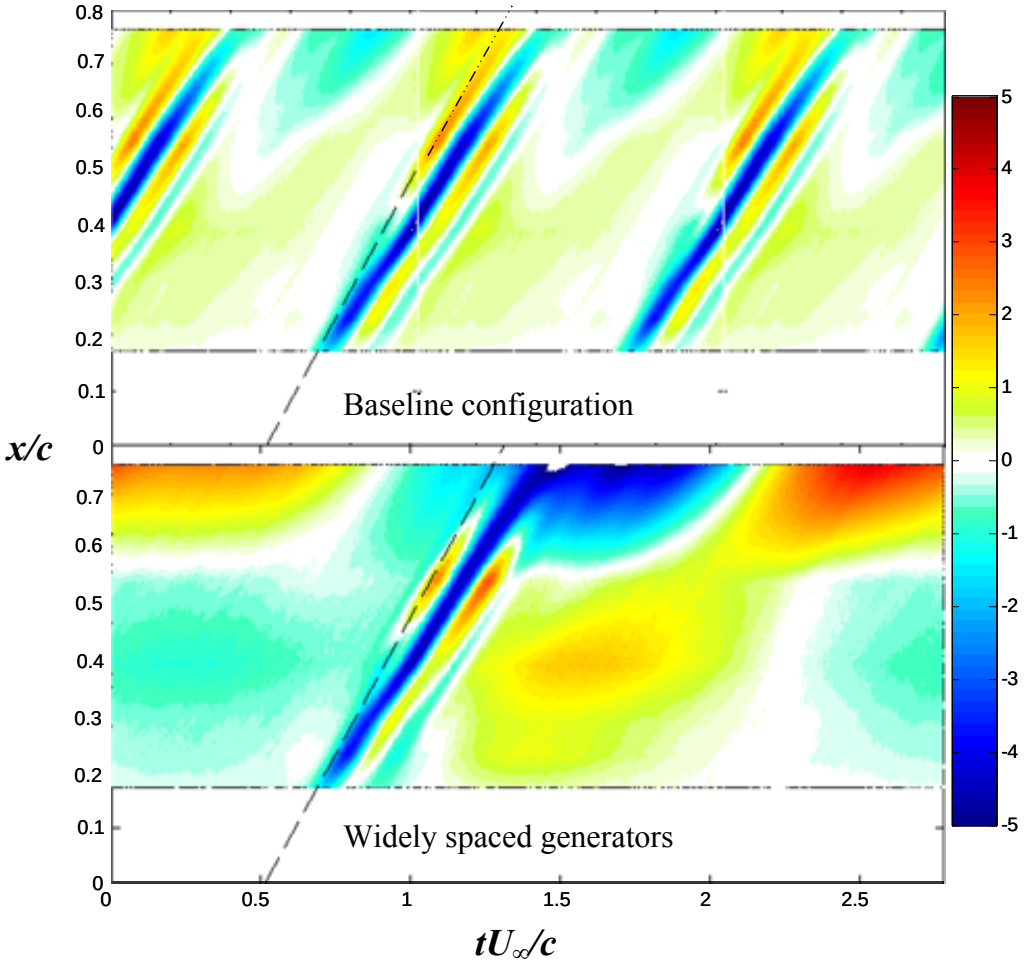

Figure 4.40 Comparison of baseline generator configuration and widely spaced generator pressure difference across blade tip normalized on the r.m.s. pressure difference across the blade tip.

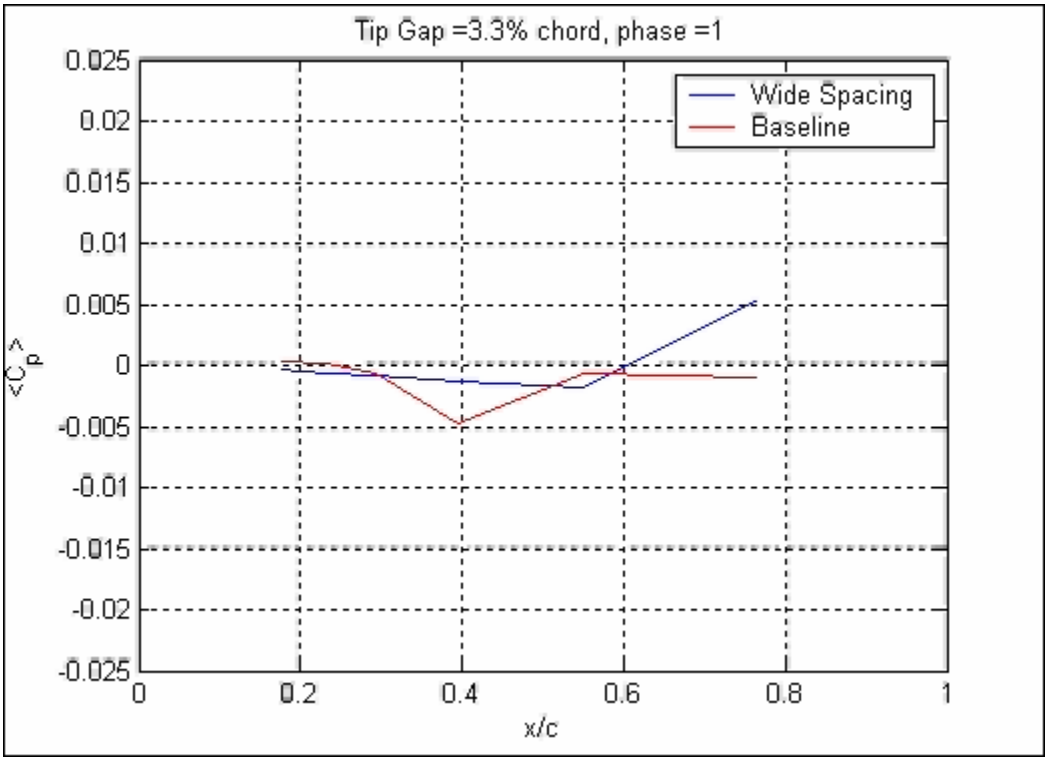

Figure 4.41 Movie of unsteady pressure fluctuation on the pressure side of the blade as a function of phase number along blade chord for widely spaced generators and baseline generator configuration for a tip clearance of 3.3%*c*.

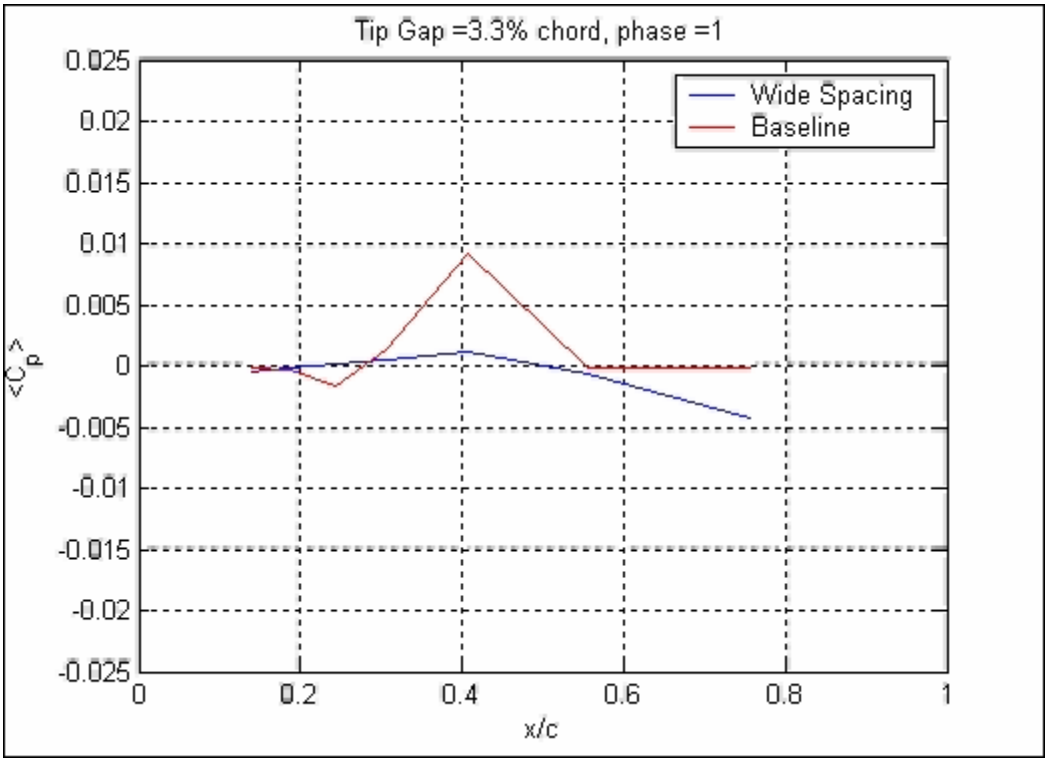

Figure 4.42 Movie of unsteady pressure fluctuation on the suction side of the blade as a function of phase number along blade chord for widely spaced generators and baseline generator configuration for a tip clearance of 3.3%*c*.

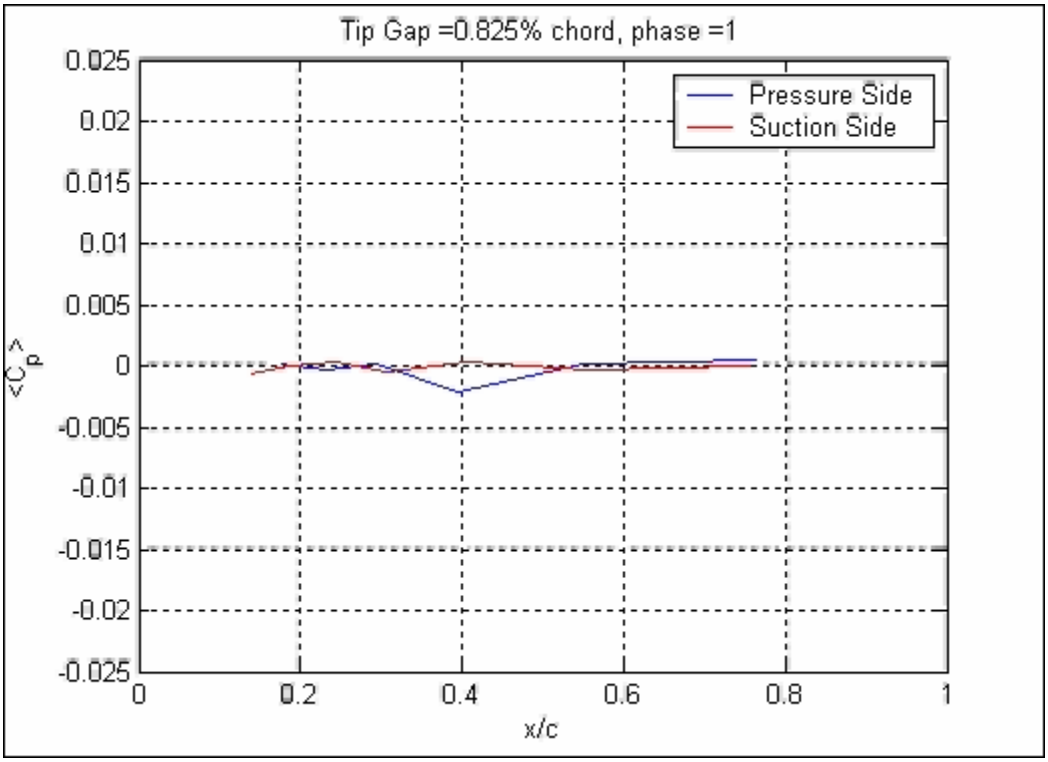

Figure 4.43 Movie of unsteady pressure fluctuation as a function of phase number along blade chord for half-height generators for a tip clearance of 0.825%*c*.

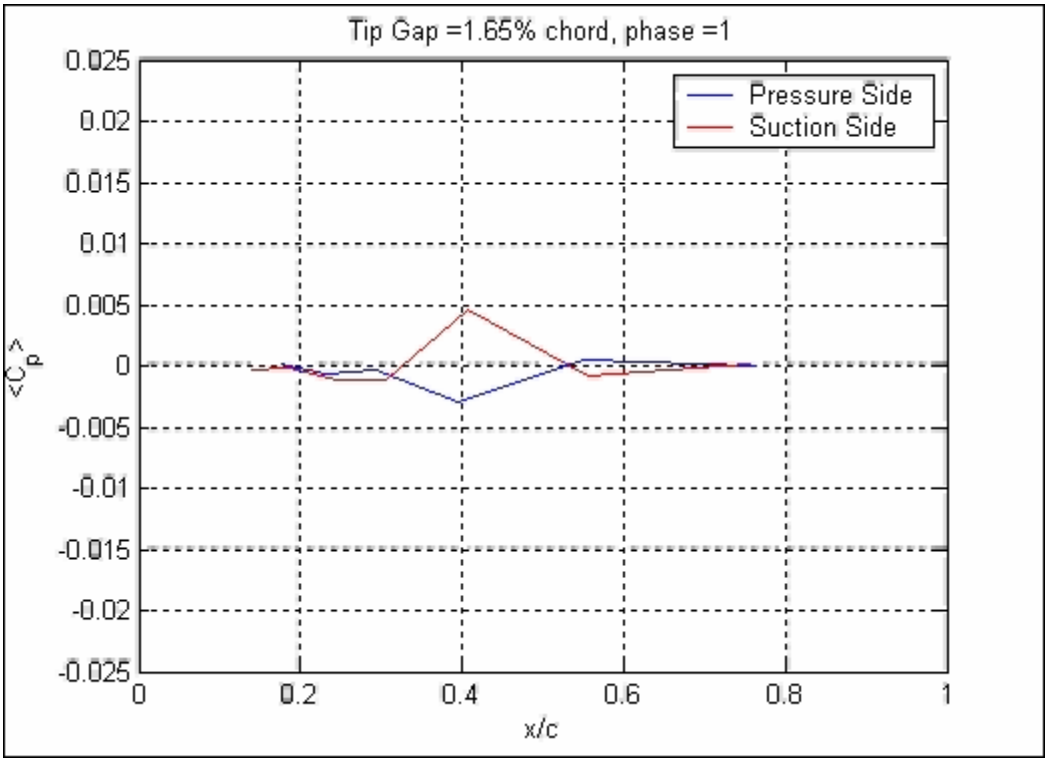

Figure 4.44 Movie of unsteady pressure fluctuation as a function of phase number along blade chord for half-height generators for a tip clearance of 1.65%*c*.

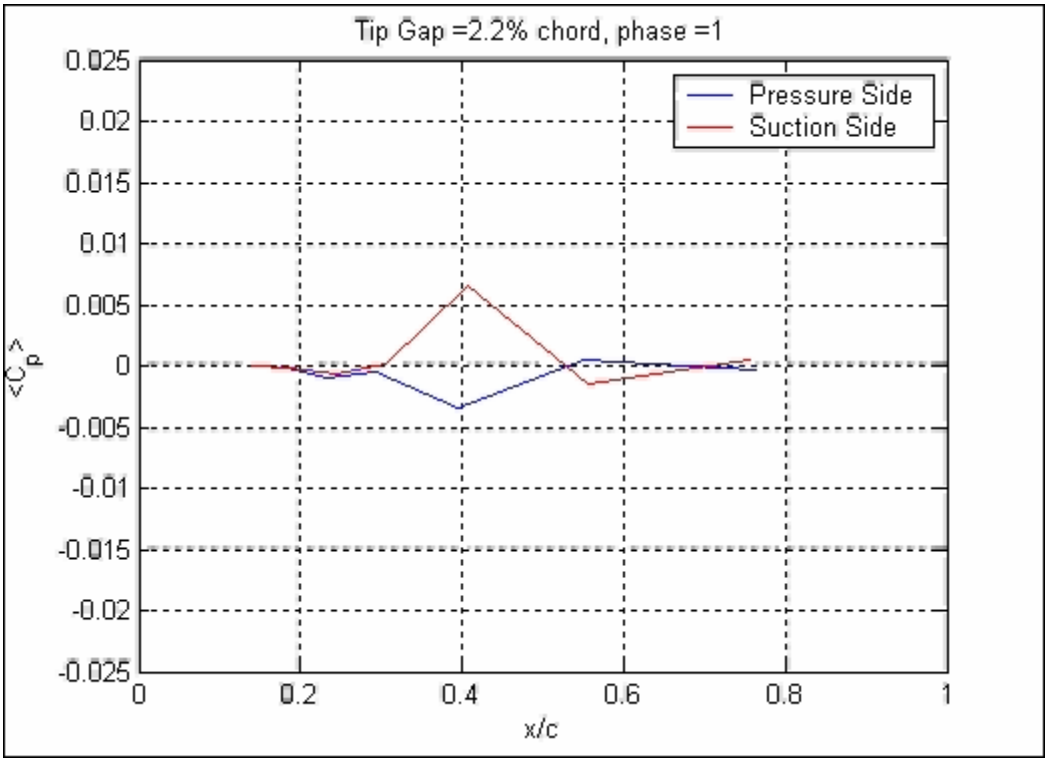

Figure 4.45 Movie of unsteady pressure fluctuation as a function of phase number along blade chord for half-height generators for a tip clearance of 2.2%*c*.

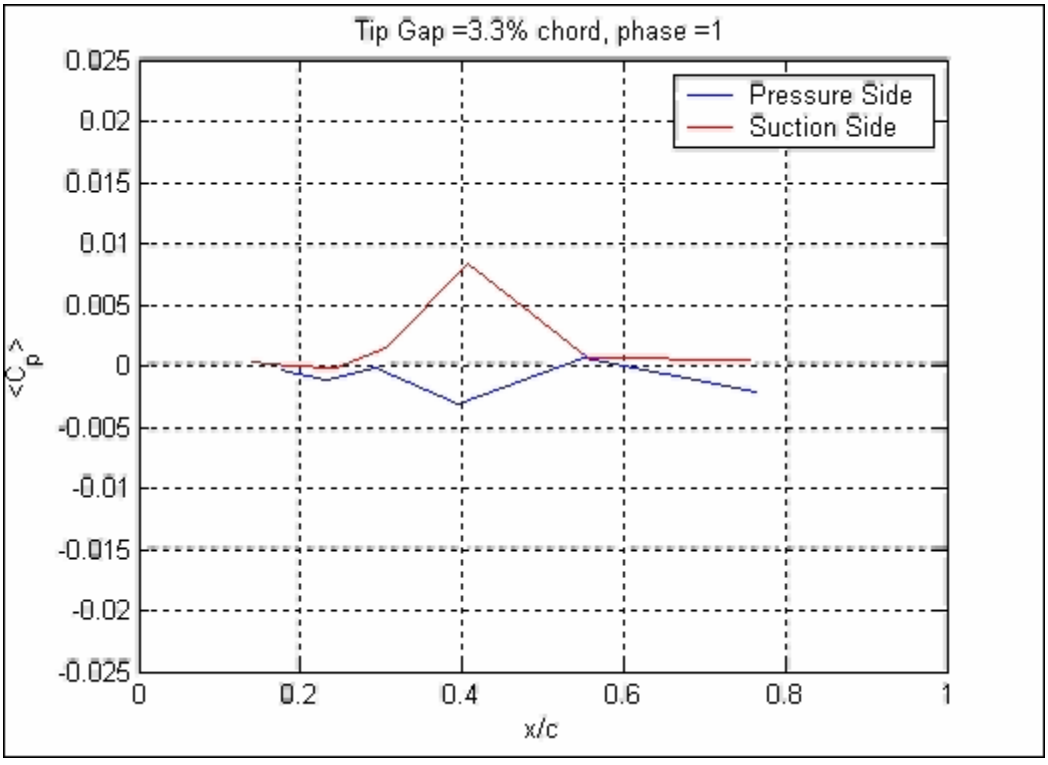

Figure 4.46 Movie of unsteady pressure fluctuation as a function of phase number along blade chord for half-height generators for a tip clearance of 3.3%*c*.

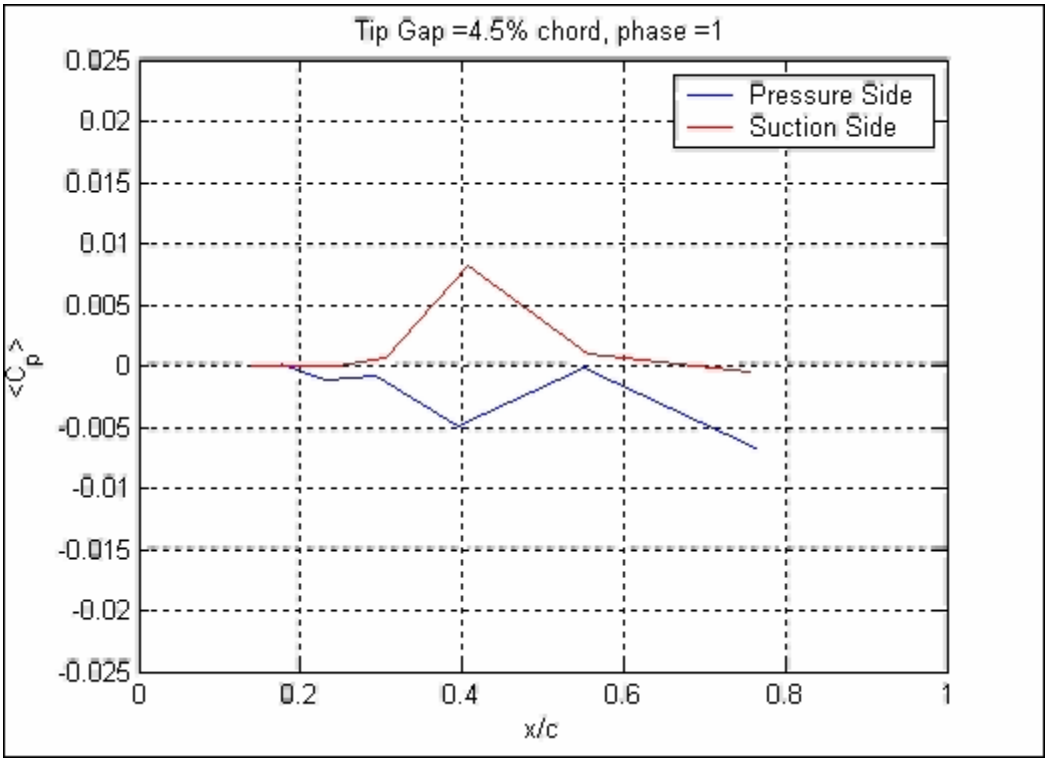

Figure 4.47 Movie of unsteady pressure fluctuation as a function of phase number along blade chord for half-height generators for a tip clearance of 4.5%*c*.

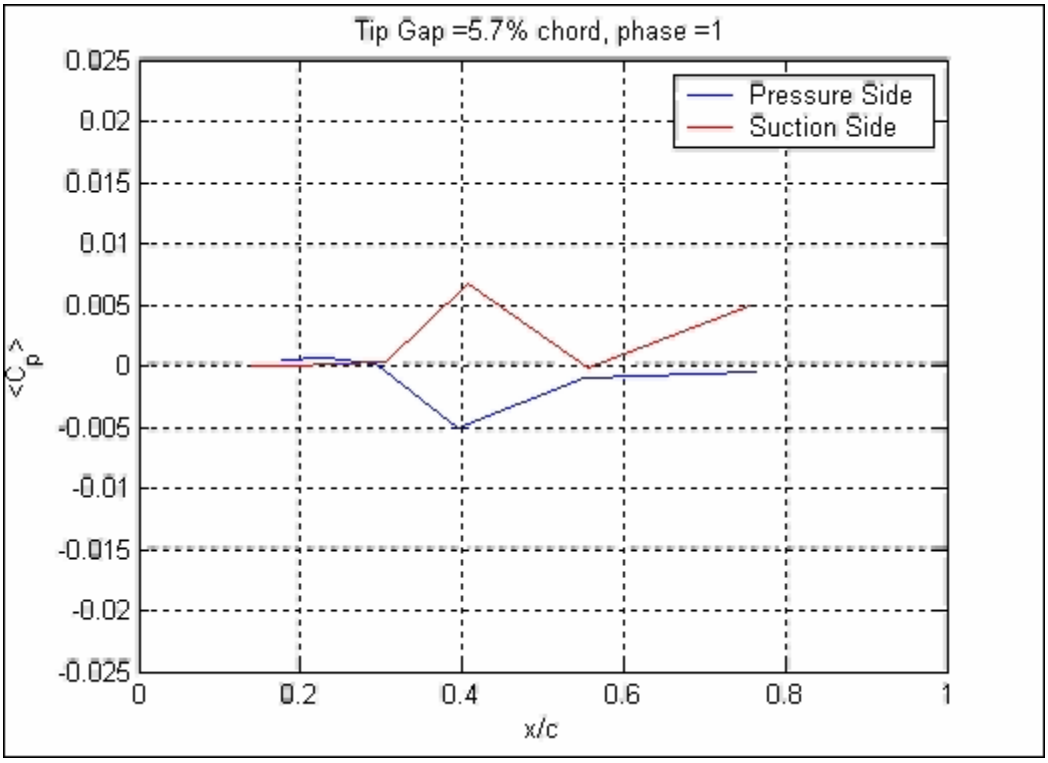

Figure 4.48 Movie of unsteady pressure fluctuation as a function of phase number along blade chord for half-height generators for a tip clearance of 5.7%*c*.

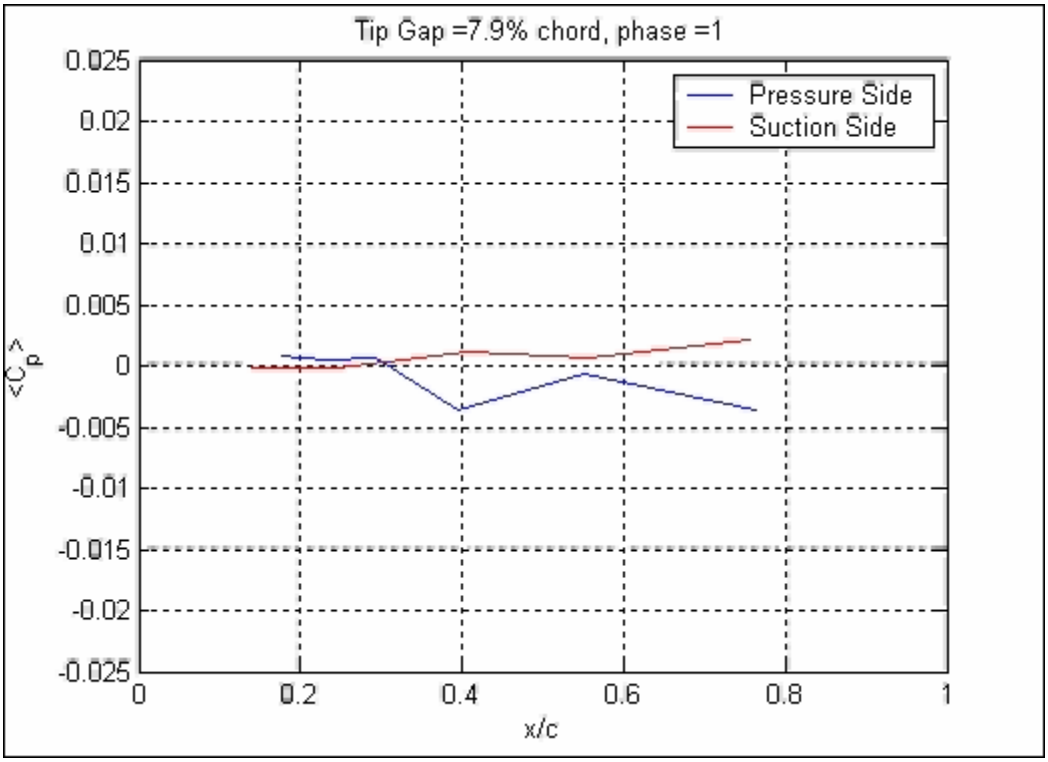

Figure 4.49 Movie of unsteady pressure fluctuation as a function of phase number along blade chord for half-height generators for a tip clearance of 7.9%*c*.

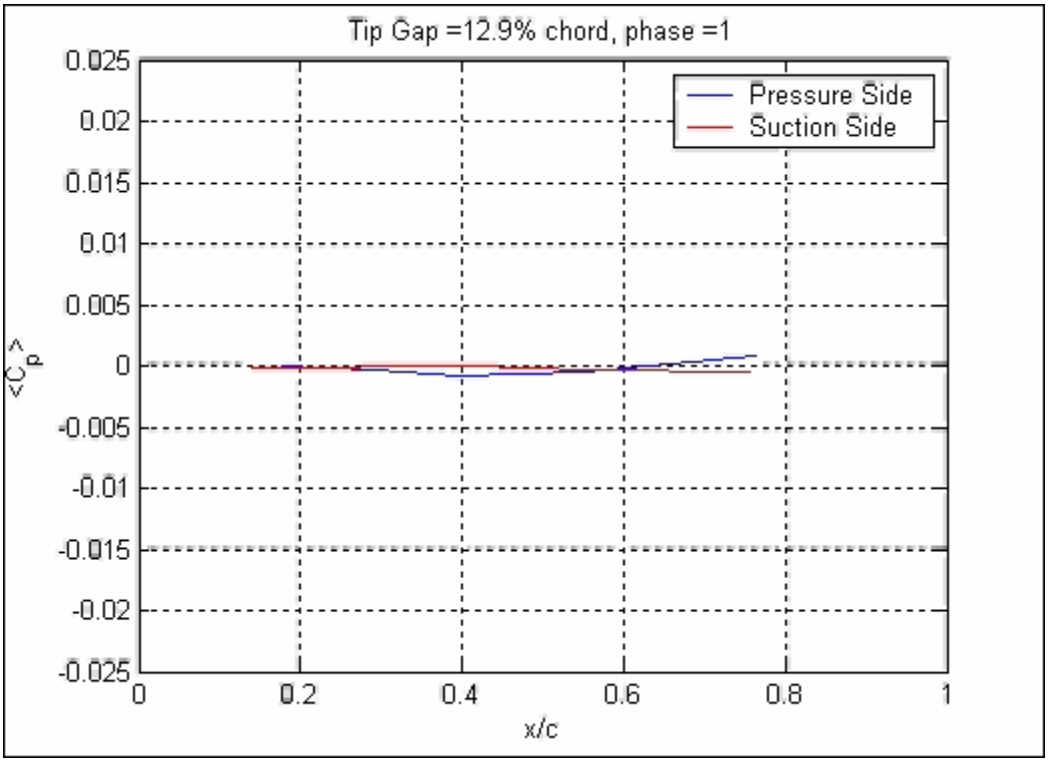

Figure 4.50 Movie of unsteady pressure fluctuation as a function of phase number along blade chord for half-height generators for a tip clearance of 12.9%*c*.

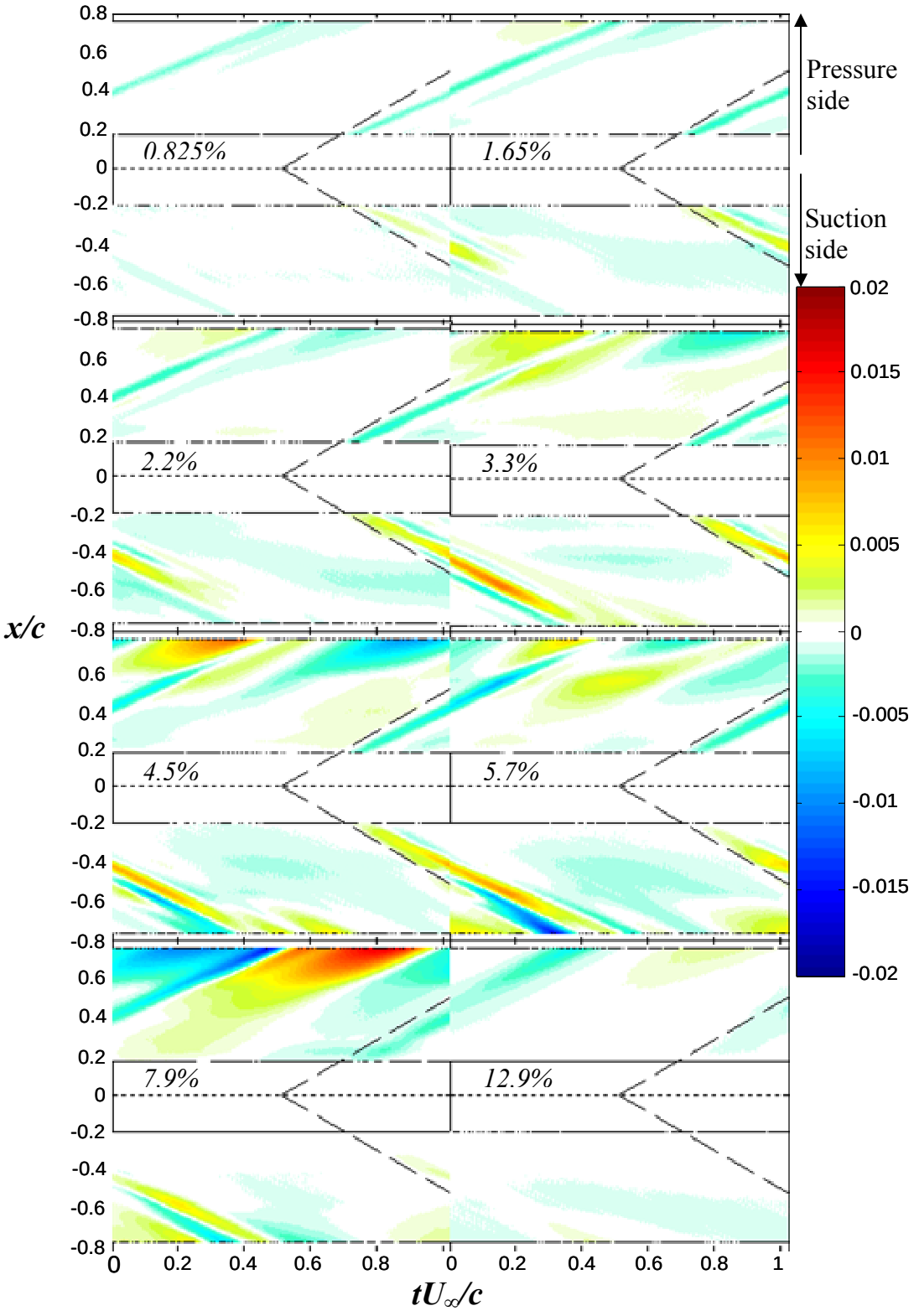

Figure 4.51 Chordwise pressure coefficient (C_p) contours for microphones on pressure and suction sides of blade for half-height generators.

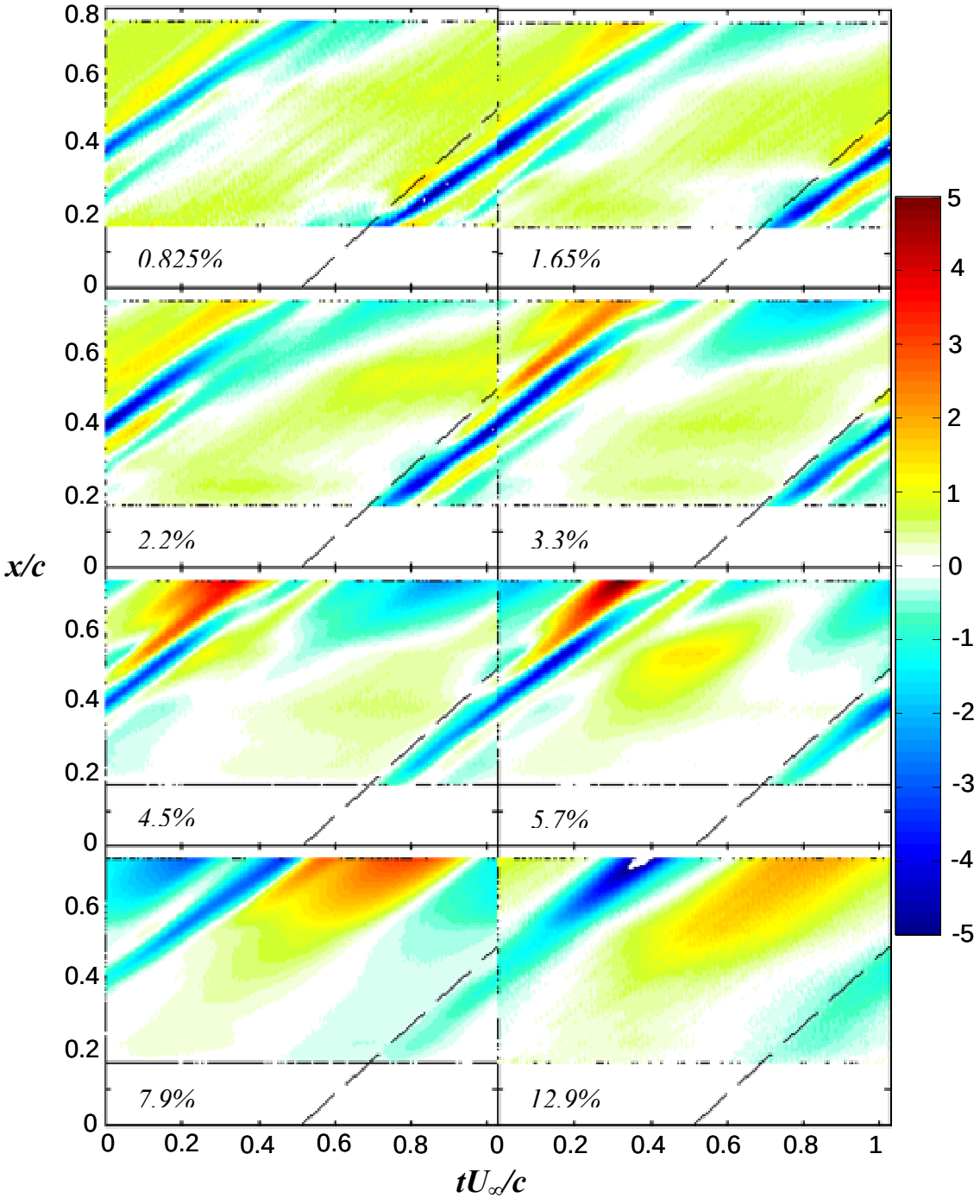

Figure 4.52 Pressure difference across blade tip normalized on the r.m.s. pressure difference across the blade tip for the half-height generators.

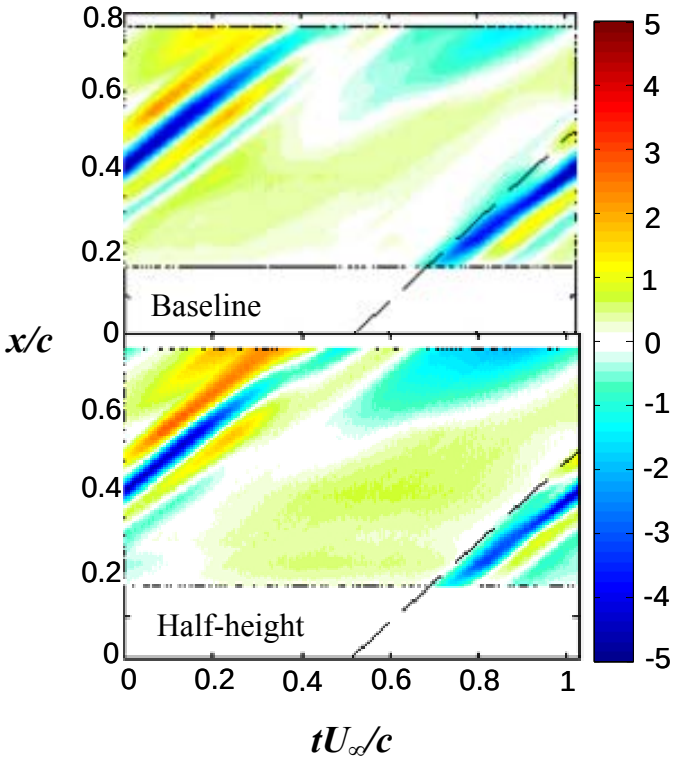

Figure 4.53 Comparison of baseline and half-height generator configurations normalized pressure difference across the blade tip.

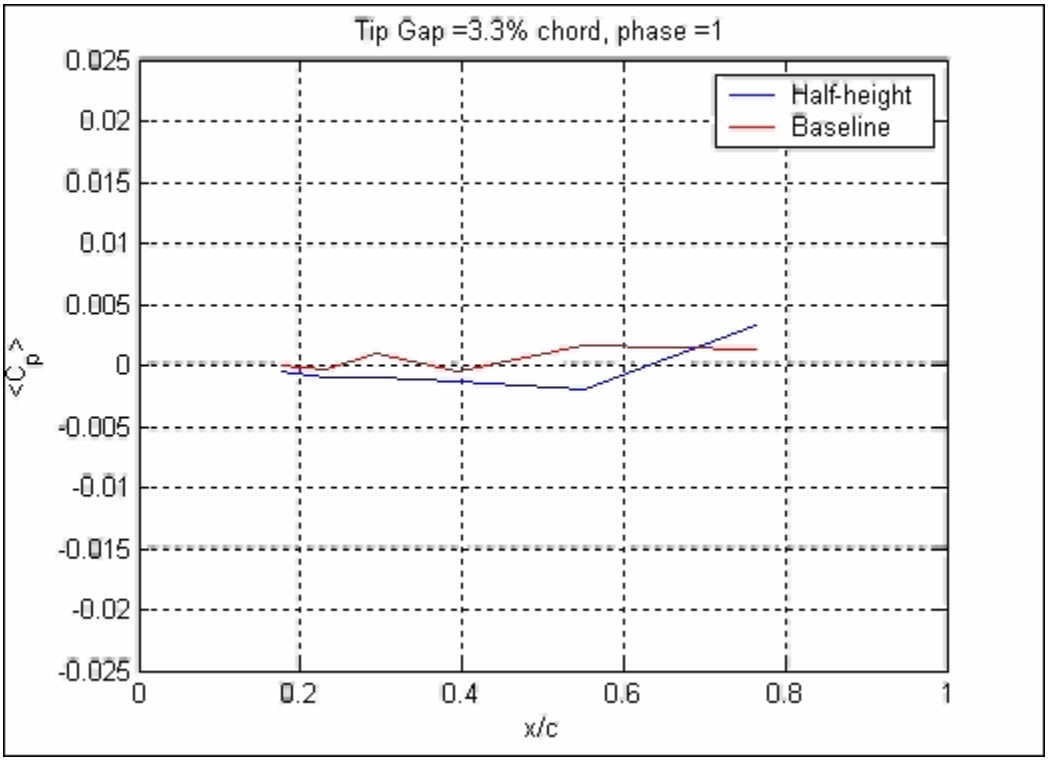

Figure 4.54 Movie of unsteady pressure fluctuation on the pressure side of the blade as a function of phase number along blade chord for widely spaced generators and baseline generator configuration for a tip clearance of 3.3%*c*.

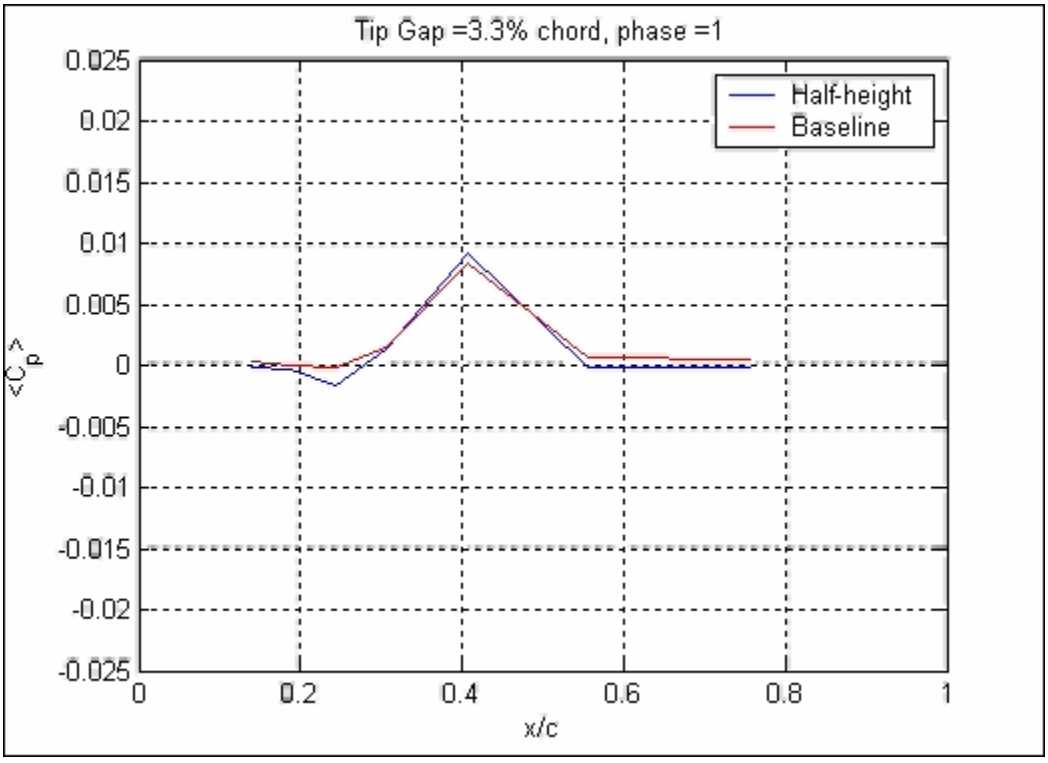

Figure 4.55 Movie of unsteady pressure fluctuation on the suction side of the blade as a function of phase number along blade chord for widely spaced generators and baseline generator configuration for a tip clearance of 3.3%*c*.

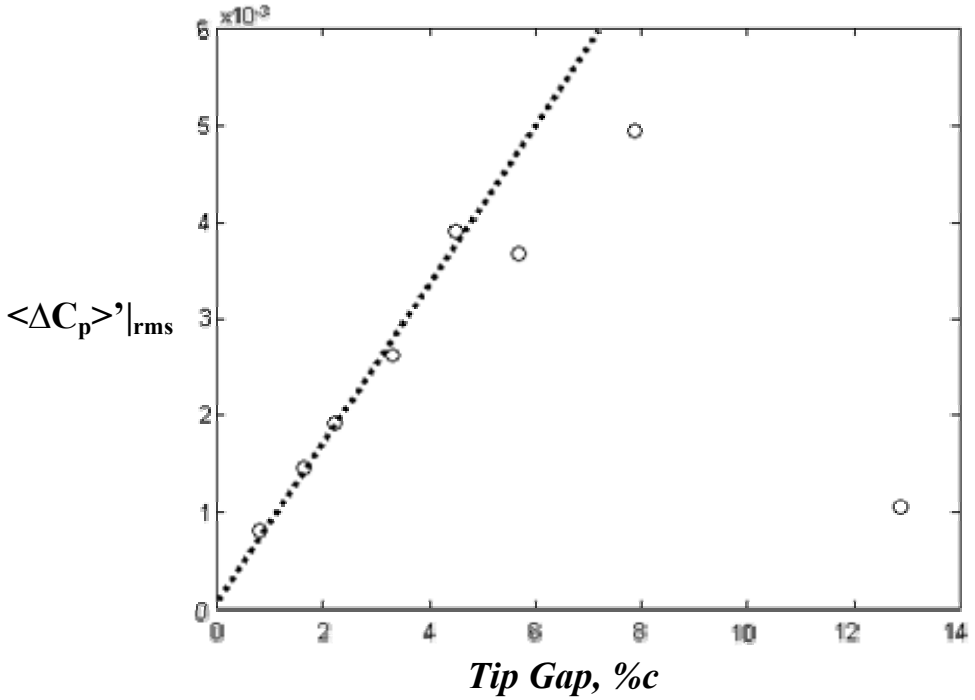

Figure 4.56 Scaled tip loading versus tip gap for half-height generators.

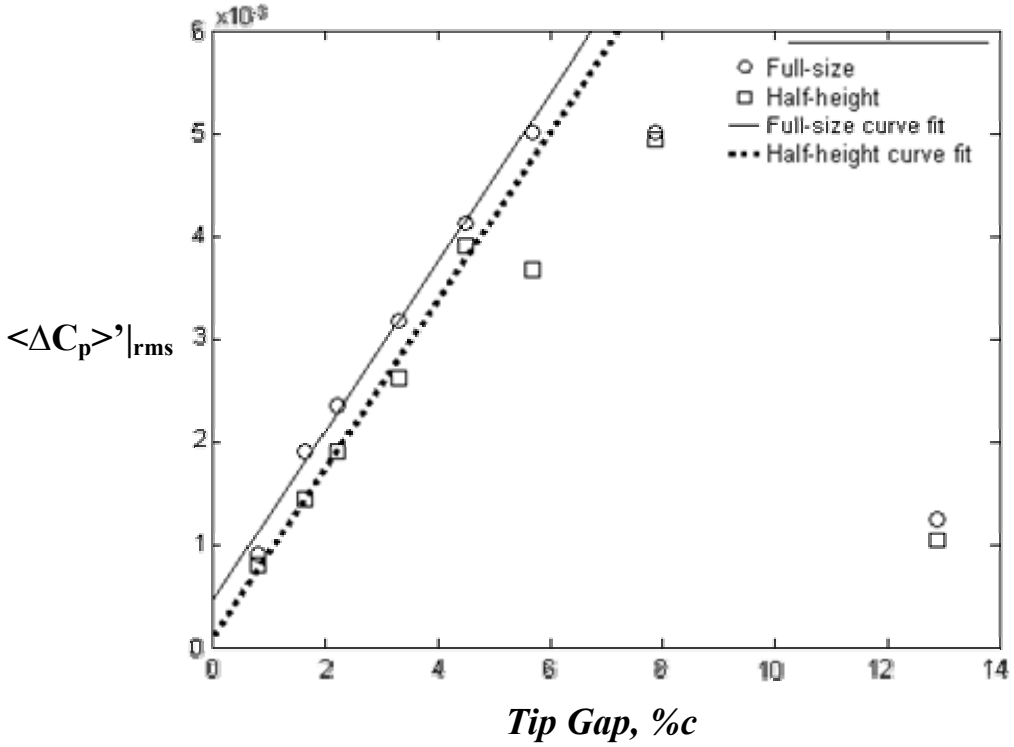

Figure 4.57 Comparison of scaled tip loading versus tip gap for full-size generators and half-height generators.

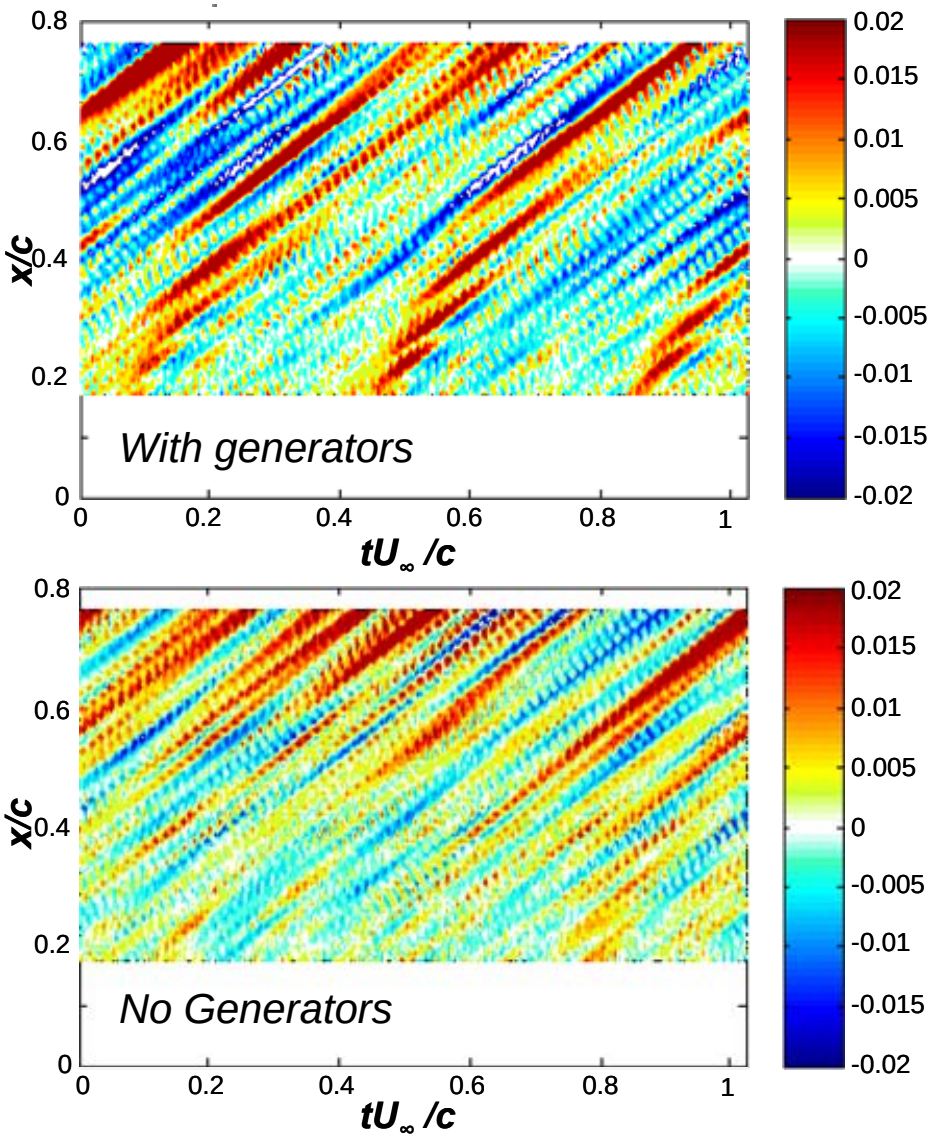

Figure 4.58 Instantaneous unsteady pressure difference comparison between moving wall with no vortex generators and moving wall with generators for 3.3%*c* tip clearance.

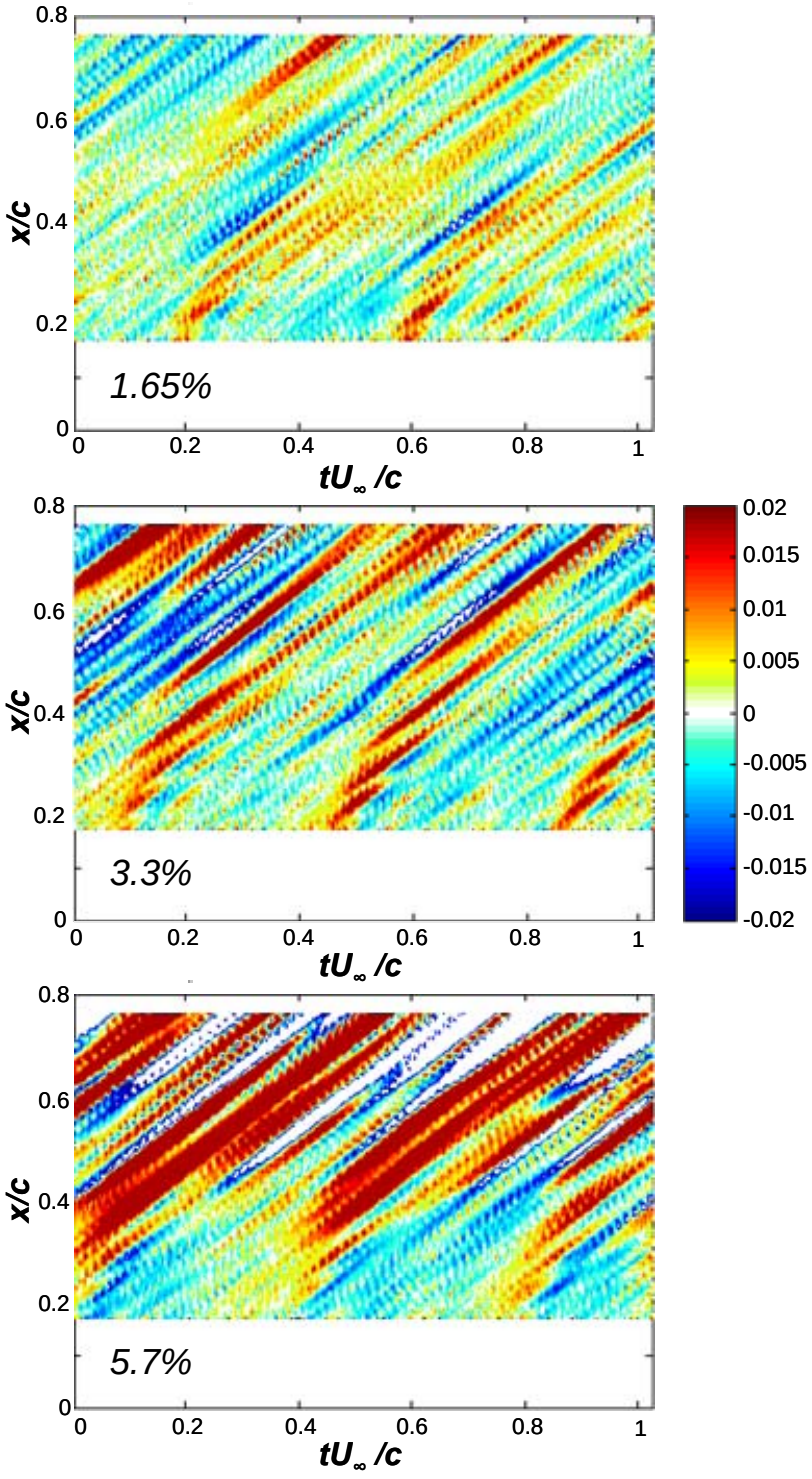

Figure 4.59 Instantaneous unsteady pressure difference contours for tip clearances of 1.65%, 3.3%, and 5.7%*c*.

5. Analysis of Unsteady Velocity

5.1 Introduction

There have been only a few studies including those by Foley and Ivey (1996), Goto (1992), Inoue and Kuroumaru (1988), Pandya and Lakshminarayana (1983a, 1983b), Lakshminarayana *et al*. (1987) and Murthy and Lakshminarayana (1986) that have investigated the flow through the tip clearance region of a compressor rotor. Foley and Ivey (1996) used static pressure taps to investigate the pressure difference near the blade tip in order to understand the flow through the tip clearance. This investigation was also performed in the current study along with unsteady instantaneous pressure measurement using microphones. Because of the difficulties involved with traversing a hot-wire anemometer within the tip clearance region, few studies have been made of the velocity within the tip clearance region including those by Goto (1992), Inoue and Kuroumaru (1988), and Pandya and Lakshminarayana (1983a, 1983b). In order to completely understand the mechanism that is driving the flow thorough the tip clearance region, it is essential to know how the pressure difference across the blade tip is affecting the mass flow through the tip clearance region. This is the goal of this part of the investigation. Using a single sensor boundary layer probe, it is possible to measure the velocity within the tip clearance region of a compressor rotor. In this chapter, the

unsteady velocity will be measured from the suction side of the tip clearance region approximately 1 mm from the exit of the tip clearance for a tip gap of 3.3%*c*. The velocity will be measured at the same locations at which the microphones were mounted on the suction side of the blade. The unsteady velocity data acquired in this manner will provide more information about the mechanisms of the flow through the tip clearance region as a result of the unsteady inflow vortices from the vortex generators. The unsteady velocity can then be compared with the unsteady pressure across the tip gap to make conclusions about the flow through the tip clearance region.

5.2 Unsteady velocity uncertainty analysis

The uncertainty in the hot-wire measurements is dependent upon a variety of factors including A/D conversion error, calibration drift, uncertainty in the velocity calibration, and the uncertainty in the free-stream velocity. Measurement uncertainty for the single sensor hot-wire measurements was calculated using the method of Kline and McClintock (1953). The uncertainties calculated at 20:1 odds are given in Table 5.1.

Table 5.1 Uncertainties for single sensor hot-wire probe.

Quantity	*Uncertainty*
$\delta\left(\langle u \rangle\right)/U_\infty$	1.3%
$\delta\left(\langle u'^2 \rangle\right)/U_\infty^2$	3%

5.3 Measurement configuration

For the investigation presented here, single sensor hot-wire anemometry measurements were made within the tip clearance, 1mm from the blade surface at the same locations at which the unsteady pressure measurements on the suction side of the blade were made using the microphones. Three extra locations were measured using the hot-wire that were not investigated using the microphones to add more measurement

locations near the blade trailing edge. The hot-wire anemometry measurements were made at nine locations including x/c = 0.19, 0.24, 0.31, 0.36, 0.41, 0.48, 0.56, 0.67, and 0.76. The hot-wire measurements were made of the velocity component in the direction perpendicular to the blade camber line as shown in Figure 5.1. These measurements were made for the case of a stationary wall, a moving wall without vortex generators, and the case of a moving wall with vortex generators. The first two configurations provide a baseline for comparison for the case when the inflow vortices are presnet. This allows a detailed investigation into the tip clearance flow for several different cases. The results obtained using the hot-wire anemometry measurements can be compared with the results of unsteady pressure on the blade surface presented in Chapter 4.

5.4 3.3%*c* unsteady velocity data

5.4.1 Velocity profiles

5.4.1.1 No moving wall versus moving wall

To provide a baseline for the phase averaged measurements, the velocity within the tip clearance region was measured for a tip clearance of 3.3%*c* for the case of no moving wall as well as the case of a moving wall with no vortex generators. These measurements were made for 6 locations along the blade chord, x/c = 0.19, 0.24, 0.31, 0.41, 0.56, and 0.76. The results of these measurements as well as the case of moving wall with no generators and moving wall with generators are presented in Figure 5.2. In this figure, the velocity normalized on the free-stream velocity is plotted on the abscissa and the y/c location within the tip clearance is plotted on the ordinate. The dotted line at y/c = 0.33 represents the location of the blade tip. From this figure it can be seen that close to the leading edge of the blade (18.75%*c*), the difference between the moving wall case and the no moving wall case is insignificant. Also the velocity within the tip clearance is less than 0.2 times the free-stream velocity over the entire tip clearance. This may be because at this location, the mean velocity vector may be approximately aligned with the camber line and therefore the velocity measured by the hot-wire may have been

only a small component of the actual velocity within the tip clearance. As the blade is traversed from leading to trailing edge, the magnitude of the velocity within the tip clearance increases, especially close to the end wall. The differences between the case of no moving wall and moving wall with no vortex generators are most prominent at the locations between 25 and 55%*c*. The differences are most evident close to the end wall which is to be expected since the wall motion should affect the boundary layer in this region. However, the velocity for the case of wall motion with no vortex generators is slightly lower than the case for no wall motion. This is an unexpected result since the wall motion should cause the flow to speed up moving from pressure to suction side. This is an interesting result since the wall motion causes the velocity within the tip clearance to decrease. These results would be better understood through a more thorough investigation of the no moving wall and the moving wall with no vortex generator cases.

The time averaged measurements made for the moving wall with vortex generators at a tip clearance of 3.3%*c* is also presented in Figure 5.2. The passing of the vortex generators across the blade leading edge should lead to significant variations in the velocity profiles within the tip clearance along the blade chord. From this figure, it can be seen that this is what occurs. Forward of 40%*c*, the velocity within the tip clearance is less than 50% of the free-stream velocity suggesting that near the blade leading edge there is not a large interaction between the inflow vortices and the blade tip. Rearward of 40%*c*, the velocity within the tip clearance increases to well above 50% of the free-stream velocity. Therefore, most of the interaction between the inflow vortices and the blade tip is occurring towards the trailing edge of the blade. This is the same phenomenon that was shown in Chapter 4 using the unsteady measurements made with the microphones. Namely, towards the leading edge there is a smaller interaction between the inflow vortices and the blade tip than that which occurs toward the trailing edge. The effect of the inflow vortices on the flow through the tip clearance can be better understood by comparing the case moving wall with vortex generators with the case of no moving wall and moving wall with no vortex generators.

When comparing the three different cases in Figure 5.2 it can be seen that there is not much of a difference in the tip clearance velocity between the three cases except at 41%*c*. This location may be close to the point at which the flow separates from the blade

forming the tip leakage vortex. The similarity between the three cases for the other eight measurement locations suggests that the mean properties of the flow within the tip gap region are nearly constant regardless of the presence of the inflow vortices or the wall motion. The presence of the inflow vortices will obviously affect the fluctuations of the velocity within the tip clearance as the vortex generators traverse across the blade passage. The effects of the unsteady inflow on the tip clearance flow will be discussed in detail in the following sections. The flow in the tip clearance region has been shown to occur predominantly because of the tip clearance and it would thus be valuable to examine the effects of tip clearance on the velocity within the tip clearance. This is something that could be further investigated in future work.

Figure 5.3 presents the phase averaged measurements for the nine locations along the blade chord. This is a movie that can be played by double clicking on the picture. This movie presents the phase averaged measurements made with vortex generators attached to the moving wall for nine locations along the blade chord. The figures presented at the top of the movie are the leading edge locations and the measurement locations progress from leading edge to trailing edge from left to right on the figure. This same statement applies to the figures at the bottom of the figure. In the center of the plot, three of the blades in the blade row are shown with the measurement locations plotted on the center blade. The blue circle that tracks across the plot shows the movement of the center of one pair of vortex generators across the blade passage. On each of the individual plots for the measurement locations, the normalized tip gap velocity (U/U_∞) is plotted on the abscissa and the location within the tip clearance is plotted on the ordinate. The flow is from right to left, with the inlet velocity being horizontal in the figure. From this movie it can be seen that when the generator pair is at phase=0, the measurement location at about 42% chord is the first location to be affected by the passing of the vortex generator pair. As the generator pair moves from phase 0 to phase 128, the effects of the generator pair travels down the blade chord and impacts the location at 75% chord at a phase number of approximately 128, which is the time when the generator pair is at the blade leading edge. As the generator pair moves from phase 128 to phase 256, the locations near the leading edge of the blade are affected by the inflow vortices. This effect moves down the blade chord as the generator pair tracks across the blade passage.

It can also be seen that there are some lingering effects on the velocity within the tip clearance for all measurement locations after the generator pair has moved past the location at which the inflow vortices should affect the tip clearance velocity. Therefore it appears as though there is a 'thump' on the blade tip clearance velocity. This may be a result of the blade tip breaking apart the inflow vortices. These vortices would then pass under the blade tip at different instances of time and therefore several velocity fluctuations would be seen over an extended period of time. The velocity fluctuations appear to be the largest at the trailing edge locations which agree well with the idea presented by the time averaged results that the velocity near the trailing edge is significantly larger than that seen at the leading edge. In order to better understand the velocity fluctuations within the tip clearance, it is beneficial to investigate the turbulence intensity within the tip clearance.

5.4.2 Turbulence intensity profiles

Turbulence intensity is defined as the fluctuations in the velocity from the mean. This quantity shows how much the velocity deviates from that of the free-stream velocity and can be calculated as a percentage. The turbulence intensity is represented by *u'* and thus the phase averaged turbulence intensity is defined as $\sqrt{\langle u'^2 \rangle}$. The investigations of the turbulence intensity profiles within the tip clearance show how much the velocity varies from the mean at each measurement location. Figure 5.4 presents the turbulence intensity for each of the six locations measured with no moving wall and for the moving wall with no vortex generators as well as moving wall with generators. This figure presents the turbulence intensity, u'/U_{ref} as a percentage on the abscissa and the y/c measurement points on the ordinate. This figure clearly shows that the peak in the turbulence intensity profiles continues to increase in magnitude as the blade chord is traversed from leading edge to trailing edge. At the leading edge, the velocity only fluctuates about 5% from the mean, while at the trailing edge the velocity fluctuates by approximately 20%. This says that the velocity within the tip clearance at the leading edge is nearly constant with only slight fluctuations. However, at the trailing edge, the

velocity fluctuates significantly from the mean. This may be caused by the interaction of the tip leakage vortex with the blade. Because the tip leakage vortex is highly turbulent, the eddies formed within this vortex have high velocity fluctuations. Since the tip leakage vortex forms at approximately 40% chord, it is this reason that the turbulence intensity begins to increase quickly at this location. The rapid change in the turbulence intensity at 40% chord may be caused by the creation of a jet with a shear layer as the flow passes through the tip clearance. The development of this shear layer downstream may be the cause of the high turbulence seen at 40% chord.

Figure 5.4 clearly shows the same results as that found in the no wall case and the moving wall with no generator case. The turbulence intensity continues to increase as the blade chord is traversed from leading to trailing edge. The turbulence intensity peaks begin to become noticeable at approximately 40% chord and continues to increase up to 20% of U_{ref} at 76% chord. It can also be seen that there is little variation between the three cases. This means that the vortex generators play only a small role in the velocity fluctuations within the tip clearance. This indicates that the tip leakage vortex is the primary reason for the velocity fluctuations within the tip clearance and the unsteady inflow provides only a small portion of this variation.

Figure 5.5 presents a movie of the phase averaged turbulence intensity as a function of location along the blade chord. This movie can be played by double clicking the plot. This movie is the same as the velocity profile movie except that it shows the turbulence intensity. On the abscissa of each individual plot within the movie, the turbulence intensity $\langle u' \rangle / U_{ref}$ as a percentage is plotted with the location in the tip clearance, y/c plotted on the ordinate. This movie shows that the turbulence intensity within the tip clearance region behaves in the same manner as the velocity. The effects of the inflow vortices travel down the blade chord as the vortex generators track across the blade passage. The same 'thump' can be seen on the tip clearance turbulence intensity as was seen on the velocity. After the generator pair is past the location where it should impact the blade tip clearance flow, the turbulence intensity still fluctuates for several phase numbers later. This can be contributed to the breaking apart of the inflow vortices.

5.4.3 Mass flow through the tip clearance

Although the velocity and turbulence intensity profiles within the tip clearance show how the flow within the tip clearance varies with location along the blade chord, it is more intuitive to investigate the mass flow through the tip clearance. The mass flow through any given region can be defined as

$$\frac{\dot{m}}{c} = \int_{0.07}^{0.33} \rho U dy \qquad 5.1$$

where $\dot{m}$ is the total mass flow through the given area, ρ is the density of the fluid, U is the velocity in the given area, and dA is the differential area. Since ρ is a constant, it can be taken out of the integral. The velocity within the tip clearance was investigated in this section and was measured for many points at each measurement location. Therefore, if the velocity is integrated over the measurement locations, the total mass flow at each measurement location can be computed using the trapezoidal rule with limits from y/c=0.07 to y/c=0.33 which is the minimum and maximum locations measured within the tip clearance, respectively. Since the velocity at all chordwise locations is unknown, because only nine locations along the blade chord were measured the mass flow can only be determined for the nine locations at which the velocity was measured. Figure 5.6 presents a contour plot of the phase averaged total mass flow through the tip clearance. On the abscissa, the normalized time tU_∞ / c is plotted against the measurement location on the ordinate. The contours are of the total mass flow through the tip clearance normalized on the density, ρ. The dashed line on the plot represents the speed at which the inflow vortices would travel down the blade chord is they were convected at the free-stream velocity. This plot is separated into colored layers because of the increasing mass flow as the chord is traversed from leading to trailing edge. From this figure it can be seen that the mass flow through the tip clearance increases as the blade is traversed from leading edge to trailing edge. This agrees with the results seen in the velocity profiles. This contour plot does not provide a intuitive means of understanding the mass flow through the tip clearance. This can be better investigated by comparing the unsteady pressure discussed in Chapter 4 with the unsteady mass flow.

5.5 Comparison of pressure and velocity

The unsteady pressure discussed in Chapter 4 was measured for eight tip clearances. A tip clearance of 3.3%*c* was used for one set of these measurements. This same tip clearance was also investigated using single sensor hot-wire anemometry. The similarity between the measurements made using the microphones and the measurements made using hot-wire anemometry are uncanny. This similarity is demonstrated by Figure 5.7. In this figure, the pressure difference across the tip clearance normalized on the root mean square pressure difference is plotted in the top part of the figure and the mass flow minus the mean mass flow is plotted in the bottom part of the figure. On the abscissa of both plots, the normalized time tU_∞ / c is plotted versus the measurement location on the ordinate. The dashed lines on both plots indicate the speed at which the inflow disturbances would move down the blade chord if they were convected at the free-stream velocity. These two plots show remarkable similarities. Both plots show that the disturbance moves down the blade chord at a speed approximately equal to that of the free-stream velocity. Both of these plots show that the speed that these disturbances move down the blade chord is nearly the same for both the unsteady pressure data and the unsteady velocity data. This implies that the pressure difference across the blade tip is influencing the mass flow through the tip clearance. The correlation between the unsteady pressure and the unsteady velocity provides a basis for better understanding the causes of the pressure fluctuations on the blade surface.

In order to better understand the relationship between the pressure and the mass flow, Figure 5.8 presents the mean mass flow, normalized on ρc where ρ is the fluid density and c is the blade chord, through the tip clearance from the hot-wire measurements versus the mean pressure difference across the blade tip from the mean pressure measurements. If the flow through the tip gap behaved like steady flow through a simple two-dimensional orifice then one would expect the mass flow to be proportional to the square root of the pressure difference given by $\dot{m} \sim \sqrt{\Delta C_p}$. This figure presents the log-log relationship between the two quantities. The data seem to follow closely to a linear trend on this log scale. However, the slope of this line is significantly greater than

the value of ½ that would be expected from the orifice analogy Figure 5.9 presents the phase averaged mass flow versus the phase averaged pressure difference for the three microphones closest to the blade leading edge (x/c = 0.19, 0.24, 0.31). This figure shows that the relationship between the two phase averaged quantities is not as simple as the mean value relationship. In fact, it shows the exact opposite relationship that was seen in the mean value comparison. Namely, the mean value comparison showed that as the pressure difference increased, the mass flow also increased. However, the phase averaged values show that as the pressure difference increases, the mass flow decreases suggesting that the two are 180 degrees out of phase. Therefore, it is more intuitive to look at the contour plots presented in Figure 5.7 to understand the relationship between the phase averaged pressure fluctuations and the phase averaged mass flow fluctuations.

5.6 Summary

In this investigation, the unsteady velocity within the tip clearance region was measured for a compressor rotor operating at a tip clearance of 3.3%c. These measurements were made using a single sensor boundary layer hot-wire anemometer placed 1mm from the suction surface of the blade that was traversed from the blade tip to the moving end wall. These measurements were made for no moving wall, moving wall with no vortex generators, and moving wall with vortex generators to study the effects of the inflow disturbances on the velocity within the tip clearance. The measurements were made at nine locations along the blade chord corresponding to the locations at which the unsteady pressure measurements were made (x/c = 0.19, 0.24, 0.31, 0.36, 0.41, 0.48, 0.56, 0.67, and 0.76). From this study several conclusions can be made:

1. For the no moving wall and the moving wall with no generator case, the velocity and turbulence intensity profiles increase in magnitude as the blade chord is traversed from leading edge to trailing edge.
2. The effect of the inflow disturbances causes only a small variation in the mean velocity and turbulence intensity profiles.

3. The inflow disturbances cause the velocity and turbulence intensity profiles to fluctuate from the mean as the vortex generator pair tracks across the blade passage.
4. A rapid change can be seen in the phase averaged velocity and turbulence intensity movies after the vortex generator pair is past the location at which the inflow disturbances should affect the tip clearance flow. This can be attributed to the breaking apart of the inflow disturbances and these pieces traveling under the blade tip.
5. The mass flow contours show that the mass flow increases as the blade chord is traversed from leading edge to trailing edge.
6. The mass flow minus the mean mass flow contour is similar to the contour of the normalized pressure difference across the blade tip. Both the mass flow and the pressure show that the disturbances travel down the blade chord at a speed approximately equal to that of the free-stream velocity.
7. The pressure difference across the blade tip drives the flow through the tip clearance region.

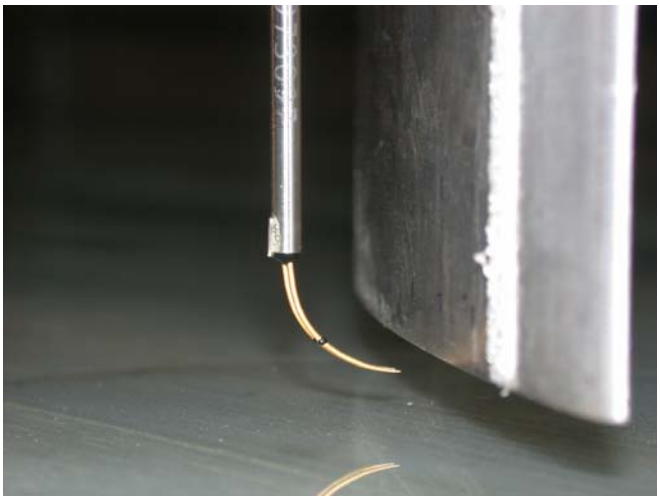

Figure 5.1 Single sensor hot-wire boundary layer probe mounted perpendicular to blade camber line.

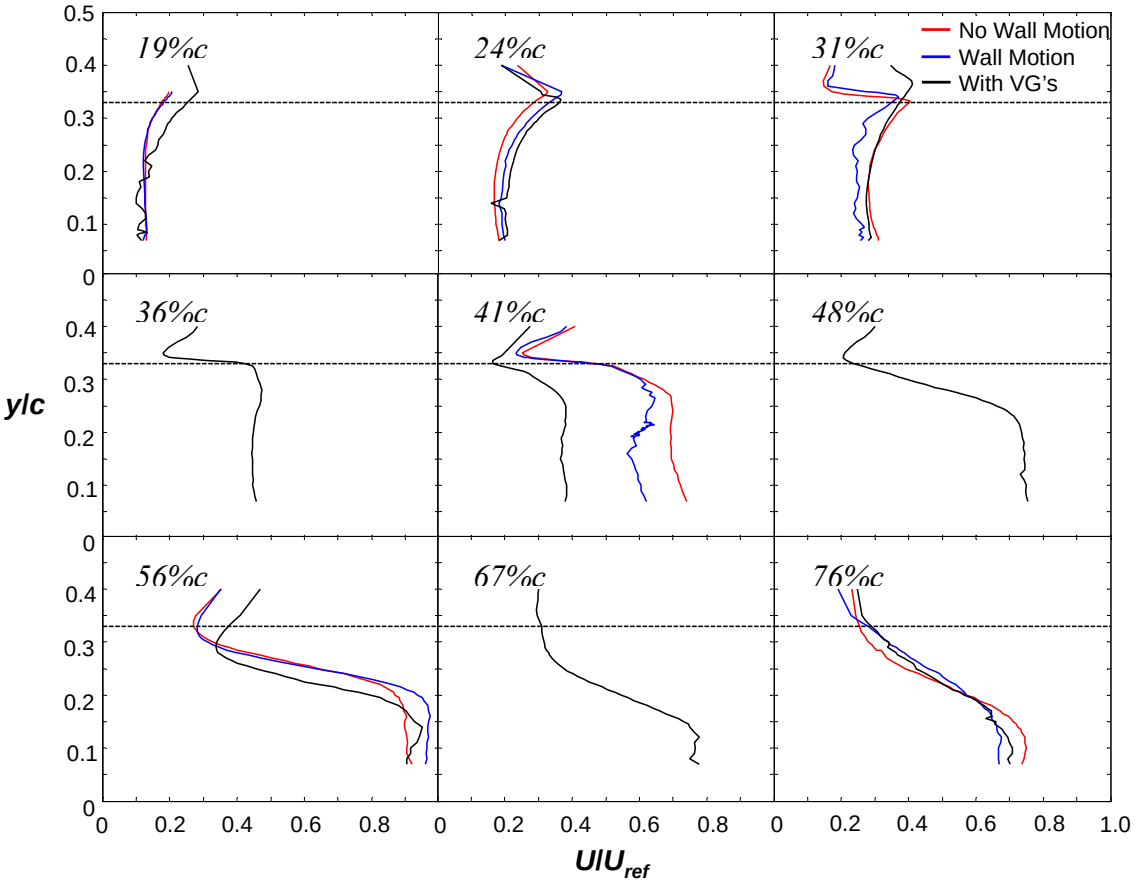

Figure 5.2 Time averaged velocity profiles for no moving wall, moving wall without vortex generators, and moving wall with vortex generators for nine chordwise locations for a tip clearance of 3.3%*c*.

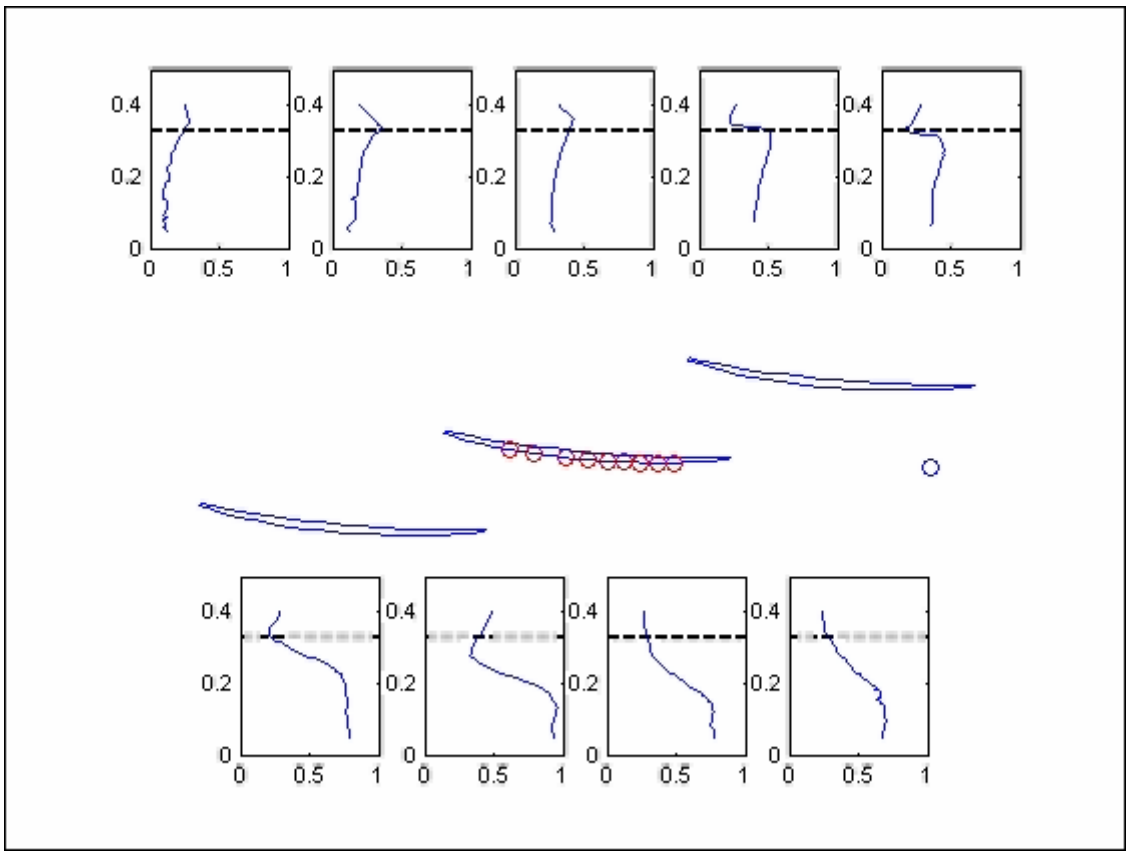

Figure 5.3 Movie of phase averaged velocity for nine measurement locations along the blade chord.

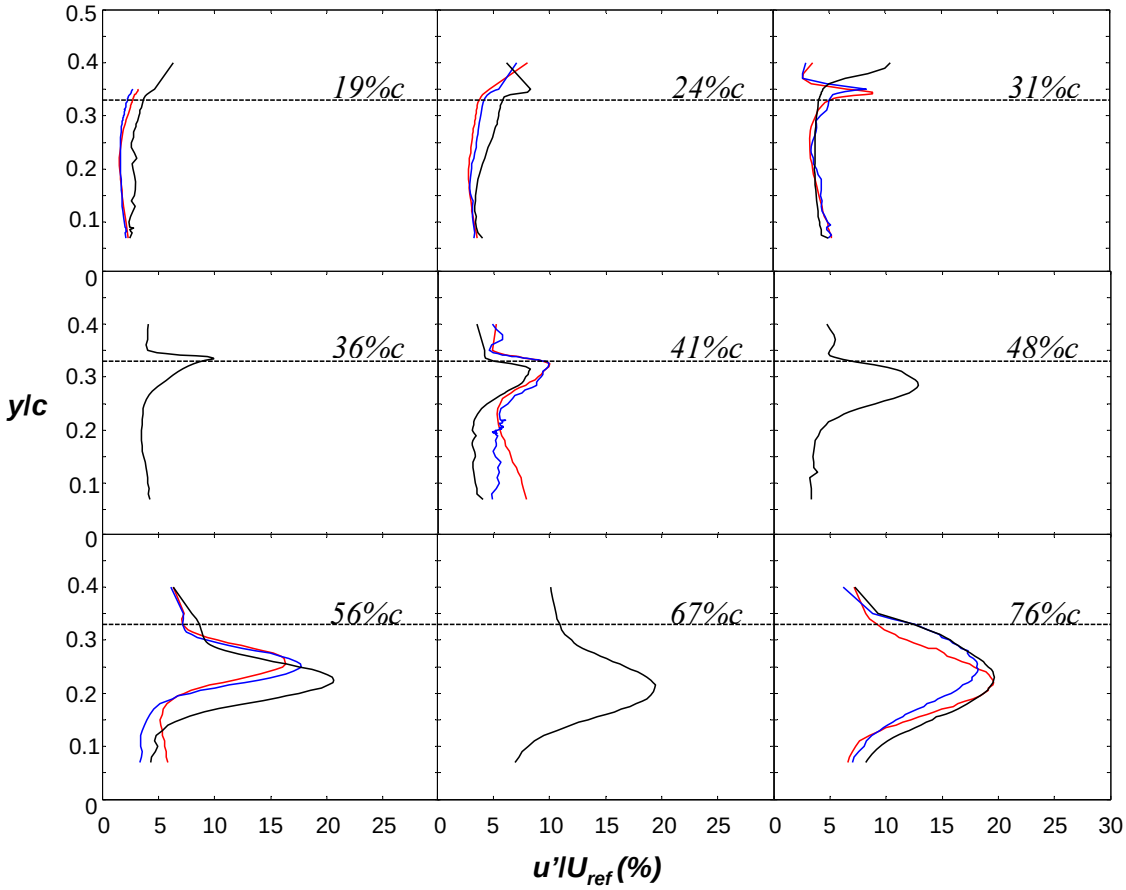

Figure 5.4 Time averaged turbulence intensity profiles for no moving wall, moving wall without vortex generators, and moving wall with vortex generators for nine chordwise locations for a tip clearance of 3.3%*c*.

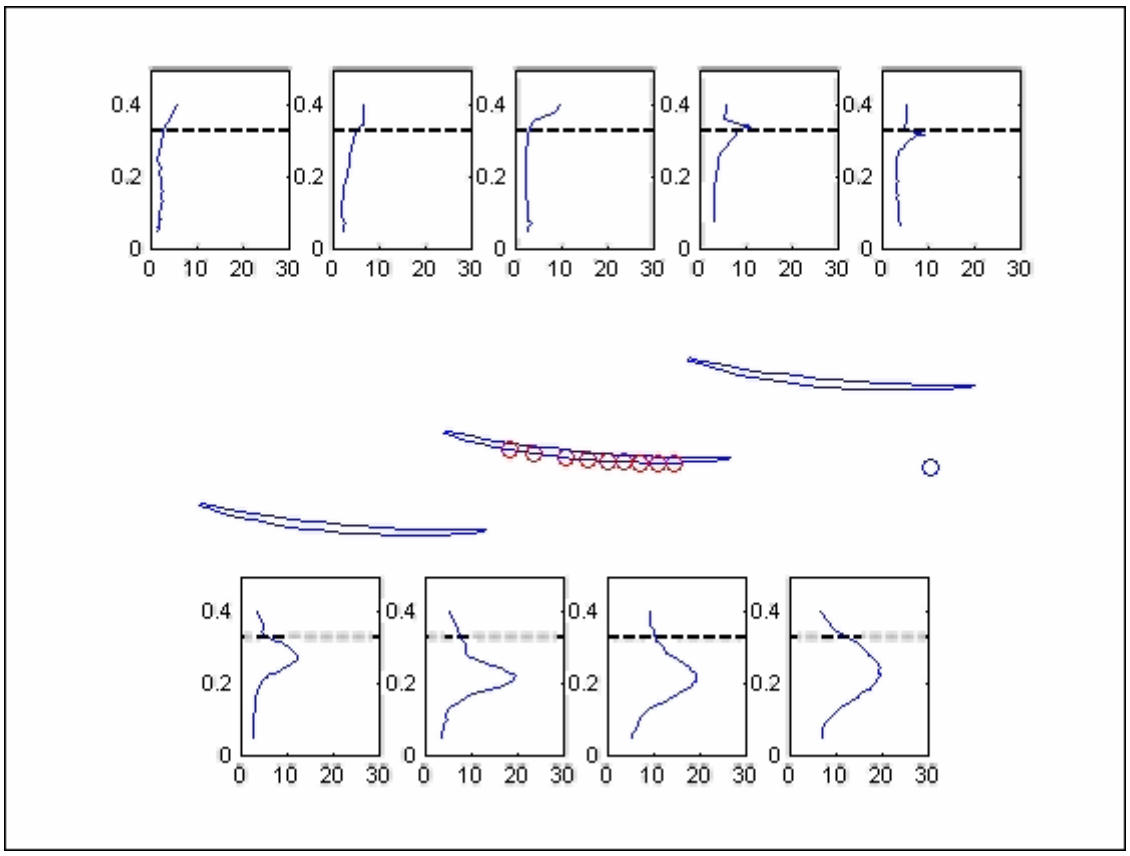

Figure 5.5 Movie of phase averaged turbulence intensity for nine measurement locations along the blade chord.

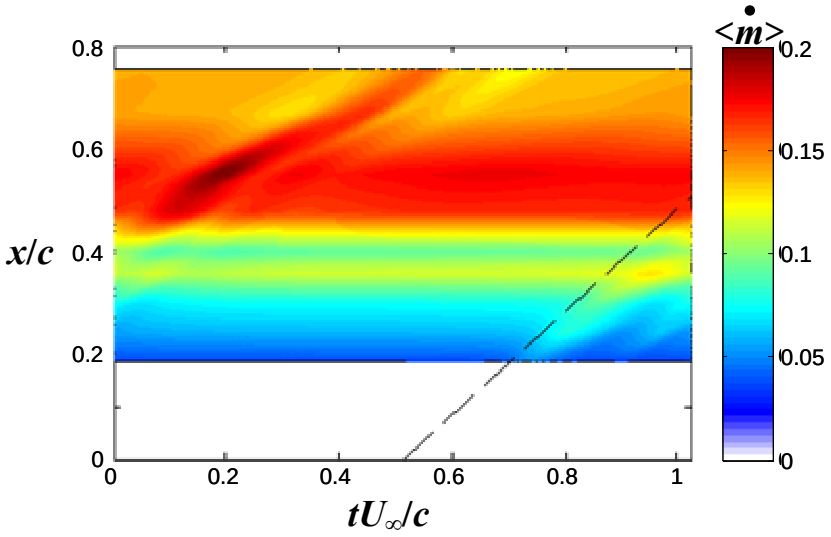

Figure 5.6 Total phase averaged mass flow through the tip clearance.

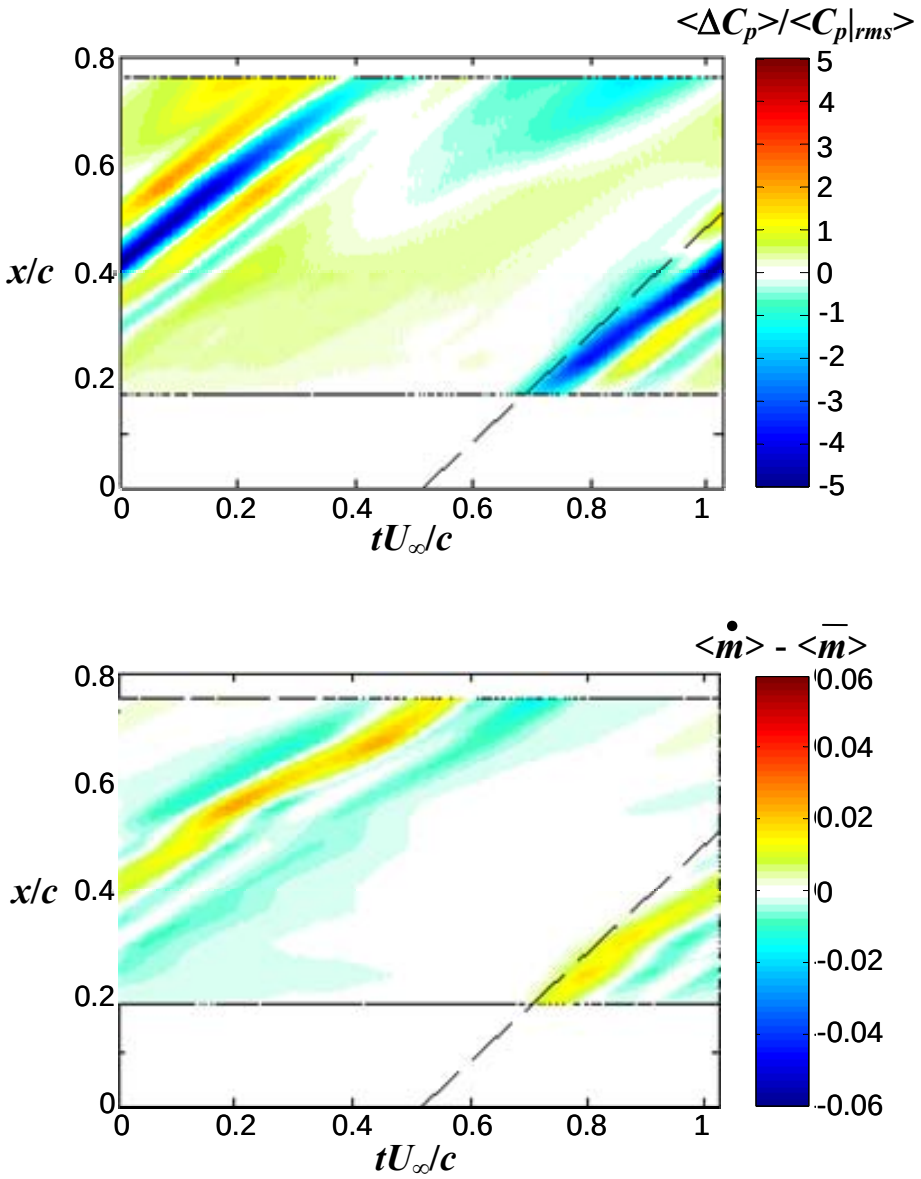

Figure 5.7 Comparison of normalized pressure difference across the blade tip and the mass flow minus the mean mass flow.

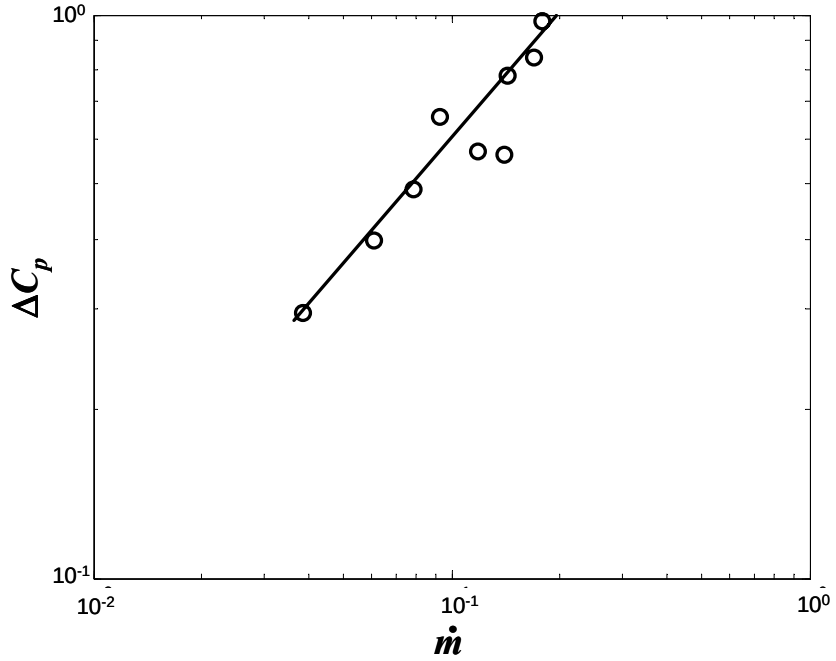

Figure 5.8 Mean mass flow through the tip clearance versus mean pressure difference across the tip clearance for a tip gap of 3.3%*c*.

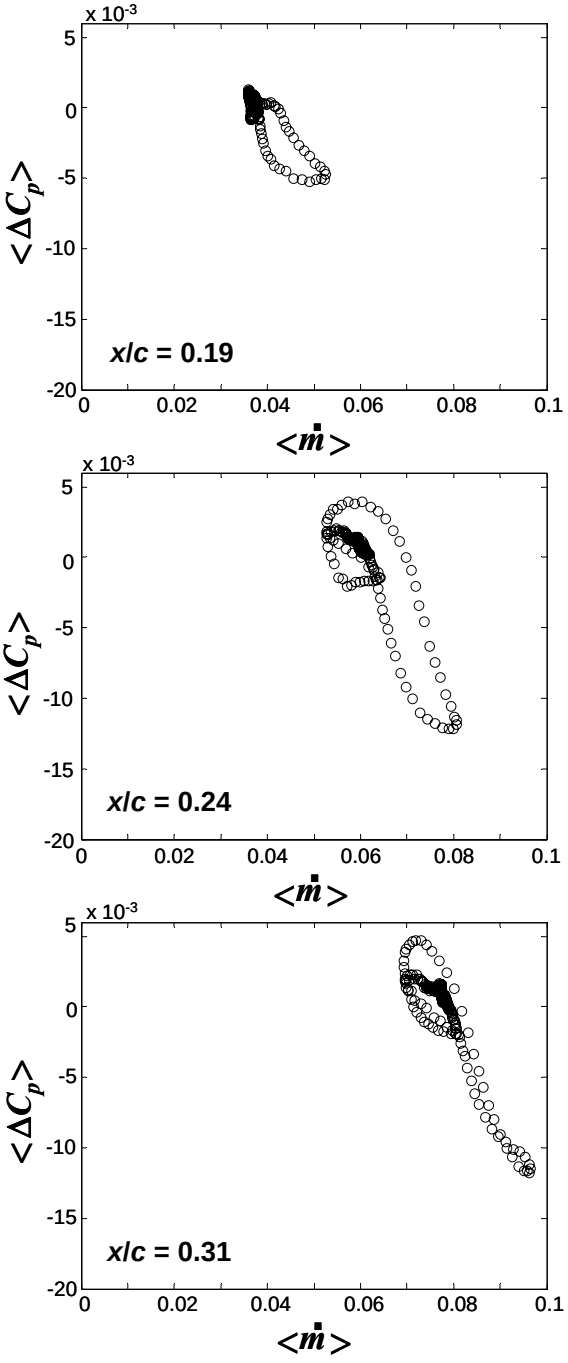

Figure 5.9 Phase averaged mass flow through the tip clearance versus phase averaged pressure difference across the tip clearance for a tip gap of 3.3%*c*.

6. Conclusions

6.1 Introduction

The Virginia Tech low speed linear cascade wind tunnel was used to model the unsteady tip clearance flow produced by a rotor operating in the vortical wake of a set of stator vanes. The cascade composed of 8 GE rotor B blades has a variable tip clearance and was operated at a blade chord Reynolds number of approximately 382,000. A moving end wall is used to simulate the relative motion between the rotor and the casing. Vortex generator pairs were attached to the moving end wall to simulate the flow created at the junction of the casing and the stator vanes. Measurements were made for no moving end wall, moving end wall with no vortex generators, and moving end wall with vortex generators to investigate the effects of simulated motion as well as the effects of the unsteady inflow vortices on the tip clearance flow.

The passing of the vortex generators through one of the blade passages was subdivided into 256 phases for the 236 mm spaced vortex generator pairs and 696 phases for the 641 mm spaced vortex generator pairs. Dividing the movement of the vortex generator pairs into phases, where one phase represents approximately 1 mm of vortex generator movement, allows for keeping track of the location of the generator pairs and thus knowing the approximate location of the counter-rotating vortices. Measurements were made at tip clearances of 0.825%, 1.65%, 2.2%, 3.3%, 4.5%, 5.7%, 7.9%, and 12.9%c to study the effects of tip clearance on the flow within the tip clearance region of a compressor rotor.

In this study, the mean pressure at the blade tip was measured using an array of static pressure ports mounted on the pressure and suction surfaces of blades 4 and 5 respectively. These measurements were made at all 8 tip clearance for no moving wall, moving wall with no vortex generators, and moving wall with vortex generators. The unsteady pressure at the blade tip was also investigated using an array of pressure microphones mounted within the surface of the blade on the pressure and suction sides of blades 4 and 5. These measurements were made at all 8 tip clearances to investigate the variation of the unsteady loading on the blade tip with the tip clearance. Unsteady velocity measurements were also made within the blade tip clearance approximately 1 mm from the blade suction surface for a tip clearance of 3.3%*c* using single sensor hot-wire anemometry. These measurements were also made for no moving wall, moving wall with no vortex generators, and moving wall with vortex generators.

6.2 Conclusions concerning unsteady blade tip loading

The mean blade loading at the blade mid-span and at the blade tip were investigated for tip clearances from 0.83%*c* to 12.9%*c* for three cases: a stationary wall case, a moving wall case, and a moving wall case with unsteady inflow created by vortex generator pairs. These measurements were made using pressure ports located on the suction and pressure surfaces of blades 4 and 5, respectively. From these measurements, we can make several conclusions:

1. The maximum pressure side C_p at the midspan decreases linearly as the tip clearance is increased.
2. For the stationary wall case, the mid-span blade loading and the tip loading are significantly different, especially at higher tip gaps, showing that the effects of the tip clearance primarily affects the region of the blade closest to the tip.
3. There is little difference in the blade tip loading between the three cases studied showing that the effects of the moving wall and unsteadiness play a small role in the mean tip loading of the blade.

4. Consistent with the measurements made by Dean (1954), the point of minimum pressure on the suction side of the blade moves closer to the blade trailing edge as the tip clearance is increased.
5. The minimum pressure on the blade suction side continues to decrease as the tip clearance is increased. This effect is evident up to a tip gap of 7.9%*c*.
6. There exists a simple relationship between the suction surface minimum pressure at the blade tip. The decrease in the suction side minimum pressure is found to be a linear function of the tip clearance for tip clearances up to 7.9%*c*.

6.3 Conclusions concerning unsteady pressure measurements

In this investigation, the effect on the surface pressure distribution from several different vortex generator configurations was studied for tip clearances from 0.825%*c* to 12.9%*c*. To determine whether the surface pressure distribution is influenced by multiple inflow vortices impacting the blade at the same instant of time, the vortex generators were placed far enough apart to eliminate this effect. The size of the vortex generators and thus the size of the inflow vortices were also investigated by using half-height generator pairs. This allows an investigation of the surface pressure for inflow vortices that should be almost twice as small as those for the baseline vortex generator configuration. From this study, several conclusions can be made:

1. The baseline generator configuration shows a self-similarity in the $\langle C_p \rangle$ contours when the pressure difference across the blade tip is normalized on the root mean square pressure difference.
2. The baseline generator configuration shows that the phase-averaged difference between suction and pressure side C_p, adjacent to the blade tip, root-mean-square averaged along the chord and over phase time varies nearly linearly up to a tip clearance of 5.7%*c* with an increasing pressure difference up through this tip clearance.

3. The RMS pressure increases as the tip clearance is increased from 0.83% to 5.7%*c* for the baseline configuration. The changes in the RMS pressure as the tip clearance is increased are mainly noticeable at the trailing edge.
4. The spacing of the vortex generators shows that there is almost no effect on the blade surface pressure distribution resulting from multiple inflow vortices impacting the blade at the same instant of time.
5. The study of the vortex generator size shows that there is almost no effect on the blade surface pressure distribution at tip clearances smaller than 5.7%*c*.
6. The half-height generators show an increase in $\langle C_p \rangle$ up to a tip clearance of 4.5%*c* while the full-size generators show an increase in $\langle C_p \rangle$ up to a tip clearance of 5.7%*c*.
7. There are only minor effects on the blade surface pressure distribution as a result of using widely spaced generator pairs and half-height generator pairs in place of the full-size generator pairs spaced 9.29" apart. Therefore, the pressure on the blade surface near the tip is affected primarily by one pair of inflow vortices and is not significantly affected by the size of these inflow vortices.
8. The instantaneous pressure results show that the response of the blade is independent of whether or not the vortex generators are present. It appears as though the inflow vortices stimulate the response of the blade. These results also show that the tip gap effect is real and is not simply a result of the phase averaging of the measurements.

6.4 Conclusions concerning unsteady velocity measurements

In this investigation, the unsteady velocity within the tip clearance region was measured for a compressor rotor operating at a tip clearance of 3.3%*c*. These measurements were made using a single sensor boundary layer hot-wire anemometer placed 1mm from the suction surface of the blade that was traversed from the blade tip to

the moving end wall. These measurements were made for no moving wall, moving wall with no vortex generators, and moving wall with vortex generators to study the effects of the inflow disturbances on the velocity within the tip clearance. The measurements were made at nine locations along the blade chord corresponding to the locations at which the unsteady pressure measurements were made (x/c = 0.1875, 0.24375, 0.30625, 0.36, 0.40625, 0.48, 0.55625, 0.67, and 0.75625). From this study several conclusions can be made:

1. For the no moving wall and the moving wall with no generator case, the velocity and turbulence intensity profiles increase in magnitude as the blade chord is traversed from leading edge to trailing edge.
2. The effect of the inflow disturbances causes only a small variation in the mean velocity and turbulence intensity profiles.
3. The inflow disturbances cause the velocity and turbulence intensity profiles to fluctuate from the mean as the vortex generator pair tracks across the blade passage.
4. A ‘thump’ can be seen in the phase averaged velocity and turbulence intensity movies after the vortex generator pair is past the location at which the inflow disturbances should affect the tip clearance flow. This can be attributed to the breaking apart of the inflow disturbances and these pieces traveling under the blade tip.
5. The mass flow contours show that the mass flow increases as the blade chord is traversed from leading edge to trailing edge.
6. The mass flow minus the mean mass flow contour is similar to the contour of the normalized pressure difference across the blade tip. Both the mass flow and the pressure show that the disturbances travel down the blade chord at a speed approximately equal to that of the free-stream velocity.
7. The pressure difference across the blade tip drives the flow through the tip clearance region.

References

Bindon J P, “The Measurement and Formation of Tip Clearance Loss”, ASME Journal of Turbomachinery, vol. 111, July 1989, pp. 257-263.

D de la Riva, 2001, “Turbulence Interaction in a Highly Staggered Cascade-Propulsor Configuration”, M.S. thesis, Aerospace and Ocean Engineering Dept., Virginia Polytechnic Institute and State University, available http://scholar.lib.vt.edu/theses/available/etd-04272001-172809/

D de La Riva, Devenport W and Muthanna C, “The Behavior of Turbulence Flowing Through a Compressor Cascade”, AIAA Journal, vol. 42, no. 7, pp. 1302-1313, July 2004.

Dean Jr. R, “The Influence of Tip Clearance on Boundary-Layer Flow in a Rectilinear Cascade”, Three-Dimensional Flow in Turbomachines Research, Report of Research Activities, 1953-1954 under the sponsorship of General Electric Company, Report Number 27-3, December 1954, MIT.

Foley A C and Ivey P C, “Measurement of Tip-Clearance Flow in a Multistage, Axial Flow Compressor”, ASME Journal of Turbomachinery, vol. 118, April 1996, pp. 211-217.

Gallus H E and Zeschky J, “Endwall and Unsteady Flow Phenomena in an Axial Turbine Stage”, ASME paper 94-GT-143, 1994.

Gearhart W S, “Tip Clearance Cavitation in Shrouded Underwater Propulsors”, Journal of Aircraft, vol. 3, no. 2, March-April 1966.

Goto A, “Three-Dimensional Flow and Mixing in an Axial Flow compressor with Different Rotor Tip Clearances”, ASME Journal of Turbomachinery, vol. 114, July 1992, pp. 675-685.

Inoue M and Kuroumaru M, “Structure of Tip Clearance Flow in an Isolated Axial Compressor Rotor”, Gas Turbine and Aeroengine Congress and Exposition, June 5-9, 1988, Amsterdam, The Netherlands.

Intaratep N, expected 2005, Ph.D. dissertation, Aerospace and Ocean Engineering Dept., Virginia Polytechnic Institute and State University.

Intaratep N, Devenport W and Staubs J, "The Tip Leakage Vortex Shed from an Unsteady Tip Clearance Flow", 34th AIAA Fluid Dynamics Conference and Exhibit, June 28-July 1, 2004, Portland OR, AIAA paper 2004-2430.

Jin P and Goldstein R J, "Local Mass/Heat Transfer on Turbine Blade Near-Tip Surface", ASME Journal of Turbomachinery, vol. 125, July 2003, pp. 521-528.

Kang S and Hirsch C, "Experimental Study on the Three-Dimensional Flow within a Compressor Cascade with Tip Clearance: Part I-Velocity and Pressure Fields", ASME Journal of Turbomachinery, vol. 115, July 1993, pp. 435-443.

Kang S and Hirsch C, "Tip Leakage Flow in Linear Compressor Cascade", Journal of Turbomachinery, vol. 116, October 1994, pp. 657-664.

Kline S J and McClintock F A, "Describing Uncertainties in Single Sample Experiments", Mechanical Engineering, vol. 75, 1953, pp. 3.

Lakshminaryana B, Zhang J and Murthy K N S, 1987, "An Experimental Study of the Effects of Tip Clearance on Flow Field and Losses in an Axial Flow Compressor Rotor", Proceedings of the 8th International Symposium on Air Breathing Engines, AIAA, New York, pp. 273-290, ISABE paper 87-7045 (including addendum).

Ma R, 2003, "Unsteady Turbulence Interaction in a Tip Leakage Flow Downstream of a Simulated Axial Compressor Rotor", Ph.D. dissertation, Aerospace and Ocean Engineering Dept., Virginia Polytechnic Institute and State University, available http://scholar.lib.vt.edu/theses/available/etd-06172003-122153/

Mish P F, 2003, "An Experimental Investigation of Unsteady Surface Pressure on Single and Multiple Airfoils", Ph.D. dissertation, Aerospace and Ocean Engineering Dept., Virginia Polytechnic Institute and State University, available http://scholar.lib.vt.edu/theses/available/etd-03312003-173021/

Moore J and Tilton J S, "Tip Leakage Flow in a Linear Turbine Cascade", ASME Journal of Turbomachinery, vol. 110, January 1988, pp. 18-26.

Moyle I N, Shreeve R P and Walker G J, "Case Wall Pressures in a Multistage Axial Compressor with Tip Clearance Variation", Journal of Propulsion and Power, vol. 12, no 5, September-October 1996, pp. 967-973.

Murthy K N S and Lakshminarayana B, "Laser Doppler Velocimeter Measurement in the Tip Region of a Compressor Rotor", AIAA Journal, vol. 24, no. 5, May 1986, pp. 807-814.

Muthanna C and Devenport W, “Wake of a Compressor Cascade with Tip Gap, Part 1: Mean Flow and Turbulence Structure”, AIAA Journal, vol. 42, no. 11, pp. 2320-2331, November 2004.

Muthanna C, 1998, “Flowfield Downstream of a Compressor Cascade with Tip Leakage”, M.S. thesis, Aerospace and Ocean Engineering Dept., Virginia Polytechnic Institute and State University, available
http://scholar.lib.vt.edu/theses/available/etd-110798-235327/

Muthanna C, 2002, “The Effects of Free Stream Turbulence on the Flow Field through a Compressor Cascade”, Ph.D. dissertation, Aerospace and Ocean Engineering Dept., Virginia Polytechnic Institute and State University, available
http://scholar.lib.vt.edu/theses/available/etd-08222002-194441/

Pandya A and Lakshminarayana B, “Investigation of the Tip Clearance Flow Inside and at the Exit of a Compressor Rotor Passage-Part I: Mean Velocity Field”, Journal of Engineering for Power, vol. 105, January 1983, pp. 1-12.

Pandya A and Lakshminarayana B, “Investigation of the Tip Clearance Flow Inside and at the Exit of a Compressor Rotor Passage-Part II: Turbulence Properties”, Journal of Engineering for Power, vol. 105, January 1983, pp. 13-17.

Pauley W R and Eaton J K, “Boundary Layer Turbulence Structure in the Presence of Embedded Streamwise Vortex Pairs”, Seventh Symposium on Turbulent Shear Flows, Stanford Universtiy, August 21-23, 1989.

Rains D A, “Tip Clearance Flow in Axial Compressors and Pumps”, California Institute of Technology, Mechanical Engineering Laboratory, Report 5, 1954.

Sjolander S A and Amrud K K, “Effects of Tip Clearance on Blade Loading in a Planar Cascade of Turbine Blades”, ASME Journal of Turbomachinery, vol. 109, April 1987, pp. 237-245.

Srinivasan V and Goldstein R J, “Effect of Endwall Motion on Blade Tip Heat Transfer”, ASME Journal of Turbomachinery, vol. 125, April 2003, pp. 267-273.

Storer J A and Barton J P, "An investigation of the flow within the clearance space of a compressor blade tip", ISABE paper 91-7013, 1991.

Storer J A and Cumpsty N A, “Tip Leakage Flow in Axial Compressors”, ASME Journal of Turbomachinery, vol. 113, April 1991, pp. 252-259.

Storer J A, 1989, "The interaction between tip clearance flow and the passage flow field in an axial compressor cascade", Proceedings of the 9th International Symposium on Air

Breathing Engines, Athens, Greece, Sept. 3-8, pp. 245-253, ISABE paper 89-7024, AIAA, Washington DC.

Tang G, 2004, "Measurements of the Tip-gap Turbulent Flow Structure in a Low-speed Compressor Cascade", Ph.D. dissertation, Aerospace and Ocean Engineering Dept., Virginia Polytechnic Institute and State University, available http://scholar.lib.vt.edu/theses/available/etd-05122004-161722/

Wang Y and Devenport W, "Wake of a Compressor Cascade with Tip Gap, Part 2: Effects of Endwall Motion", AIAA Journal, vol. 42, no. 11, pp.2332-2340, November 2004.

Wang Y, 2000, "Tip Leakage Flow Downstream a Compressor Cascade with Moving End Wall", M.S. thesis, Aerospace and Ocean Engineering Dept., Virginia Polytechnic Institute and State University, available http://scholar.lib.vt.edu/theses/available/etd-04052000-14200057/

Wenger C W, 1999, "Analysis of Two-point Turbulence Measurements for Aeroacoustics", M.S. thesis, Aerospace and Ocean Engineering Dept., Virginia Polytechnic Institute and State University, available http://scholar.lib.vt.edu/theses/available/etd-010699-132153/

Wenger C W, Devenport W, Wittmer K S and Muthanna C, "Wake of a Compressor Cascade with Tip Gap, Part 3: Two Point Statistics", AIAA Journal, vol. 42, no. 11, pp.2341-2346, November 2004.

Yamamoto A, Mimura F, Tominaga J, Tomihisa S, Outa E and Matsuki M, "Unsteady Three-Dimensional Flow Behavior Due to Rotor-Stator Interaction in an Axial-Flow Turbine", ASME paper 93-GT-404, 1993.

Yaras M, Yingkang Z and Sjolander S A, "Flow Field in the Tip Gap of a Planar Cascade of Turbine Blades", ASME Journal of Turbomachinery, vol. 111, July 1989, pp. 276-283.

Zeschky J and Gallus H E, "Effects of Stator Wakes and Spanwise Nonuniform Inlet Conditions on the Rotor Flow of an Axial Turbine Stage", Journal of Turbomachinery, vol. 115, pp. 128-136, January 1993.

Zierke W C, Farrell K J and Straka W A, "Measurements of the Tip Clearance Flow for a High-Reynolds-Number Axial-Flow Pump", Journal of Turbomachinery, vol. 117, October 1994, pp. 522-532.